L'information quantique encodé en gravité semi-classique

Dongsheng Ge

PSL
UNIVERSITÉ PARIS

THÈSE DE DOCTORAT
DE L'UNIVERSITÉ PSL

Préparée à l'École Normale Supérieure

Quantum Information Encoded in Semi-Classical Gravity

Soutenue par

Dongsheng GE

Le 28 September 2020

École doctorale n°564

Physique en Île-de-France

Spécialité

Physique Théorique

Composition du jury :

Constantin BACHAS École Normale Supérieure	*Président*
Johanna ERDMENGER Universität Würzburg	*Rapporteuse*
Blaise GOUTÉRAUX École Polytechnique	*Examinateur*
Francesco NITTI Université Paris-Diderot	*Examinateur*
Michela PETRINI Sorbonne Université	*Examinatrice*
Simon ROSS Durham University	*Rapporteur*
Giuseppe POLICASTRO École Normale Supérieure	*Directeur de thèse*

ENS | PSL

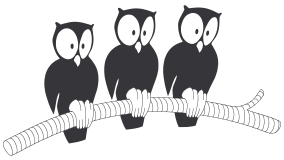

To my parents.

Abstract

The holographic duality renders a way to encode certain quantum information in a semi-classical gravity theory. In this thesis, we start with the quantum complexity, considering the universality of its two holographic conjectures, "Complexity=Volume" (CV) and "Complexity=Action" (CA), in terms of the thin brane model in AdS_3. Our result shows that the divergence structures for the two are not identical as CV has an extra brane tension dependent logarithmic divergence. Though preliminary considerations on the field theory side of complexity favor CA, the universality question is still kept open. Next we move to a study on the gate dependence of circuit complexity by explicit calculation in the two-dimensional bosonized model where we show that the influence of the gate set choice is different for different subsets of states under consideration, not significant for "bosonic coherent-fermionic Gaussian" case, while dramatically different in the bi-Gaussian case. Then, we reconsider the thin-brane model in the canonical holographic manner, finding that the brane tension is related to the energy transport coefficients defined in the dCFT, in addition to the relation to the boundary entropy of the interface which has been commonly advertised in the literature. In the last part, we propose a new bulk geometric quantity dual to the Berry curvature in the space of boundary modular Hamiltonians, which is the Riemann curvature in the vicinity of the Hubeny-Rangamani-Takayanagi surface. A sanity test has been done in pure AdS_3 which shows a nice agreement due to the simplicity and nice symmetries of this system. The studies in this thesis have opened many interesting directions, which hopefully will be explored in the future.

Acknowledgement

The four years of doctoral study has been a wonderful journey for me to realize myself and expand my toolkits to explore our world, from a physicist perspective. My growth in those years is such that noticeable, even myself could not neglect. Like a tree, from a sapling, it requires water, sunshine, air and various nutritions to become bigger. The development as a theoretical physicist wouldn't be possible without the supports and assistance from all the people I have met. At this very moment, my gratitudes to all the nice figures are the only stuff appearing in my mind.

I wouldn't be blamed if I would like to thank my parents who are always behind me to provide love and supports whenever there is need, like most parents. If there can be any peculiarity of them, it would be their undoubted respects for all the decisions I have made, and constant encouragements to pursue my interests, without which my professional life would be another story. I feel also very lucky to have been born in such a big family with many solidary relatives, the close relations among us help me go through the obstacles from time to time. I wouldn't make myself regretful for having not taken the chance to thank them all.

Now it is time to thank my supervisor, Giuseppe Policastro, who introduced me to the amazing world of holography, without him this journey would be much harder. I really appreciate the long hours of discussions we have spent together during the last four years. He guides me on how to think about the problems, how to tackle them and eventually how to solve them. Through our countless interactions, I start to build my own way of understanding physics, to a better level. I am also grateful for his nomination of the KITP graduate fellowship, which is a precious opportunity for me to open up my horizon and expand my knowledge from interactions with the American physicists.

Next I want to thank all my collaborators, from whom I have gained practical knowledge through the common projects. I would like to thank Shira Chapman, who helped me on my first publication and made my first academic trip to PI become reality. I would like to thank Lampros Lamprou, who introduced me to the interesting subject of modular Berry problem. His passion and enthusiasm on understanding physics bring me the air of creativity. I would like to thank Bartek Czech, who has a special perspective to understand physics and who always reminds me to think positively. I would like to thank Jan de Boer, who presented me to see things at a higher level. I would like to thank Costas Bachas, who taught me how to find a simpler way to solve a problem. I would also like to thank Bruno Le Floch, who is willing to teach me about the beauty of the $T\bar{T}$ deformation theory.

The last period of my doctoral study was spent at KITP, in the city of Goleta. I am very grateful for the hospitality and various supports from all the stuffs and faculties. Especially I

want to thank Xi Dong and Don Marolf, for offering me the opportunity to join their group meetings, Gary Horowitz for organizing the Friday gravity lunch discussion and Juan Maldacena for valuable discussions and inspirations on information paradox. I benefit as well through the interactions with the other graduate fellows, in particular, Alex Cole, Mike Staddon, Marija Tomašević and Xuzhe Ying. Besides, I am grateful for Wayne Weng, who helped me on the accommodation before my arrival in the US.

Through discussions at various occasions, conferences, academic visits etc., my understanding about different physical concepts have been pushed forward non-negligibly. I would like to take this opportunity to show my gratitude to Ahmed Almheiri, Vijay Balasubramanian, Alex Belin, David Berenstein, Alice Bernamonti, Oblak Blagoje, Joan Camps, Pawel Caputa, Horacio Casini, Alejandra Castro, Aldo Cotrone, Lorenzo Di Pietro, Tom Faulkner, Ben Freivogel, Federico Galli, Steve Giddings, Daniel Harlow, Tom Hartman, Daniel Kabat, Hong Liu, Vinay Malvimat, Henry Maxfield, Eric Mefford, Ruben Montent, Rob Myers, Tatsuma Nishioka, Onkar Parrikar, Đjorđje Radičević, Suvrat Raju, Douglas Stanford, Wei Song, Tin Sulejmanpasic, James Sully, Eduardo Testé, Erik Tonni, Gustavo Joaquin Turiaci, Eric Verlinde, Huajia Wang, Jieqiang Wu, Tadashi Yakayanagi, Zhenbin Yang, and Beni Yoshida. I would also like to thank Johanna Erdmenger, Blaise Goutéraux, Michela Petrini and Simon Ross, for accepting my requests to join the Jury of my defence.

LPTENS has been home to me for the last four years, I would like to show my gratitude to all the administrative stuffs and faculty members who made my research life easier and more enjoyable. In particular, I would like to thank Jan Troost, for his inspirations during Monday lunches through numerous semi-physical conversations, and Francesco Nitti, Jesper Jacobsen, Jean-François Allemand and Jean-Marc Berroir, for their help on getting the fourth-year funding for my doctoral study. I am also grateful for the supports and accompany of the friends who shared the same office with me, Clément Le Priol, Gwenaël Ferrando, and Songyuan Li. The lab friends are undoubtedly another cheering force, I would like to thank Zhihao Duan, Arnaud Fanthomme, Tristan Gautié, Etienne Granet, Tony Jin, Alexandre Krajenbrink, Augustin Lafay, Cathelijne ter Burg and Deliang Zhong.

Finally, I would like to say that I feel very lucky to have those wonderful friends from my master years, Raphael Sgier, Daniele Ruini, Ioannis Lavdas and Andrea Dei, who are always on my side, share stories with me and cheer me up from time to time.

葛东胜 (Dongsheng Ge)
Goleta, in the quarantine time of COVID-19

Contents

List of Figures

Chapter 1

Introduction

Geometry has fascinated us as human beings ever since the start of the history of human's civilization, due to our curiosity about nature, who hides a large amount of information in a certain geometric manner. If one ever thinks of the discovery of the first irrational number "$\sqrt{2}$", which appears to be the length of the hypotenuse of a right triangle with legs of length 1, or Archimedes' constant "π", which acts as the ratio of a circle's circumference to its diameter, one would be amazed at how nature could encode such important information with beauty and simplicity. It is safe to say that, the deeper we understand about our nature, the more information we are able to extract from its associated geometries, and vice versa.

The 20th century has witnessed a breakthrough in the understanding of gravity, a fundamental piece of our nature, initiated by the unconventional work of Einstein and Großman on the generalized theory of relativity in 1915 [1]. This revolutionary theory refines Newton's outlook on the split of space and time by treating them as a whole and on equal footing, which leads to a novel understanding of the gravitation as the geometric property of spacetime. As have been put by Misner, Thorne and Wheeler, "space tells matter how to move, matter tells space how to curve" [2], General Relativity beautifully illustrated how the dynamics of the spacetime geometry conveys the message from nature in terms of gravitation.

Another pillar that can not be circumvented in the last century is the microscopic understanding of many macroscopic phenomena, for instance, the photonic explanation of photoelectric effect in 1905 by Einstein [3], the orbital model for the spectral of emission lines of atomic hydrogen in 1913 by Bohr [4] and so on so forth, which updated the classical mechanics to the quantum level through further developments, forming a modern subject named Quantum Mechanics. A natural question one might quest on the lessons from General Relativity is that, does this new type of theory share some common features such that it have some geometric interpretation as well? To answer this question would require a particular theory which incorporates both General Relativity and Quantum Mechanics in the same framework. In the sixties, it might still be a pie in the sky though both theories have been mathematically formulated.

Nevertheless, this among other questions stimulated the search for a new theory which can depict the quantum behaviours of gravity as well as a complete unified theory for everything. A prominent candidate theory then emerged starting from the late sixties, by generalizing the point-like particle to one-dimensional fundamental vibrating strings living in tiny scales, which

can give rise to the desired properties of standard particles, such as charge, mass, spin etc., at the observational level and automatically contains the graviton, the quantum of gravity as one of its oscillating modes by construction. These fascinating features of the so called String Theory have attracted vast investigations, including the extension to supersymmetric case which relates the bosonic system to the fermionic one via a symmetry transformation, thus laid a fairly good foundation for building a rather concrete connection between General Relativity and Quantum Mechanics.

It was not until 1997, when Maldacena proposed a correspondence between the type IIB supergravity theory in the five-dimensional anti-de Sitter (AdS) space with a negative cosmological constant compactified on a five-sphere, and the four-dimensional superconformal Yang-Mills theory with four supersymmetries [5], that things become more tractable. The novel feature of this conjecture is that it offers a new perspective to understand the relation between the gravity theory and quantum field theory which are related by the so called holographic duality[1] or gauge/gravity duality. In this setup, a $(d+1)$-dimensional conformal field theory (CFT) which roughly speaking is a quantum field theory with additional scale invariance, is regarded to live on the asymptotic boundary of the $(d+2)$-dimensional AdS spacetime. Therefore, the boundary CFT can be taken on as the projection of the gravity theory in one higher dimension, hence the name holographic duality or *AdS/CFT* correspondence. A very successful application of this duality was the calculation on the transport coefficient, more precisely the shear viscosity of the strongly correlated quark-gluon plasma system at finite temperature by Policastro, Son and Starinets [9], whose result is remarkably in the same order of magnitude as the experimental measurement in RHIC [10], while the other perturbative analysis leads to infinity. With a huge amount of further tests being made to show the validity of the holographic duality, it has become commonly accepted as a principle among considerably many theoretical physicists, which lays the foundation for the present dissertation.

Due to this established duality, it becomes rather natural to endow some information about the quantum systems with the geometric interpretations, through the corresponding suitable quantities in the spacetime manifold. In 2006, after almost ten years of the birth of the holographic duality, Ryu and Takayanagi made the first trial towards this direction in their seminal work [11] by relating the entanglement entropy, a measure of the degrees of quantum entanglement between a many-body subsystem with its complement, to a certain bulk[2] codimensional-two extremal surface anchored to the boundary subregion where the entanglement entropy is evaluated. Their intuition comes from the counting of Black Hole entropy via the Bekenstein-Hawking formula, where gravitational entropy is proportional to the area of the Black Hole horizon. In the context of $\mathrm{AdS}_3/\mathrm{CFT}_2$ correspondence, the bulk geometric quantity to encode the boundary entanglement pattern is simply the length of a spatial geodesic anchored to the interval considered, with the proportionality factor being a quarter of the inverse Newton's constant.

The success of understanding the quantum entanglement in the holographic manner then

[1] Some preliminary considerations on viewing the universe as a hologram have been articulated by Thorn [6], 't Hooft [7] and Susskind [8] in the early nineties.

[2] In the context of holographic duality, "bulk" means the spacetime where the gravity theory is living as opposed to the asymptotic AdS boundary where the CFT is living. Usually the asymptotic boundary is reached by following a spatial coordinate to one of its limits in the bulk frame.

initiated many researches along the line to decode the quantum information via the holographic principle in the semi-classical gravitational system, such as the holographic derivation of the entropic inequalities [12,13], butterfly effect in Black hole system [14], gravitational dual of Rényi Entropy [15] and so on so forth. Thus in a way it reinforces the geometric essence of certain quantum theories and to some degree tightens the connections between the gravity theory and the quantum theory. The current dissertation aims to continue to explore these connections, either to analyse some existing conjectured correspondences or to propose new geometric quantities that encode the quantum information in the gravitational language.

The first part of the thesis focuses on a quantity arising from the quantum computing theory, called the quantum complexity, defined as the minimal number of gates required to conduct a quantum computation task which starts from a reference state and ends approximately in a target state. In 2014, Susskind et al proposed a connection to the gravity theory, arguing that this quantity could be related to a bulk codimension-one volume in AdS spacetime [16], or the action in a certain bulk codimension-zero region called Wheeler-DeWitt patch [17] which was conjectured in the following year. The "volume" conjecture is named as "Complexity=Volume" (CV) while the "action" conjecture is named as "Complexity=Action" (CA), whether they are universally equivalent remains an unknown issue. Therefore, in Chapter 3 based on [18], the universality of the two proposals was studied by introducing a thin tensile AdS_2 brane in the middle of AdS_3, where the brane acts as a defect and leads to an extra volume in its transverse direction. The results show that an extra tension dependent *log* divergence is present for CV while no tension-dependent divergence appears for CA. Through a preliminary consideration of the complexity of a free scalar model on the boundary, it seems that CA rather than CV is more favoured. However, a definite claim of the universality of the current holographic conjectures requires further investigation, which is left to the future studies.

As an episode, in Chapter 4 based on [19], we reconsider the thin AdS_2 brane model in the canonical holographic manner, assuming it is indeed the bulk dual of a generic defect CFT_2. On the dCFT side, an interesting property arises in terms of the two-point functions of the stress energy tensor which are universally fixed with only one new parameter other than the central charges of the CFTs on the two sides of the defect if they are generally different from each other. Furthermore, a scattering process could be set up with this parameter encoding the information for the energy transport coefficients. Through our analysis on the scattering of the boundary gravitons, we give the first calculation to relate the brane tension to the reflection/transmission coefficients. The limits of the brane setup introduces both an upper bound and a lower bound to the those coefficients where the lower bound for the reflection coefficient coincides with the one from the average null energy condition (ANEC) while the upper bound tightens the result from ANEC.

In Chapter 5 based on [20], the attention is drawn to the field theory consideration of the quantum complexity, since to understand the holographic conjectures to a better level requires a clearer understanding of the boundary theory, like the process for understanding holographic entanglement entropy. A known fact in the consideration of quantum complexity is that, it is highly influenced by the choices of gates, states and penalty factor. In the previous literature, there is no work that has considered the dependence of the gates choice explicitly, hence giving

the spirit for this chapter where the work was performed in the "$1+1$" free-fermion, equivalently free-boson model by calculating the relative complexity between the same reference state and target state, using two different sets of operators (gates) which are related non-linearly through the bosonisation formula. As limited by the computability, the states under consideration are either of coherent type or Gaussian type, where two methods are available for the computation, the *Nielsen* method and the *Fubini-Study* (FS) method. Both methods are based on the idea of geometrizing the problem and finding the shortest path, in which FS geometrizes the states on a manifold while *Nielsen* geometrizes the unitary transformations on the states. The analysis shows that the quantum complexity is highly sensitive to the gate choice for the "bosonic coherent-fermionic Gaussian" states while non-significantly impacted by the "bosonic Gaussian-fermionic Gaussian" states.

Though many bulk geometric quantities have been endowed with some meaning from quantum information, there is on another different geometric object, which is very simple yet poorly understood in holography, is the curvature of the bulk spacetime. In Chapter 6 based on [21], special attention is payed to understand this quantity. The inspirations come from the following: in a gravitational system, when a vector, representing a frame orientation, is parallel transported along a loop, it differs from its initial orientation by an amount governed by the curvature of the spacetime manifold; similarly, when a quantum state is transported along a loop in Hilbert space, it will incur an extra phase called *Berry phase*, which is an integral of *Berry curvature*. Based on those, a pioneering proposal was made by claiming the duality between those two curvatures, through careful analysis on the definition of the corresponding connections for the two kinds of parallel transports. In addition, the consistency of the conjecture was tested in a pure $\mathrm{AdS}_3/\mathrm{CFT}_2$ setup, taking advantage of the equivalence between the local isometry of the AdS_3 and global conformal symmetry of the CFT_2. Potentially, this part will provide a new test for the emergence of bulk geometry at a semi-classical level.

In the last part of the dissertation, Chapter 7, a summary of the results obtained during the doctorate is presented, thus putting a beautiful end to the doctoral study of the author.

Chapter 2

Fundamentals of Holography and its Applications

Holography, as its name suggests, is the study of making holograms where a one-dimension higher system could be reconstructed by a lower system, specifically in the current context, it is regarded as a synonym of the *AdS/CFT* correspondence. As an attractive subject which has been developed for more than twenty years, it has become a large field of study, which roughly can be divided into two categories based on the approaches to study the subject. The first one is the *top-down* approach, where clear descriptions on both sides are available from the UV complete theory perspective (superstring theory or supergravity theory), as well as the existence of precise matching of the symmetries, spectra, coupling constants, amplitudes etc. The first prominent example is given by Maldacena [5], and later by Witten [22] and Gubser, Klebanov and Polyackov [23] stating that

$$4D\ \ \mathcal{N}=4,\ SU(N)\ \text{Yang-Mills theory} \equiv \text{Type IIB string theory on } AdS_5\times S^5\,, \tag{2.1}$$

which is realized through $N-$stack of coincident D3 branes in the ten-dimensional spacetime whose near horizon geometry is $AdS_5\times S^5$, while the low energy dynamics of the brane volumes is governed by the $\mathcal{N}=4$ $U(N)$ gauge theory[1]. A quick look at the symmetries on both sides reveals the consistency of the duality, since on the left side, we have the $SO(4,2)$ global conformal symmetry as well as the global $SU(4)$ R-symmetry, while on the right side, these symmetries correspond to the isometries of the full spacetime, $SO(4,2)\times SO(6)$, which are equivalent to each other, since $SO(6)\cong SU(4)$. Notably, the duality relates the parameters on both sides in the following manner,

$$(\ell/l_s)^4 \equiv \ell^4/\alpha'^2 = 4\pi g_s N = g_{\rm YM}^2 N = \lambda, \tag{2.2}$$

where λ is the 't Hooft coupling and $g_{\rm YM}$ is the coupling for the term $-\frac{1}{2g_{\rm YM}^2}{\rm Tr}F_{\mu\nu}F^{\mu\nu}$ in the YM theory, l_s is the string length related to the string tension $(2\pi\alpha')^{-1}$ as $\alpha'=l_s^2$ and g_s is the string coupling. To have a classical gravity description requires that $N\to\infty$ and $\lambda\to\infty$, physically this means that we consider the planar limit of a strongly coupled gauge theory. For

[1]The missing U(1) part represents the overall collective motion of the stack of branes, which moves away in the near horizon limit, thus can be omitted [24].

more interesting aspects and details on this duality or some other top-down models, one can refer to the thorough AGMOO review [25].

The second approach is the opposite, called *bottom-up* approach, where we consider an effective AdS gravity theory that is dual to a one dimension lower quantum field theory, with the belief that there exists a UV completed theory in higher dimensions that can make precise the duality, usually a ten-dimensional superstring theory or eleven-dimensional M-theory if can be consistently constructed. This gives an advantage of this approach, since one only needs to consider the necessary relavant bulk ingredients without complicating the system by finding a consistent theory including the compactified directions. Considering its nice features, the bottom-up approach will be the main melody of the current thesis.

In the following sections, I will start with some basic ingredients about the holographic duality, with emphasis on the geometric features of the AdS space and the most useful extrapolating method to obtain the CFT correlation functions. After that, I will introduce the application of the holographic duality on the subjects that have been studied in this thesis.

2.1 Basic Ingredients of Holographic Duality

In this part, I only include the most necessary ingredients that will be used in the current thesis. For more details, one can refer to the thorough review [25] by Aharony, Gubser, Maldacena, Ooguri and Oz, or lecture notes by, for example, Skenderis [26] and Polchinski [24].

2.1.1 A Glimpse of the Anti-de Sitter Space

As is known, the AdS_{d+1} space is a maximally symmetric spacetime, which means that its Riemann tensor is fixed by the metric tensor g_{ab} up to a total factor related to the AdS scale ℓ

$$R_{abcd} = -\frac{1}{\ell^2}(g_{ac}g_{bd} - g_{ad}g_{bc})\,, \tag{2.3}$$

where a runs from 0 to d. It has the right scale dimension and is antisymmetric under the change of $a \leftrightarrow c$ and $b \leftrightarrow d$ and symmetric under the exchange of $\{ab\} \leftrightarrow \{cd\}$ as expected. Tracing twice of the indices, we have the Ricci scale $R = -\frac{d(d+1)}{\ell^2}$, which simply tells us that AdS space has a constant negative curvature, resulting in a negative cosmological constant $\Lambda = \frac{d(1-d)}{2\ell^2}$ when applying the Einstein equation.

The isometry group for the AdS space as aforementioned is $SO(d,2)$, which can also be looked as the Lorentz group for $(d+2)$-Minkowski space with two negative signatures. In fact, one can embed AdS_{d+1} space as a hyperboloid surface in the $(d+2)$-Minkowski space with the following surface equation

$$-X_0^2 + \sum_{i=1}^{d} X_i^2 - X_{d+1}^2 = -\ell^2, \tag{2.4}$$

where X^M $(M = 0, \ldots, d+1)$ are the Minkowski coordinates. Through different coordinate choices[2], one would get different patches of the AdS space. Notably, there is the global embedding,

[2]There are at least three common coordinate choices, global, Poincaré and Rindler. In the main text, the first two are introduced due to the relevance for the later chapters, if one is interested in the Rindler coordinates, one

which is a result of the following relation between the global AdS coordinates with the Minkowski coordinates,

$$\begin{aligned} X_0 &= \ell \cosh\rho \cos\tau\,, \quad X_{d+1} = \ell \cosh\rho \sin\tau\,, \\ X_i &= \ell \sinh\rho \sin\theta_1 \sin\theta_2 \ldots \sin\theta_{i-1} \cos\theta_i \quad (i = 1, \ldots, d-1)\,, \\ X_d &= \ell \sinh\rho \sin\theta_1 \sin\theta_2 \ldots \sin\theta_{d-2} \sin\theta_{d-1} \end{aligned} \tag{2.5}$$

where $\theta_i \in [0, \pi]$ for $i = 1, \ldots, d-1$ and $\theta_{d-1} \in [0, 2\pi)$. To cover the hyperboloid once, one can take $\rho \geq 0$ and $\tau \in [0, 2\pi)$, hence the name global coordinates, which leads to the metric

$$ds^2 = \ell^2(-\cosh^2\rho d\tau^2 + d\rho^2 + \sinh^2\rho d\Omega^2) \tag{2.6}$$

with Ω being all the spherical coordinates and the asymptotic boundary locates at $\rho \to \infty$. Another embedding worth mentioning is given by the Poincaré coordinate, which is often used with the embedding relation

$$\begin{aligned} X_0 &= \frac{z}{2}\left(1 + \frac{1}{z^2}(\ell^2 + \vec{x}^2 - t^2)\right)\,, \quad X_{d+1} = \frac{\ell t}{z}\,, \\ X^i &= \frac{\ell x^i}{z} \quad (i = 1, \ldots, d-1)\,, \quad X^d = \frac{z}{2}\left(1 - \frac{1}{z^2}(\ell^2 - \vec{x}^2 + t^2)\right)\,, \end{aligned} \tag{2.7}$$

which covers a patch of the AdS space, with the asymptotic boundary located at $z \to 0$. The Poincaré metric is given by

$$ds^2 = \frac{\ell^2}{z^2}(dz^2 + \eta_{\mu\nu} dx^\mu dx^\nu)\,, \tag{2.8}$$

where one see clearly that the asymptotic boundary is conformally flat. By a coordinate change $\tan\theta = \sinh\rho$ ($\theta \in [0, \pi/2)$ for the global coordinate (2.6), it is easy to see the conformal flatness when approaching the asymptotic boundary $\theta \to \pi/2$. The consistency of the duality proposal is self-revealed in this manner where on the boundary lives a conformal field theory.

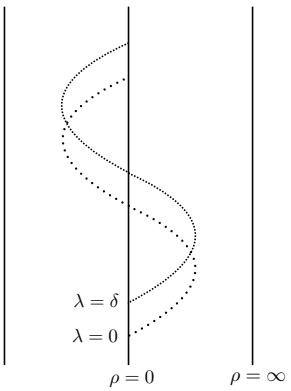

Figure 2.1: Massive particles moving in AdS are attracted towards the center, as illustrated by two timelike geodesics in AdS_2, one begins at $\lambda = 0$ while the other is the shifted one with δ displacement.

As AdS space has a negative cosmological constant, it is an attractor, which can be seen

could refer to, for example the appendix of [27].

from the trajectory of a massive particle in the global coordinates. To obtain that trajectory, in principle, one has to solve the timelike geodesic equation or the equivalent Euler-Lagrangian equation, however, thanks to the embedding picture, we could use a simpler manner to obtain a glimpse of the trajectory without solving the second-order differential equation. The observation is that in (2.6), a known timelike geodesic is

$$\rho = 0, \quad \tau = \lambda\,, \tag{2.9}$$

where λ is the affine parameter. Then one can use the isometries to obtain all the timelike geodesics. We can see the simplest example explicitly in the AdS_2 space, if we perform a boost η in (01) direction in the embedding space, which means

$$\ell \begin{pmatrix} \cos\lambda \\ 0 \\ \sin\lambda \end{pmatrix} \to \ell \begin{pmatrix} \cos\lambda\cosh\eta \\ \cos\lambda\sinh\eta \\ \sin\lambda \end{pmatrix} = \ell \begin{pmatrix} \cosh\rho\cos\tau \\ \sinh\rho \\ \cosh\rho\sin\tau \end{pmatrix}, \tag{2.10}$$

expressing $\rho,\ \tau$ in terms of $\lambda,\ \eta$ within half a period $\tau \in [0,\pi]$ where $\tau(\lambda = 0) = 0$ gives,

$$\rho = \sinh^{-1}(\cos\lambda\sinh\eta), \tag{2.11}$$

$$\tau = \tan^{-1}\left(\frac{\tan\lambda}{\cosh\eta}\right). \tag{2.12}$$

The above solution gives a set of new timelike geodesics in AdS_2. In a full period $\tau \in [0, 2\pi]$, one see that the geodesic will emanate from the center $\rho = 0$, then at some point turn back, go pass the centeral axis to the other side, later turn back again and end on the central axis, as Fig 2.1 shows. We can also get another geodesic from this one by performing a shift δ in τ direction, which amounts to a rotation in (02) directions in the embedding space. Taking advantages of all the isometries, one is able to obtain all the timelike geodesics for an AdS space with arbitrary dimensions, where anyone of those can reveal the attracting property of the AdS space due to its negative cosmological constant.

2.1.2 CFT Correlation functions via the Duality

Holography realizes a deep connection between the low energy supergravity in AdS space and a CFT theory living on its boundary. From a CFT perspective, one might wonder how the correlation functions are encoded in the gravity theory, since those correlators carry the whole CFT data. This piece of hidden information has been dug out by two independent works, Witten [22] and Gubser, Klebanov and Polyakov [23], giving rise to the name GKPW relation. The idea is to identify the generating functional of the CFT on the boundary side to the bulk gravity action at evaluated at the saddle point[3], subject to the asymptotical Dirichlet boundary condition for the bulk fields which act as sources for the gauge invariant CFT operators. In practice, the saddle point is approximated by the solution to the equation of motion of the field respecting the chosen

[3] A subtlety might arise when there is more than one saddle points to extremize the gravity action, then one solution is to consider the most important one. However, in the following parts of the thesis, this issue will not be encountered.

boundary condition. In the Euclidean signature[4], the relation can be formulated as

$$W_{\rm CFT}[\phi_0] = -\ln\left\langle \exp\left(\int_\partial \phi_0 \mathcal{O}\right)\right\rangle_{\rm CFT} = -I^{\rm extremal}_{\rm grav}[\Phi_\partial = \phi_0]\,, \tag{2.13}$$

where ϕ_0 is the asymptotic boundary condition for the bulk field Φ, which carries spin index implicitly. Holographic dictionary shows that the bulk scalar field is dual to the boundary scalar field, the bulk gauge field is dual to the boundary conserved current, the bulk graviton is dual to the boundary stress energy tensor, etc. In this manner, the connected CFT correlation functions are given by the functional derivatives of the extremized gravity action with respect to its boundary value,

$$\langle \mathcal{O}(x_1)\mathcal{O}(x_2)\cdots\mathcal{O}(x_n)\rangle_c = -\frac{\delta^n I^{\rm extremal}_{\rm grav}[\Phi_\partial=\phi_0]}{\delta\phi_0(x_1)\delta\phi_0(x_2)\cdots\delta\phi_0(x_n)}\Big|_{\phi_0=0}\,. \tag{2.14}$$

For higher (than two) correlation functions, the issue becomes more complicated. In the following part of this section, we will consider an example with free massive scalar in the bulk, and get an idea how to obtain its two-point correlator holographically.

An example: two-point function for a massive scalar field in the bulk

Now as an illustration to obtain the two point function holographically, we will consider the canonical example with a free scalar field in the bulk,

$$I = \frac{1}{2}\int d^dx dz\sqrt{g}\phi(x)(-\Box + m^2)\phi(x) + \frac{1}{2}\int_{\partial\rm AdS} d^dx\sqrt{\gamma}\partial_\perp\phi(x) + I_{\rm ct} \tag{2.15}$$

where the second integral is the boundary action and the third one is the counter term needed to make the action finite. Varying the Lagrangian with respect to ϕ gives the equation of motion,

$$\frac{1}{\sqrt{g}}\partial_a(g^{ab}\sqrt{g}\partial_b)\phi = m^2\phi\,. \tag{2.16}$$

A similar equation of the above also appears when considering spin fields like a vector field or graviton in the AdS [28], that's the reason we will focus on this as an illustration. The back reaction of the scalar field to the geometry can be neglected since it is of order $O(G_N^{-1})$ with G_N being the Newton's constant in $(d+1)$ dimension. Therefore, we are safe to use the metric for pure AdS. In the following, we will use the Euclidean version of the Poincaré coordinate (2.8) to give the explicit result, substituting into the equation of motion (2.16) gives

$$\left(\frac{z}{\ell}\right)^{d+1}\partial_z\left(\left(\frac{\ell}{z}\right)^{d-1}\partial_z\right)\phi + \frac{z^2}{\ell^2}\partial_\mu\partial^\mu\phi - m^2\phi = 0\,, \tag{2.17}$$

[4]The advantage of working in the Euclidean signature is that one can avoid the subtlety of between the advanced and retarded Green functions.

whose solution contains two branches, depending on the leading power of $z \to 0$. The full ansatz can be written as a power series of the radial coordinate z

$$\phi(z,x) = \underbrace{z^{\Delta_-}(\phi_0(x) + z^2\phi_2(x) + \dots)}_{\phi_-} + \underbrace{z^{\Delta_+}(\phi_{2\nu}(x) + z^2\phi_{\nu+2}(x) + \dots)}_{\phi_+} \tag{2.18}$$

where $\Delta_\pm = \frac{d}{2} \pm \nu$ with $\nu = \sqrt{\frac{d^2}{4} + m^2\ell^2}$ and $\phi_2(x)$ stands for two-derivative term which can actually be obtained explicitly as well as the other higher derivative terms. Let's assume that $\nu \notin \mathbb{Z}$ in the following analysis. One can see that ϕ_- is the dominant branch and contains the non-normalisable mode when approaching the asymptotic boundary if $\Delta_- < 0 < \Delta_+$[5], thus most of the time ϕ_0 is identified as the source for the dual CFT operator, as well as the boundary condition for the bulk scalar. It is not hard to see that when substituting the ansatz (2.18) back to the action (2.15) assuming some conterterms like a quadratic term in ϕ on the boundary [26], one could obtain the expectation value of the boundary dual operator $\mathcal{O}(x)$ by using the description (2.14),

$$\langle \mathcal{O}(x) \rangle = -\frac{\delta I_{\text{on-shell}}}{\delta\phi_0(x)} = (2\Delta_+ - d)\,\ell^{d-1}\phi_{2\nu}(x)\,, \tag{2.19}$$

which shows that, the asymptotically leading power the other branch ϕ_+ works as the response to the source ϕ_0 and provides one-point function in presence of the source.[6] Once we have identified the source, in principle, one could write the bulk solution as an integral of the source

$$\phi(z,x) = \int d^d y K(x,z;y)\phi_0(y) \tag{2.20}$$

where $K(x,z;y)$ is the alleged bulk-to-boundary propagator, encoding the way how the boundary source ϕ_0 propagates into the bulk. The explicit form for $K(x,z;y)$ can be obtained by solving the scalar e.o.m[7] assuming a localized boundary source $\phi_0(x) = \delta^{(d)}(x - x')$, given by

$$K(x,z;y) = \pi^{-d/2}\frac{\Gamma(\Delta_+)}{\Gamma(\nu)}\frac{z^{\Delta_+}}{(z^2 + (x-y)^2)^{\Delta_+}}\,, \tag{2.21}$$

one sees that when $z \to 0$, $K(x,z;y) \to 0$ as expected. Finally, one arrives the two-point function

$$\langle \mathcal{O}(x)\mathcal{O}(y) \rangle = \frac{\delta\langle \mathcal{O}(x) \rangle}{\delta\phi_0(y)} = (2\Delta_+ - d)\,\ell^{d-1}\frac{\delta\phi_{2\nu}(x)}{\delta\phi_0(y)} = (2\Delta_+ - d)\pi^{-d/2}\frac{\Gamma(\Delta_+)}{\Gamma(\nu)}\frac{1}{(x-y)^{2\Delta_+}}\,. \tag{2.22}$$

One can read the conformal dimension of the scalar operator from the power of the proper distance between the two operators, which is Δ_+, the unitarity bound requires that Δ_+ is bounded from below, *i.e.*, $\Delta \geq d/2 - 1$, as in [29, 30].

[5] This relation is obtained assuming $m^2 \geq 0$, in general, one only has to work on the condition $m^2 \geq -d/4$, known as the Breitenlohner-Freedman stability bound, though the leading asymptotic mode in ϕ_- is no longer necessarily non-normalizable.

[6] In fact, $\phi_{2\nu}(x)$ can be expressed as an integral of the source $\phi_0(x)$ where $\phi_{2\nu}(x) = \int d^d y F(x,y)\phi_0(x)$, with $F(x,y) = \lim_{z\to 0} z^{-\Delta_+}K(x,z;y)$.

[7] An interesting way to get this Green function using symmetry argument by Witten can be found in his paper [22].

2.2 Holography and Two-Dimensional Defect CFT

In the study of AdS/CFT correspondence, a special case arises when the bulk dimension is "2+1" whose dual boundary theory is the "1+1" conformal field theory. The speciality in this dimension is that there are infinitely many conserved charges due to an enhancement of global $SL(2,\mathbb{R}) \times SL(2,\mathbb{R})$ symmetry to two sets of local Virasoro symmtries whose generators satisfy the Virasoro algebra, the unique central extension of Witt algebra [31]. In the bulk side, if one choose the asymptotic boundary conditions for the metric as Brown and Henneaux did in [32], the asymptotic symmetries will be enlarged as well to the complete two dimensional conformal symmetries. In this manner, the central charge is identified as the ratio of the AdS radius over Newton's constant for Einstein gravity, $c = \frac{3\ell}{2G}$. For a general higher derivative theory of AdS_3 gravity taking into account the quantum corrections, the central charge has a more covariant form $c = \frac{\ell}{2G} g_{ab} \frac{\partial \mathcal{L}}{\partial R_{ab}}$ [33, 34], one sees it coincides with Brown-Henneaux formula for Einstein gravity.

While the above should be regarded as a bottom-up consideration of the correspondence, the AdS_3 geometry could also be constructed from a top-down approach, *i.e.,* have an origin of an underlined string theory. The most well known realization comes from the near horizon geometry of D1-D5 brane system. Supposing we have a type IIB string theory on the background $R^{1,4} \times S^1 \times M_4$ with N_5 D5-branes wrapped on $S^1 \times M_4$ while N_1 D1-branes wrapped on the S^1, taking the near horizon limit yields the ten dimensional geometry $AdS_3 \times S^3 \times M_4$ with M_4 being T^4 or K^3 [25, 35, 36]. The central charge can be obtained through an analysis of the anomaly on the field theory living on D1-D5 branes whose IR fixed point is the dual conformal field theory. In [25], the central charge is $c = 6(k_a + 1) = 6(N_1 N_5 + 1)$, which is the same as six times the dimension of the instanton (D1 brane) moduli space for a large number of branes. Substituting the values for AdS_3 radius $\ell = (g_6 N_1 N_5)^{1/4} l_s$ and the three dimensional Newton's constant $G^{(3)} = g_6^2 l_s^4/(4\ell^3)$, one recovers the Brown-Henneaux central charge. Some recent process on understanding the duality for $M_4 = S^3 \times S$ could be found, for example [37, 38] and references therein. However, this is outside the scope of the current thesis and we will not use too much space to talk about that.

In the following part of this section, we will consider only from the bottom-up perspective without questioning if there is a microscopic string theory. To start with, we will make some brief introductions on the holographic Weyl Anomaly and then reach the 2D defect CFT and its energy transport coefficients. A careful holographic consideration on how to obtain those coefficients and the bounds associated will be discussed in Chapter 4.

2.2.1 Holographic Weyl Anomaly

It is known that in conformal field theories, there exists Weyl anomalies in even spacetime dimensions ($d = 2n$) which can be described purely in terms of geometric quantities [39], falling into two types of classes, type A anomaly and type B anomaly.[8] Type A is proportional to the Euler density of the dimension $E_{(d)}$ which is a topological term, in the sense that its integral over the spacetime manifold is the Euler characteristic, hence scale invariant. Type B constitutes of all

[8] When the spacetime has a boundary, there will be some corrections on from the boundary and there can also be integral Weyl anomaly in odd dimensions, one can see, for example [40, 41].

the conformal scalar polynomials constructed by the Weyl tensor[9] and its derivatives, denoted as $I_{(d)}$. There is also a third class consisting of total derivatives, however, it is trivial since it can be removed by adding finite local counterterms to the action [39, 42, 43]. Hence the universal form for the expectation value of the trace of the stress tensor can be written as

$$\langle T^{\mu}{}_{\mu} \rangle = c_1 E_{(d)} + c_2 I_{(d)} + \text{total derivatives}\,. \tag{2.24}$$

In $d = 4$, this universal form can be written as [44]

$$\langle T^{\mu}{}_{\mu} \rangle = -2aE_{(4)} - bI_{(4)} - \frac{b}{24\pi^2}\nabla^2 R\,, \tag{2.25}$$

$$E_{(4)} = \frac{1}{32\pi^2}\left[R^2 - 4R_{ab}R^{ab} + R_{abcd}R^{abcd}\right]\,, \tag{2.26}$$

$$I_{(4)} = -\frac{1}{16\pi^2}C_{abcd}C^{abcd}\,, \tag{2.27}$$

where a and b are called charges as an analog of 2d CFT and in [45] it has been proved that $a_{UV} > a_{IR}$ for all unitary RG flows from a critical point to another one, which is called $a-$theorem. In $d = 2$, the Weyl tensor vanishes identically and the Euler density is proportional to the Ricci scalar, the trace anomaly gives

$$\langle T^{\mu}{}_{\mu} \rangle = -\frac{c}{24\pi}R\,, \tag{2.28}$$

where c is the central charge and was proven by Zamolodchikov [46] to decrease monotonically as RG flows to the IR fixed point, *i.e.,* the $c-$theorem.

To see how the conformal anomaly can appear from the holographic setup, we have to rely on the GKPW relation (2.13) and consider the metric field or the graviton since it is the gravitational partner of the stress energy tensor according to the holographic dictionary. Following [42, 47], if one adopts the Fefferman-Graham Gauge for the metric as following

$$ds^2 = \frac{\ell^2}{4\rho^2}d\rho^2 + \frac{1}{\rho}g_{\mu\nu}dx^{\mu}dx^{\nu} \tag{2.29}$$

where ρ is the radial direction and the conformal boundary is located as $\rho \to 0$. Since our consideration is the conformal anomaly, we can turn off the other fields, then the vacuum Einstein equation is solved order by order in ρ such that

$$g = g_{(0)} + \rho g_{(2)} + \rho^2 g_{(4)} + \ldots, \qquad \text{for } d \text{ odd}\,, \tag{2.30}$$

$$g = g_{(0)} + \rho g_{(2)} + \cdots + \rho^{d/2} g_{(d)} + \rho^{d/2}\ln\rho\, h_{(d)} + O(\rho^{d/2+1})\,, \qquad \text{for } d \text{ even} \tag{2.31}$$

where $\mathrm{Tr}(g_{(0)}^{-1}g_{(d)})$ is covariant while $\mathrm{Tr}(g_{(0)}^{-1}h_{(d)})$ vanishes identically [42]. One thing worth noting is that in $d = 2$ case, the metric expansion doesn't contain the logarithmic term as $h_{(2)}$ vanishes which is shown in the appendix A of [47]. In [48], it has been shown that the metric expansion

[9] The Weyl tensor is defined as

$$C_{abcd} = R_{abcd} + (P_{bc}\,g_{ad} + P_{ad}\,g_{bc} - P_{ac}\,g_{bd} - P_{bd}\,g_{ac}) \tag{2.23}$$

with $P_{ab} \equiv \frac{1}{d-2}\left(R_{ab} - \frac{R}{2(d-1)}g_{ab}\right)$. One sees that the Weyl tensor has the same symmetries as Riemann tensor under the exchange of indices.

terminates at $g_{(4)}$ due to that the Weyl tensor vanishes identically at this very dimension. Since the bulk volume is infinite, one needs to introduce a regularization scale $\rho = \epsilon$ and evaluate the gravitational action[10] till this cutoff surface. If we pause the integration over the boundary coordinates x^μ for the moment, and only do the integral in terms of the radial direction, we can obtain the boundary Lagrangian containing both divergent terms in ϵ and finite terms,

$$\mathcal{L} = \frac{1}{16\pi G^{(d+1)}}\sqrt{g_{(0)}}(\epsilon^{-d/2}a_{(0)} + \epsilon^{-d/2+1}a_{(2)} + \cdots + \epsilon^{-1/2}a_{(d-1)}) + \mathcal{L}_{\text{finite}}, \qquad d \text{ odd}\,, \tag{2.33}$$

$$\mathcal{L} = \frac{1}{16\pi G^{(d+1)}}\sqrt{g_{(0)}}(\epsilon^{-d/2}a_{(0)} + \cdots + \epsilon^{-1}a_{(d-2)} - \ln\epsilon\ a_{(d)}) + \mathcal{L}_{\text{finite}}, \qquad d \text{ even}\,, \tag{2.34}$$

where $\mathcal{L}_{\text{finite}}$ collects all the finite terms as $\epsilon \to 0$ and the log divergence comes only from the bulk integral. Since the whole Lagrangian and the divergent terms proportional to the negative powers of ϵ are invariant under the combined transformations $\delta g_{(0)} = 2\delta\sigma g_{(0)}$ and $\delta\epsilon = 2\delta\sigma\epsilon$ with constant rescaling, the variation of the finite Lagrangian gains a finite piece from the log divergent term in even dimensions (see eq. (2.34)), which will be identified with the conformal anomaly

$$\langle T^\mu{}_\mu \rangle = \frac{1}{16\pi G^{(d+1)}}(-2a_{(d)})\,. \tag{2.35}$$

In $d = 2$, one recovers (2.28) by using the Brown-Henneaux formula with $a_{(2)} = \ell\text{Tr}(g_{(0)}^{-1}g_{(2)})$. One will see in [49] that the Weyl anomaly contains all the information one needs to obtain the correct two point functions of the stress energy tensor, both with and without defects, as in two dimension every metric is conformally equivalent.

2.2.2 2D Defect CFT and Energy Transport Coefficients

Two dimensional conformal field theory, widely studied, is an appealing subject due to its infinite-dimensional symmetries [31]. A natural way to break its symmetries can be adopted by introducing a defect in the spacetime. A certain class of defect preserving half of the symmetries is the main interest in this dissertation, which is called conformal defect or conformal interfaces. On the two sides of the interface, two generically different CFTs, possibly with two different central charges can live,, as shown in Figure 2.2, subject to certain boundary conditions. In physical language, this boundary condition amounts to have the conservation of the energy across the interface, which means the off-diagonal component of the stress energy tensor T_{xt} in the Euclidean[11] flat metric $ds^2 = dx^2 + d\tau^2$ is continuous across the interface. In holomorphic coordinates, the above continuity can be expressed as

$$\lim_{x\to 0^-} T_L(x + i\tau) - \bar{T}_L(x - i\tau) = \lim_{x\to 0^+} T_R(x + i\tau) - \bar{T}_R(x - i\tau)\,, \tag{2.36}$$

[10] If we follow [42], the gravitational action is the following,

$$S = \frac{1}{16\pi G^{(d+1)}}\left(\int_{AdS}\sqrt{g}(R + 2\Lambda) - \int_{\partial AdS}(K + \alpha)\right)\,, \tag{2.32}$$

which contains the bulk Einstein-Hilbert term and some boundary terms including the Gibbons-Hawking-York term.

[11] The same works in Lorentzian signature upon the Wick rotation $\tau \to -it$.

where the unbarred and barred notation are the usual notations for the left and right movers, which are holomorphic and antiholomorphic functions in terms of $z = x + i\tau$ and $\bar{z} = x - i\tau$. Two extremal cases are worth noting, one corresponds to the *totally transmissive* interface (topological interface) where each component of the stress energy tensor is continuous by itself, *i.e.*, $T_L(i\tau) = T_R(i\tau)$ and $\bar{T}_L(i\tau) = \bar{T}_R(i\tau)$, the other marks the *totally reflective* interface where the two theories decouple from each other, in terms of the stress energy tensor, the relation is $T_{L/R}(i\tau) = \bar{T}_{L/R}(-i\tau)$.

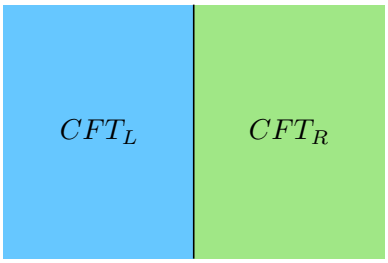

Figure 2.2: Two generically different CFTs, CFT_L and CFT_R in the geographic sense, are glued together along the interface, the black line, which acts as a defect in the whole theory.

If one perform a folding trick, the interface then becomes the boundary of the system, represented by a boundary state $|\mathcal{B}\rangle$ in the bulk Hilbert space which is the tensor product of the Hilbert spaces of the two CFTs [50]. Continuity relation (2.36) then becomes

$$((L^1_n + L^2_n) - (\bar{L}^1_{-n} + \bar{L}^2_{-n}))\,|\mathcal{B}\rangle = 0\,, \tag{2.37}$$

which allows for an infinite-dimensional conformal symmetry in the defect system. With such a class of boundary states, one can define a scattering matrix[12]

$$M_{ij} = \frac{\langle 0|\, L^i_2 L^j_2\, |\mathcal{B}\rangle}{\langle 0|\mathcal{B}\rangle}\,, \tag{2.38}$$

where the indices are either "L" or "R" and it is normalized by the $g-$factor, $g = \langle 0|\mathcal{B}\rangle$, which gives the degeneracy of the boundary state on the vacuum state. The above matrix elements can be further used to define two transport coefficients of the energy in the following manner,

$$\mathcal{R} = \frac{2}{c_L + c_R}\,(M_{LL} + M_{RR}) = \frac{c_L^2 + 2c_L c_R \omega_b + c_R^2}{(c_L + c_R)^2}\,, \tag{2.39}$$

$$\mathcal{T} = \frac{2}{c_L + c_R}\,(M_{LR} + M_{RL}) = \frac{2c_L c_R\,(1 - \omega_b)}{(c_L + c_R)^2}\,, \tag{2.40}$$

where an extra parameter ω_b appears and the reflection and transmission coefficients add up to one,*i.e.*, $\mathcal{R} + \mathcal{T} = 1$. The defect characterizing parameter ω_b is related to the only new parameter appearing in the two-point function of the left and right (anti-)holomorphic stress tensors, $\langle T_L T_R\rangle \sim \langle \bar{T}_L \bar{T}_R\rangle \sim c_{LR}/2$ as $c_{LR} = c_L c_R(1 - \omega_b)$ [51]. In terms of the transport

[12] One can also use level-n generator to define the scattering matrix, however, $\langle 0|\, L^i_n L^j_n\, |\mathcal{B}\rangle = \frac{n(n^2-1)}{6}\,\langle 0|\, L^i_2 L^j_2\, |\mathcal{B}\rangle$ which can be easily checked by acting $\langle 0|\, L^i_n \bar{L}^j_{n+1}$ on equation (2.37) as indicated in [50].

coefficients, the totally transmissive(reflective) case has $\mathcal{T} = 1(\mathcal{R} = 1)$ respectively. In Chapter 4, one will see how these transport coefficients arise holographically through analyzing the scattering process on the boundary. More discussions on obtaining the two-point functions holographically will be presented in [49].

To get an intuition of the energy transport coefficients, one could refer to [52] for a free boson consideration, where the transport coefficients are determined by the boundary condition of the boson across the interface. For free fermions, one can refer to [50, 51]. Some other interesting consideration on defining the transmission-reflection algebra can be found, for example in [53].

2.3 Quantum Complexity and the Holographic Conjectures

In the last few years a lot of effort has been devoted to understanding the relation between certain properties of complex quantum systems (such as thermalization, scrambling, and chaos) and their counterparts on the holographically dual gravitational side. The quest for such relations dates back to the discovery of the holographic duality in 1997 [5], but a more recent facet of this story is the incorporation of quantum information-theoretic aspects on top of more traditional physics considerations.

Thinking of black holes as quantum computers, along the lines first advocated by [54], Susskind and collaborators have argued that some of the puzzles associated to the region behind the horizon of black holes could be clarified if one considers a quantity associated to the quantum state, that they named quantum complexity, which is the main topic of this section. I will start with some general discussion about this quantity, then in Section 2.3.1, the geometric interpretations in the holographic setup will be introduced, later in Section 2.3.2 we will see some recent developments on the field theory definition of quantum complexity.

As is known, this quantity is a concept borrowed from quantum computation theory as a means of characterizing the difficulty (in the sense of the amount of resources needed) of performing a task on a quantum computer; more precisely, if the task can be described as producing a certain quantum state $|\psi_T\rangle$ from a given initial state $|\psi_R\rangle$ using a circuit made of elementary unitary operations (gates), the quantum complexity can be defined as the minimum number of gates required for such a circuit

$$\mathcal{C}(|\psi_R\rangle \to |\psi_T\rangle) = \text{min } \# \text{ of gates required for the circuit}\,. \tag{2.41}$$

Therefore, it if of no surprise that quantum complexity will be dependent on the choices of the states, the gate set, as well as the penalty factor, a weight of the cost assigned to gates. In Chapter 5, we will see explicitly how the gate sets will influence this quantity in a bosonized model. As of now, let me use a simple example of two qubits to get the readers a feeling of the gates dependence.

A simple example of two qubits

Let's consider the following elementary gates

$$A : |n\rangle \to \frac{1}{\sqrt{2}}(|0\rangle + (-1)^n |1\rangle), \quad B : |0\,\cdot\rangle \to |0\,\cdot\rangle \;\; or \;\; |1\,\cdot\rangle \to |1\,\times\rangle\,, \quad C : |\cdot\rangle \to e^{i\phi}\,|\cdot\rangle \tag{2.42}$$

where A is a gate that will map a qubit to a superposition of the spin up and down depending on the type of the qubit acted on, with $n = 0, 1$, B is a gate that will map the second qubit to itself or its opposite depending on the spin of the first qubit, and C is a gate that will assign a phase to the qubit acted on. For the reference and target states, we consider the following

$$|\psi_R\rangle = |00\rangle\,, \quad |\psi_T\rangle = \frac{1}{\sqrt{2}}(|00\rangle - |11\rangle)\,, \tag{2.43}$$

by two simple set of gates, the corresponding complexity is

$$\text{gate set} = \{A, B\}: \quad \mathcal{C} = \infty; \quad \text{gate set} = \{A, B, C\}: \quad \mathcal{C} = 3\,. \tag{2.44}$$

Applying the full set of gates, we obtained a finite value of complexity by using each of the gate once: first acting A on the first qubit, followed by B, finally acting C on the second qubit with the phase to be $\phi = \pi$. If the gate set does not contain C, no matter how one tries, the target state cannot be reached since neither A or B can change the sign of a qubit without changing the spin, resulting in a value of infinity. Such a simple example concludes that gate sets have a strong influence on the complexity, though at a discrete level. In Chapter 5, we will see more in the free field theory setup about the influence of the gate set choice.

2.3.1 The Two Holographic Conjectures

Having got a glimpse of the definition of quantum complexity, it is time to introduce how this quantity is linked to the gravitational interpretations. The story started from the work by Stanford and Susskind [16], where they proposed quantum computational complexity to be a boundary dual quantity that captures the long time behaviour of the growth of the Einstein-Rosen bridge, a wormhole structure connecting two black holes. Therefore in a way, quantum complexity can be used as a probe to study the scrambling of the black hole interior. Although a similar consideration has been made by Hartman and Maldacena [55] in the eternal AdS black hole case (see [56] for early discussions) in terms of entanglement entropy between the left and right asymptotic boundary subregions, the growth of entanglement entropy continues only for a short time till the system is thermalized.

This proposal utilises a codimensional-one Cauchy surface, which by construction extends into the black hole in the eternal AdS BH geometry, claiming that its maximal volume can encapsulate the evolution of the scrambling of the BH interior when the Cauchy slice advances in time. Furthermore, it states that the same behaviour is encoded in the time evolution the quantum complexity of corresponding thermal field double states on each Cauchy slice. Thus this

conjecture is called "Complexity = Volume" (CV), the precise formulation is given as

$$\mathcal{C}_V = \frac{\max V_{\text{Cauchy}}}{4G_{\text{N}}\ell}, \tag{2.45}$$

where G_{N} is the Newton's constant in AdS_{d+1} which is introduced by hand to relate to the gravitational theory. The dimensional analysis shows that the denominator should have length dimension $[L]^d$ while the length dimension of the Newton's content has length dimension $[G_{\text{N}}] = [L]^{d-1}$, thus the necessity for the introduction of another length scale ℓ, which constitutes one of the drawbacks for the CV conjecture. In order to cure this problem, a second conjecture, the Complexity=Action (CA) was proposed by Brown, Susskind et al. [17, 57] in the following year, which states

$$\mathcal{C}_A = \frac{I_{\text{WDW}}}{\pi}, \tag{2.46}$$

where I_{WDW} is the on-shell gravitational action evaluated on the Wheeler-DeWitt (WDW) patch[13] which is a solid double cone as shown in Figure 2.3. Technically speaking, the action approach is more subtle than the volume one, since codimension-1 boundary surface terms and codimension-2 joint terms have to be included in the action, see [58–63] (a summarized prescription is outlined in appendix A of [64]).

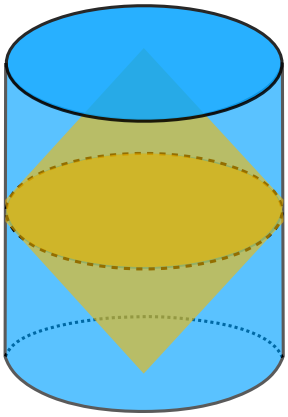

Figure 2.3: WDW patch in AdS_3 represented by the yellow double cone asymptotic to a certain boundary time slice.

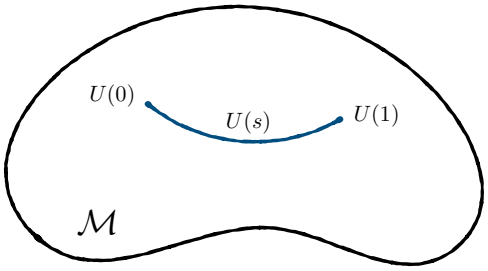

Figure 2.4: Geometrizing the space of unitary operations, the curve connecting the initial states and the final states is a geodesic which represents a sequence of operators to reach the target states.

2.3.2 Field Theory Approach for Complexity: *Nielsen* Method

In order to have a better understanding about quantum complexity in the holographic manner, it is essential to have a proper definition of quantum complexity in the continuum limit through field theory approach. Although such a formulation for a general consideration is not yet available, there have been some developments along this line [65–73]. In this section, we will focus on the Nielsen's approach on the Gaussian states complexity for free fields based on [65, 66]. The *Nielsen*

[13] The WDW patch is the bulk causal development of the slice from the CV conjecture, and is bounded by light sheets sent from the boundary time slice where the state is defined. For the case of the two-sided AdS black hole the WDW patch is anchored at both boundaries at the relevant times where the thermofield double state is studied.

method can be understood as a way to geometrize the notion of complexity. As an analog to the minimum number of gates, this geometrization relates the geodesic length, which has a minimal sense on the metric space, to the definition of circuit complexity, as illustrated in Figure 2.4. In contrast to the *Fubini-Study* method which geometrizes the space of states, the *Nielsen* approach considers instead the space of unitary operations (gates). Since there is a one-to-one map between the states and operations, those two approaches in principle are identical to each other, however, the concepts behind differs.

From now on we will focus the *Nielsen* method. In this approach, the circuit is replaced by a continuous path of unitary operators

$$U(s) = \mathcal{P}\exp\left(-i\int_0^s ds' Y^I(s')\mathcal{O}_I\right), \tag{2.47}$$

such that $U(s=1)$ gives the desired unitary operator (i.e., implements the circuit we want), and $\mathcal{O}_I$ is a basis of operators that can be used to build the circuit (we can think of them as the generators of the infinitesimal gates $e^{i\epsilon\mathcal{O}_I}$). One can think that the final state is being prepared by means of an evolution in a fictitious time s with a time-dependent Hamiltonian $H = Y^I(s)\mathcal{O}_I$. The complexity is then determined by the choice of a suitable *cost functional*

$$\mathcal{C}[U(s)] = \int_0^1 F\left(U(s), Y(s)\right). \tag{2.48}$$

The minimization of this functional will determine the form of the functions $Y^I(s)$ and thus the optimal circuit. With an appropriate choice, the cost functional determines a distance on the space of unitary operators, and the problem of minimizing the complexity of a circuit is mapped to the problem of finding a geodesic path on a Riemannian manifold. The cost functional can for instance have the form

$$F_2\left(U(s), Y(s)\right) = \sqrt{G_{IJ}(U(s))Y^I(s)Y^J(s)}\,. \tag{2.49}$$

Often the metric $G_{IJ}(U)$ is choosen to be a right-invariant metric, but not necessarily the canonical biinvariant metric defined by $\langle A, B\rangle = tr(AB)$ for A, B self-adjoint. In fact, the possibility of choosing different metrics can be thought of as introducing penalty factors for moving along certain directions, corresponding to gates that may be more difficult to implement (for instance, in a system of qubits, one wants to penalize gates that act on many qubits simultaneously). A more general choice of the cost functional would lead to a Finsler geometry, where there is notion of a distance but not induced by a metric on the tangent space [65]. For instance one can consider the family of cost functionals dependent on a parameter κ:

$$F_\kappa\left(U(s), Y(s)\right) = \sum_I |Y^I|^\kappa\,. \tag{2.50}$$

Sometimes the ambiguity is reduced: the functional (2.50) with $\kappa = 1$ is parametrization-independent. Another cost functional, which we will use in Chapter 5, is basis-independent

and makes use of the *Schatten p-norm*:[14]

$$F_p\left(U(s), Y(s)\right) = ||Y^I(s)\mathcal{O}_I||_p\,, \tag{2.51}$$

$$||A||_p \equiv \left(\mathrm{tr}(A^\dagger A)^{\frac{p}{2}}\right)^{\frac{1}{p}}\,. \tag{2.52}$$

Application on Gaussian States for Free Fermion

In Nielsen's approach, the metric is defined not on the space of states, but on the manifold of a group of operators that act on the states. For fermions, the relevant group turns out to be the orthogonal group [66]. To see this, it is convenient to use the Majorana basis

$$\xi^a = \{q_{+\infty}, \ldots, q_1, q_0, q_{-1}, \ldots, q_{-\infty}, p_{+\infty}, \ldots, p_1, p_0, p_{-1} \ldots p_{-\infty}\} \tag{2.53}$$

which is related to the annihilation and creation modes in the following way

$$c_l^\dagger = \frac{1}{\sqrt{2}}(q_l - ip_l), \quad c_l = \frac{1}{\sqrt{2}}(q_l + ip_l). \tag{2.54}$$

In the Majorana basis the anticommutation relations read $\{\xi^a, \xi^b\} = \delta^{ab}$.

A general Gaussian state $|\psi\rangle$ is completely characterized by the two-point function, or covariance matrix,

$$\langle\psi|\,\xi^a\xi^b\,|\psi\rangle = \frac{1}{2}(G^{ab} + i\Omega_\psi^{ab}) \tag{2.55}$$

which can be decomposed in the symmetric and antisymmetric part, respectively G^{ab} and Ω_ψ^{ab}. The symmetric part is determined by the anticommutation relation, therefore it is state-independent, while the antisymmetric part encodes the state. In terms of the covariance matrix, the fermionic vacuum state $|0\rangle$ defined in (5.17) would be expressed as,

$$G^{ab} = \delta^{ab}, \quad \Omega_0^{ab} = \begin{pmatrix} 0 & C \\ -C & 0 \end{pmatrix} \text{ with } C = \begin{pmatrix} \mathbb{1} & 0 \\ 0 & -\mathbb{1} \end{pmatrix}. \tag{2.56}$$

As will be discussed in Section 5.1.3 the Gaussian states are obtained by Bogoliubov transformations; in the Majorana basis, these are linear transformations $\tilde{\xi} = M\xi$ that leave the anticommutation relation invariant, therefore they are orthogonal transformations. If we put a UV cutoff so that there are $2N$ modes, $M \in SO(2N)$.[15] However there is a subgroup that acts trivially on the state, which only change the state by a phase. The covariance matrix transforms as

$$\tilde{\Omega} = M\Omega M^T\,. \tag{2.57}$$

The covariance matrix of the vacuum can be considered as a symplectic form, from this we see that the orthogonal matrices that leave Ω invariant should be symplectic as well, *i.e.,* , they should be unitary. The manifold of Gaussian states is then $SO(2N)/U(N)$. A convenient way to

[14] Despite a certain resemblance, the Schatten p-norm is not directly related to the κ cost function (2.50), although one might speculate that the two give the same result for a particular choice of basis.

[15] We consider for simplicity only the component connected with the identity. It turns out that this is the subgroup that does not change the parity $(-1)^F$ of the fermion number of the state.

parametrize this coset is by using the relative covariance matrix

$$\Delta(M) = \tilde{\Omega}\,\Omega_0^{-1} = M\Omega_0 M^T \Omega_0^{-1}. \tag{2.58}$$

Conversely, if we are given the reference and target states Ω_0 and $\tilde{\Omega}$, we can recover the transformation matrix up to a unitary transformation. The polar decomposition of orthogonal matrices allows us to write $M = u\hat{M}$ with $u \in U(N)$ and $\hat{M}$ antisymmetric. In this manner, u and $\hat{M}$ are uniquely defined by the polar decomposition.

At the level of Lie algebra, the splitting $so(2N) = u(N) \oplus \text{asym(N)}$ is an orthogonal decomposition with respect to the Killing metric of $so(2N)$. We expect then that the shortest path in the coset space will be obtained by moving only along the second subspace. Indeed it is shown in [66] that the geodesic connecting Ω_0 and $\tilde{\Omega}$ is given by a straight curve $\gamma(s) = e^{sA}$ with $s \in [0, 1]$ which has a constant direction $A \in \text{asym(N)}$. Finally the geodesic length is given by the norm of $A = \frac{1}{2}\ln\Delta$, which is the inner product with itself $||A|| = \sqrt{\langle A, A\rangle}$ using the embedded metric on the Lie manifold $SO(2N)$. This definition of norm is basis independent and will coincide with the *Schatten* $p = 2$ norm. The *Schatten* $p-$norm for a general matrix T is defined as

$$||T||_p = \left(\sum_{n\geq 1} s_n^p(T)\right)^{1/p} \tag{2.59}$$

with $s_n(T)$ being the singular values of the $n \times n$ matrix T, *i.e.,* , the eigenvalues of the matrix $\sqrt{T^\dagger T}$. Due to the decreasing monotonicity of the *Schatten* $p-$norm, an interesting case is the $p = 1$ norm, defined as

$$||T||_p = \text{Tr}(\sqrt{T^\dagger T}) = \sum_{n\geq 1} s_n(T) \tag{2.60}$$

which will impose an upper bound to the $p = 2$ norm. The $p = 1$ norm has been considered before for quantum information purposes, for example it has been found that it is the only one among the p-norms to provide a consistent measure for quantum correlations, called quantum discord [74].

To summarize, the complexity of fermionic Gaussian states, defined as the geodesic length with respect to the Killing metric on the orthogonal group:

$$\mathcal{C}_f(|0\rangle, |\psi\rangle) \equiv ||A|| = ||A||_{p=2} = \frac{1}{2}\sqrt{\text{Tr}|(i\ln\Delta)^2|} = \frac{1}{2}\sqrt{\sum_r (i\ln\lambda_r)^2} \tag{2.61}$$

$$\leq ||A||_{p=1} = \frac{1}{2}\text{Tr}|i\ln\Delta| = \frac{1}{2}\sum_r |i\ln\lambda_r|. \tag{2.62}$$

In the above formula λ_i are the eigenvalues of Δ which come in pairs $e^{\pm i\theta}$ since $\Delta \in SO(2N)$. Although the $p = 1$ norm loses its geometric meaning in the current case, it is interesting because in some cases discussed in the later sections, it poses an analytical bound on the Gaussian state complexity.

Application on Gaussian States for Free Boson

In the case of free bosonic theory with N degrees of freedom, the gates group corresponding to Gaussian states is $Sp(2N)$. Contrary to the fermionic case, the role of covariance matrices G and Ω defined in (2.55) is exchanged, in the way that G represents the state and Ω encodes the algebraic relation. The main objective is still to find the relative covariance matrix relating the reference state and the target state, given as

$$\Delta = \tilde{G}G_0 = MG_0M^TG_0^{-1} \tag{2.63}$$

where $M \in Sp(2N)$ encodes the basis transformation. Similar to the fermionic case, Δ is an element in the coset space $Sp(2N)/U(N)$ and the geodesic connecting $\tilde{G}$ and G_0 will be again $\gamma(s) = e^{sA}$ with however $A \in \mathrm{sym}(N)$ being an element in the symmetric algebra. In the same manner, the geodesic length is given by the norm of $A = \frac{1}{2}\ln\Delta$, hence the complexity

$$\mathcal{C}_b(|0\rangle, |\psi\rangle) \equiv ||A|| = ||A||_{p=2} = \frac{1}{2}\sqrt{\mathrm{Tr}|(\ln\Delta)^2|} = \frac{1}{2}\sqrt{\sum_r (\ln\lambda_r)^2} \tag{2.64}$$

$$\leq ||A||_{p=1} = \frac{1}{2}\mathrm{Tr}|\ln\Delta| = \frac{1}{2}\sum_r |\ln\lambda_r|. \tag{2.65}$$

Compared to the eq. (2.61), there is an "i" difference, which is due to the fact that the eigenvalues of a real symmetric symplectic matrix are in pairs of $e^{\pm r}$ with $r \in \mathbb{R}$. If the covariance matrix G for the reference state is the identity matrix, the covariance matrix will simply be $\Delta = MM^T$, which we shall use in Section 5.4. Detailed studies of the free bosonic complexity can be found in [66, 75].

2.4 Modular Flow and Bulk Reconstruction

2.4.1 Entanglement Entropy and Modular Hamiltonian

Quantum entanglement is a special feature in the quantum many-body systems, dating back to the Einstein-Podolsky-Rosen paradox in 1935, a thought expriment that indicates that the speed of the interaction transmitter is faster than light between two entangled particles if the interaction is local. Later in the sixties, it has been argued that this kind of interaction should actually be regarded as nonlocal thus assigning quantum entanglement a special property which cannot be integrated into action formulation.

Though the entanglement is nonlocal, the degrees of freedom get involved in the entanglement between subsystems can still be quantified via the entropy of entanglement or simply entanglement entropy. Supposing we have a quantum system which is bipartite into two subsystems A and its complement $\bar{A}$, the full Hilbert space will be factorized as

$$\mathcal{H} = \mathcal{H}_A \otimes \mathcal{H}_{\bar{A}}\,. \tag{2.66}$$

For an entangled state $|\psi\rangle \in \mathcal{H}$ between the two subsystems, $\rho = |\psi\rangle\langle\psi|$, the entanglement

entropy is defined via the the reduced density matrix by tracing out one of the subsystems

$$\rho_{A/\bar{A}} = \mathrm{Tr}_{\bar{A}/A}\,\rho\,. \tag{2.67}$$

Then the *von Neumann entropy* is defined as

$$-\mathrm{Tr}_{\bar{A}}(\rho_{\bar{A}}\ln\rho_{\bar{A}}) = S_{\bar{A}} = S_A = -\mathrm{Tr}_A(\rho_A\ln\rho_A) \tag{2.68}$$

where we see that the entanglement entropy is independent on which system we are conducting the calculation since it should be regarded as common property. Another definition that appears often is called *Rényi entropy*[16], defined as

$$S_A^{(n)} = \frac{1}{1-n}\ln\mathrm{Tr}_A(\rho_A^n)\,, \tag{2.69}$$

where $n \in \mathbb{Z}_+$ in the canonical definition. However it is often possible to analytically continue the range of n to $\mathbb{R}_+$, as a result, in the limit of $n \to 1$, the *Rényi entropy* coincides with the *von Neumann entropy*

$$S_A = \lim_{n\to 1} S_A^{(n)}\,. \tag{2.70}$$

It is worth noting that the entanglement entropies are defined using the trace of the reduced density matrices, therefore, any unitary transformation on one of the subsystem will not affect the entanglement degrees of freedom. Another quantity related to the reduced density matrix that plays a vital role in the proposed duality in Chapter 6 is named as *Modular Hamiltonian*, which goes back the *Tomita-Takesaki*'s study on the modular automorphism of *von Neumann algebra* [77], defined as minus of the logarithm of the reduced density matrix

$$H_A = -\ln\rho_A\,. \tag{2.71}$$

The modular Hamiltonian in general is a non-local operator and hard to compute, however, for the reduced matrix of the Rindler wedge of a flat Minkowski space, it simply acts as a Minkowski boost generator or the Rindler time translation (see Figure 2.5) as the *Bisognano-Wichmann theorem* [78] suggests, thus will be a local operator in this case [79]. An identical case has been studied by Unruh [80] is that the Minkowski vacuum acquires a non-zero temperature when observed by a uniformly accelerated observer. The Rindler modular Hamiltonian for the Rindler vacuum state in $\mathbb{R}^{d-1,1}$ can always be written as an integration of the stress energy tensor with the following covariant form

$$H_A^{\mathrm{Rindler}} = 2\pi\int_\Sigma d^{d-1}x\sqrt{\gamma}\,\eta^\mu T_{\mu\nu}n^\nu\,, \tag{2.72}$$

where Σ is an Cauchy slice with n^μ the future pointing normal and η^μ a Lorentz boost vector. One can see from the expression that indeed the Rindler modular Hamiltonian generates the translation along the direction of η^μ as can be shown using *Peierls Bracket* [81].[17] For a CFT,

[16] In practice, the *Rényi entropy* is more calculable than the *von Neumann entropy* via the replica trick, one can read for example the review of Takayanagi and Rangamani [76] for more technical details.

[17] *Peierls Bracket* is the covariant form of *Poisson Bracket*, defined as $[X,Y] = D_X^- Y - D_X^+ Y$, where $D_X^\pm$ are

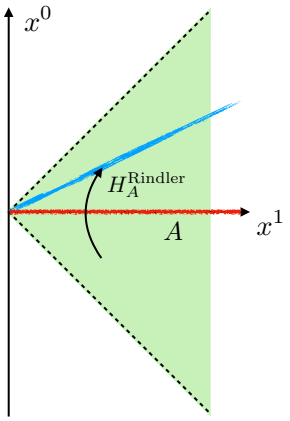

Figure 2.5: Rindler wedge for the region $x^1 > 0$, where the Rindler modular Hamiltonian generates the Rindler time translation from the red time slice to the blue one.

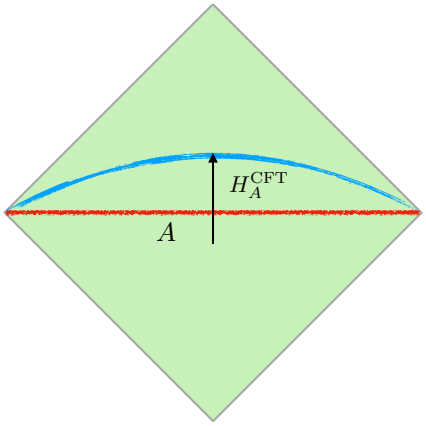

Figure 2.6: Causal wedge for a CFT, where the modular Hamiltonian generates the modular time translation from the red time slice to the blue one.

one can always map the Rindler wedge to the causal development region of a ball, as a result the modular Hamiltonian for the ball region is the same as eq. (2.72) up to some constant to normalise the reduced density matrix [79], which generates the modular flow in that causal wedge, as shown in Figure 2.6.

2.4.2 Modular Hamiltonians in Holography: JLMS Relation

For a quantum field theory that has a gravity dual, it has been stated in [82] by Jafferis, Lewkowycz, Maldacena and Suh (JLMS), that there is a simple relation between the modular Hamiltonian corresponding to a boundary subregion A and its bulk dual partner, given as

$$H_A^{\text{boundry}} = \frac{\text{Area}_{\text{ext}}}{4G_{\text{N}}} + H_A^{\text{bulk}} + \hat{S}_{\text{Wald-like}} + O(G_{\text{N}})\,. \tag{2.73}$$

The first term on the right hand side originates from the proposal of Ryu and Takayanagi on the holographic dual of the entanglement entropy for the subregion A on the asymptotic boundary [11], as shown in Figure 2.7. They argued that this dual is given by the area of an extremal bulk codimensional-two surface Σ, *i.e.,* the Ryu-Takayangi (RT) surface homologous to A. The area term can also be regarded as an operator in the bulk effective theory, containing both the classical area and changes in the area that result from the backreaction of quantum effects. The bulk modular Hamiltonian H_A^{bulk} is the modular hamiltonian for the bulk region a enclosed by the RT surface and the asymptotic boundary, which behaves as a boost in the vicinity of the RT surface. The Wald-like contributions come from the expectation values of local operators on the RT surface Σ. It is worth nothing that the JLMS relation (2.73) implies the subregion-subregion duality in the entanglement wedge[18], since causal domain of the region a. While the boundary modular Hamiltonian H_A^{boundry} generates a modular flow on the boundary causal wedge, the bulk

corresponding advanced and retarded derivative along X.

[18]The entanglement wedge corresponds to A is defined as the whole set of bulk points that are spacelike separated from the RT surface on the side of A.

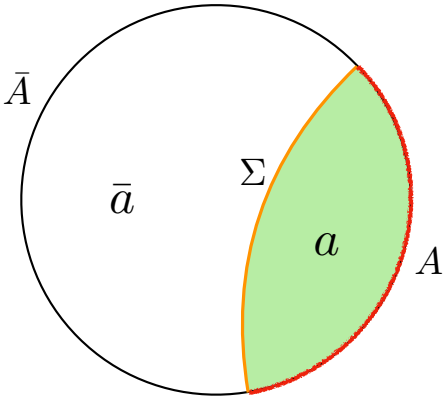

Figure 2.7: Illustration of the Ryu-Takayanagi surface Σ (orange curve) in a given time slice for the boundary entangling region A (red curve) with $\bar{A}$ being its complement. The green shaded region a is enclosed by the RT surface and boundary subregion, with its complement bulk region being $\bar{a}$.

modular Hamitonian H_A^{bulk} generates a bulk modular flow in the interior of the entanglement wedge.

The JLMS relation also leads to the equivalence of the bulk and boundary relative entropy, which is defined via a reference state σ which can be taken to be the vacuum state, as following

$$\begin{aligned} S(\rho||\sigma) \equiv \operatorname{Tr}\rho\ln\rho - \operatorname{Tr}\rho\ln\sigma &= \underbrace{\operatorname{Tr}\rho\ln\rho - \operatorname{Tr}\sigma\ln\sigma}_{S_\sigma - S_\rho = -\Delta S} + \underbrace{\operatorname{Tr}\sigma\ln\sigma - \operatorname{Tr}\rho\ln\sigma}_{\langle H_\rho\rangle - \langle H_\sigma\rangle = \Delta\langle H_\sigma\rangle} \\ &= \Delta\langle H_\sigma\rangle - \Delta S \end{aligned} \tag{2.74}$$

which is positive definite and monotonic [83]. When the state ρ is a small perturbation around σ, *i.e.,* $\rho = \sigma + \delta\rho$, due to the positivity of the relative entropy, it has a global minimal at $\rho = \sigma$, therefore, to the linear order in the perturbation, the relative entropy remains zero as $\operatorname{Tr}\delta\rho = 0$, which gives rise to the first law of entanglement[19]

$$\delta S = \delta\langle H_\sigma\rangle\,. \tag{2.76}$$

2.4.3 Code Subspace and Entanglement Wedge Reconstruction

As mentioned in the last section, the JLMS relation implies bulk reconstruction within the entanglement wedge $\mathcal{E}_A$, which is the spacelike causal domain of the HRT *(Hubeny, Rangamani and Takayanagi)* surface Σ [84] (a covariant generalisation of the RT surface) on the side of A. This consideration of entanglement wedge reconstruction is made more clear if we consider the duality problem in the code subspace [85], which is a sub Hilbert space in the whole Hilbert space for the quantum gravity, $\mathcal{H}_{\text{code}} \in \mathcal{H}$. As shown in Figure 2.7, when there the boundary CFT Hilbert

[19] As a comparison, the first law of black hole thermodynamics is

$$dE = \frac{\kappa}{8\pi G_{\text{N}}} dA + \Omega dJ + \Phi dQ\,, \tag{2.75}$$

where for non-rotating, non-charged black, by using Bekenstein-Hawking formula, one obtain the usual first law of thermodynamics.

space factorizes as in equation (2.66), the code subspace factorises in a similar way in the bulk entanglement wedge

$$\mathcal{H}_{\text{code}} = \mathcal{H}_a \otimes \mathcal{H}_{\bar{a}} \,, \tag{2.77}$$

where $\mathcal{H}_a$ denotes excitations in the entanglement wedge $\mathcal{E}_A$ while $\mathcal{H}_{\bar{a}}$ for $\mathcal{E}_{\bar{a}}$. Through a projection onto the code subspace, the JLMS relation is reproduced,

$$\Pi_c \, H_\sigma^{\text{boundary}} \, \Pi_c = \frac{\text{Area}_{\text{ext}}}{4G_{\text{N}}} + H_A^{\text{bulk}} \tag{2.78}$$

where Π_c is a projection onto the code subspace and on the right hand side, the operators are defined to annihilate the orthogonal subspace to the code subspace $\mathcal{H}_{\text{code}}^{\perp}$.

In the work of [85], the bulk reconstruction theorem suggests that for an operator in the entanglement wedge $\mathcal{E}_A$, the reconstruction will only receive support from the boundary subregion A within the code subspace. Besides that, a local bulk field will have vanishing commutators with operators that are spatially separated. A simple model of three qutrits code could be found for example in [86, 87].

In the spirit of the entanglement wedge reconstruction, we could in principle link many geometric quantities in the bulk to some dual quantities on the boundary. In Chapter 6, we will see how the JLMS relation help build a bridge to study the between the new duality we would like to propose, *i.e.,* the modular Berry connection with the bulk Riemann connection.

Chapter 3

Holographic complexity: "CA" or "CV" ?

This Chapter is based on the work [18].

Various aspects of the two holographic proposals have been explored in recent years, including their structure of divergences [64, 88], their time dependence [17, 57, 63, 89, 90], their reaction to shockwaves [16, 91–93] and studies of complexity in JT gravity and nearly extremal black holes [94–97]. In general, it appears that the predictions of the action and volume proposals tend to coincide up to overall numerical factors. For instance, the complexity grows linearly for a long period of time at a rate which is proportional to the energy of the system.[1] In shockwave geometries the complexity exhibits characteristic delays in its growth related to the scrambling time of the system both for the CV and CA proposals. It is therefore of interest to extend the study of complexity to systems where a clear-cut distinction can be made between the predictions of the action and the volume proposals.

In order to explore this question, we consider the modification of the complexity associated to the introduction of a conformal defect in the boundary field theory. Defect CFTs (DCFTs) have been studied extensively in the literature (see, e.g., [100] and references therein), both on the field theory side and holographically, so we can draw on existing constructions. For simplicity, we focus on the case of a 2d DCFT, and consider its ground state complexity. On the gravitational side, we consider a bottom-up Randall-Sundrum type model [101] of a thin AdS_2 brane embedded in AdS_3 spacetime [102]. The brane, which acts as a defect in this geometry, has two anchoring points on the boundary, which introduce defects in the boundary theory on opposite sides of the circular domain (analogous to a quark-antiquark pair). The brane backreacts and modifies the geometry, therefore entailing a modification of the complexity depending on a parameter, namely the tension of the brane. It is worth noting that after our study, there exist some works which consider the holographic complexity with one end-of-world brane in a general dimension [103] or in AdS_3 [104], which confirm our conclusion in three dimensions.

The main results of the study in this chapter can be found in eqs. (3.23) and (3.52), for the CV and CA proposals, respectively. In particular we observe that while for the CV proposal the

[1] For the volume this statement holds in the high temperature limit, and for hyperscaling violating geometries [98, 99] the late time growth rate from the CV proposal includes an additional temperature dependent proportionality coefficient required from dimensional analysis considerations.

complexity contains a logarithmically divergent term due to the presence of the defect, which is related to the central charge and to the Affleck-Ludwig boundary entropy [105],[2] in the CA proposal no such term appears; the (absence of a) logarithmically divergent contribution to the CA complexity does not depend on the tension of the brane. In fact even the finite part of (3.52) is independent of the tension, so the CA appears completely unaffected by the presence of the defect; however it is only the logarithmically divergent part that has a universal meaning, as the finite part is dependent on the regularization scheme. It is worth noting that this is the first case in which the results of the holographic CV and CA proposals disagree so dramatically. This offers an opportunity to discriminate between the two prescriptions. It may seem surprising to find a vanishing contribution to the complexity, especially if we compare the results with the change in the entanglement entropy, and this could be seen as an argument in favor of the CV proposal. However we prefer to suggest a more cautious interpretation, namely that the CV and CA proposals correspond to different measures of complexity.[3]

In the original proposals, the complexity is associated to the state of the whole system. Inspired by the Ryu-Takayanagi prescription for the holographic entanglement entropy [11, 108], and motivated by the suggestion that the reduced density matrix of a boundary subregion is encoded in its "entanglement wedge" [109, 110],[4] proposals have been made [64, 111] for an extension of the complexity conjectures for states (reduced density matrices) associated to subregions. For static geometries, the CV prescription is generalized to the volume enclosed between the RT surface and the AdS boundary, while for the CA prescription, one considers the gravitational action of the region enclosed between the WDW patch and the entanglement wedge. We consider the subregion complexity for the defect geometry for subregions which include a single defect; For the CA proposal we are able to perform the computation only in the case of a symmetric region, i.e., when the defect is at its midpoint. The results are in eq. (3.69) for the CV proposal and in eqs. (3.89), (3.90) for CA proposal. Again we find no change in the logarithmically divergent contribution to the CA complexity (nor do we find a change in the finite contribution, with our choice of cutoff) due to the presence of the defect. Interestingly, we find that the structure of divergences of the subregion CA complexity is not the same as the one of the total CA complexity. In particular, we observe a $\ln \Lambda$ divergence where Λ is the UV momentum cutoff.

The evidence for the validity of the CV and CA proposals is far from being conclusive since the notion of complexity in QFT is still not well understood. Some progress has been made [65–69, 72, 73, 75, 112–123], but a precise definition in strongly interacting CFTs, from first principles, is still absent. In particular, one can put together an operative definition for the case of free fields [65, 67], and arrive at a result that matches with holography in terms of the divergence structure. However, it is not clear at the moment what is the universal content which can be extracted from the coefficients of the complexity as a series expansion in the cutoff scale, similarly to the case of entanglement entropy, where the coefficient of the logarithmic divergence

[2] The system with the defect is related to a similar system with a boundary via a folding trick.

[3] Previous studies of the CV complexity in the presence of boundaries can be found in [106] where a holographic Kondo model was explored and it was pointed out that for constant tension branes the complexity increases with the tension of the brane. We reach a similar conclusion in our model using the CV proposal. For an alternative proposal of world sheet complexity, see Section 4 of [107].

[4] The entanglement wedge is defined as the set of bulk points that are spacelike separated from the RT surface and causally connected to the causal wedge on the boundary of AdS.

is associated to the central charge in the CFT. An operative definition for subregion complexity is also absent, although some proposals have been made in [124].

The definition of complexity in QFT is subject to many ambiguities. In particular, one is free to choose a reference state as well as a set of gates that can act on the state. It was initially suggested [65, 67] that the ambiguity associated with the reference state is mirrored by a similar ambiguity on the gravitational side of the correspondence, related to the choice of normalization of the null normals at the boundaries of the WDW patch. More recently it has been understood that in evaluating the complexity one has to include a certain counter term needed to restore reparametrization invariance on the null boundaries [91, 92]. This counter term comes accompanied with a length scale which could be the one reproducing the effect of the various ambiguities on the complexity. For a more elaborate discussion, see Section 5 of [92].

We make a naive attempt to match our holographic results with the dual field theory. As mentioned before, the definition of complexity for a generic field theory is unknown, and furthermore, the precise CFT dual of our holographic setup is not known. However, we can look at free field models of CFTs with defects, analogous to our holographic setup and study their complexities. We consider first a model with permeable domain walls [52] on opposite sides of a periodic domain. We observe in this case that a logarithmic contribution proportional to the parameters of the defect is absent, similarly to what happens for the CA proposal. We then briefly discuss a solvable model with a boundary interaction [125]. It seems that in this case a logarithmic contribution which depends on the strength of the boundary interaction is present in the result for the complexity (in the case of a single boundary, but not if there are two boundaries), though we have to make an assumption that the formula derived for free fields, which computes the complexity in terms of the (single particle) spectrum, can be extended to these cases. An extension of the current holographic calculation to a case where the dual field theory is known would be required in order to identify which one of the field theory models (if any) is relevant for the analogy with holography. Since we are focusing on models of compact bosons, we point out that the effects of zero modes could have an influence on the complexity and might need to be incorporated into the existing definitions.

The following parts of this chapter is organized as follows: In Section 3.1, we descibe the defect AdS_3 geometry, employing different coordinate systems. We also discuss the choice of cutoff and the shape of the WDW patch in this geometry. In Section 3.2, we present the calculations of the holographic complexity of the full boundary state using both the CV and CA proposals. In Section 3.3, we consider the subregion complexity proposals for subregions including one defect. In Section 3.4, we describe a free bosonic field theory model with defects as well as an exactly solvable model with a boundary interaction and compute their complexities. We conclude with a summary of the main results and a discussion in Section 3.5. A number of technical details of the calculation are discussed in Appendixes A.1 and A.2, and the subregion CV proposal in the Poincaré patch with two distinct cosmological constants on the two sides of the defect is discussed in Appendix A.3.

3.1 Warm up with the Defect Toy Model

In the following section we provide various ingredients of the defect toy model which we use to study the complexity of defects in this chapter. As mentioned in the last section, we focus our attention on a Randall-Sundrum solution for a 2d brane of tension λ embedded in a 3d geometry which is a solution of Einstein equations with negative cosmological constant. Various aspects of this simple solution were already studied in [102]. We start by reviewing the solution in a number of convenient coordinate choices. We then address the choice of cutoff surface and describe how to obtain null geodesics emanating from a point on the boundary in order to construct the WDW patch for the CA proposal.

3.1.1 Two-Dimensional Branes in AdS_3

We begin by considering the solution for a symmetric defect in AdS_3 which solves Einstein equations for the action

$$S = \frac{1}{16\pi G_{\rm N}} \int d^3x\sqrt{-g}\left(R + \frac{2}{L^2}\right) - \lambda \int d^2x\sqrt{-h}, \tag{3.1}$$

where R is the Ricci scalar, L is the AdS curvature scale, λ is the tension of the brane and h is the determinant of the induced metric on the defect. For brane tension in the range $0 < \lambda < \frac{1}{4\pi G_{\rm N} L}$, the gravitational equations of motion admit stable solutions which include a thin AdS_2 brane. These solutions preserve the symmetries expected from a dual CFT with a conformal defect. The full solution reads

$$ds^2 = L^2\left(d\bar{y}^2 + \cosh^2(|\bar{y}| - y^*)(-\cosh^2 r dt^2 + dr^2)\right), \tag{3.2}$$

with

$$\tanh y^* = 4\pi G_{\rm N} L\lambda\,, \tag{3.3}$$

and the brane is situated at $\bar{y} = 0$, where one finds a discontinuity of the extrinsic curvature. These coordinates correspond to a foliation in terms of AdS_2 slices with coordinates (r, t) on each slice.

The solution (3.2) can also be seen as two (slightly larger than half) patches of vacuum AdS_3, glued together at the location of the defect.[5] This is most simply seen by redefining $y = \bar{y} - y^*$ for $\bar{y} > 0$ $(-y^* < y < \infty)$ and $y = \bar{y} + y^*$ for $\bar{y} < 0$ $(-\infty < y < y^*)$. Of course this coordinate system has a discontinuity at the position of the brane. The metric is then given on each patch by,

$$ds^2 = L^2\left(dy^2 + \cosh^2 y(-\cosh^2 r dt^2 + dr^2)\right), \tag{3.4}$$

where $-y^* < y < \infty$ on one side of the defect and $-\infty < y < y^*$ on the other. The ranges of the coordinates indicate that we have two patches of AdS_3 bounded by curves of constant $y = \mp y^*$. A cross section of the two patches, as well as their constant y and r slices are depicted in figure

[5] To be more precise, the coordinate system (3.2), with $r > 0$ only covers half of each patch. We will later translate our expressions to global coordinates where the full patches are covered.

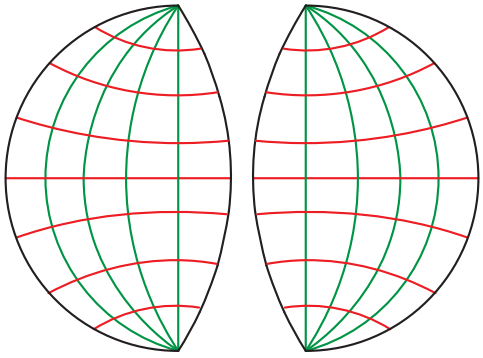

Figure 3.1: Constant time slices of the two AdS patches on the two sides of the defect, corresponding to the metric (3.4), glued together at the location of the defect along $y = \pm y^*$ curves. Lines of constant r are indicated in red and lines of constant y are indicated in green.

3.1. In this coordinate system, the boundary of AdS_3 is located at $y = \infty$ or $r = \infty$, constant r lines are geodesics, constant y curves are perpendicular to $r = 0$ and constant r curves are perpendicular to the boundary.

The (t, y, r) coordinates can be related to the usual global AdS_3 coordinates (t, ρ, θ) in the following way,

$$\cosh y \cosh r = \cosh \rho; \qquad \sinh y = \sinh \rho \sin \theta, \tag{3.5}$$

and the metric becomes

$$ds^2 = L^2 \left(-\cosh \rho^2 dt^2 + d\rho^2 + \sinh^2 \rho d\theta^2 \right). \tag{3.6}$$

Another useful set of coordinates maps the global AdS_3 coordinates to a circle of finite radius, it reads

$$\tan \phi = \sinh \rho, \tag{3.7}$$

which leads to the following metric,

$$ds^2 = \frac{L^2}{\cos^2 \phi} \left(-dt^2 + d\phi^2 + \sin^2 \phi \, d\theta^2 \right). \tag{3.8}$$

In this way, we obtain a third coordinate system (t, ϕ, θ) where the constant time slices are Poincaré disks with $\phi \in [0, \pi/2]$ playing the role of a radial coordinate and θ an angular coordinate on the disk. Note that constant θ curves are geodesics. The (t, y, r) coordinates are related to the (t, ϕ, θ) coordinates according to

$$\tanh r = \sin \phi \cos \theta; \qquad \sinh y = \tan \phi \sin \theta, \tag{3.9}$$

and these coordinates cover half the space.

Our previous coordinate systems (3.4), (3.6) and (3.8) were dimensionless and so the curvature of the boundary will naturally be set by the AdS scale L. In order to separate the radius of curvature of the boundary from the AdS curvature scale (see, e.g., [90]) we rescale the time

coordinate by a new length scale $L_{\mathcal{B}}$ [64]

$$\tau = L_{\mathcal{B}}\, t, \tag{3.10}$$

which will set the curvature of the spatial geometry of the boundary. This leads to the metric

$$ds^2 = \frac{L^2}{\cos^2\phi}\left(-\frac{d\tau^2}{L_{\mathcal{B}}^2} + d\phi^2 + \sin^2\phi d\theta^2\right) \tag{3.11}$$

where the boundary time is now given by τ.

3.1.2 Fefferman-Graham Expansion and the Cutoff Surface

The gravitational observables that come into play in the two holographic complexity conjectures (2.45)-(2.46) yield divergent results and need to be regularized. The standard procedure, used also in previous studies of the holographic complexity, is to introduce a cutoff of constant $z = \delta$ in a Fefferman-Graham (FG) expansion of the relevant metric (see, e.g., [64, 126]). In the case of vacuum AdS_3, ignoring the defect, one needs to bring the metric (3.11) to the form

$$ds^2 = \frac{L^2}{z^2}\left(dz^2 + g_{ij}(x,z)dx^i dx^j\right), \tag{3.12}$$

where the boundary is situated at $z = 0$ and $g_{ij}(x,z)$ can be expanded in a power series in z where $g_{ij}(x, z = 0)$ is the boundary metric. This can be achieved by the following coordinate transformation

$$z = 2L_{\mathcal{B}}\frac{\cos(\phi/2) - \sin(\phi/2)}{\cos(\phi/2) + \sin(\phi/2)}, \tag{3.13}$$

and of course, scaling the metric in the asymptotic region by z^2/L^2 then yields the boundary metric

$$ds^2_{bdy} = -d\tau^2 + L_{\mathcal{B}}^2 d\theta^2. \tag{3.14}$$

The FG cutoff $z = \delta$ is then expressed using eq. (3.13) as

$$\phi = \pi/2 - \hat{\delta} + \mathcal{O}(\hat{\delta}^3), \qquad \text{or} \qquad \cosh y \cosh r = \frac{1}{\sin\hat{\delta}} + \mathcal{O}(\hat{\delta}), \qquad \hat{\delta} \equiv \frac{\delta}{L_{\mathcal{B}}}. \tag{3.15}$$

In the presence of the defect, however, it was shown in [127] that the Fefferman-Graham expansion breaks down near the defect and fails to cover a bulk wedge-shaped region originating from the defect. Different solutions to this problem have been proposed in the literature, see the discussion in [128] and references therein. In particular, one suggestion is to use two different cutoffs, one for the region near the defect and another one away from the defect; in the defect region, the cutoff is expressed in term of the FG coordinates of an AdS_2 slicing of the geometry (in our coordinates (3.4) these are the slices of constant y). We adopt this suggestion for regularizing the complexity in the defect region, but continue to use the standard FG cutoff away from the defect. Moreover, we choose the two cutoffs in such a way that the cutoff surface is smooth.[6]

[6] Although we do not have a strong justification, it seems natural to require smoothness of the cutoff surface; moreover this avoids some problems that would arise in the CA computation where a lack of smoothness would

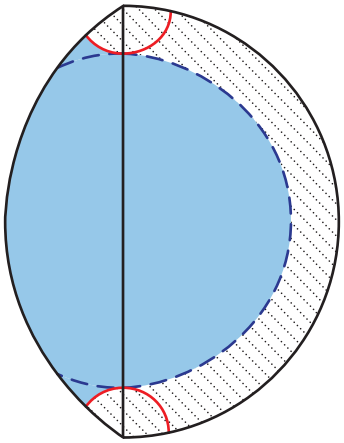

Figure 3.2: Extension of the cutoff surface in the region of the defect following lines of constant r. This generates a cutoff surface which is perpendicular to the defect and connects smoothly the two sides. We have indicated in light blue the region inside the cutoff surface.

Note that naively extending the cutoff surface of constant radius ϕ in eq. (3.15) up to the defect would give a surface that does not match smoothly across the defect. One way to see this is to check that the FG cutoff surface is not perpendicular to the line of constant $y = y^*$, where it crosses the defect. The proposed extension of the cutoff surface in the region of the defect ($y < 0$) is given by constant r curves on each side, see figure 3.2. Explicitly the constant r extension of the cutoff surface can be expressed using eq. (3.9) and it reads[7]

$$\tanh r = \sin\phi\cos\theta = \cos\hat{\delta}\,. \tag{3.16}$$

The two parts of the cutoff surface (3.15) and (3.16) are smoothly connected at $y = 0$.

3.1.3 Wheeler-DeWitt Patch in Defect AdS_3

The Wheeler-DeWitt (WDW) patch is defined as the union of all spacelike surfaces anchored at the boundary time slice where the state is defined. A practical way to obtain its shape is to identify the parts of space which are not contained within the lightcones generated from any of the points on the given boundary time slice. Without loss of generality we choose this time slice to be $t = 0$. In the case of pure AdS_3 (without the defect), the WDW patch takes the form of a cone generated from the relevant time slice on the boundary, bounded by light sheets (see, e.g., the left panel of figure 2 in [126]). In the defect geometry however, the WDW patch will be bounded by additional surfaces in the defect region, see figure 3.3. Those surfaces correspond to the lightcones generated from the points at the intersection of the boundary and the defect on the $t = 0$ time slice, namely $\theta = 0$ and $\phi = \pi/2$ or $\theta = \pm\pi$ and $\phi = \pi/2$. To understand

introduce additional joints, see footnote 17. We would like to thank Rob Myers for suggesting this choice of cutoff.

[7] A more general choice for a smooth cutoff surface is given by $\tanh r = \cos(\hat{\delta} f(y))$, where $f(y)$ is a general function satisfying $f(0) = f(-y^*) = 1$ and $f'(0) = f'(-y^*) = 0$. Such a choice does not affect the divergent contributions to the complexity using either the CV or the CA conjectures, and in particular it does not change the coefficient of the logarithmic divergence. Changing the cutoff will however change the finite contributions to the complexity in a way which depends on the tension of the brane and we comment on this issue further in the discussion.

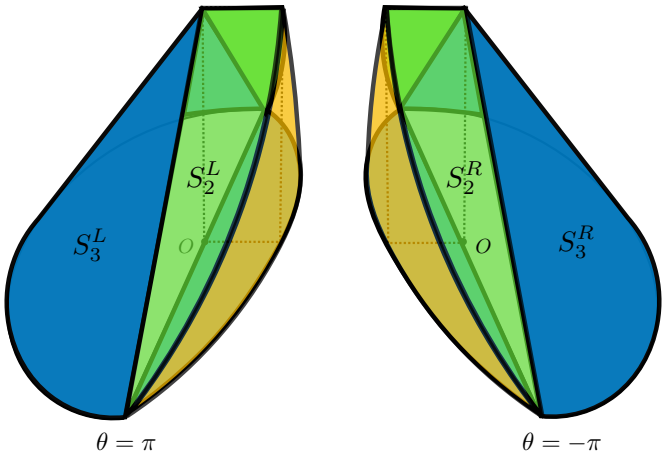

Figure 3.3: Illustration of the (future half of the) WDW patch in defect AdS_3. S_3^L and S_3^R are the two half cones, already present for the case of vacuum AdS_3. S_2^L and S_2^R are the additional boundaries of the WDW patch in the defect region, fixed by parts of the lightcones generated from the points $\theta = 0, \pm\pi$ on the boundary ($\phi = \pi/2$). Those null surfaces are smoothly connected across the defect and they terminate along a ridge at the top of the WDW patch. The yellow surfaces correspond to the defect brane, where the left and right patches are glued together.

the shape of these extra boundaries of the WDW patch, we need to obtain the relevant surfaces in the defect region by explicitly analyzing the lightcone generated from a given point on the boundary, e.g., $\theta = 0$.[8] As we demonstrate below, the lightcone takes a very simple form in the (t, y, r) coordinate system.

We will study the null geodesics starting from the boundary point $t = 0$, $r = \infty$ in the metric (3.4). Since the (y, r) coordinate system is singular at $r = \infty$, one of the initial conditions is replaced by a regularity condition at this point, which as we show below amounts to having the geodesic follow an initial angular orientation along some $y = y_0$, with $\dot{y} = 0$, where the derivative is taken with respect to some parameter σ along the null geodesics. In Appendix A.1 we derive the same geodesics directly in global coordinates as a consistency check. With the change of variables $\tanh(r(\sigma)) = R(\sigma)$ and $\tanh(y(\sigma)) = Y(\sigma)$ and a choice of parametrization $\sigma = t$ we obtain the following equations of motion by minimizing the line element

$$\ddot{R}(t) = -R(t), \qquad \ddot{Y} = Y\left[\frac{\dot{R}^2}{(R^2-1)^2} + \frac{1}{R^2-1}\right] - \frac{2R\dot{R}\dot{Y}}{R^2-1}, \tag{3.17}$$

and the requirement that the geodesics are null, namely the vanishing line element, reads

$$\dot{Y}^2 = (Y^2-1)\left[\frac{\dot{R}^2}{(R^2-1)^2} + \frac{1}{R^2-1}\right]. \tag{3.18}$$

Eq. (3.17) is solved by

$$R(t) = c_1 \cos t + c_2 \sin t. \tag{3.19}$$

The boundary condition $R(t = 0) = 1$ fixes $c_1 = 1$ and substituting eq. (3.19) into eq. (3.18) we

[8] The result for $\theta = \pm\pi$ is easily obtained using symmetry arguments.

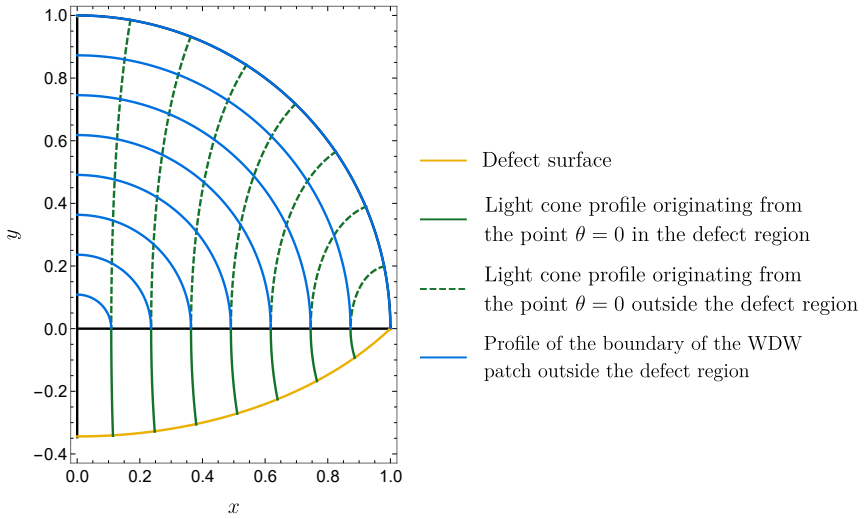

Figure 3.4: Cross section of the boundary of the WDW patch for different times t denoted by the green and blue lines inside and outside the defect region respectively. In the defect region the boundary of the WDW patch is fixed by the light cone emanating from the boundary at $\theta = 0$, indicated by solid green curves, and it meets the lightcone surface coming from $\theta = \pi$ along a ridge at $\theta = -\pi/2$ (and $t = \pi/2$). The rest of the boundary of the WDW patch is the conical region fixed by straight infalling light rays coming from different boundary points along lines of constant θ and its cross section for different times t is indicated by the blue circular arcs. The plot corresponds to a defect parameter of $y^* = 0.6$, see eq. (3.3), and is presented using the x and y coordinates defined in eq. (A.11).

find that $\dot{y}$ diverges at $t = 0$ unless $c_2 = 0$. This constraint is analogous to setting to zero the angular momentum of a geodesic passing through the radial origin of a polar coordinate system. The null equation is then solved by $Y(t) = Y_0$ where Y_0 is a constant, and this also solves the second equation of (3.17). Reverting the change of variables we finally obtain

$$\tanh r = \cos t, \qquad y = y_0. \tag{3.20}$$

This means that the null geodesics are following lines of constant y while r and t are changing. Because of this fact it is very natural to work with y, r coordinates in the defect region, while we will keep working with the ϕ, θ coordinates outside the defect region. A cross section of this surface for different values of t is depicted by the green slices in figure 3.4. We see that the constant time slices on our null cone straighten up as we go deeper into the bulk and they finally follow the constant angular surface of $\theta = -\pi/2$. We conclude that the two new boundaries of the WDW patch, see the green surfaces in figure 3.3, meet along a ridge at $\theta = -\pi/2$ and $t = \pi/2$. For $y > 0$ the WDW patch is fixed by the light rays which come from other boundary points, and its constant t profile is represented in figure 3.4 as blue curves which correspond to the blue conical surface in figure 3.3. This surface is the same as the boundary of the WDW patch in the absence of the defect.

3.2 Holographic Complexity with a Defect

With the geometric understanding developed in the previous section, we are now ready to investigate the predictions of the two holographic proposals (CA and CV) for the complexity of the DCFT ground state in our holographic defect toy model.

3.2.1 CV Conjecture

We start with the CV conjecture (2.45). In this case we have to evaluate the volume of a constant time slice in the presence of the defect. Since the two sides of the defect are identical, we focus on the region $-y^* < y < \infty$ below. We will eventually multiply the final result by two in order to account for the two sides of the defect. The defect is located at constant $y = -y^*$ which according to eqs. (3.5) and (3.7) corresponds to

$$\tan\phi \sin\theta = -\sinh y^*. \tag{3.21}$$

Since the volume is divergent we will use the cutoff surface in eqs. (3.15) and (3.16), see figure 3.2. We divide our volume to two parts V_1 and V_2 as indicated in figure 3.5. Integrating the volume element, given by the square root of the induced metric, in each of these regions yields

$$\begin{aligned} V_1 &= 2L^2 \int_{-y^*}^{0} dy \cosh y \int_0^{\tanh^{-1}(\cos\hat{\delta})} dr = 2L^2 \sinh y^* \ln\left(\frac{2}{\hat{\delta}}\right), \\ V_2 &= L^2 \int_0^{\pi} d\theta \int_0^{\pi/2-\hat{\delta}} d\phi \, \frac{\sin\phi}{\cos^2\phi} = L^2\left(\frac{\pi}{\hat{\delta}} - \pi\right), \end{aligned} \tag{3.22}$$

up to terms of order $\hat{\delta}$. Summing everything up and using eq. (2.45) we obtain the following result for the complexity using the CV proposal

$$\mathcal{C}_V = \frac{2}{G_N L}(V_1 + V_2) = \frac{4c_T}{3}\left(\frac{\pi}{\hat{\delta}} + 2\sinh y^* \ln\left(\frac{2}{\hat{\delta}}\right) - \pi\right) \tag{3.23}$$

where we have included an overall factor of 2 to account for the two sides of the defect and expressed the result in terms of the central charge $c_T = 3L/(2G_N)$. The leading contribution is the same as in the case without the defect and it follows a volume law (recall from eq. (3.15) that $\hat{\delta} = \delta/L_{\mathcal{B}}$). We see that the contribution introduced by the defect includes a logarithmic UV divergence with a coefficient which is proportional to $\sinh y^*$ where y^* is related to the tension of the brane according to eq. (3.3). For a brane with small tension for instance we will have a linear relation $\sinh y^* \sim y^* \sim \lambda$. On the CFT side we expect the relevant parameter to encode properties of the defect CFT. Of course, this result is larger than in the absence of the defect since due to the defect, the space was extended and so the volume has increased. We also note that the result is proportional to the central charge (equivalently, the number of degrees of freedom in the system). We will compare these results to those of simple CFT models with defects in Section 3.4.

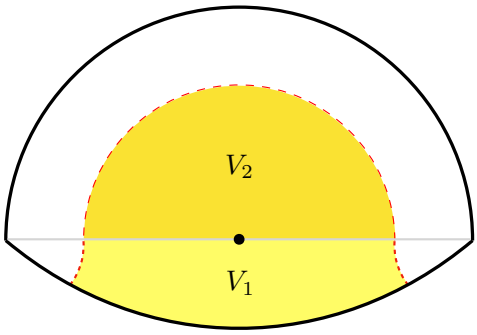

Figure 3.5: Division of the constant time slice inside the cutoff surface to two different portions which we use in evaluating the volume integrals for the CV conjecture. V_1 is the volume in the defect region and V_2 is the volume outside the defect region.

3.2.2 CA Conjecture

Next we evaluate the complexity using the CA conjecture (2.46), which states that, up to an overall numerical coefficient, the complexity is given by the gravitational action of the WDW patch. The gravitational action consists of a number of different contributions including bulk (codimension-0), boundary (codimension-1) and joint (codimension-2) terms.[9] The relevant contributions involving null joints have recently been analyzed in [63], which we will follow in our calculation below, and other relevant boundary and joint contributions were previously explored in [58–62]. For the current setup the relevant contributions in the gravitational action read

$$\begin{aligned} I = &\frac{1}{16\pi G_{\rm N}}\int_{\mathcal{M}} d^3x\sqrt{-g}\,(R-2\Lambda) + \frac{\epsilon_{_K}}{8\pi G_{\rm N}}\int_{\mathcal{B}_{t/s}} d^2x\sqrt{|h|}K \\ &+ \frac{\epsilon_\kappa}{8\pi G_{\rm N}}\int_{\mathcal{B}_n} d\lambda\, d\theta\sqrt{\gamma}\,\kappa - \frac{1}{8\pi G_{\rm N}}\int_{\mathcal{B}_n} d\lambda\, d\theta\sqrt{\gamma}\,\Theta\ln(\ell_{ct}|\Theta|) \\ &+ \frac{\epsilon_{\mathfrak{a}}}{8\pi G_{\rm N}}\int_{\Sigma} dx\sqrt{\gamma}\,\mathfrak{a} - \lambda\int_{D\cap WDW} d^2x\sqrt{-h}\,. \end{aligned} \tag{3.24}$$

The various contributions are: the bulk Einstein-Hilbert action with negative cosmological constant; the Gibbons-Hawking-York (GHY) extrinsic curvature term for timelike/spacelike boundaries;[10] the null boundary contribution given in terms of κ which measures how far is the parameter λ from providing an affine parametrization of the null generators of the null surface[11] and a counterterm added in order to ensure parametrization invariance given in terms of the null

[9] We also encounter caustics, e.g., at the tip of the blue cone in figure 3.3. The contribution of the tip can effectively be calculated by regulating it using a cutoff surface at constant $t = \pi/2 - \epsilon$. In this way we are able to demonstrate that this caustic does not make an additional contribution to the gravitational action by smoothly taking the limit $\epsilon \to 0$. We are not aware of an explicit prescription for such contributions in the literature, but we would like to point out that it is hard to come up with an action for such point-like elements which is consistent with dimensional analysis since (before dividing by $G_{\rm N}$) it should have mass dimension -1.

[10] We will only need to evaluate the GHY contribution for timelike surfaces. In this case $\epsilon_{_K} = 1$ and the normal vector s^μ should be oriented away from the volume of interest. We evaluate the extrinsic curvature according to $K_{ab} = e^\mu_a e^\nu_b \nabla_\mu s_\nu$ and its trace is given by $K = h^{ab}K_{ab}$ where the vielbeins are defined as $e^\mu_a = \partial_a x^\mu$, the induced metric is given by $h_{ab} = g_{\mu\nu}e^\mu_a e^\nu_b$ and the indexes a, b label coordinates inside the surface.

[11] κ is defined according to $k^\mu\nabla_\mu k_\nu = \kappa k_\nu$, where $k^\mu = dx^\mu/d\lambda$ is the future oriented null normal vector and λ is a parameter along the null generators increasing toward the future. As noted in reference [91], the κ term in references [63] and [64] had a sign mistake which we corrected for in eq. (3.24). $\epsilon_\kappa = \pm 1$ if the volume of interest lies to the future (past) of the boundary segment.

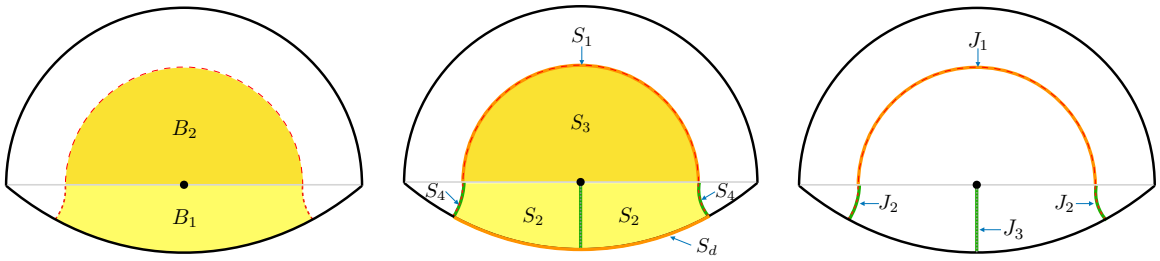

(a) Bulk contributions **(b)** Surface contributions **(c)** Joint contributions

Figure 3.6: Different contributions for the CA conjecture projected onto a constant time slice. The bulk contributions consist of those above and below the indicated regions (B_1 and B_2). The surface contributions include S_1 and S_4 which are due to the cutoff surface and S_2 and S_3 which are due to the null boundaries of the WDW patch. S_d stands for the defect contribution. The joint contributions consist of J_1 and J_2 which stand for the joints at the intersection of the cutoff surface and the null boundaries of the WDW patch and of J_3 which stands for the joint at the ridge at the top of the WDW patch, see also figure 3.3.

expansion Θ;[12] contributions from spacelike joints involving null surfaces given in terms of $\mathfrak{a}$;[13] and the new contribution due to the gravitational action for the defect itself in the region enclosed inside the WDW patch. We excluded from the action (3.24) other joint contributions which did not enter our calculations, see appendix C of [63]. In the following subsections we evaluate all these contributions and finally sum them up to produce a result for the complexity at the end of the section. The shape of the WDW patch has already been described in Section 3.1.3, see figure 3.3, and the various contributions are depicted and enumerated in figures 3.6 and 3.7.

Bulk Contributions

We start by evaluating the bulk Einstein-Hilbert and cosmological constant contributions. The Ricci scalar is the same as for the case of vacuum AdS_3 everywhere except at the position of the brane where it has an extra delta function. The effect of this additional delta function integrated over the infinitesimal thickness of the brane will be dealt with later on, together with the brane action contribution in subsection 3.2.2. For the case of vacuum AdS_3 we have $R = -6/L^2$ and $\Lambda = -1/L^2$ and therefore

$$I_{\text{bulk}} \equiv \frac{1}{16\pi G_{\text{N}}} \int_{\mathcal{M}} d^3x\sqrt{-g}\,(R - 2\Lambda) = -\frac{1}{4\pi G_{\text{N}}} \int_{\mathcal{M}} d^3x \frac{\sqrt{-g}}{L^2}. \tag{3.25}$$

This will allow us to evaluate the Einstein-Hilbert contribution everywhere except for an infinitesimally thin shell surrounding the brane. The relevant contributions can be divided into two regions B_1 and B_2 whose projections on a constant time slice are depicted in figure 3.6a. Due to

[12] The expansion parameter is defined according to $\Theta = \partial_\lambda \ln\sqrt{\gamma}$ where γ is the (one dimensional) metric on the null surface. The addition of this counterterm was recently pointed out to be an essential ingredient of the CA conjecture in refs. [91, 92].

[13] $\mathfrak{a}$ is given by $\mathfrak{a} = \ln|s \cdot k|$ for the case of the intersection between a timelike and a null boundary with normal vectors s and k respectively, and by $\mathfrak{a} = \ln|k_1 \cdot k_2/2|$ for the intersection between two null boundaries with normal vectors k_1 and k_2. The sign $\epsilon_{\mathfrak{a}} = -1$ if the volume of interest lies to the future (past) of the null segment and the joint lies to the future (past) of the segment and $\epsilon_{\mathfrak{a}} = 1$ otherwise. For more details see Appendix C of [63].

the symmetries of the problem, we focus on the future part of the WDW patch on one side of the defect and eventually multiply our result by a factor of four. We start from the contribution of the region B_1:

$$\begin{aligned} B_1 &= -\frac{L}{2\pi G_{\rm N}}\int_{-y^*}^{0} dy\cosh^2 y\int_0^{\tanh^{-1}(\cos\hat{\delta})} dr\cosh r\int_0^{\cos^{-1}(\tanh r)} dt \\ &= \frac{L}{4\pi G_{\rm N}}\left[y^*+\frac{1}{2}\sinh(2y^*)\right]\left(\ln\hat{\delta}-1\right). \end{aligned} \tag{3.26}$$

Next, we evaluate the contribution from the region B_2:

$$B_2 = -\frac{L}{4\pi G_{\rm N}}\int_0^{\pi} d\theta\int_0^{\pi/2-\hat{\delta}} d\phi\int_0^{\pi/2-\phi} dt\frac{\sin\phi}{\cos^3\phi} = -\frac{L}{4\pi G_{\rm N}}\left[\frac{\pi}{\hat{\delta}}-\frac{\pi^2}{4}\right]. \tag{3.27}$$

Summing together eqs. (3.26) and (3.27) and multiplying by a factor of four for the two sides of the defect as well as the future and past parts of the WDW patch we obtain

$$I_{\rm bulk} = \frac{L}{\pi G_{\rm N}}\left(-\frac{\pi}{\hat{\delta}}+\gamma(\ln\hat{\delta}-1)+\frac{\pi^2}{4}\right), \qquad \gamma\equiv y^*+\frac{1}{2}\sinh(2y^*), \tag{3.28}$$

where the parameter γ encodes the influence of the defect. For a brane with small tension we have a linear relation between γ and the tension of the brane, namely $\gamma\sim\lambda$.

Boundary and Joint Contributions

In this section we evaluate the various boundary and joint contributions to the gravitational action of the WDW patch. The different surfaces and joints which come into play in this calculation are illustrated and labeled in figure 3.7 and their projections on a constant time slice are presented in figures 3.6b-3.6c. They consist of the half cylindrical cutoff surface outside the defect region which is labeled as S_1, the two additional null boundaries consisting of lightcones generated from antipodal points on the boundary of the WDW patch in the defect region, both labeled as S_2, the half cone outside the defect region labeled as S_3, and the two additional constant r extensions of the cutoff surface in the defect region labeled as S_4. The joint between S_1 and S_3 is labeled as J_1 and the one between S_2 and S_4 is labeled as J_2. Finally, the joint at the ridge at the top of the WDW patch between the two S_2 surfaces is labeled as J_3. Note that S_2 and S_3 are connected smoothly, as well as the various surfaces on two different sides of the defect and we therefore do not include additional joint contributions there.

Contributions outside the defect region We start by evaluating the various contributions outside the defect region. The half cylindrical cutoff surface S_1 corresponds to $\phi=\pi/2-\hat{\delta}$ and its normal one-form and induced metric read

$$\mathbf{s^{(1)}}\equiv s^{(1)}_\mu dx^\mu = \frac{L}{\sin\hat{\delta}}\,d\phi, \qquad dh^2_{(1)} = \frac{L^2}{\sin^2\hat{\delta}}\left(-dt^2+\cos^2\hat{\delta}\,d\theta^2\right). \tag{3.29}$$

The extrinsic curvature reads

$$K_{(1)} = \frac{1}{L}\left(\cos\hat{\delta}+\frac{1}{\cos\hat{\delta}}\right), \tag{3.30}$$

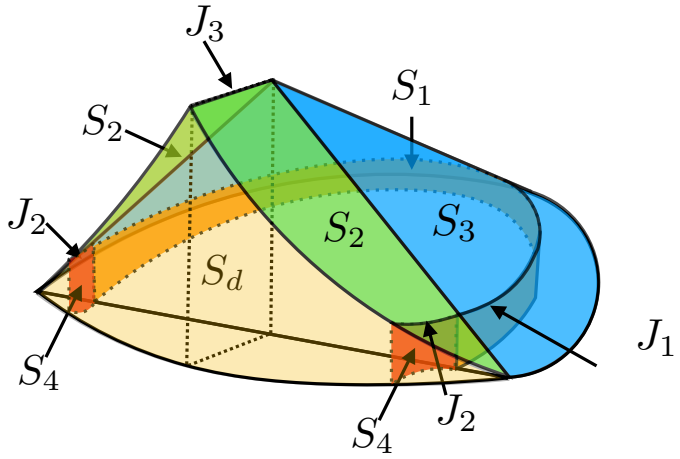

Figure 3.7: Various joint and surface contributions to the action of the WDW patch. We have focused on the future half of the patch on one side of the defect.

which yields the following GHY contribution to the gravitational action

$$S_1 = \frac{L}{8\pi G_{\rm N}} \int_0^{\hat{\delta}} dt \int_0^{\pi} d\theta \, \frac{\cos\hat{\delta}}{\sin^2\hat{\delta}} \left(\cos\hat{\delta} + \frac{1}{\cos\hat{\delta}}\right) = \frac{L}{4G_{\rm N}\hat{\delta}} \,. \tag{3.31}$$

The half cone S_3 can be parameterized by the coordinates $\lambda = t/\mathcal{N}_3$ and θ as follows[14]

$$x^\mu(\lambda,\theta) \equiv (t,\phi,\theta) = (\mathcal{N}_3\lambda, \pi/2 - \mathcal{N}_3\lambda, \theta), \tag{3.32}$$

and the normal vector to the surface reads

$$k^\mu_{(3)} = \frac{dx^\mu}{d\lambda} = \mathcal{N}_3(1,-1,0) \,. \tag{3.33}$$

The (one dimensional) induced metric, expansion and κ on the surface S_3 are given by

$$\gamma_{\theta\theta} = L^2\cot^2 t, \qquad \Theta = -\frac{2\mathcal{N}_3}{\sin(2t)}, \qquad \kappa_{(3)} = -2\mathcal{N}_3\cot t \,. \tag{3.34}$$

We can now use these results to evaluate the surface contribution S_3, including both the κ term and the counterterm contribution $\Theta\ln(\ell_{ct}|\Theta|)$ from eq. (3.24). This leads to

$$S_3 = \frac{L}{8\pi G_{\rm N}} \int_{\hat{\delta}}^{\pi/2} dt \int_0^{\pi} d\theta \, \frac{\ln\left(\frac{2\ell_{ct}\mathcal{N}_3}{\sin(2t)}\right) + 2\cos^2 t}{\sin^2 t} = \frac{L}{8G_{\rm N}\hat{\delta}} \left(\ln\left(\frac{\ell_{ct}\mathcal{N}_3}{\hat{\delta}}\right) + 1\right) . \tag{3.35}$$

The joint J_1, where the half-cone intersects with the cylindrical cutoff surface, is given as

$$J_1 = -\frac{L}{8\pi G_{\rm N}} \int_0^{\pi} d\theta \, \cot(\hat{\delta}) \ln\left(\frac{\mathcal{N}_3 L}{\sin\hat{\delta}}\right) = -\frac{L}{8G_{\rm N}\hat{\delta}} \ln\left(\frac{\mathcal{N}_3 L}{\hat{\delta}}\right) . \tag{3.36}$$

[14] In [63] it was suggested that as a part of the prescription to evaluate the complexity we should choose a parametrization of the null generators such that $\kappa = 0$ and such a parametrization is given by the choice $\lambda \propto \cot(t)$. However, since we are adding the counterterm the choice of parametrization will not modify the final result and we may proceed with $\lambda \propto t$.

Combining all these contributions for the surfaces and joints outside the defect region together and multiplying by a factor of four for the future and past parts of the WDW patch as well as the two sides of the defect we obtain

$$I_{\text{sj,out}} = 4(S_1 + S_3 + J_1) = \frac{L}{2G_{\text{N}}\hat{\delta}} \left(\ln(\ell_{ct}/L) + 3\right). \tag{3.37}$$

We see that the parametrization choice $\mathcal{N}_3$ canceled out as expected due to the addition of the counterterm.

Contributions inside the defect region Here we focus on the various surfaces and joints inside the defect region, namely S_2, S_4, J_2 and J_3, see figures 3.6-3.7. The constant r cutoff extension in the defect region corresponds to the constraint $\tanh r = \cos\hat{\delta}$, see eq. (3.16), and its normal one-form and induced metric read

$$\begin{aligned} \mathbf{s}^{(4)} &\equiv s^{(4)}_{\mu} dx^{\mu} = L\cosh y\, dr, \\ dh^2_{(4)} &= L^2 \left(dy^2 - \frac{\cosh^2 y}{\sin^2\hat{\delta}}\, dt^2 \right). \end{aligned} \tag{3.38}$$

The extrinsic curvature reads

$$K_{(4)} = \frac{\cos\hat{\delta}}{L\cosh y}. \tag{3.39}$$

We can use these results to evaluate the S_4 surface contribution given by

$$S_4 = \frac{L}{8\pi G_{\text{N}}} \int_{-y^*}^{0} dy \int_0^{\hat{\delta}} dt \cot\hat{\delta} = \frac{L}{8\pi G_{\text{N}}} y^*. \tag{3.40}$$

The additional lightcone surface S_2 generated from the boundary point at $\theta = 0$ can be parameterized in terms of t and y as follows

$$x^{\mu}(t, y) = (t, y, \tanh^{-1}(\cos t)), \tag{3.41}$$

where $t \in [\hat{\delta}, \pi/2]$ and $y \in [-y^*, 0]$ and where $y = -y^*$ corresponds to a light ray which parallels the defect. It is possible to verify, as we do below that this surface has zero null-expansion ($\Theta = 0$) and as a result it is reparametrization invariant without the addition of the counterterm in eq. (3.24) (in [63] this was referred to as a stationary hypersurface).[15] If we parameterize the surface with λ such that $\lambda = \frac{L}{\mathcal{N}_2}\cosh(y)\ln\left(\tan\left(\frac{t}{2}\right)\right)$, we obtain for the normal vector[16]

$$k^{\mu}_{(2)} = \frac{dx^{\mu}}{d\lambda} = \frac{\mathcal{N}_2}{L\cosh y}\left(\sin t, 0, -1\right), \tag{3.42}$$

[15] One way to understand this statement is that the surface S_2 is in fact a part of an entanglement wedge [109, 110]. For the case of vacuum AdS and a spherical entangling surface, it is well known that the boundary of the entanglement wedge is a Killing horizon and the corresponding normals are null killing vectors [79, 129]. Hence this surface is known to have vanishing expansion and constant cross-sectional area when moving along its null generators.

[16] A guiding principle for this choice of parametrization is that it simplifies greatly the factor inside the logarithm, and as a consequence, the integration in the corner contributions J_2 and J_3.

as well as the other properties of the surface S_2

$$\gamma_{yy} = g_{\alpha\beta} e_y^\alpha e_y^\beta = L^2, \qquad \Theta = 0, \qquad \kappa_{(2)} = -\frac{\mathcal{N}_2}{L} \frac{\cos t}{\cosh y} \,. \tag{3.43}$$

We can use these results to evaluate the surface contribution S_2 which reads

$$S_2 = \frac{L}{8\pi G_{\rm N}} \int_{-y^*}^{0} dy \int_{\hat{\delta}}^{\pi/2} dt \, \cot t = -\frac{L}{8\pi G_{\rm N}} y^* \ln \hat{\delta} \,, \tag{3.44}$$

where in evaluating this expression we have changed the variable of integration from λ to t using the chain rule. We proceed to evaluate the contribution of the joint J_2, associated with the surface of constant $t = \hat{\delta}$ and $y \in [-y^*, 0]$

$$J_2 = -\frac{L \ln \mathcal{N}_2}{8\pi G_{\rm N}} \int_{-y^*}^{0} dy = -\frac{L \ln \mathcal{N}_2}{8\pi G_{\rm N}} y^* \,. \tag{3.45}$$

The joint J_3, formed by the intersection of the two lightcone surfaces generated from the two antipodal points on the boundary, is characterized by $t = \pi/2$, $r = 0$ and $y \in [-y^*, 0]$. At this intersection the normal vectors to the two null surfaces take the form

$$k^\mu_{(2)} = \frac{\mathcal{N}_2}{L \cosh y} (1, 0, -1) \,, \qquad \bar{k}^\mu_{(2)} = \frac{\mathcal{N}_2}{L \cosh y} (1, 0, 1) \,, \tag{3.46}$$

which yields the following joint contribution

$$J_3 = \frac{L \ln \mathcal{N}_2}{4\pi G_{\rm N}} \int_{-y^*}^{0} dy = \frac{L \ln \mathcal{N}_2}{4\pi G_{\rm N}} y^* \,. \tag{3.47}$$

Summing together all the contributions for the surfaces and joints inside the defect region we finally obtain

$$I_{\rm sj,in} = 8(S_2 + S_4 + J_2) + 4J_3 = -\frac{L}{\pi G_{\rm N}} y^* \left(\ln \hat{\delta} - 1 \right) , \tag{3.48}$$

and of course, the parametrization freedom $\mathcal{N}_2$ canceled from this result.

Defect Contribution

We now proceed to consider the defect contribution. We will include here both the brane action as well as the integration of the Einstein-Hilbert term over the infinitesimal thickness of the defect. The relation between these two contributions has been explored in [130] using the Israel junction conditions [131], where it was demonstrated that the Einstein-Hilbert contribution can be expressed in terms of the discontinuity of the extrinsic curvature across the defect, and this yields a contribution that is (-2) times the brane action. Summing the two together results in a flipped sign for defect contribution

$$I_d = I_\lambda + I_{EH} = -I_\lambda = \lambda \int_{\rm defect} \sqrt{-h} = \frac{\tanh y^*}{4\pi G_{\rm N} L} \int_{\rm defect} \sqrt{-h} \tag{3.49}$$

where h is the induced metric on the defect and we have used the relation (3.3) to relate λ and y^*. Of course, in the context of the CA conjecture we will be integrating over the part of the

defect enclosed in the WDW patch. Since the defect lies inside the patch we do not need to add additional boundary contributions and joints at the location of the defect.[17] The defect brane corresponds to the constraint $y = -y^*$, see eq. (3.21). We parameterize it by the coordinates t and r, and its normal vector and induced metric are given by

$$\begin{aligned} \mathbf{s}^{(\mathbf{d})} &\equiv s^{(d)}_{\mu} dx^{\mu} = L\, dy, \\ dh^2_{(d)} &= ds^2 = L^2 \cosh^2 y(-\cosh^2 r dt^2 + dr^2)\,. \end{aligned} \tag{3.50}$$

This yields the following defect contribution

$$I_d = \frac{L\sinh(2y^*)}{2\pi G_{\rm N}} \int_0^{\tanh^{-1}(\cos\hat{\delta})} dr \cosh r \int_0^{\cos^{-1}(\tanh r)} dt = -\frac{L\sinh(2y^*)}{2\pi G_{\rm N}} \left(\ln\hat{\delta} - 1\right), \tag{3.51}$$

where we have included an overall factor of two to account for the future and past portions of the defect brane.

Total CA Contribution

We can now collect all the terms to obtain the total result for CA complexity using eq. (2.46)[18]

$$\mathcal{C}_A = \frac{I_{\rm WDW}}{\pi} = \frac{1}{\pi}\left(I_d + I_{\rm sj,in} + I_{\rm sj,out} + I_{\rm bulk}\right) = \frac{c_T}{3\pi}\left(\frac{1}{\hat{\delta}}\left[\ln\left(\frac{\ell_{ct}}{L}\right) + 1\right] + \frac{\pi}{2}\right), \tag{3.52}$$

where we have expressed the result in terms of the central charge $c_T = 3L/(2G_{\rm N})$ of the boundary theory. We see that the presence of the defect does not change the result! This is in contrast to the logarithmic contribution introduced into the CV complexity due to the presence of the defect, cf. eq. (3.23). There is an ambiguity related to the new scale ℓ_{ct} introduced by the counterterm which has been suggested to be related to certain choices that can be made in defining the complexity in the QFT side [65, 67], see section 5 of [92].

3.3 Holographic Complexity for Subregions

Next, we investigate extensions of the CV and CA conjectures for mixed states produced by tracing out the degrees of freedom outside a subregion A of the full boundary time slice, see [64, 111]. Both proposals are motivated by the suggestion that the natural bulk region encoding the reduced density matrix is the entanglement wedge [109, 110]. In the presence of the defect, the non-trivial case is when the subregion A includes the defect and we focus on this case below.

3.3.1 Subregion CV Conjecture

The extension of the CV conjecture for the complexity of mixed states [64, 111] suggests that the complexity is proportional to the maximal volume of a codimension-one surface enclosed between the boundary region A and its corresponding Ryu-Takayanagi (RT) surface [11, 108] with the same

[17] As an aside, we note that a naive extension of the prescription for joint terms between the defect surface and the additional S_2 boundary would fail, since in this case the null normal is included in the timelike defect surface which would result in a vanishing product of the normals to these two hypersurfaces.

[18] We have set $\hbar = 1$.

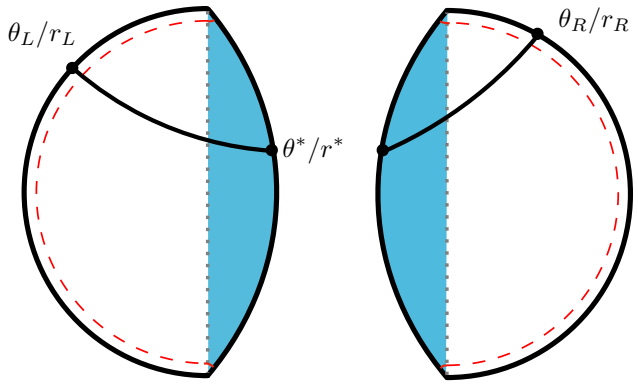

Figure 3.8: Defect AdS geometry consisting of two AdS patches glued together along lines of constant $y = \pm y^*$ at the location of the defect. The spacelike geodesic connecting θ_L and θ_R (alternatively r_L and r_R) will pass through $\theta = \pm\theta^*$ (alternatively $r = r_*$) on the left/right patches respectively. On the right patch we have $-y^* \leq y < \infty$ while on the left patch we have $-\infty < y \leq y^*$. We have extended the definition of r in both patches such that all the patch is covered and $-\infty \leq r \leq \infty$. Angles are measured with respect to the vertical upward direction.

proportionality coefficient as in equation (2.45). We will use this prescription in the defect-AdS geometry for the case in which the subregion A contains the defect. For this purpose, we need to find the RT surface (the spacelike geodesic, in our case) connecting two points on opposite sides of the defect as illustrated in figure 3.8. This is done by matching two geodesics connecting the two boundary points on each side of the defect to the same point on the defect surface and minimizing the total length.

Finding the Geodesics

Let us start with the metric on a constant time slice in global coordinates on the right patch, see eq. (3.8)

$$ds^2 = \frac{L^2}{\cos^2\phi}\left(d\phi^2 + \sin^2\phi\, d\theta^2\right). \tag{3.53}$$

The geodesics for this metric can be found by minimizing the line element. This leads to the following geodesic equation parameterized by θ, where we have used the change of variables $\Phi(\theta) = \sin(\phi(\theta))$

$$-\Phi(\theta)\Phi''(\theta) + 2\Phi'(\theta)^2 + \Phi(\theta)^2 = 0\,, \tag{3.54}$$

which admits the general solution

$$\sin\phi\,\cos(\theta - \alpha) = c\,. \tag{3.55}$$

α and c are two constants of integration which will be fixed by the boundary conditions θ_L and θ_R where the geodesic meets the boundary of AdS. This demonstrates that these are simply curves of constant r, rotated by an angle α cf. eq. (3.9).

Alternatively, we can work with the y and r coordinates by extending the definition of r to

negative values, in order to cover the full space. This is done by formally extending the coordinate transformation in eq. (3.9) to angles $\theta > \pi/2$ or $\theta < -\pi/2$. This choice of coordinates turns out to be the most convenient when evaluating the relation between the integration constants and the boundary conditions of the geodesics. The geodesic in the y and r coordinates can be obtained by considering the restriction of the metric (3.4) onto a constant time slice

$$ds^2 = L^2 \left(\left(\frac{dy}{dr} \right)^2 + \cosh^2 y \right) dr^2. \tag{3.56}$$

This leads to the following geodesic equation where we have used the change of variables $Y(r) = \tanh(y(r))$

$$\frac{d^2Y}{dr^2} - Y = 0. \tag{3.57}$$

This equation admits the general solution

$$\tanh(y(r)) = c_1 e^r + c_2 e^{-r} \tag{3.58}$$

where c_1 and c_2 will be fixed by the boundary conditions. In general these constants will be different for the left and right sections of the geodesic and we will have to match them at the position where the geodesic meets the defect. Fixing the boundary conditions $y = \infty$, $r = r_R$ for the right section of the geodesic and $y = -\infty$, $r = r_L$ for the left section we can express the geodesic solutions as follows

$$\begin{aligned} \sinh(r - r_R + \tanh^{-1}(a_R)) &= \frac{a_R}{\sqrt{1 - a_R^2}} \tanh y, \\ \sinh(r - r_L - \tanh^{-1}(a_L)) &= \frac{a_L}{\sqrt{1 - a_L^2}} \tanh y, \end{aligned} \tag{3.59}$$

where the constants of integration a_L and a_R will be fixed by matching the two geodesics on the two sides of the defect.

Since the metric is continuous at the location of the defect (only its derivative with respect to the y coordinate is discontinuous), one can show by integrating the equations of motion in a small pillbox around the defect that dy/dr is continuous at the point where the geodesics cross the defect. This is a local matching condition which is equivalent to minimizing the total length of the geodesics. Explicitly, the matching condition reads

$$\frac{\sqrt{1 - a_R^2}}{a_R} \cosh(r_* - r_R + \tanh^{-1}(a_R)) = \frac{\sqrt{1 - a_L^2}}{a_L} \cosh(r_* - r_L - \tanh^{-1}(a_L)) \tag{3.60}$$

where $r = r_*$ is the value of r at the point where the geodesics cross the defect. In addition, the

fact that the geodesics in eq. (3.59) cross the defect at $r = r_*$ yields the following conditions

$$\sinh(r_* - r_R + \tanh^{-1}(a_R)) = -\frac{a_R}{\sqrt{1-a_R^2}} \tanh y^*, \tag{3.61}$$

$$\sinh(r_* - r_L - \tanh^{-1}(a_L)) = \frac{a_L}{\sqrt{1-a_L^2}} \tanh y^*. \tag{3.62}$$

Solving these three equations leads to

$$a \equiv a_L = a_R = \frac{\sinh(\frac{r_R - r_L}{2})}{\cosh(\frac{r_R - r_L}{2}) + \tanh y^*}, \qquad r_* = \frac{r_L + r_R}{2}. \tag{3.63}$$

We note that the point r_* is simply the arithmetic mean of the two asymptotic values of r on the two sides of the defect. We also note that $|a| < 1$, and the sign depends on whether $r_R > r_L$ or $r_L > r_R$.

Evaluating the Volume

We are now in the position to evaluate the volume enclosed inside the geodesic studied in the previous subsection as suggested by the CV proposal. We have divided the volume to the part inside the defect region and the part outside the defect region. Throughout the calculation we have assumed that $r_L, r_R \ll \ln(2/\hat{\delta})$, namely that the size of the boundary interval as well as the distance between its end points and the defect are kept finite and far below the cutoff value. The volume of the part inside the defect region on the right patch can be evaluated as

$$V_1^R = L^2 \int_{-y^*}^{0} dy \cosh y \int_{r_R - \tanh^{-1}(a) + \sinh^{-1}\left(\frac{a}{\sqrt{1-a^2}} \tanh y\right)}^{\tanh^{-1}(\cos\hat{\delta})} dr \tag{3.64}$$

and for the left patch we have

$$V_1^L = L^2 \int_{0}^{y^*} dy \cosh y \int_{r_L + \tanh^{-1}(a) + \sinh^{-1}\left(\frac{a}{\sqrt{1-a^2}} \tanh y\right)}^{\tanh^{-1}(\cos\hat{\delta})} dr. \tag{3.65}$$

Using the change of variables $y \to -y$ in the first integral, we can combine the two integrals. Some of the contributions cancel out and we are left with

$$\begin{aligned} V_1 = V_1^L + V_1^R &= L^2 \int_0^{y^*} dy \cosh y \left(2\tanh^{-1}(\cos\hat{\delta}) - r_L - r_R\right) \\ &= \sinh y^* \left(2\ln\left(\frac{2}{\hat{\delta}}\right) - r_L - r_R\right). \end{aligned} \tag{3.66}$$

The volume outside the defect region for the right patch is given by

$$\begin{aligned} V_2^R &= L^2 \int_{r_R+\mathcal{O}(\hat{\delta}^2)}^{\tanh^{-1}(\cos\hat{\delta})} dr \int_0^{\cosh^{-1}\left(\frac{1}{\cosh r \sin\hat{\delta}}\right)} \cosh y \, dy \\ &\quad + L^2 \int_{r_0}^{r_R+\mathcal{O}(\hat{\delta}^2)} dr \int_0^{\tanh^{-1}\left(\frac{\sqrt{1-a^2}}{a}\sinh\left(r-r_R+\tanh^{-1}(a)\right)\right)} \cosh y \, dy \\ &= L^2\left(\frac{1}{\hat{\delta}}\cos^{-1}(\tanh r_R) - \pi/2\right) + L^2 \arcsin(a), \end{aligned} \tag{3.67}$$

where we have decomposed the volume integration into two parts along the black dashed line in figure 3.9, and the first integral was carried out using the change of variables $t = \sinh r$. We have also defined $r_0 = r_R - \tanh^{-1}(a)$ which is the point on the spatial geodesic (3.59) where $y = 0$. Note that in some cases the limits of integration in the second integral may be flipped which accounts for a subtraction rather than an addition. The volume in the left patch can be effectively obtained by replacing $a \to -a$ and $r_R \to r_L$ in the above expression which yields

$$V_2 = V_2^R + V_2^L = \frac{L^2}{\hat{\delta}}\left(\cos^{-1}(\tanh r_R) + \cos^{-1}(\tanh r_L)\right) - L^2\pi. \tag{3.68}$$

Finally summing the different contributions yields the following result for the subregion complexity using the CV conjecture

$$\mathcal{C}_V^{\text{sub}}(r_R, r_L) = \frac{2c_T}{3}\left(\frac{\theta_R - \theta_L}{\hat{\delta}} + \sinh y^* \left(2\ln\left(\frac{2}{\hat{\delta}}\right) - r_L - r_R\right) - \pi\right), \tag{3.69}$$

where we have expressed the result in terms of the central charge $c_T = 3L/(2G_{\text{N}})$ and the opening angle $\theta_R - \theta_L$ where

$$\theta_R = \cos^{-1}(\tanh r_R), \qquad \theta_L = -\cos^{-1}(\tanh r_L), \tag{3.70}$$

cf. (3.9) with $\phi = \pi/2$. One consistency check on our result is to check that when $r_L = r_R = 0$ we recover half the volume of the full time slice, which is indeed the case, cf. eq. (3.23). The leading divergence in eq. (3.69) is proportional to the size the interval A measured in terms of its opening angle $\theta_R - \theta_L$, which is the same result as obtained without the defect, see [64]. The last term $-\pi$ is a topological term, already mentioned in reference [132]. There, the authors concluded that the holographic subregion complexity of q intervals living on the boundary of AdS_3 is proportional to $\frac{x}{\delta} + \pi q - 2\pi\chi$, where x is the total length of the entangling intervals on the boundary and χ is the Euler characteristic of the codimension-one volume entering in the CV proposal. In our case, we obtain exactly the same result for the theory without a defect by setting $y^* = 0$, with $\chi = 1$ and $q = 1$ (or alternatively $q = 0$ for the full boundary, cf. eq. (3.23)). Compared to the full CV calculation in eq. (3.23), the subregion complexity has half of the log divergent contribution which is due to the fact that the subregion encloses only one boundary defect and the finite piece has an additional negative contribution proportional to $r_L + r_R$.

Finally, with the tools we have developed here we can also generalize the result of [102] for the entanglement entropy in the presence of the defect to the case of an entangling region which is not symmetric around the defect. The entanglement entropy is determined by the minimal

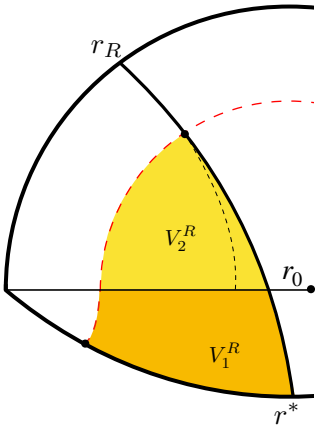

Figure 3.9: A corner of the right defect patch illustrating the relevant volumes in the evaluation of the subregion CV proposal. The red dashed curve indicates the cutoff surface and the volumes V_1^R in eq. (3.64) and V_2^R in eq. (3.67) are colored in dark and light yellow respectively. The dashed black line indicates the division between the two integration regions in eq. (3.67).

area surface anchored at the boundary of the entangling region according to the Ryu-Takayanagi (RT) formula $S_{EE} = A/(4G_{\mathrm{N}})$ [11, 108], where for AdS_3, A is simply the length of the geodesic (3.59) according to the length element in eq. (3.56). In total we have

$$S_{EE} = S_{EE,\mathrm{empty}} + \Delta S_{EE,\mathrm{defect}} \tag{3.71}$$

where the entropy in the absence of the defect is given by [133]

$$S_{EE,\mathrm{empty}} = \frac{c_T}{3} \ln \left(\frac{2 \sin\left(\frac{\theta_R - \theta_L}{2}\right)}{\hat{\delta}} \right) \tag{3.72}$$

and the entropy associated with the defect is given by

$$\Delta S_{EE,\mathrm{defect}} = \frac{c_T}{3} \ln \left(\cosh y^* + \frac{\sinh y^*}{\cosh\left(\frac{r_R - r_L}{2}\right)} \right) . \tag{3.73}$$

For the case $r_R = r_L = 0$ where the geodesic passes through the center of the AdS_3 this matches eq. (3.9) of [102]. In fact, the authors there note that as long as the entangling surface is symmetric around the defect, the result does not depend on the size of the subsystem, and is related by means of a folding trick to the boundary entropy $\ln g$. Indeed we observe that when setting $r_L = r_R$ the dependence on the boundary points r_L, r_R disappears from the above equation. If the defect is not located at the midpoint of the interval, the entanglement entropy is no longer determined solely by the two universal numbers c_T and g but rather depends also on the location of the end points of the entangling region.

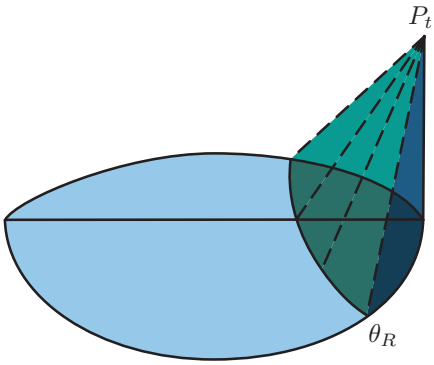

Figure 3.10: Illustration of the entanglement wedge for a subregion centered around the defect in the right patch of the defect AdS_3 geometry. P_t is the point on the boundary at the edge of the causal diamond associated with the relevant boundary region, whose past bulk lightcone will pass through the spatial geodesic connecting θ_L and θ_R.

3.3.2 Subregion CA Conjecture

In [64], a proposal was made for extending the CA conjecture to subregions (corresponding to mixed states); the proposal is that the complexity of the mixed state is proportional to the action of a codimension-zero bulk region, defined as the intersection of the WDW patch and the entanglement wedge associated to the relevant subregion with the proportionality coefficient as in eq. (2.46). The WDW patch does not depend on the subregion and is therefore identical to the one described in Section 3.1.3. The entanglement wedge associated to a boundary subregion A is the set of bulk points which are spacelike separated from the RT surface and connected to the boundary domain of dependence of the subregion A, see [109, 110]. Its boundary is then formed by the light-front of the past and future light cones emanating from the various points on the RT surface. For the case of vacuum AdS_3 the null geodesics which form the boundaries of the entanglement wedge meet on the boundary at the two ends of the causal diamond associated with the subregion A.

To simplify the calculation we will be focusing on the case where the entangling region is symmetric about the defect, i.e., $r_R = r_L$ or $\theta_L + \theta_R = 0$, see eq. (3.70). In this case, the RT surface is simply a curve of constant $r = r_L = r_R$, see eqs. (3.59) and (3.63). The entanglement wedge then naturally coincides with the one of empty AdS_3 and consists of the light rays emanating from the boundary point $P_t = (t, \phi, \theta) = (\theta_R, \pi/2, 0)$, see figure 3.10. In fact, recall that we have already considered a similar lightcone, when we were looking at the extension of the boundary of the WDW patch in the defect region in Section 3.1.3, where it was described by the relation (3.20). Adapting this expression to our case by the substitution $t \to \theta_R - t$ results in the following parametrization for the boundary of the entanglement wedge

$$\tanh r = \cos(\theta_R - t)\,. \tag{3.74}$$

For the case of vacuum AdS and spherical entangling regions, it is well known that the boundary of the entanglement wedge is a Killing horizon which has vanishing expansion [79, 129] and therefore

the counterterm in eq. (3.24) will vanish for this surface.

In the following, we will divide the contributions to the CA proposal for the subregion to two parts — inside, and outside the defect region

$$\mathcal{C}_{A,\text{sub}} = \mathcal{C}^{\text{vac}}_{A,\text{sub}} + \mathcal{C}^{d}_{A,\text{sub}}. \tag{3.75}$$

Since we are mainly interested in studying the special properties that the defect induces in our system, we will focus here on evaluating the contributions to the complexity from the defect region. Those will be the ones important for the conclusions of this chapter. For completeness we also extract the divergent contributions outside the defect region in Appendix A.2. We will demonstrate below that $\mathcal{C}^{d}_{A,\text{sub}}$ vanishes for all symmetric subregions around the defect.

In what follows it will be useful to have an explicit expression for the intersection of the WDW patch and the entanglement wedge in the defect region. Combining (3.74) and (3.20) for this joint yields

$$t = \theta_R/2\,. \tag{3.76}$$

Evaluating the Action

In this subsection we focus on contributions from the defect region. We quote the result for the structure of divergences outside the defect region at the end of the subsection and the details can be found in Appendix A.2. The projections of the various relevant contributions onto the $t = 0$ time slice are illustrated in figure 3.11. They consist of bulk, boundary, joint and defect contributions. In the defect region, those are the two bulk contributions B_1 (region under the WDW patch) and B_3 (region under the entanglement wedge), the three surface contributions S_4 (cutoff surface), S_2 (null boundary of the WDW patch) and S_8 (null boundary of the entanglement wedge), the three joint contributions J_2 (between the cutoff surface and the boundary of the WDW patch), J_5 (between the boundary of the WDW patch and the boundary of the entanglement wedge) and J_6 (between the past and future boundaries of the entanglement wedge), and the two defect contributions $S_d^{(a)}$ (enclosed under the WDW patch) and $S_d^{(b)}$ (enclosed under the entanglement wedge). We evaluate them below.

Bulk contributions We start from the bulk contribution B_1, bounded by the WDW patch (3.20), which reads

$$\begin{aligned} B_1 &= -\frac{L}{4\pi G_{\text{N}}}\int_{-y^*}^{0}\cosh^2 y\,dy\int_{\tanh^{-1}(\cos\frac{\theta_R}{2})}^{\tanh^{-1}(\cos\hat{\delta})}\cosh r\,dr\int_0^{\cos^{-1}(\tanh r)}dt \\ &= \frac{L}{8\pi G_{\text{N}}}\left(y^* + \frac{1}{2}\sinh(2y^*)\right)\left(\ln\hat{\delta} + \frac{\theta_R}{2}\cot\left(\frac{\theta_R}{2}\right) - \ln\left(\sin\left(\frac{\theta_R}{2}\right)\right) - 1\right). \end{aligned} \tag{3.77}$$

Next, we evaluate the bulk contribution B_3, under the entanglement wedge (3.74), which reads

$$\begin{aligned} B_3 &= -\frac{L}{4\pi G_{\text{N}}}\int_{-y^*}^{0}\cosh^2 y\,dy\int_{\tanh^{-1}(\cos\theta_R)}^{\tanh^{-1}(\cos\frac{\theta_R}{2})}\cosh r\,dr\int_0^{\theta_R-\cos^{-1}(\tanh r)}dt \\ &= -\frac{L}{8\pi G_{\text{N}}}\left(y^* + \frac{1}{2}\sinh(2y^*)\right)\left(\frac{\theta_R}{2}\cot\left(\frac{\theta_R}{2}\right) + \ln\left(\sin\left(\frac{\theta_R}{2}\right)\csc\theta_R\right)\right). \end{aligned} \tag{3.78}$$

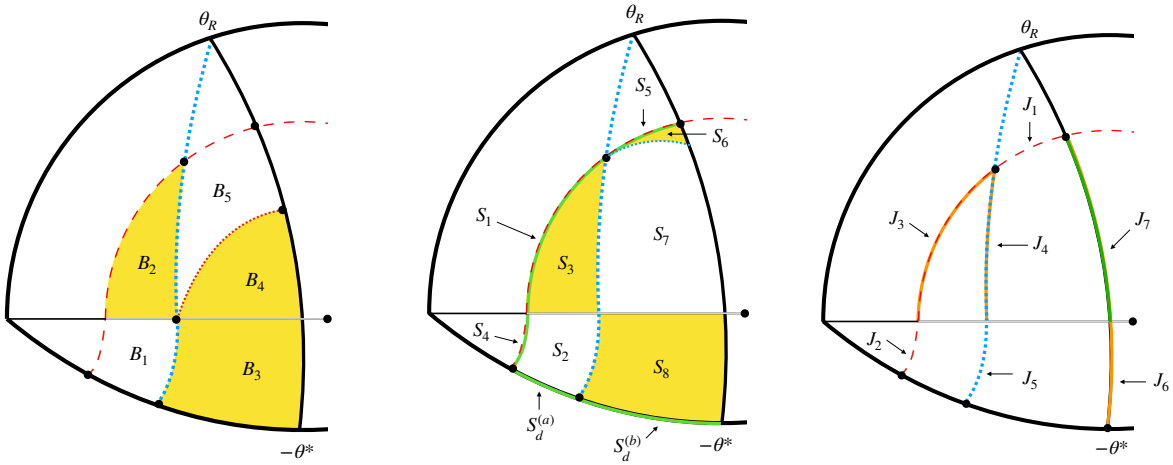

(a) Bulk contributions **(b)** Surface contributions **(c)** Joint contributions

Figure 3.11: Illustrations of the various contributions in the evaluation of the subregion CA proposal for an interval which is symmetric around the defect. The illustrations focus on the right patch, but of course, equivalent contributions exist for the left patch. The red dashed line represents the cutoff and the middle dotted blue curve represents the projection of the joint formed at the intersection between the boundary of the WDW patch and the entanglement wedge. We have also included certain internal divisions between B_4 and B_5 and between S_6 and S_7 outside the defect region which we use in evaluating the relevant integrals in Appendix A.2.

Multiplying by four to account for the equivalent contributions from both sides of the defect, as well as above and below the $t = 0$ time slice, we find that the total bulk contribution inside the defect region is given by

$$I_{\text{bulk,in}} = \frac{L}{2\pi G_{\text{N}}}\left(y^* + \frac{1}{2}\sinh(2y^*)\right)\left(\ln\hat{\delta} - \ln\left(\frac{1}{2}\tan\left(\frac{\theta_R}{2}\right)\right) - 1\right) . \tag{3.79}$$

Surface and joint contributions The contribution from the cutoff surface S_4 has already been evaluated in Section 3.2.2, see eq. (3.40), and is given by

$$S_4 = \frac{L}{8\pi G_{\text{N}}} y^* . \tag{3.80}$$

The contribution of the null surface S_2 is very closely related to the one evaluated in eq. (3.44). All one has to do is modify the limits of integration according to eq. (3.76) which yields

$$S_2 = \frac{L}{8\pi G_{\text{N}}}\int_{-y^*}^{0} dy \int_{\hat{\delta}}^{\theta_R/2} dt\, \cot t = \frac{L}{8\pi G_{\text{N}}} y^*\left(-\ln\hat{\delta} + \ln\left(\sin\left(\frac{\theta_R}{2}\right)\right)\right) . \tag{3.81}$$

The details of the null boundary of the entanglement wedge S_8 can be easily obtained from those of the null boundary of the WDW patch in eq. (3.41)-(3.43) by substituting $t \to \theta_R - t$ in the relevant places. However, we have to make sure that the parametrization λ increases from past to future, hence we choose $\lambda = -\frac{L}{\mathcal{N}_{\text{EW}}}\cosh y \, \ln\left(\tan\left(\frac{\theta_R - t}{2}\right)\right)$, where we have included a constant $\mathcal{N}_{\text{EW}}$ to account for the choice of parametrization at the boundaries of the entanglement wedge.

The surface data is given by

$$\begin{aligned} &x^\mu(t,y) = (t, y, \tanh^{-1}(\cos(\theta_R - t))), \quad k^\mu_{(2)} = \frac{\mathcal{N}_{\text{EW}}}{L\cosh y}\left(\sin(\theta_R - t), 0, 1\right), \\ &\gamma_{yy} = L^2, \qquad \Theta = 0, \qquad \kappa_{(2)} = \frac{\mathcal{N}_{\text{EW}}}{L}\frac{\cos(\theta_R - t)}{\cosh y}, \end{aligned} \tag{3.82}$$

which leads to the following surface contribution

$$S_8 = -\frac{L}{8\pi G_{\text{N}}}\int_{-y^*}^{0} dy \int_0^{\theta_R/2} dt\, \cot(\theta_R - t) = -\frac{L}{8\pi G_{\text{N}}} y^* \ln\left(2\cos\left(\frac{\theta_R}{2}\right)\right). \tag{3.83}$$

Next, we evaluate the relevant joints. The joint J_2 at the intersection of the WDW patch and the cutoff surface is identical to the one evaluated in eq. (3.45) and reads

$$J_2 = -\frac{L\ln\mathcal{N}_2}{8\pi G_{\text{N}}} y^*. \tag{3.84}$$

The joint J_5 at the intersection of the WDW patch and the entangling wedge can be obtained using the normal vectors in eqs. (3.82) and (3.42) evaluated at $t = \theta_R/2$ which yields

$$J_5 = \frac{L\ln\left(\mathcal{N}_{\text{EW}}\mathcal{N}_2\right)}{8\pi G_{\text{N}}} y^*. \tag{3.85}$$

The joint J_6 is obtained by contracting the normal vector in eq. (3.82) for $t = 0$ with the normal vector of the past null boundary of the entanglement wedge obtained from the former by flipping the sign of its t component. This yields

$$J_6 = -\frac{L\ln\mathcal{N}_{\text{EW}}}{4\pi G_{\text{N}}} y^*. \tag{3.86}$$

Summing all these contributions together yields the following result for the action of the surfaces and joints inside the defect region

$$\begin{aligned} I_{\text{sj,in}} &= 4(S_2 + S_4 + S_8 + J_2 + J_5) + 2J_6 \\ &= \frac{L}{2\pi G_{\text{N}}} y^* \left(-\ln\hat{\delta} + \ln\left(\frac{1}{2}\tan\left(\frac{\theta_R}{2}\right)\right) + 1\right) \end{aligned} \tag{3.87}$$

and of course, we note that the parametrization choices $\mathcal{N}_2$ and $\mathcal{N}_{\text{EW}}$ canceled out.

Defect contribution The defect contribution is given according to eq. (3.49). One has to subdivide the integration into two parts. First, we consider the defect brane portion $S_d^{(a)}$ under the WDW patch

$$\begin{aligned} S_d^{(a)} &= \frac{L\sinh 2y^*}{8\pi G_{\text{N}}} \int_{\tanh^{-1}(\cos\frac{\theta_R}{2})}^{\tanh^{-1}(\cos\hat{\delta})} \cosh r\, dr \int_0^{\cos^{-1}(\tanh r)} dt \\ &= \frac{L\sinh 2y^*}{8\pi G_{\text{N}}} \left(-\ln\hat{\delta} - \frac{\theta_R}{2}\cot\left(\frac{\theta_R}{2}\right) + \ln\left(\sin\left(\frac{\theta_R}{2}\right)\right) + 1\right). \end{aligned}$$

Next we evaluate the defect brane contribution under the entanglement wedge

$$\begin{aligned} S_d^{(b)} &= \frac{L\sinh 2y^*}{8\pi G_{\rm N}} \int_{\tanh^{-1}(\cos\theta_R)}^{\tanh^{-1}(\cos\frac{\theta_R}{2})} \cosh r dr \int_0^{\theta_R - \cos^{-1}(\tanh r)} dt \\ &= \frac{L\sinh 2y^*}{8\pi G_{\rm N}} \left(\frac{\theta_R}{2}\cot\left(\frac{\theta_R}{2}\right) + \ln\left(\sin\left(\frac{\theta_R}{2}\right)\csc\theta_R\right)\right). \end{aligned}$$

Those contributions are counted twice to account for the parts of the defect brane to the future and past of the $t = 0$ time slice. Finally, we obtain

$$I_d = 2\left(S_d^{(a)} + S_d^{(b)}\right) = \frac{L\sinh(2y^*)}{4\pi G_{\rm N}}\left(-\ln\hat{\delta} + \ln\left(\frac{1}{2}\tan\left(\frac{\theta_R}{2}\right)\right) + 1\right). \tag{3.88}$$

Total contributions from defect region Adding up the contributions (3.79), (3.87) and (3.88), we find that the defect region contribution to the subregion complexity vanishes

$$\mathcal{C}^d_{A,\rm sub} = \frac{1}{\pi}\left(I_{\rm bulk,in} + I_{\rm sj,in} + I_d\right) = 0 \tag{3.89}$$

as was the case for the complexity of the state on the entire time slice. This means that the subregion complexity for an interval centered around the defect will be identical to the result for a subregion of the same size in empty AdS. This is again in stark contrast to the results of the subregion CV complexity in eq. (3.69), where the defect introduced a logarithmic contribution which also depended on the location of the end points of the subregion.

Contributions outside the defect region In Appendix A.2 we consider the contribution to the complexity from outside the defect region. This is the same as evaluating the subregion complexity for empty AdS.[19] We are able to extract the structure of divergences analytically and obtain

$$\mathcal{C}^{\rm vac}_{A,\rm sub} = \frac{c_T}{3\pi^2}\left(\frac{\theta_R}{\hat{\delta}}\left[\ln\left(\frac{\ell_{ct}}{L}\right) + 1\right] + \ln\hat{\delta}\,\ln\left(\frac{2\ell_{ct}}{L}\right)\right) + \text{finite}. \tag{3.90}$$

We note that upon setting $\theta_R = \pi$ we recover the leading divergence of the full boundary complexity (3.52). However, note that in expanding this result we have everywhere assumed that θ_R was not too close to the cutoff, and therefore we cannot expect to recover the subleading divergences in the full boundary complexity in this way. We see that the result here has an additional logarithmic contribution compared to that in eq. (3.52) which depends on the scale ℓ_{ct} associated with the counter term.

3.4 Complexity in QFT

In this section we consider the problem of calculating the defect contribution to the complexity of the ground state from the dual field theory point of view.

At the moment it is not known, even in principle, how one should compute the complexity for a generic interacting field theory, although some progress has been made for weakly interacting

[19] For the case of a flat boundary, the divergence structure of the subregion complexity in vacuum AdS was studied in [64].

QFTs, see [72]. For the case of a free field theory one can follow the methods developed in [65] which allows to compute the complexity in the case where the reference state and the target states are Gaussian (as is the case for the vacuum of a free field theory). A Gaussian state can be characterized in normal coordinates by a set of characteristic frequencies ω_k; if the reference state is taken to have all frequencies equal to a constant ω_0, the complexity is given by

$$\mathcal{C} = \frac{1}{2}\sum_k \left|\ln\left(\frac{\omega_k}{\omega_0}\right)\right| . \tag{3.91}$$

This formula is obtained as a geodesic distance, calculated in a certain metric defined on the space of unitary operators that are used to move within the set of Gaussian states. An essentially equivalent result was obtained in [67] via a different method, where the metric was computed from the Fubini-Study metric on the set of quantum states.[20]

In order to make a connection between eq. (3.91) and the holographic model studied in the previous sections, we look at a free 1+1-dimensional CFT with a conformal defect, i.e., a defect which preserves at least one copy of the Virasoro algebra. A single defect on the real line can be mapped to a boundary using the "folding trick", and the problem of constructing conformally invariant boundary conditions has been considered by Cardy [135] who derived a set of consistency conditions that boundary states have to satisfy. However these conditions cannot be solved in full generality. In the simplest case of a single free boson, which we denote as ϕ_+ and ϕ_- on the right and left sides of the defect respectively, it is possible to show [52] that the most general current-preserving conformal boundary condition relating the derivatives of the fields is

$$\begin{pmatrix}\partial_x\phi_-\\ \partial_t\phi_-\end{pmatrix} = M(\lambda)\begin{pmatrix}\partial_x\phi_+\\ \partial_t\phi_+\end{pmatrix}, \qquad M(\lambda) = \begin{pmatrix}\lambda & 0\\ 0 & \lambda^{-1}\end{pmatrix}, \quad \text{or} \tag{3.92}$$

$$\begin{pmatrix}\partial_x\phi_-\\ \partial_t\phi_-\end{pmatrix} = M'(\lambda)\begin{pmatrix}\partial_x\phi_+\\ \partial_t\phi_+\end{pmatrix}, \qquad M'(\lambda) = \begin{pmatrix}0 & \lambda^{-1}\\ \lambda & 0\end{pmatrix} . \tag{3.93}$$

If the boson is compact, the first condition amounts to a change of the compactification radius, with $\lambda = R_+/R_-$. The second type of defect is related to the first type by a T-duality on one side of the defect, i.e, $\partial_\mu\phi_+ = \epsilon_{\mu\nu}\partial^\nu\tilde{\phi}_+$. These boundary conditions can be obtained by requiring that energy is conserved (i.e., the stress tensor component T_{xt} is continuous) at the location of the defect.

In order to mimic the setup of our holographic model we will consider a scalar field, living on a periodic boundary of length $2L_{\mathcal{B}}$, namely $x \in [-L_{\mathcal{B}}, L_{\mathcal{B}}]$, with defects at the diametrically opposed points $x = 0$ and $x = L_{\mathcal{B}}$, as indicated in figure 3.12.

If the boson is compact, then its compactification radius must be unchanged after going once around the circle; this implies that the matrix associated to one defect must be the inverse of the other; if at $x = 0$ we have a defect $M(\lambda)$, at the opposite side the defect has to be $M(\lambda^{-1})$. This amounts to choosing $\lambda' = \lambda^{-1}$ in figure 3.12. It is a simple exercise to show that imposing these boundary conditions on the boson leads to a spectrum that is the same as in the theory without

[20] It has been shown in [134] that the two methods will not be equivalent in general, and an explicit counterexample can be found using coherent states.

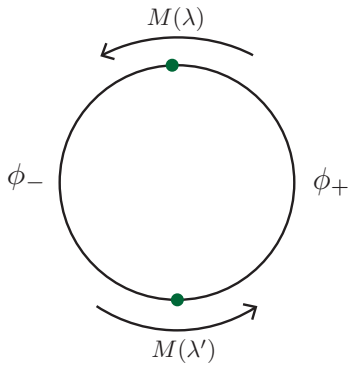

Figure 3.12: Illustration of two CFT domain walls at the opposite sides of a periodic domain.

defects, namely

$$\omega_n = \frac{\pi n}{L_{\mathcal{B}}}\,. \tag{3.94}$$

Applying the formula (3.91) then obviously leads to the result that the complexity does not depend on the presence of the defect. This is in agreement with the result for the CA conjecture that we obtained in (3.52), but not with the result for the CV conjecture (3.23), which may be seen as an argument in favor of the CA conjecture. However, we should be cautious in drawing such a conclusion, as the model we consider is a very simple one and we do not know if the result is generic. Moreover, the fact that the normal frequencies are the same does not imply that there is no effect of the defect. The zero modes play an important role in determining the entanglement entropy, more precisely its finite part, which can be identified with the Affleck-Ludwig boundary entropy [102,136,137]. This potentially hints that one has to incorporate the effect of zero modes, or winding modes, into the free field theory definitions of complexity [65,67].

We can make a few further observations. First, notice that if the two defects are not placed at antipodal points, then the spectrum will change (the defects are not topological, so the theory depends on the distance between them). In the field theory we can put the defects wherever we want, but in the gravitational dual it seems difficult to find a corresponding solution where the brane would have to bend, so something would have to pull on it to stabilize the solution. Second, if the boson is not compact, then there is no reason a priori why the two defects should be related to each other. We can allow for a more general pair of defects $M(\lambda), M(\lambda')$. The boundary conditions lead to a set of allowed momenta and corresponding frequencies

$$\omega_{n\pm} = |k_{n\pm}|\,, \quad k_{n\pm} = \frac{n\pi}{L_{\mathcal{B}}} \pm \frac{1}{L_{\mathcal{B}}} \tan^{-1}\left(\frac{\lambda\lambda' - 1}{\lambda + \lambda'}\right) \equiv \frac{\pi}{L_{\mathcal{B}}}(n \pm \Delta)\,. \tag{3.95}$$

Alternatively, if one considers a pair of defects with transfer matrices $M(\lambda)$ and $M'(\lambda')$ the frequencies are again identical to those in the vacuum state, while for transfer matrices $M'(\lambda), M'(\lambda')$ we obtain the same result as in eq. (3.95).

Even though we have no reason to think that this model has anything to do with our holographic model, we may hope that the corresponding complexity will have a sufficiently generic form. Then using the prescription (3.91), and assuming for simplicity that we use a reference

frequency larger than the cutoff, we find

$$\begin{aligned}\mathcal{C} &= \sum_{n=1}^{N} \ln \frac{L_{\mathcal{B}}^2 \omega_0^2}{\pi^2 |n^2 - \Delta^2|} \sim 2N \ln\left(\frac{L_{\mathcal{B}}\omega_0}{\pi N}\right) + 2N - \ln N - \ln\left(\frac{2\sin(\pi\Delta)}{\Delta}\right) \\ &= 2\left(\frac{L_{\mathcal{B}}\Lambda}{\pi}\right)\left[\ln\left(\frac{\omega_0}{\Lambda}\right) + 1\right] - \ln\left(\frac{L_{\mathcal{B}}\Lambda}{\pi}\right) - \ln\left(\frac{2\sin(\pi\Delta)}{\Delta}\right),\end{aligned} \tag{3.96}$$

where we have used $N = L_{\mathcal{B}}\Lambda/\pi$ with Λ the momentum UV cutoff. In the above expression we have not included the contribution of the mode $n = 0$ since this mode would have to be IR regularized when considering the theory without the defect $\Delta = 0$. Note that since we have assumed that $\omega_0 > \Lambda$ the leading term in the complexity will be positive, as expected.

We can compare this result to the one of the holographic CV (3.23) and CA (3.52) proposals. The field theory result has a $\Lambda \ln \Lambda$ divergence, which is expected in field theory [67] but is absent both in CV and in CA when ℓ_{ct} is taken to be a constant. If we consider $\ell_{ct} \sim 1/\Lambda$ in the CA proposal, the leading divergence is reproduced, but not the subleading $\ln \Lambda$. The fact that the subleading divergences do not agree is not surprising given the simplicity of our model and was already observed in the complexity of the vacuum state in [65, 67]. This choice of ℓ_{ct} would also lead to a $\ln^2 \Lambda$ divergence in the subregion complexity (3.90), which despite being an unusual divergence to encounter in field theory quantities that need to be renormalized, does appear in quantum information measures, e.g., the entanglement and Rényi entropies for entangling surfaces which contains a conical singularity [138]. Another option would be to choose the reference frequency $\omega_0 \sim \Lambda$. In this case the divergences are only Λ and $\ln \Lambda$ and the structure is the same as for CV (3.23), except for the fact that the coefficient of the log depends on the parameter of the defect in CV, whereas in the field theory the defect affects only the finite part. Comparing eq. (3.96) to the results of the CA proposal (3.52) we see that in both cases a defect dependent log contribution is absent.

It appears that the absence of a defect-dependent log is due to a cancelation that occurs between modes of momentum k and $-k$; they are degenerate in the free model, and the defect lifts the degeneracy symmetrically, i.e., $\omega \to \omega \pm \delta\omega$. This suggests that the result can change if parity invariance is broken, for instance in a chiral theory, or if the defect has degrees of freedom living on it; in this case there is a channel of inelastic scattering of the modes, so that k is not coupled only to $-k$.[21] This idea can be checked explicitly in a solvable model [125] of a free boson with a boundary interaction of the form

$$L = \frac{1}{8\pi}\int dx\, (\partial_\mu \phi \partial^\mu \phi) - g\cos\left(\frac{\phi(0)}{\sqrt{2}}\right). \tag{3.97}$$

The interaction term is of dimension one and is exactly marginal. By taking the boson at the self-dual radius, one can see that the interaction term can be reabsorbed into a redefinition of the SU(2) currents $J^3 = \frac{i}{\sqrt{2}}\partial\phi, J^\pm = e^{\pm i\sqrt{2}\phi}$:

$$J^1(x) \to \mathcal{J}^1(x) = J^1(x) - \frac{g}{2}\delta(x). \tag{3.98}$$

[21] Note, however, that the notion of degrees of freedom localized on the defect is not well-defined outside of the perturbative regime, see, e.g., [139].

The effect of this shift is to change the allowed $U(1)$ charges (i.e., momenta) of the modes. On a segment $[0, L_{\mathcal{B}}]$ with Dirichlet boundary conditions at $x = L_{\mathcal{B}}$, one finds that $k_n = \frac{\pi}{L_{\mathcal{B}}}(n + g/2)$; the complexity in this case gives a result similar to (3.96), but with a term $g \ln \Lambda$. However, if the interaction term is added at both endpoints, the spectrum is different [140]: it forms continuous bands centered around each integer, of width $1 - 2\alpha$ for $g \in \alpha + \mathbb{Z}$. In this case the asymmetry disappears again.

3.5 Discussion

In this chapter we have studied how the results of the holographic complexity proposals change when the boundary theory includes a conformal defect. We have focused on a simple gravity model which includes an AdS_2 brane embedded inside an AdS_3 geometry for which the full solution is known including backreaction [102]. The solution consists of two, slightly more than half, patches of empty AdS_3.

In Section 3.2, we evaluated the complexity of the full boundary state according to the complexity=volume proposal and found that it has an additional logarithmic divergence, compared to the case of vacuum AdS_3, see eq. (3.23). We define the difference as the defect formation complexity

$$\Delta C^{\text{form}}_{\text{defect}} \equiv \mathcal{C}_V - \mathcal{C}_{V,\text{vac}} = \frac{8 c_T \, \sinh y^*}{3} \ln\left(\frac{2L_{\mathcal{B}}}{\delta}\right), \tag{3.99}$$

where we have used eq. (3.15) to express $\hat{\delta}$ as a function of the UV-cutoff δ and the boundary radius $L_{\mathcal{B}}$, and where y^* is related to the tension of the brane as in eq. (3.3), i.e., $\tanh y^* = 4\pi G_{\text{N}} L \lambda$. Since the coefficient of the logarithmic divergence does not depend on the regularization scheme, we expect that it is related to the physical data of our system. Indeed, we demonstrate below that in addition to the explicit dependence on the central charge, the coefficient of the logarithm in the above equation is related to the Affleck-Ludwig boundary entropy [105], which manifests itself as the finite part of the entanglement entropy [133] in the presence of a boundary. In the case of the conformal defect studied in this chapter, when the entanglement region is symmetric around the defect, it is possible to use a folding trick to relate the system with the defect to a finite system with boundaries and in this case the finite part of the entanglement entropy is also related to the boundary entropy. In the holographic setup when evaluating the entanglement (3.73) for an entangling region which is symmetric around the defect one obtains

$$S_{EE} = \frac{c_T}{3} \ln\left(\frac{2L_{\mathcal{B}}}{\delta} \sin\left(\frac{\ell}{2L_{\mathcal{B}}}\right)\right) + \ln g; \qquad \ln g = \frac{c_T \, y^*}{3}, \tag{3.100}$$

where $\ell \equiv L_{\mathcal{B}} \Delta\theta$ is the length of the interval on the boundary and $\ln g$ is the boundary entropy. This result was already obtained in [102] and eq. (3.73) generalizes it to the case of asymmetric regions around the defect; we find that in the latter case the finite part of the entanglement is no longer a constant but depends on the location of the endpoints. As far as we know, this result has not appeared in the literature before, and it would be interesting to have a field theory derivation of it.

Next, we evaluated the complexity according to the complexity=action proposal and found

that the result was identical to the one obtained for empty AdS_3

$$\Delta C^{\text{form}}_{\text{defect}} = \mathcal{C}_A - \mathcal{C}_{A,\text{vac}} = 0. \tag{3.101}$$

We stress once more that the exact vanishing, and in particular the independence on the tension of the brane, is obtained with a particular choice of regularization. As discussed in footnote 7, a change of cutoff can induce finite contributions that are in general dependent on the tension. The robust part of this result is the vanishing of the defect contribution to the logarithmic divergence which contains universal information. Previous studies of the two holographic proposals have found that the two results generally coincide up to an overall numerical factor. This includes the late time growth rate of complexity in black hole backgrounds which is proportional to the mass of the black hole (for the CV proposal this is valid in the high temperature limit) [17, 57, 89],[22] characteristic delays in the complexity growth due to the introduction of shockwaves in the system [16, 91–93], as well as the structure of divergences in holographic complexity (this is true when including a counter term in the action proposal), see [64, 88]. It is therefore interesting that for the case of the defect the results of the two holographic proposals dramatically differ. However, we have to be careful about the generality of this result. Holographic complexity is known to have special features for the case of $d = 2$, e.g., the complexity of formation is not proportional to the entropy for this particular boundary dimension [126]. It is therefore important to carry this analysis in higher dimensional cases before a definite conclusion can be drawn. One possibility would be to use the setup of AdS/BCFT to study the complexity in the presence of a boundary [141, 142] or in various holographic models proposed for systems with defects [143–146]. It would also be interesting to try and explore the effect of defects of codimension different than one on the complexity. Another possible extension of our results would be to explore the effect of the defect at finite temperature when a black hole is present in the bulk.

It is important to point out that, at least naively, in order to study the complexity using the volume conjecture we have to include the backreaction of the brane. It would be interesting to see if this could somehow be avoided as was done for the entanglement entropy in [147] by using the Casini-Huerta-Myers trick [79], or in an expansion for small tension of the brane, see [148]. Note that the analysis of the action cannot be performed in the probe approximation by simply considering the action of the brane itself since the gravitational action for the region surrounding the brane contributes at the same order in an expansion in the tension of the brane, as explicitly seen in our calculation.

In Section 3.3 we evaluated the holographic complexity for subregions using the generalizations of the CA and CV proposals [64, 111] motivated by the suggestion that the natural bulk region to encode the information about the reduced density matrix is the entanglement wedge [109, 110]. Using the complexity=volume we found in eq. (3.69) that the leading divergence in the complexity was proportional to the size of the boundary region. This was already noted in [64, 111]. The defect introduced a subleading logarithmic divergence, which was exactly half of the one given in eq. (3.99) for the full boundary state. The reason is that the subregion covers only one defect in the boundary theory. It is also interesting to compare this result to the entanglement entropy in

[22] See also [90] for the full time dependence.

equation (3.73) where the contribution due to the defect was finite rather than logarithmic.

For the complexity=action for a symmetric region around the defect, we found again that the complexity with the defect was identical to the result for vacuum AdS_3 in the cutoff choice presented in Section 3.1.2, see eq. (3.89). We derived the result for empty AdS_3 in global coordinates in Appendix A.2 and the final result can be found in eq. (3.90) (previous results for subregions in vacuum AdS with a flat boundary can be found in [64]). We observed that the leading divergence is proportional to the size of the interval and that a certain ambiguity was introduced by the parameter ℓ_{ct}, with dimension of a length, due to the gravitational counterterm needed to restore reparametrization invariance of the gravitational action. This counterterm was recently shown to be an essential ingredient in the CA proposal in order to reproduce certain desired properties of the complexity in the presence of shockwaves [91, 92]. We also observed a subleading logarithmic divergence which depends on the same ambiguity due to the counterterm. If the characteristic length ℓ_{ct} is chosen to be of the order of the cutoff, this introduces a $\ln^2 \hat{\delta}$ divergence in the holographic complexity. It would be interesting to generalize this result to the case of a region which is not symmetric around the defect which cannot be related to a system with boundary using the folding trick.

In Section 3.4 we studied the complexity of the ground state for two simple models of bosonic QFTs including two defects at the two opposite sides of a periodic domain. We evaluated the complexity according to the methods introduced in [65, 67] for Gaussian states in free quantum field theories, starting from an unentangled product state with characteristic frequency ω_0. The first model consists of a free boson with permeable domain wall defects. In this model, we found that the logarithmic contribution to the complexity does not depend on the permeability parameter λ characterizing the defect, see eq. (3.96). This is similar to what happened in holography using the complexity=action proposal. Later, we considered an exactly solvable model with a boundary interaction given in eq. (3.97). In this model a logarithmic divergence which depends on the defect parameters appeared in the complexity, analogously to our result for the complexity=volume conjecture, although the logarithmic term is absent even in this case if the system has two boundaries.

No embedding of the precise holographic model studied in this chapter into string theory is known. It would therefore be very interesting to reproduce our holographic calculation for a model that comes from a solution of string theory, for instance, one could consider the exact string background of AdS_3 with NS-NS fluxes, in which AdS_2 D-brane probes can be embedded, see [149]. Presumably the fluxes would contribute to CA but not to CV, so there is a possibility that the discrepancy found in this chapter would not be present in a full top-down model. Another interesting possibility is to study the complexity in a smooth defect geometry, e.g., the Janus solution [150], and check whether a defect-dependent logarithmic contribution is obtained using the CA/CV proposals.

It is possible to gain further intuition into the influence of the defect on the complexity by considering MERA circuits, for a review see [151]. MERA tensor networks constitute an efficient way of approximating the ground state of critical systems. It has been suggested that they have a natural interpretation in holography where the MERA constitutes a lattice representation of a constant time slice in AdS and where the additional direction in the MERA circuit corresponds

to the holographic RG scale [152]. More precisely, the number of layers in the tensor network is proportional to $\log z$ where z is the holographic FG coordinate. The lattice points in this description represent the MERA gates and so counting them (equivalently evaluating the volume of the time slice) would naturally result in a measure of the complexity of the state.

It was pointed out in [153, 154] that in order to find the ground state of a system whose Hamiltonian has been modified in a certain region due to an impurity or a defect it is sufficient to minimally update the tensor network, namely to replace the tensors in the causal cone of the defect, defined as the part of MERA which traces the evolution of the defect under coarse-graining transformations. Furthermore, if the defect is conformal, it is enough to replace the pair of tensors representing disentanglers and isometries with another (single) pair in the causal cone of the defect. For impurities spread over a small spatial region, the causal cone consists of approximately a fixed number of tensors at each layer.

We have seen in our CA calculations that the defect itself makes a large positive contribution logarithmic in the cutoff, see eq. (3.51), while the geometry around the defect introduces a negative contribution, which exactly cancels the one of the defect. This can be naturally interpreted in terms of the minimally updated MERA. Introducing a cost for the tensors in the causal cone would give a log contribution, since it would be proportional to the length of the cone in the bulk; at the same time, we would have to subtract the contribution of the tensors that have been replaced. The exact cancellation that we observe seems to indicate that the CA proposal corresponds to microscopic rules where the defect gates and the ordinary gates are equally costly while in the CV, the defect gates are more costly.

An alternative interpretation was suggested in [155] according to which the additional volume in the extension of the AdS space created by a thin defect could be interpreted as additional portions added to the tensor network, and this would resemble a discretized version of the time slice in our CV calculation. Another interesting possibility would be to incorporate a defect into the path integral complexity proposal based on Liouville action studied in [68, 69, 118, 119].

We should point out that for entanglement entropy calculations in the free setup with a compact boson and two permeable domain walls, the zero modes play an important role; the finite boundary entanglement can be understood as arising essentially from the log of the volume of the zero modes [102]. This raises the question of whether the prescription for computing complexity using Gaussian states needs to be extended to account for a contribution of the zero modes. We leave this interesting issue for future study.

Chapter 4

A Careful Consideration of Holographic 2D dCFT

This Chapter is based on the work [19].

Conformal interfaces are ubiquitous both in condensed-matter systems and in studies of the holographic duality. Such interfaces describe the local, scale-invariant gluing of two conformal field theories, CFT_L on the left and CFT_R on the right. Examples include junctions of quantum wires [156], line or surface defects in the critical 2D or 3D Ising models [157], or the gluing of superconformal gauge theories with different couplings and/or gauge groups. In bottom-up AdS/CFT, interfaces are often modeled by codimension-one branes anchored at the AdS boundary. Smooth (super)gravity solutions describing top-down embeddings in string theory are also known. Some early papers on the subject are [52, 143, 145, 146, 158, 159]. Additional references will be given as we proceed.

Folding spacetime along an interface converts the latter to a conformal boundary of the product theory $\mathrm{CFT}_L \otimes \overline{\mathrm{CFT}}_R$, where the bar indicates space reflection.[1] The folded theory has two energy-momentum tensors, T_L and $\bar{T}_R$, that are separately conserved in the bulk while only their sum, $T_{\rm tot} \equiv T_L + \bar{T}_R$, needs to be conserved at the boundary. What distinguishes interfaces from boundaries (and ICFTs from BCFTs) is the existence of another, relative spin-2 current $T_{\rm rel} = c_R T_L - c_L \bar{T}_R$,[2] which measures the exchange of energy between left and right. Here c_L and c_R are the central charges of the two CFTs. As usual, things simplify considerably in two dimensions. In this case, it was noted in [50] and further analyzed in [51, 160, 161] that the transfer of energy across the interface is controlled by a single transmission or reflection coefficient, $\mathcal{T}$ or $\mathcal{R}$, with $\mathcal{T} + \mathcal{R} = 1$. The purpose of the present note is to derive a formula for these coefficients in the simplest holographic-interface model.

The model consists of two AdS_3 slices separated by a string of tension σ. The AdS_3 slices have radii ℓ_L and ℓ_R,[3] related to the CFT central charges by the Brown-Henneaux formula $c_{L,R} = 3\ell_{L,R}/2G$ [32], where G is the three-dimensional Newton's constant. With no loss of generality we take $\ell_L \geq \ell_R$, so that the 'false' higher-energy AdS vacuum is on the left, while the

[1] We will actually restrict our discussion to non-chiral theories, for which $\overline{\mathrm{CFT}}_R = \mathrm{CFT}_R$.
[2] This combination of the energy-momentum tensors is a conformal primary of the folded theory.
[3] We will work in the semiclassical limit, so the radii must be much larger than G.

'true' AdS vacuum is on the right. For tensions inside the interval

$$0 \leq \frac{1}{\ell_R} - \frac{1}{\ell_L} \leq 8\pi G\sigma \leq \frac{1}{\ell_R} + \frac{1}{\ell_L} \tag{4.1}$$

the string-worldsheet geometry is AdS_2 corresponding to the ground state of the ICFT [130,145]. At the extremal values of the interval the worldsheet flattens out, *i.e.,* the AdS_2 radius diverges. The lower σ limit in (4.1) actually corresponds to the Coleman-De Lucia bound [162] below which the false AdS_3 vacuum is unstable to nucleation of bubbles. This is also the BPS bound for supergravity domain walls [163]. The upper limit, on the other hand, corresponds to the Randall-Sundrum fine-tuned tension, beyond which the string worldsheet becomes de Sitter and gets anchored on a spacelike curve of the conformal boundary [145].

This model has been used as a toy model of holographic defects, in particular for calculations of holographic entanglement entropy, see *e.g.,* [102]. In this letter we provide the first calculation of its transport properties. Our main result is the following formula for the energy-transmission coefficient defined in [50],

$$\mathcal{T} = \frac{4}{\ell_L + \ell_R}\left[\frac{1}{\ell_L} + \frac{1}{\ell_R} + 8\pi G\sigma\right]^{-1} . \tag{4.2}$$

Together with the central charges, $\mathcal{T}$ was shown [50] to parametrize the most general two-point functions of energy-momentum tensors allowed by the symmetries of the problem.

As explained in [51,160], what was actually defined in [50] is the *weighted-average* transmission coefficient

$$\mathcal{T} = \frac{c_L\mathcal{T}_L + c_R\mathcal{T}_R}{c_L + c_R} , \quad \text{where} \quad \mathcal{T}_{L,R} = \frac{(c_L + c_R)\mathcal{T}}{2c_{L,R}} \tag{4.3}$$

are the transmission coefficients for excitations incident on the interface from the left and right, respectively. Our formula for these directional transmission coefficients reads

$$\mathcal{T}_{L,R} = \frac{2}{\ell_{L,R}}\left[\frac{1}{\ell_L} + \frac{1}{\ell_R} + 8\pi G\sigma\right]^{-1} . \tag{4.4}$$

The calculation of (4.2) and (4.4) is performed by scattering surface-gravity waves in a semi-classical geometry dual to the ground state of the ICFT. It relies on the usual condition of no outgoing waves at the Poincaré horizon, whose subtle implementation we explain below.

Before describing the calculation in detail, let us comment on some salient features of our result. First, both $\mathcal{T}_L$ and $\mathcal{T}_R$ are monotonically-decreasing functions of the tension σ. Their maximal and minimal values (in terms of the central charges) read

$$\mathcal{T}^{\max}_{L,R} = \frac{c_R}{c_{L,R}} , \qquad \mathcal{T}^{\min}_{L,R} = \frac{c_{R,L}}{c_L + c_R} , \tag{4.5}$$

or equivalently for the average coefficients

$$\frac{2c_Lc_R}{(c_L + c_R)^2} \leq \mathcal{T} \leq \frac{2c_R}{c_L + c_R} \quad \Longleftrightarrow \quad \frac{c_L^2 + c_R^2}{(c_L + c_R)^2} \geq \mathcal{R} \geq \frac{c_L - c_R}{c_L + c_R} . \tag{4.6}$$

The above lower bound on $\mathcal{R}$ is the same as the one following from the achronal average-null-

energy condition (AANEC) in the ICFT [51]. As stressed in that reference, this lower bound is stronger than the bound imposed by reflection positivity of the Euclidean theory [161], $\mathcal{R} \geq (\frac{c_L-c_R}{c_L+c_R})^2$. This shows that reflection positivity does not necessarily imply the ANEC in ICFTs.[4]

If the inequality $c_L > c_R$ is strict, both $\mathcal{T}_L$ and $\mathcal{T}$ are less than 1. Total transmission to signals incident from both sides is therefore only possible between degenerate AdS_3 vacua separated by a tensionless string. This is the gravitational counterpart of a topological interface.

The opposite limit of total reflection, $\mathcal{R} \to 1$, can only be reached by taking $c_R/c_L \to 0$, *i.e.*, by depleting CFT_R of degrees of freedom, relative to CFT_L. This should be contrasted with the fact that in more general ICFTs, factorizable interfaces can impose reflecting boundary conditions on each side for any values of c_L, c_R. In our minimal holographic model, on the other hand, the transmission of energy incident from the left can be shut down only if there are no degrees of freedom in the right side. Note however that in this limit $\mathcal{T}_R = 1$, so that the (scarce) signals incident from the right are fully transmitted to the other side.[5]

We should here stress that the transport coefficient $\mathcal{T}$ (or $\mathcal{R}$) and the ground-state entropy (the logarithm of the g-factor) [105] are independent properties of an interface. This is illustrated by topological interfaces in free-field models which can have arbitrarily large entropy [165, 166] even though their transmission coefficient is always $\mathcal{T} = 1$. The holographic duals of such interfaces are tensionless branes [167, 168], so tension is not necessarily tied to entropy. Entanglement entropy, which contains the ground-state entropy as a finite correction to the leading logarithmically divergent term, has been computed in a variety of holographic ICFT models, *e.g.*, [102, 147, 169–171]. It would be interesting to calculate transport coefficients in these models to see how, if at all, they are correlated with entropy.

4.1 Holographic Scattering States and Matching

We describe now the main steps in the calculation of the reflection and transmission coefficients. As mentioned above, we use a minimal holographic model for the ICFT, consisting of two manifolds $M_{L,R}$ that are locally AdS_3 and are joined on the worldsheet of a tensile string. The asymptotic boundaries of these manifolds are the left, respectively right half-planes glued along the CFT interface P. The latter extends in the bulk to surfaces $Q_L \subset M_L$ and $Q_R \subset M_R$ that are identified with each other and with the worldsheet of the string, see figure 4.1. The gluing of M_L to M_R must obey the matching conditions [131]

$$\gamma_{L,\alpha\beta} = \gamma_{R,\alpha\beta} \,, \tag{4.7a}$$

$$[K_{\alpha\beta}] - [\mathrm{tr}K]\gamma_{\alpha\beta} = 8\pi G\sigma\, \gamma_{\alpha\beta} \,, \tag{4.7b}$$

where we have denoted by $\gamma_{L,R}$ and $K_{L,R}$ the induced metric and extrinsic curvature on $Q_{L,R}$, respectively, and we use $[X] \equiv X_L - X_R$ to indicate discontinuities on the two sides of the interface.

[4] Contrary to what happens for quantum states built by the action of local operators on the Poincaré-invariant vacuum of a pure CFT [164].

[5] From the perspective of the false AdS vacuum, the string looks in this limit like the end-of-the-world brane of holographic BCFT [141, 142]. As we will see from eq. (4.10) below, this requires $G\ell_L\sigma$ to diverge. What is referred to as tension in [141, 142] is a finite leftover piece of σ.

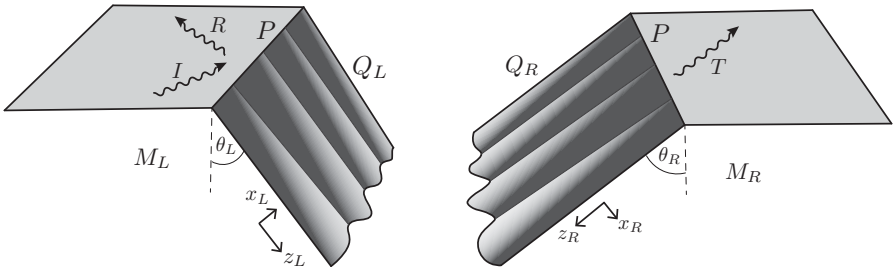

Figure 4.1: Illustration of the holographic-interface geometry. The two spacetimes are glued together at the location of the worldsheet $Q_L \equiv Q_R$. The interface P is the intersection of the worldsheet with the conformal boundary. The incident wave is denoted by I, and the reflected and transmitted waves are denoted by R and T.

The ICFT vacuum is described in Fefferman-Graham coordinates by the solution [130, 145]

$$ds_L^2 = \frac{\ell_L^2}{y_L^2}[dy_L^2 + du_L^2 - dt_L^2] \quad \text{for } u_L \leq y_L \tan\theta_L, \tag{4.8}$$

$$ds_R^2 = \frac{\ell_R^2}{y_R^2}[dy_R^2 + du_R^2 - dt_R^2] \quad \text{for } u_R \geq -y_R \tan\theta_R, \tag{4.9}$$

where $0 \leq y_{L,R} < \infty$. The worldsheet $u_L = y_L \tan\theta_L$ or $u_R = -y_R \tan\theta_R$ subtends an angle $\frac{\pi}{2} + \theta_L$, respectively $\frac{\pi}{2} + \theta_R$, to the left/right halves of the conformal boundary. The worldsheet metric is AdS_2 with radius ℓ_W obeying

$$\ell_W = \frac{\ell_L}{\cos\theta_L} = \frac{\ell_R}{\cos\theta_R} = \frac{\tan\theta_L + \tan\theta_R}{8\pi G\sigma}\,. \tag{4.10}$$

The first two equalities follow from (4.7a) and the last one from (4.7b). It will be later convenient to employ the rotated coordinates

$$\begin{aligned} \begin{pmatrix} u_L \\ y_L \end{pmatrix} &= \begin{pmatrix} \cos\theta_L & \sin\theta_L \\ -\sin\theta_L & \cos\theta_L \end{pmatrix} \begin{pmatrix} x_L \\ z_L \end{pmatrix}, \\ \begin{pmatrix} u_R \\ y_R \end{pmatrix} &= \begin{pmatrix} \cos\theta_R & -\sin\theta_R \\ \sin\theta_R & \cos\theta_R \end{pmatrix} \begin{pmatrix} x_R \\ z_R \end{pmatrix}, \end{aligned} \tag{4.11}$$

in which the unperturbed string sits at $x_L = x_R = 0$, and its worldsheet can be parametrized by $t_L = t_R \equiv t$ and $z_L = z_R \equiv z$.

In principle one would like to solve the matching problem (4.7) for a generic metric and a fluctuating interface on the conformal boundary. It is however sufficient for our purposes here to set all ICFT sources to zero, and only consider normalizable excitations of the fields. These are particularly simple in pure AdS_3 where the most general solution of the Einstein equations in Fefferman-Graham coordinates can be written as [48] (see also [172–175])

$$ds^2 = \frac{\ell^2 dy^2}{y^2} + \Big[\frac{\ell^2 g^{(0)}_{\alpha\beta}}{y^2} + g^{(2)}_{\alpha\beta} + \frac{y^2}{4\,\ell^2} g^{(4)}_{\alpha\beta}\Big] dw^\alpha dw^\beta \tag{4.12}$$

with $g^{(4)} = g^{(2)}(g^{(0)})^{-1}g^{(2)}$ and, for flat boundary metric, $g^{(2)}_{\alpha\beta} = 4G\ell\langle T_{\alpha\beta}\rangle$. Here $\langle T_{\alpha\beta}\rangle$ is the

vev of the canonically-normalized, traceless conserved energy-momentum tensor in some state of the dual CFT. Linearizing in the perturbation allows us to drop $g^{(4)}$, so that the correction to the standard AdS_3 Poincaré metric has arbitrary left- and right-moving waves, $g^{(2)}_{++}(w^+)$ and $g^{(2)}_{--}(w^-)$.

In order to reproduce the setup of ref. [51] we consider a configuration with an incoming wave from the left, giving rise to a reflected wave on the left and a transmitted wave on the right. Explicitly, identifying the $w^\pm$ of (4.12) with $u \pm t$, and using monochromatic waves,[6] we have

$$\big[ds^2\big]^{(2)}_L = 4G\ell_L\epsilon\Big[e^{i\omega(t_L-u_L)}\, d(t_L-u_L)^2 + \mathcal{R}_L\, e^{i\omega(t_L+u_L)}\, d(t_L+u_L)^2\Big] + c.c.\ , \tag{4.13}$$

$$\big[ds^2\big]^{(2)}_R = 4G\ell_R\epsilon\, \mathcal{T}_L e^{i\omega(t_R-u_R)}\, d(t_R-u_R)^2 + c.c.\ , \tag{4.14}$$

where $\mathcal{R}_L$ and $\mathcal{T}_L$ are the (a priori complex) relative amplitudes of the reflected and transmitted waves, and the subscript L indicates that the incident wave came from the left. Anticipating the final result, we give the same names to these amplitudes as to the (real) reflection and transmission coefficients. In what follows, we will linearize our equations in the incoming flux $|\langle T_{--}\rangle| = \epsilon$.

Gluing M_L with M_R requires matching coordinates on the worldsheet. We allow for this by writing $z_{L,R} = z + \tilde\epsilon\,\zeta_{L,R}(z,t)$ and $t_{L,R} = t + \tilde\epsilon\,\lambda_{L,R}(z,t)$, where z, t are the Poincaré coordinates of the AdS_2 worldsheet and we defined for convenience $\tilde\epsilon = \frac{4G}{\ell_W}\,\epsilon$. Since we are keeping only linear order in ϵ, we can set $t_L = t_R = t$ and $z_L = z_R = z$ in the perturbation (4.13). The above changes of coordinates enter only through the expansion of the leading worldsheet metric and extrinsic curvatures in (4.7). We also let $x_{L,R} = \tilde\epsilon\,\delta_{L,R}(z,t)$ be the fluctuating position of the string in the transverse dimension.[7]

Thanks to time-translation invariance we are allowed to work at fixed frequency,

$$\delta_{L,R}(z,t) = e^{i\omega t}\delta_{L,R}(z) + c.c. \tag{4.15}$$

and similarly for $\zeta_{L,R}$ and $\lambda_{L,R}$.

We have then six equations for the six functions $\delta_{L,R}$, $\zeta_{L,R}$ and $\lambda_{L,R}$. But common reparametrizations of the two charts are pure gauge, so only the transition functions

$$\zeta \equiv \zeta_L - \zeta_R \quad \text{and} \quad \lambda \equiv \lambda_L - \lambda_R \tag{4.16}$$

enter in the equations (4.7). The problem may now look overconstrained, but two of the matching conditions (4.7b) are not actually independent equations. The reason is that all foliations of AdS_3 obey the momentum constraints

$$D^\alpha K_{\alpha\beta} - D_\beta K = 0\ , \tag{4.17}$$

where D_α is the covariant derivative with respect to the induced metric. Thus, once one of the equations (4.7b) has been solved, the other two are automatically satisfied up to constants.[8]

[6] Since we are working at the linearized level, the plane wave solutions can be superposed to wave packets.

[7] We use units where the metric is dimensionless, t, x, z have dimensions of length, ϵ and $\tilde\epsilon$ have dimensions of mass squared, and hence the functions $\zeta_{L,R}, \lambda_{L,R}, \delta_{L,R}$ have dimensions of length cubed.

[8] Since the time dependence is fixed, (4.17) implies that the z derivatives of two matching conditions are identi-

The brane fluctuations are induced by the gravity waves (4.13). The equations are more compact in terms of the combinations

$$D \equiv \delta_L - \delta_R\,, \quad \Delta \equiv \tan\theta_L \delta_L + \tan\theta_R \delta_R - \zeta\,. \tag{4.18}$$

The four independent matching conditions read

$$\Delta + i\omega z\lambda = z^3\Big[\frac{\cos\theta_L}{2}(\mathbf{I}+\mathbf{R}) - \frac{\cos\theta_R}{2}\mathbf{T}\Big]\,, \tag{4.19}$$

$$i\omega z\zeta - z\partial_z\lambda = z^3\Big[\sin\theta_R\cos\theta_R\mathbf{T} + \sin\theta_L\cos\theta_L(\mathbf{I}-\mathbf{R})\Big]\,, \tag{4.20}$$

$$z\partial_z\zeta + \Delta = z^3\Big[\frac{\sin^2\theta_R\cos\theta_R}{2}\mathbf{T} - \frac{\sin^2\theta_L\cos\theta_L}{2}(\mathbf{I}+\mathbf{R})\Big]\,, \tag{4.21}$$

$$z\partial_z D = z^3\Big[\frac{1}{i\omega z}(\mathbf{I}-\mathbf{R}-\mathbf{T}) - \frac{\sin\theta_L\cos^2\theta_L}{2}(\mathbf{I}+\mathbf{R}) - \frac{\sin\theta_R\cos^2\theta_R}{2}\mathbf{T}\Big]\,, \tag{4.22}$$

where

$$\mathbf{I} \equiv e^{-i\omega\sin\theta_L z}, \quad \mathbf{R} = \mathcal{R}_L\, e^{i\omega\sin\theta_L z}, \quad \mathbf{T} \equiv \mathcal{T}_L e^{i\omega\sin\theta_R z} \tag{4.23}$$

are the exponentials imprinted on the worldsheet by the graviton waves (4.13). The first three equations are the matching conditions (4.7a) while the fourth is the (tz) component of (4.7b), where we have used the second equation to simplify it. The three (almost) redundant matching conditions can be actually combined into an algebraic equation for D, so the integration constant in the last equation of (4.19) is fixed as in eq. (4.25), see below.

Consider first the homogeneous equations obtained by setting the right-hand sides in (4.19) to zero. The general solution reads

$$\begin{aligned} -i\omega\lambda(z) &= \frac{\Delta(z)}{z} = a_+ e^{i\omega z} + a_- e^{-i\omega z}\,, \\ -i\omega\zeta(z) &= a_+ e^{i\omega z} - a_- e^{-i\omega z}\,, \quad D = 0\,. \end{aligned} \tag{4.24}$$

The $z = 0$ limit of these functions corresponds to sources in the dual ICFT. For instance $\delta_L(0) = \delta_R(0)$ is a source for the interface displacement operator.[9] Linearizing in this source gives an $O(z^{-3})$ correction to the induced metric. This is consistent with the fact that the scaling dimension of the displacement operator is $\mathfrak{D} = 2$ [161]. In the absence of gravity waves, setting the sources to zero implies $a_+ = a_- = 0$. This shows that there are no normalizable states supported entirely by the interface.

Let's go back now to the inhomogeneous equations (4.19). Since these are linear equations, the general solution is given by (4.24) plus some special solution. The result after straightforward manipulations is

cally zero. Note that in D spacetime dimensions the same counting gives $(D-1)^2$ matching conditions for $D+1$ arbitrary functions, so that for $D > 3$ two generic spacetimes cannot be matched.

[9] Similarly, $\lambda(0)$ is the source for the dual operator that generates a relative reparametrization of the interface [49].

$$\frac{\Delta(z)}{z} = \frac{1}{\omega^2\cos\theta_L}(\mathbf{I}+\mathbf{R}) - \frac{1}{\omega^2\cos\theta_R}\mathbf{T} + a_+e^{i\omega z} + a_-e^{-i\omega z}\,, \tag{4.25}$$

$$\zeta(z) = -\frac{\cos\theta_L z}{\omega^2}(\mathbf{I}+\mathbf{R}) - \frac{i}{\omega^3}(\mathbf{I}-\mathbf{R})\left(\tan\theta_L + \frac{\sin\theta_L\cos\theta_L}{2}\omega^2z^2\right) \tag{4.26}$$

$$- \frac{i}{\omega^3}\mathbf{T}\left(\tan\theta_R + i\cos\theta_R\omega z + \frac{\sin\theta_R\cos\theta_R}{2}\omega^2z^2\right) + \frac{i}{\omega}\left(a_+e^{i\omega z} - a_-e^{-i\omega z}\right)\,, \tag{4.27}$$

$$\lambda(z) = \frac{i}{\cos\theta_L\omega^3}(\mathbf{I}+\mathbf{R})\left(1 - \frac{\cos^2\theta_L}{2}\omega^2z^2\right) - \frac{i}{\cos\theta_R\omega^3}\mathbf{T}\left(1 - \frac{\cos^2\theta_R}{2}\omega^2z^2\right)$$

$$+ \frac{i}{\omega}\left(a_+e^{i\omega z} + a_-e^{-i\omega z}\right)\,, \tag{4.28}$$

$$D(z) = -\frac{i}{\omega^3}(\mathbf{I}-\mathbf{R})\left(1 + \frac{\cos^2\theta_L}{2}\omega^2z^2\right) + \frac{\sin\theta_L z}{\omega^2}(\mathbf{I}+\mathbf{R})$$

$$+ \frac{i}{\omega^3}\mathbf{T}\left(1 - i\sin\theta_R\omega z + \frac{\cos^2\theta_R}{2}\omega^2z^2\right)\,. \tag{4.29}$$

Requiring that the sources vanish now gives

$$D(0) = 0 \implies \mathcal{R}_L + \mathcal{T}_L = 1\,, \tag{4.30}$$

and further from $\zeta(0) = \lambda(0) = 0$ we obtain:

$$a_+ = \frac{1}{2\omega^2}\Big[\mathcal{T}_L\Big(\frac{1+\sin\theta_R}{\cos\theta_R} + \tan\theta_L\Big) - \frac{(1+\mathcal{R}_L)}{\cos\theta_L}\Big]\,, \tag{4.31}$$

$$a_- = \frac{1}{2\omega^2}\Big[\mathcal{T}_L\Big(\frac{1-\sin\theta_R}{\cos\theta_R} - \tan\theta_L\Big) - \frac{(1+\mathcal{R}_L)}{\cos\theta_L}\Big]\,. \tag{4.32}$$

The reader can verify that with these choices all four functions are $O(z^3)$ near the conformal boundary, and make $O(1)$ contributions to the worldsheet metric which can be interpreted as ICFT vevs. This agrees again with the fact that the scaling dimension of the displacement operator is two [161].

Inserting the solution for $\delta_{L,R}$ in the expression for the induced metric shows that the latter is locally AdS_2 (constant intrinsic Ricci curvature). Thus, as is the case for homogeneous AdS_3/CFT_2, here too the dynamics happens at the conformal boundary in spite of the presence of the string/interface.

Up to this point, we have obtained a solution for the equations of motion of our model, that is valid for any value of $\mathcal{T}_L$. To proceed further, we have to make an assumption about the behaviour of the solution at the Poincaré horizon, as mentioned in the introduction. It is well-known that in the Lorentzian AdS/CFT correspondence the boundary conditions at the conformal boundary do not determine the solution uniquely, because there are normalizable modes that vanish at the boundary and are regular in the interior [173]; this is the dual of the property that there are different Minkowskian QFT propagators, depending on the choice of the initial state (retarded, advanced, Feynman etc.).[10]

[10] One could try to circumvent the problem by going to Euclidean signature, however in AdS_3 there are subtleties because one finds infrared divergences at $z \to \infty$ that must be regulated (in [48] an IR cutoff was used) and this

The prescription of [176,177] (generalized by [178]), frequently used in the literature, requires the absence of modes coming out of the horizon for the computation of a retarded correlator. In our case it is not immediately obvious how to apply this prescription, since the problem is not formulated as the computation of a causal response.[11] One difficulty is that wave packets formed from (4.13) are localized in $u_{L,R}$ but not in the radial AdS coordinates $y_{L,R}$. Such wavepackets imprint superluminal waves on the functions $\delta_{L,R}$, ζ and λ of the form $e^{i\omega t} \times (\mathbf{I}, \mathbf{R}$ or $\mathbf{T})$, see eq. (4.23). But as illustrated by seawaves hitting an oblique seashore, these superluminal waves carry no energy. To see why, one must look at gauge-invariant quantities left unchanged by common reparametrizations of the two charts, $\delta\zeta_L = \delta\zeta_R$ and $\delta\lambda_L = \delta\lambda_R$. One such quantity, at the linearized order considered here, is the traceless part of the extrinsic curvature which is continuous across the worldsheet by Israel's matching condition (4.7b).[12] A simple calculation gives

$$\hat{K}_{\pm\pm} = \frac{a_\pm\, \omega^2 \epsilon}{2\pi\sigma\ell_W} e^{i\omega x^\pm} + \mathcal{O}(\epsilon^2)\ , \tag{4.33}$$

where $x^\pm = t \pm z$ and $\hat{K}_{\alpha\beta}$ denotes the traceless part of $K_{\alpha\beta}$. Note that the superluminal waves disappeared from the above expression, and that the 'no outgoing wave' condition reduces to $a_+ = 0$. Note in addition that the (discontinuous) trace parts, $K_{L,R} = \pm\frac{2}{\ell_W}\tan(\theta_{L,R}) + \mathcal{O}(\epsilon^2)$, are not perturbed at linear order.

With the help of equations (4.30) and (4.31), the no-outgoing-wave condition implies

$$\mathcal{T}_L = \frac{2\cos\theta_R}{\cos\theta_R(1+\sin\theta_L) + \cos\theta_L(1+\sin\theta_R)}\ . \tag{4.34}$$

Trading the angles for $\ell_{L,R}$ and σ gives our result (4.4). It is non-trivial that $\mathcal{R}_L$ and $\mathcal{T}_L$, which started out as complex amplitudes in the gravitational-scattering problem, ended up as real, positive reflection and transmission coefficients as required for a proper ICFT interpretation. This together with the fact that our result obeys the non-trivial ANEC bound (4.6) is a strong *a posteriori* argument for the correctness of the above assumption.[13]

4.2 Summary and Outlook

In this letter we evaluated the reflection and transmission from thin-brane holographic interfaces in AdS_3. We found that the result (4.6) for the reflection coefficient is consistent with the lower ANEC bound, while its maximum approaches $\mathcal{R} = 1$ only in the limit of infinite ratio of the central charges. This imperfect reflection might be a generic feature of holographic interfaces.

It would be interesting to study applications of our work in condensed matter systems, as well as explore other holographic models, higher dimensions and quantum-gravitational corrections. Of special interest are the 1/2-BPS holographic interfaces of $N = 4$ super Yang-Mills [180, 181] and the associated top-down embedding of massive gravity [182]. Another important issue that will be discussed in a future publication [49] is universality, in particular why $\mathcal{R}_{L,R}$ and $\mathcal{T}_{L,R}$ are

would introduce some ambiguities.

[11] Perhaps this can be done using an alternative definition of $\mathcal{T}$ in terms of a 3-point function [51].

[12] It is also covariant under Weyl transformations of the bulk geometry [179].

[13] For instance, one can check that the condition $a_- = 0$ would lead to unphysical values for $\mathcal{T}$.

independent of the nature of the incident wave as has been shown in the dual CFT_2 [51].

It is also interesting to explore the relation of our work to the recent discussions of the Page curve that describe the entanglement entropy between an evaporating black hole and its Hawking radiation through the appearance of islands behind the horizon. This has been evaluated in a class of toy models where the black hole is coupled to a heat bath via transparent boundary conditions [183, 184]. Holographic realizations corresponding to this scenario were put forward for example in [185–189] in terms of doubly holographic BCFT/ICFT models. Our results on reflection and transmission could come to use when coupling the black hole to the bath – we hope to return to this question in the future.

In this context it has been also pointed out that the transmission of energy across an interface differs from the transmission of information. It would be interesting to compare our results to various information theoretic measures and their dynamics in the presence of defects, see *e.g.,* [18, 102, 128, 136, 147, 155, 170].

Chapter 5

Revisiting Circuit Complexity in 2d Bosonisation

This Chapter is based on the work [20].

Recently, much attention has been devoted to the study of quantum complexity in connection with the holographic correspondence. Quantum complexity is a concept that has its origin in quantum computation theory as a means of characterizing the difficulty (in the sense of the amount of resources needed) of performing a task on a quantum computer; more precisely, if the task can be described as producing a certain quantum state $|\psi_T\rangle$ from a given initial state $|\psi_R\rangle$ using a circuit made of elementary unitary operations (gates), the quantum complexity can be defined as the minimum number of gates required for such a circuit. It has been suggested by Susskind and collaborators [16, 89, 190, 191] that the notion of complexity may be an important component in our understanding of the properties of emergent spacetime, and possibly point to a solution of the information loss paradox, by giving additional insight, beyond what can be obtained from entanglement entropy, into the information-theoretic properties associated to spacetime and in particular to the region inside black hole horizons (see the recent lectures [192]).

It was further conjectured that, similarly to entanglement entropy which is described holographically by the area of a minimal surface [11], quantum complexity is also captured, in a theory with a holographic dual, by a simple gravitational observable. However what precisely is the observable is unclear. There are two different proposals: one takes the volume of a maximal spatial slice of the geometry [16], the other takes the action evaluated on the *Wheeler-DeWitt* patch [17, 57]. Each proposal has its merits and drawbacks, and a clear-cut way to choose one over the other has not been found yet. In particular, both prescription lead to similar behavior for the late-time growth of complexity during the formation of a black-hole (i.e., linear growth in time, albeit with different coefficients [91, 92]), and have similar structure of UV divergence

$$\mathcal{C} \sim a \frac{V}{\delta^{d-1}} (1 + \mathcal{O}(\delta)) \,, \tag{5.1}$$

where d is the spacetime dimension of the dual field theory, δ is a short-distance cutoff, and a is a coefficient that depends on the prescription.[1]

[1] In the case of the action, there can be a further divergence of the form $\frac{1}{\delta^{d-1}} \ln \delta$ [64], but it can be removed by a boundary counterterm [63] which is also needed to make the prescription reparametrization invariant.

Even in cases when the two prescriptions give different results (e.g., in the case of an AdS_3 space with a defect brane, as we found in our paper with S. Chapman [18]), we do not have at present a criterion for choosing one over the other, absent any independent calculation that can serve as benchmark. By contrast, in the case of the entanglement entropy, one can compute it in a 2d CFT, for an interval of length ℓ, and obtain the famous exact result [193]

$$S_{EE} = \frac{c}{3} \log\left(\frac{\ell}{\delta}\right) , \tag{5.2}$$

which depend only on the central charge c. Because the coefficient of the log does not change under a rescaling of the cutoff, it can be considered a universal quantity with a well-defined physical meaning. By analogy, one could try to attribute a similar universal meaning to the coefficient of the "log" in the complexity, but the situation is less clear.

The problem is that the definition in terms of gates, which is applicable to a finite quantum system, does not translate easily to a definition that is applicable to a continuum quantum field theory. In other words, we do not know how to associate the notion of complexity to a well-defined observable in QFT. This problem was considered in [65, 67], who provided a partial answer by proposing a definition of complexity for free scalar fields. The proposal of [65] used the Nielsen's approach of *geometrization* of quantum computation [194], while [67] used a method based on the Fubini-Study metric [2]. In Nielsen's method, described in more detail in Section 2.3.2, the circuit is replaced by a continuous version that is a path in the space of unitary operators, of the form

$$U(s) = \mathcal{P}\exp\left(-i \int_0^s ds' \, Y^I(s') \mathcal{O}_I\right) , \tag{5.3}$$

The functions $Y^I(s)$ are determined by minimization of a certain functional $F[Y^I(s)]$ that determines the *cost* associated to a given path. The complexity of a unitary operator V is then defined as the minimum of the cost functional over all paths (5.3) such that $U(s=1) = V$.

What is important to notice here is that this definition of complexity depends on several choices: the choice of the allowed space of operators used to build the circuit [3], and indeed of a specific basis $\mathcal{O}_I$, the choice of a cost functional, and a choice of parametrization of the path.

The space of unitary operators acting on the Hilbert space of a QFT is very large, but one of the main points of [65] was to reduce it to a tractable setup by considering operators that act within the subset of Gaussian states. This allows one to consider the complexity of any state that is the ground state of any Hamiltonian quadratic in the fields. Discretizing the free scalar field to a set of N harmonic oscillators, a Gaussian state is described by a symmetric $2N \times 2N$ matrix, and the group of unitary operators that preserves the Gaussian states is $Sp(2N)$. In [65] the behaviour of the complexity between Gaussian states was investigated for various choices of cost functions, mostly focusing on the one corresponding to the Cartan-Killing metric on the symplectic group.

The approach used in [67] considers a path in the space of states; the complexity is identified with the minimal length of a path connecting two states, calculated in the standard Fubini-Study metric on the space of normalized states. For a parametrized path of quantum states $|\psi(\sigma)\rangle$, the

[2] For other approaches and follow-ups see [68–72, 75, 123, 195, 196].

[3] If the space of all operators is allowed, then obviously all circuits would have the same complexity.

line element is

$$ds = d\sigma \sqrt{\langle \partial_\sigma \psi(\sigma) | \partial_\sigma \psi(\sigma) \rangle - |\langle \psi(\sigma) | \partial_\sigma \psi(\sigma) \rangle|^2}\,. \tag{5.4}$$

This definition may seem more canonical, but if one allows the most general path in the space of states, then the geodesic distance between normalized states is always less or equal to $\pi/2$. In order to have a sensible measure of complexity, one must somehow restrict the possible paths. The proposal of [67] is to use paths that can be obtained using unitary operators similar to (5.3), with the basis operators being a subset of the bilinears the creation and annihilation operators; thus in both approaches one does not leave the space of Gaussian states, and the results are comparable.

Nielsen's approach was extended to the case of free fermions in [66, 73]. In comparison to the bosonic case, the main difference is that the relevant group of operators acting on Gaussian states is $SO(2N)$, which is a compact group, with the consequence that the complexity (again measured using the Cartan-Killing metric) cannot grow very large. Considering a field theory in d spacetime dimension with spatial volume V and a UV cutoff Λ, it turns out that the leading divergent term in the bosonic complexity is

$$\mathcal{C}^b_\Lambda \sim V \Lambda^{d-1} |\ln(\Lambda/\omega_0)|^\kappa, \tag{5.5}$$

where ω_0 is an arbitrary reference scale and κ is a parameter related to the choice of the cost function, whereas for a free fermion field theory is

$$\mathcal{C}^f_\Lambda \sim V \Lambda^{d-1}. \tag{5.6}$$

The discrepancy seems at odds with the holographic interpretation, as the holographic result is relatively blind to the fermionic or bosonic nature of the dual fields. Moreover, for the case of a two-dimensional theory, we might think that the bosonization map between bosons and fermions should imply the equality of the two results. These observations do not constitute a strong objection to the results of [65–67, 73], because states with a holographic dual are not Gaussian states, the theory is strongly coupled whereas (5.5) and (5.6) are obtained for free fields, and complexity is not a well-defined field theory observable in the usual sense, as we stressed. Nevertheless, they provide the motivation for the present chapter, where we look more closely at the complexity for bosons and fermions in 1+1 dimensions, comparing states that are related by bosonisation. From this point of view, the results (5.5) and (5.6) do not constitute a discrepancy, rather they illustrate the effect of a different choice of operator spaces.

In the context of quantum computation, the question of the choice of gates is of obvious importance, and there are some known results: when the gates act on arrays of qubits, it is possible to show that there is a universal finite set of gates, such that any unitary operator can be approximated by a circuit made of universal gates with an arbitrarily small error ϵ (see *e.g.* [197]), and the size of the circuit is $\mathcal{O}(\ln^c(1/\epsilon))$, for some constant c. Moreover, if a circuit has complexity m with some choice of basic gates, a different choice will give complexity $\mathcal{O}(m \ln^c(m/\epsilon))$ [198], so the dependence on the basis choice is at most logarithmic.

It would be nice to establish similar results in the QFT context, but so far almost nothing can be said about the gate dependence. In most of the works on the complexity, the choice of

gates was restricted to gates quadratic in the fields, in order not to depart from the space of Gaussian states. No fundamental reason underlies this choice except that it allows to do explicit computations, and it is not obvious how to make an alternative choice: in general it is difficult to find an algebraically closed set of gates that is larger than the set of quadratic operators but not as large as the full space [72, 199]. But it turns out that such a set is provided by the magic of bosonisation.

The reason for this is that the bosonisation map is very non-linear, so Gaussian states in one description generically do not correspond to Gaussian states in the other, and similarly gates that are oscillator bilinears in one description will map to more complicated gates in the other. Thus we can have a completely solvable example where it is possible to explore the effect of different choice of gate sets on the complexity.

We have started to undertaken this exploration in the present chapter. We are not yet in a position to make general statements about the effect of a change of gates, since we are limited to the states whose complexity can be computed using the available technology. We have identified two such classes of states. In the first class, the states are bosonic-coherent and fermionic-gaussian. For the states in this class, we can compute the complexity analytically, and we find that it has a similar form in the two descriptions, see the results in (5.43) and (5.63), however the fermionic complexity appears to have a cost that depends on the mode number of the bosonic oscillator that is excited. Thus, the difference of complexity can become arbitrarily large, even with a single mode.

In the second class, the states are both bosonic-gaussian and fermionic-gaussian [4]. These states can be understood as ground states of a system with a free but inhomogeneous hamiltonian. They are parametrized by an arbitrary function; we considered some examples with the function having only one or only two Fourier components. We cannot find analytic results in this case but have to resort to numerics. The numerical results are given in Figures 5.5, 5.6 and 5.7, and show striking differences between the bosonic and the fermionic result. The bosonic complexity for these states is cutoff-independent, and smoothly dependent on the parameters corresponding to the Fourier modes, whereas for fermions it grows like $\ln(\Lambda)$, and it is much less regular (it appears to be quasi-periodic in the simplest case).

The plan of the chapter is the following: in Section 5.1 we recall the basic properties of the bosonisation equivalence and the correspondence between fermionic and bosonic states. In Section 5.2 we compute the complexity of a class of bosonic coherent states in terms of bosonic gates by using the *Fubini-Study* metric method. In Section 5.3 we use the *Nielsen* method to compute the complexity of bosonic coherent states using fermionic gates. In Section 5.4 we describe a class of states that are of gaussian type both in the fermionic and in the bosonic description, and we compare the results for the complexity computed in either description. In Section 5.5 we present our conclusions. Some additional details of the computations are presented in Appendix B.

[4] The existence of such states has not been remarked before, to our knowledge.

5.1 2D Bosonisation

5.1.1 Basic Ingredients

In this section, we will review the basics of the 2D bosonisation formalisms, for free bosons and fermions, which we will use in the rest of the chapter. We follow the presentation in [200]. In two dimensions, the bosonisation can be proved exactly for a system on a finite size interval $[-L/2, L/2]$. In such a system, the unbounded momentum k satisfies

$$k = \frac{2\pi}{L}\left(n_k - \frac{\delta_b}{2}\right), \qquad n_k \in \mathbb{Z}, \qquad \delta_b \in [0, 2) \tag{5.7}$$

where δ_b depends on the periodicity condition of the fermionic fields, 0 for complete periodicity and 1 for anti-periodicity. If there are M chiral fermions with periodic conditions ($\delta_b = 0$) in the system, an index η could be used to denote different types of fermions, and the mode decomposition for each fermion type is given as

$$\psi_\eta(x) = \left(\frac{2\pi}{L}\right)^{1/2} \sum_{n=-\infty}^{\infty} e^{-i\frac{2\pi n}{L}x} c_{n\eta}, \qquad c_{n\eta} = (2\pi L)^{-1/2} \int_{-L/2}^{L/2} dx e^{i\frac{2\pi n}{L}x} \psi_\eta(x)\,, \tag{5.8}$$

where $\eta = 1, 2, \ldots, M$, can be *spin, handedness, flavor* etc. The bosonic chiral fields are given by the mode decomposition

$$\phi_\eta(x) = -\sum_{n>0} \frac{1}{\sqrt{n}} (e^{-i\frac{2\pi n}{L}x} b_{n\eta} + e^{i\frac{2\pi n}{L}x} b^\dagger_{n\eta}) e^{-a\frac{\pi n}{L}}\,, \tag{5.9}$$

where the zero mode is omitted. Notice that only $n > 0$ modes are included, because of the chirality. The a appearing in the last factor is a regularisation parameter that should be sent to zero when computing physical quantities.[5]

By construction, there is an operator identity at the level of annihilation and creation operators between fermions and bosons,

$$b_{n\eta} = \frac{-i}{\sqrt{n}} \sum_{l=-\infty}^{\infty} c^\dagger_{l-n\ \eta} c_{l\eta}, \qquad b^\dagger_{n\eta} = \frac{i}{\sqrt{n}} \sum_{l=-\infty}^{\infty} c^\dagger_{l+n\ \eta} c_{l\eta} \tag{5.10}$$

from where we see that the bosonic operators are always an infinite sum of fermionic operators of quadratic type containing both the creation and annihilation ones. We can take (5.10) as a definition of the bosonic modes; the proof of bosonisation amounts to showing that, with this definition, the bosonic commutation relations are satisfied if the fermionic ones are:

$$\{c_{l\eta}, c^\dagger_{\tilde{l}\tilde{\eta}}\} = \delta_{\eta\tilde{\eta}}\delta_{l\tilde{l}} = [b_{l\eta}, b^\dagger_{\tilde{l}\tilde{\eta}}]. \tag{5.11}$$

The bosonisation formula can also be stated in terms of the local fields:

$$i\partial_x \phi_\eta(x) = :\psi^\dagger_\eta(x)\psi_\eta(x):\,, \tag{5.12}$$

[5] Notice that the bosonisation is exact only when all the modes are included. In practice we often need to introduce a UV cutoff on the mode number; we still expect that we can match quantities that are cutoff-independent.

with the colon denoting normal ordering. The inverse formula is more complicated:

$$\psi_\eta(x) = F_\eta\, a^{-1/2} e^{-i\frac{2\pi}{L}(\hat{N}_\eta - \frac{\delta_b}{2})x}\, :e^{-i\phi_\eta(x)}:, \tag{5.13}$$

where $\hat{N}_\eta = \sum_l : c_{l\ \eta}^\dagger c_{l\ \eta} :$ is the fermionic number operator with respect to the ηth spiecies. From (5.10), it is easy to see that the bosonic operators commute with the fermionic number operator, *i.e.,*

$$[b_{n\ \eta}, \hat{N}_\eta] = 0, \qquad [b_{n\ \eta}^\dagger, \hat{N}_\eta] = 0\,, \tag{5.14}$$

so only fermionic operators that don't change the fermion number can strictly speaking be bosonised. The so-called Klein factor F_η in (5.13) has the role of compensating the mismatch in fermion number (this factor is often omitted in many presentations of bosonisation). However we will not need its explicit expression.

The commutation relation between bosonic and fermionic modes is

$$[b_l, c_{\tilde{l}}] = \frac{i}{\sqrt{l}} c_{\tilde{l}+l}, \qquad [b_l^\dagger, c_{\tilde{l}}^\dagger] = \frac{i}{\sqrt{l}} c_{\tilde{l}+l}^\dagger, \tag{5.15}$$

$$[b_l, c_{\tilde{l}}^\dagger] = \frac{-i}{\sqrt{l}} c_{\tilde{l}-l}^\dagger, \qquad [b_l^\dagger, c_{\tilde{l}}] = \frac{-i}{\sqrt{l}} c_{\tilde{l}-l}. \tag{5.16}$$

Intuitively we can think that $b_l^\dagger$ creates, and b_l annihilates, a particle-hole pair of total momentum l.

In the following, we will consider the simplest case with only two chiral fermions and one chiral bosons, thus the species index will be omitted.

5.1.2 Fermionic Fock space

In the fermionic Fock space $\mathcal{F}$, a unique vacuum $|0\rangle$ is defined in terms of the fermionic modes,

$$c_n |0\rangle = 0, \quad n > 0; \qquad c_n^\dagger |0\rangle = 0, \quad n \leq 0. \tag{5.17}$$

In the bosonised picture, the Fock space can be reorganised as a direct sum of all the Hilbert space with fixed fermionic particle number, i.e.,

$$\mathcal{F} = \oplus_N \mathcal{H}_N. \tag{5.18}$$

Each $\mathcal{H}_N$ with fixed fermion number can be regarded as the bosonic Hilbert space since the bosonic operators commute with the fermionic number operator as mentioned before. The condition for a bosonic ground state is to be annihilated by all the bosonic annihilation operators

$$b_n |\mathcal{G}_B\rangle = 0, \qquad n > 0. \tag{5.19}$$

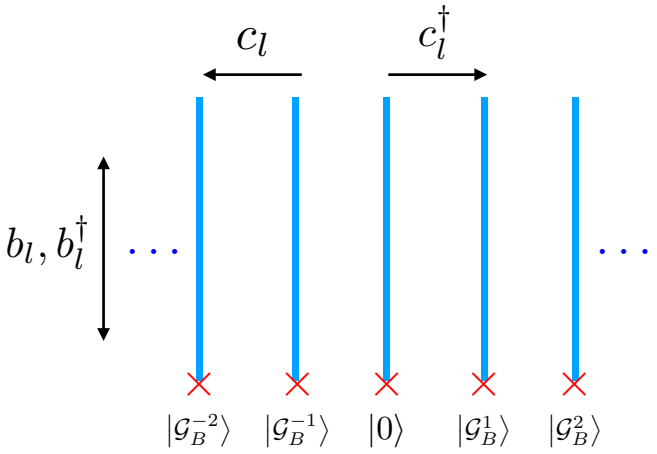

Figure 5.1: The base manifold $\mathcal{G}_B$ is made of all the bosonic ground states which are denoted as the red crosses. The vertical blue lines are modules of the fermionic fock space where each represents a bosonic Hilbert space with fixed fermion number. The operators of bosonic type can only move vertically while the fermionic ones span the whole Fock space with a single fermionic operator moving horizontally.

This condition uniquely defines a state in each module $\mathcal{H}_N$; then the ground state $|\mathcal{G}_B\rangle$ in the N-particle module is denoted as

$$|\mathcal{G}_B^N\rangle = \begin{cases} c_N^\dagger c_{N-1}^\dagger \cdots c_1^\dagger |0\rangle\,, & N > 0 \\ |0\rangle\,, & N = 0 \\ c_{N+1} c_N \cdots c_0 |0\rangle\,, & N < 0 \end{cases} . \tag{5.20}$$

Figure 5.1 gives a depiction of the Fock space as a bundle, with the base given by the ground states and the fiber by the bosonic Hilbert space. The bosonic operators act inside a single fiber, whereas fermionic operator can move between different fibers.

5.1.3 Correspondence between states

Our main purpose in this note is to compare the circuit complexity of states in the bosonic and fermionic descriptions. We cannot consider the most general state, since the techniques developed so far only allow to deal with Gaussian states or coherent states. Our first task is to determine the correspondence between Gaussian/coherent states in both descriptions.

It is clear that, since the bosonisation relations (5.12)-(5.13) are non-linear, Gaussian states in one description will not correspond in general to Gaussian states in the other. It is shown in [66] that all Gaussian states can be obtained from the fermionic vacuum (5.17) by the action of a unitary operator of the form

$$\mathcal{O}_F = e^{A^{lm} c_l c_m + B^{lm} c_l c_m^\dagger + D^{lm} c_l^\dagger c_m^\dagger}\,. \tag{5.21}$$

Equivalently, each such states is a vacuum under a set of modes related to the original ones by a Bogoliubov transformation

$$\tilde{c}_l = \mathcal{A}_{lm} c_m + \mathcal{B}_{lm} c_m^\dagger\,. \tag{5.22}$$

It is easy to see then that states of the form

$$c^\dagger_{n_1} c^\dagger_{n_2} \cdots c^\dagger_{n_k} c_{m_1} c_{m_2} \cdots c_{m_q} |0\rangle \tag{5.23}$$

with $n_1 > n_2 > \cdots > n_k > 0 \geq m_1 > m_2 > \cdots > m_q$, are Gaussian states; these include in particular the bosonic ground states of (5.20).

Another class of fermionic Gaussian states is given by

$$|\{\alpha_k, n_k\}, N\rangle = e^{\sum_k \alpha_k b^\dagger_{n_k} - \alpha^*_k b_{n_k}} |\mathcal{G}^N_B\rangle \,, \tag{5.24}$$

obtained from the ground state with the action of the *displacement operator* which is a fermion bilinear (see (5.10)). These are bosonic coherent states, therefore not Gaussian but still tractable. In the next sections we will analyze the complexity of the last class of states, first from the bosonic and then from the fermionic perspective.

5.2 *Fubini-Study* Method for Bosonic Coherent States

In the FS approach, the complexity $\mathcal{C}(|\psi_1\rangle, |\psi_2\rangle)$ is computed as the geodesic distance between two states $|\psi_1\rangle$ and $|\psi_2\rangle$, with respect to the Fubini-Study metric on the projective Hilbert space $\mathcal{H}/\mathbb{C}^*$. The metric can be described as follows: given a parametrised path $|\psi(\sigma)\rangle$ on the manifold of normalized states, the line element, *i.e.,* the length of the tangent vector to the path, is

$$ds = d\sigma \sqrt{\langle \partial_\sigma \psi(\sigma) | \partial_\sigma \psi(\sigma)\rangle - |\langle \psi(\sigma) | \partial_\sigma \psi(\sigma)\rangle|^2} \,. \tag{5.25}$$

Equivalently, for a family of states $\psi(\lambda)$ parametrized by coordinates λ^i, the FS metric is $g_{ij} d\lambda^i d\lambda^j$, with

$$g_{ij} = \langle \partial_{(i} \psi | \partial_{j)} \psi\rangle - \langle \partial_i \psi | \psi\rangle \langle \psi | \partial_j \psi\rangle \ . \tag{5.26}$$

The complexity of coherent states of a set of harmonic oscillators was considered in [134] using both the Nielsen approach and the Fubini-Study approach. In order to use the Nielsen's approach with bosonic gates, we would need to to embed the coherent states in a larger space acted on by $GL(n)$, therefore in this section we will use the FS method for simplicity. The results of [134] show that the FS complexity is very closely related to the Nielsen complexity with the cost function given by the invariant metric on the group. See also [112] for a different approach based on Finsler geometry.

Let us consider the coherent states as described in the previous section. For simplicity we start with the case of a displacement operator acting only on one mode of the bosons. We consider the one-complex-parameter family of states

$$|\psi(\alpha)\rangle = |\alpha, n, N\rangle = U_n(\alpha) |\mathcal{G}^N_B\rangle \ , \tag{5.27}$$

where the displacement operators

$$U_n(\alpha) = e^{\alpha b_n^\dagger - \alpha^* b_n} = e^{\alpha b_n^\dagger} e^{-\alpha^* b_n} e^{-\frac{1}{2}\alpha\alpha^*}, \tag{5.28}$$

$$U_n^\dagger(\alpha) = e^{-\alpha b_n^\dagger + \alpha^* b_n} = e^{-\alpha b_n^\dagger} e^{\alpha^* b_n} e^{-\frac{1}{2}\alpha\alpha^*} \tag{5.29}$$

satisfy

$$\partial_\alpha U_n(\alpha) = b_n^\dagger\, U_n(\alpha) - \frac{1}{2}\alpha^*\, U_n(\alpha), \quad \partial_{\alpha^*} U_n(\alpha) = -U_n(\alpha) b_n - \frac{1}{2}\alpha\, U_n(\alpha), \tag{5.30}$$

$$\partial_\alpha U_n^\dagger(\alpha) = -b_n^\dagger U_n^\dagger(\alpha) - \frac{1}{2}\alpha^*\, U_n^\dagger(\alpha), \quad \partial_{\alpha^*} U_n^\dagger(\alpha) = U_n^\dagger(\alpha) b_n - \frac{1}{2}\alpha\, U_n^\dagger(\alpha)\,. \tag{5.31}$$

It is useful to notice the commutation relations

$$[b_n, U_l(\alpha)] = \delta_{ln}\,\alpha\, U_n(\alpha), \qquad [U_l^\dagger(\alpha), b_n^\dagger] = \delta_{ln}\,\alpha^*\, U_n^\dagger(\alpha)\,, \tag{5.32}$$

from which it follows that

$$\langle U_n^\dagger(\alpha) b_n U_n(\alpha)\rangle = \alpha\,, \quad \langle U_n^\dagger(\alpha) b_n^\dagger U_n(\alpha)\rangle = \alpha^*\,, \tag{5.33}$$

where $\langle \ldots \rangle$ denotes the vev in the state $|\mathcal{G}_B^N\rangle$. The FS metric components can be computed:

$$g_{\alpha\alpha} = \langle \partial_\alpha U_n^\dagger(\alpha)\, \partial_\alpha U_n(\alpha)\rangle - \langle \partial_\alpha U_n^\dagger(\alpha)\, U_n(\alpha)\rangle \langle U_n^\dagger(\alpha) \partial_\alpha U_n(\alpha)\rangle = 0\,, \tag{5.34}$$

$$g_{\alpha^*\alpha} = \langle \partial_{\alpha^*} U_n^\dagger(\alpha)\, \partial_\alpha U_n(\alpha)\rangle - \langle \partial_{\alpha^*} U_n^\dagger(\alpha) U_n(\alpha)\rangle \langle U_n^\dagger(\alpha) \partial_\alpha U_n(\alpha)\rangle = 1\,. \tag{5.35}$$

We obtain then that the FS metric is a flat Kähler metric

$$ds^2 = d\alpha\, d\alpha^*, \tag{5.36}$$

as expected, since it is known that in quantum mechanics coherent states form a two-dimensional *Kähler manifold* which can be parametrized by classical phase space variables [201].

For our purposes it is important to notice that the result does not depend on either the fermion number N, or the bosonic oscillator number n. We can easily understand the N-independence since all the bosonic Hilbert spaces $\mathcal{H}_\mathcal{N}$ are equivalent to each other. The independence on the mode number indicates that the FS metric corresponds to a cost function that assigns the same cost to all displacement operators U_n. This is also natural since the FS metric is derived from the scalar product in the Hilbert space, which has no information about the energy levels apart from the fact that they are orthogonal to each other. It is trivial to compute the geodesic length in the flat metric:

$$\mathcal{C}_{FS}(|\mathcal{G}_B^N\rangle\,, |\psi(\alpha)\rangle) = |\alpha|\,. \tag{5.37}$$

This agrees with the result of [112]; the result of [134] is $\mathcal{C}_{FS}(\alpha) = \operatorname{arccosh}(1 + \frac{|\alpha|^2}{2})$, which agrees with (5.37) for small α, while for larger α it is smaller, which means that one can find shorter geodesics if the coherent states are embedded in the larger space mentioned at the beginning of this section.

The general case of coherent states contains displacement operators acting on several modes:

$$|\psi(\alpha)\rangle = \prod_{i=1}^{k} U_{n_i}(\alpha_i)\,|\mathcal{G}_B^N\rangle\ , \tag{5.38}$$

with $n_i \neq n_k$ for $i \neq k$. In order to compute the metric it is enough to consider the case of two modes:

$$|\psi(\alpha,\beta)\rangle = |\alpha,\beta;m,n;N\rangle = U(\alpha,\beta)\,|\mathcal{G}_B^N\rangle\ , \quad U(\alpha,\beta) = U_m(\alpha)U_n(\beta)\,. \tag{5.39}$$

The off-diagonal metric components are

$$g_{\alpha\beta} = \frac{1}{2}\langle\partial_\alpha U^\dagger\partial_\beta U\rangle + \frac{1}{2}\langle\partial_\beta U^\dagger\partial_\alpha U\rangle - \langle\partial_\alpha U^\dagger U\rangle\langle U^\dagger\partial_\beta U\rangle = 0\,, \tag{5.40}$$

$$g_{\alpha^*\beta} = \langle\partial_\alpha^* U^\dagger\partial_\beta U\rangle - \langle\partial_\alpha^* U^\dagger U\rangle\langle U^\dagger\partial_\beta U\rangle = 0\,. \tag{5.41}$$

It is easy to see that since the displacement operators of different modes commute, this applies for any number of excited modes. Therefore the metric is a direct product of the metrics for the individual modes:

$$ds^2 = \sum_i d\alpha_i d\alpha_i^* \tag{5.42}$$

and the complexity of a general coherent state is

$$\mathcal{C}_{FS}(|\mathcal{G}_B^N\rangle\,, \prod_i^k U_{n_i}(\alpha_i)\,|\mathcal{G}_B^N\rangle) = \sqrt{\sum_{i=1}^{k}|\alpha_i|^2}\,. \tag{5.43}$$

5.3 Application of *Nielsen* Method on Bosonic Coherent States

In this section, we apply the method introduced in Section 2.3.2 on the bosonic coherent states with instead fermionic gates.

5.3.1 Complexity between Bosonic Ground States

As a first simple application of the formalism, we can compute the complexity of the bosonic ground states $\mathcal{G}_B^N$ defined in (5.20), which constitute a subset of the fermionic gaussian states, as already noticed. These states are labeled by the fermion number N. The Bogoliubov transformation that takes from $|\mathcal{G}_B^0\rangle$ to $|\mathcal{G}_B^m\rangle$ is (for m positive)

$$\tilde{c}_l = c_l^\dagger\,, \qquad \tilde{c}_l^\dagger = c_l\,, \qquad 1 \leq l \leq m\,. \tag{5.44}$$

The corresponding matrix M changes the sign of $p_l, 1 \leq l \leq m$ and it is in $SO(2N)$ only if m is even. As noticed before, we can only find geodesic paths between states that have the same parity of fermion number.

The covariance matrix Δ in this case is the identity, except for $2n$ diagonal entries that are equal to -1. Applying (2.61) we find

$$\mathcal{C}(|\mathcal{G}_B^m\rangle\,, |\mathcal{G}_B^{m+2k}\rangle) = 2\pi|k|\,. \tag{5.45}$$

As observed before, the bosonic operators act vertically in the fibers, so there is no corresponding bosonic complexity in this class of states.

5.3.2 Bosonic Coherent States with One Excited Mode

We consider next the coherent states analysed in Section 5.2, but now in the fermionic description. We start again from the coherent states involving excitations of only one bosonic mode, namely the states $U_n(\alpha)\,|\mathcal{G}_B^N\rangle$ and consider within the states module of zero fermion number $N=0$, the analysis can be applied in the same manner to the other states module having a different fermion number with only a shift in the fermionic modes.

As discussed in Section 5.1.3, the unitary operator $U_n(\alpha) = e^{\alpha b_n^\dagger - \alpha^* b_n}$ is the exponential of a fermion bilinear, therefore the states are fermionic gaussian and the formalism developed in the first part of this section can be applied. Using the Baker-Campbell-Hausdorff formula

$$e^X Y e^{-X} = Y + [X,Y] + \frac{1}{2!}[X,[X,Y]] + \frac{1}{3!}[X,[X,[X,Y]]] + \cdots\,, \tag{5.46}$$

we can find the transformation of the oscillators in closed form, writing $\alpha = |\alpha| e^{i\theta}$ we have

$$\begin{aligned}
\tilde{c}_q(n) = U_n(\alpha) c_q U_n^\dagger(\alpha) &= \sum_{l,m\geq 0} \frac{(\alpha^*)^l \alpha^m}{m!l!} \left(\frac{-i}{\sqrt{n}}\right)^{l+m} c_{q+(l-m)n} \\
&= \sum_{r\geq 0} (-i)^r e^{-ir\theta} J_r\left(\frac{2|\alpha|}{\sqrt{n}}\right) c_{q+nr} + \sum_{r<0} i^r e^{-ir\theta} J_{-r}\left(\frac{2|\alpha|}{\sqrt{n}}\right) c_{q+nr}, \qquad (5.47) \\
\tilde{c}_q^\dagger(n) = U_n(\alpha) c_q^\dagger U_n^\dagger(\alpha) &= \sum_{l,m\geq 0} \frac{(\alpha^*)^l \alpha^m}{m!l!} \left(\frac{i}{\sqrt{n}}\right)^{l+m} c_{q-(l-m)n}^\dagger \\
&= \sum_{r\geq 0} i^r e^{ir\theta} J_r\left(\frac{2|\alpha|}{\sqrt{n}}\right) c_{q+nr}^\dagger + \sum_{r<0} (-i)^r e^{ir\theta} J_{-r}\left(\frac{2|\alpha|}{\sqrt{n}}\right) c_{q+nr}^\dagger, \qquad (5.48)
\end{aligned}$$

where $J_r\left(\frac{2|\alpha|}{\sqrt{n}}\right)$ is the Bessel function of the first kind and n is the excitation mode of boson. Notice that the mixing occurs only within fermionic modes that differ by a multiple of n. In the Majorana basis the transformation reads

$$\tilde{q}_l = \sum_r J_{|r|}\left(\frac{2|\alpha|}{\sqrt{n}}\right) \cos\left(\frac{\pi}{2}|r| + r\theta\right) q_{l+nr} + \sum_r J_{|r|}\left(\frac{2|\alpha|}{\sqrt{n}}\right) \sin\left(\frac{\pi}{2}|r| + r\theta\right) p_{l+nr}, \tag{5.49}$$

$$\tilde{p}_l = \sum_r J_{|r|}\left(\frac{2|\alpha|}{\sqrt{n}}\right) \cos\left(\frac{\pi}{2}|r| + r\theta\right) p_{l+nr} - \sum_r J_{|r|}\left(\frac{2|\alpha|}{\sqrt{n}}\right) \sin\left(\frac{\pi}{2}|r| + r\theta\right) q_{l+nr}\,, \tag{5.50}$$

and the corresponding orthogonal matrix has the form

$$M(n) = \begin{pmatrix} A(n) & B(n) \\ -B(n) & A(n) \end{pmatrix} \tag{5.51}$$

which is indeed orthogonal as we show in appendix B for the case that $\theta = 0$. Recall that the fermionic Gaussian state $|\psi\rangle$ is given in terms of the transformed oscillators by

$$\tilde{c}_q(n)\,|\psi\rangle = 0, \quad q > 0; \qquad \tilde{c}_q^\dagger(n)\,|\psi\rangle = 0, \quad q \leq 0. \tag{5.52}$$

We observe that the θ-dependence in (5.47),(5.48) can be eliminated by the following field redefinition

$$c_q \to e^{iq\theta/n} c_q \,, \qquad \tilde{c}_q(n) \to e^{iq\theta/n} \tilde{c}_q(n) \,, \tag{5.53}$$

which does not affect the state (5.52). It is a unitary transformation, so it does not affect the complexity, as discussed in Section 2.3.2. This is also in agreement with the result for the bosonic complexity (5.37) which is independent of the phase of α. We find that the most convenient choice for the present calculation is to set $\theta = \pi/2$.

In this case the off-diagonal block $B(n)$ of the transformation matrix $M(n)$ vanishes identically, and the non-vanishing entries of $A(n)$ are given by

$$A(n)_{i(i+nj)} = \begin{cases} J_{|j|}\left(\frac{2|\alpha|}{\sqrt{n}}\right) & (j \leq 0) \\ (-1)^j J_{|j|}\left(\frac{2|\alpha|}{\sqrt{n}}\right) & (j > 0) \end{cases} , \tag{5.54}$$

The relative covariance matrix $\Delta(n)$ is made of two identical blocks

$$\Delta(n) = \begin{pmatrix} A(n)CA^T(n)C & 0 \\ 0 & A(n)CA^T(n)C \end{pmatrix} , \tag{5.55}$$

with C given in (2.56). We can observe that $A^T(n)$ and $A(n)$ are related by an orthogonal transformation

$$A^T(n) = O^T A(n) O \tag{5.56}$$

with $O_{ij} = (-1)^i \delta_{ij}$, which is symmetric and also commutes with C. The diagonal block can be rewritten as $(A(n)OC)^2$, so the problem is reduced to the diagonalization of $A(n)OC$.

We have not been able to obtain the eigenvalues analytically. Instead, we notice that the matrix elements $A(n)_{ij}$ (and those of $A(n)OC$ as well, they just differ by some minus signs) are of the form of Bessel functions $J_\nu(z)$ with index $\nu = |i-j|$ and argument $z = \frac{2\alpha}{\sqrt{n}}$. Recalling the power series expansion

$$J_\nu(z) = \left(\frac{z}{2}\right)^\nu \sum_{k=0}^{\infty} \frac{\left(-\frac{z^2}{4}\right)^k}{k!\Gamma(\nu+k+1)}, \tag{5.57}$$

we see that for small z the matrix is dominated by the diagonal elements, while off-diagonal ones are suppressed exponentially with the distance from the diagonal. This has the consequence that the eigenvalues can be computed numerically with good accuracy, and they are weakly dependent on the cutoff that we put on the length of the matrix considered. One has to keep in mind that each entry in eq. (5.55) contains the full contributions of all the modes.

Result with $p = 1$ norm In Figure 5.2 we plot the complexity with $p = 1$ norm, as a function of α, for different values of the number n, the excited bosonic mode. The cutoff is chosen to be $10n$, although the result does not depend on it. We observe that the ratio between the complexity $\mathcal{C}_{p=1}$ and $\frac{|\alpha|}{\sqrt{n}}$ which is the argument of the Bessel function, is constant in α.

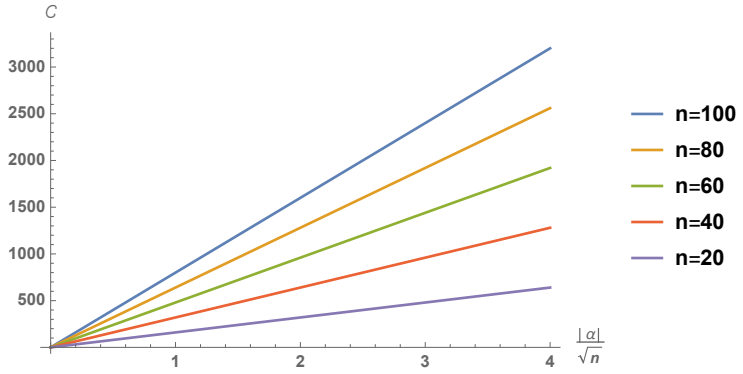

Figure 5.2: Complexity $\mathcal{C}_{p=1}$ over $\frac{\alpha}{\sqrt{n}}$ is constant in $|\alpha|$, for $n \in [20, 100]$ with an interval of 20, where n labels the bosonic excitation $b_n^\dagger$ in (5.27). The cutoff on the size of the matrices $A(n)$ and $B(n)$ is set equal to $10n$.

Therefore, we claim that the complexity between the bosonic ground state $|\mathcal{G}_B^N\rangle$ and the coherent state $|\alpha, n\rangle$ generated from it by using the *Schatten* $p = 1$ norm is

$$\mathcal{C}_{p=1}(|\mathcal{G}_B^N\rangle, U_n(\alpha)\,|\mathcal{G}_B^N\rangle) = 4\sqrt{n}|\alpha| \tag{5.58}$$

where we have taken into account the two diagonal blocks and an overall factor 1/2 in (2.62). Comparing to the result (5.37) obtained in terms of bosonic gates, we see that the fermionic complexity has an extra dependence on the excitation mode n.

Result with $p = 2$ norm The *Schatten* $p = 2$ norm, as aforementioned, endows the complexity with the meaning of geodesic length on the gates' manifold. In Figure 5.3, we plot the complexity similar to the previous case with different number of excitations n. We see here that the complexity is still increasing but not at all in a linear manner. The rate of the increase in each curve decreases with $|\alpha|$, consistently with the monotonicity of the $p-$norms.

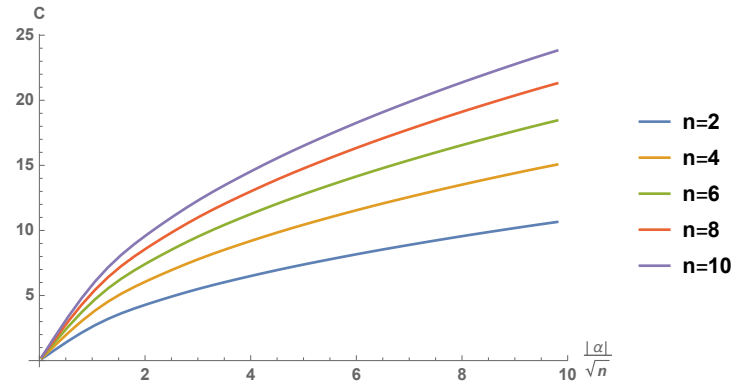

Figure 5.3: Complexity $\mathcal{C}_{p=2}$ increases when $|\alpha|$ increases for $n \in [2, 10]$ with an interval of 2, where n labels the bosonic excitation $b_n^\dagger$ in (5.27). The length of the matrices $A(n)$ and $B(n)$ is cut to be twenty times of the bosonic excitation n for the plot.

Finally the complexity with the $p = 2$ norm is bounded by $p = 1$ norm result

$$\mathcal{C}(|\mathcal{G}_B^N\rangle \to U_n(\alpha)\,|\mathcal{G}_B^N\rangle) = \mathcal{C}_{p=2}(|\mathcal{G}_B^N\rangle \to U_n(\alpha)\,|\mathcal{G}_B^N\rangle) \leq 4\sqrt{n}|\alpha|. \tag{5.59}$$

5.3.3 Complexity for Bosonic Coherent States with Shifts in More Modes

As has been considered in Section 5.2, one can also extend the result (5.58) to shifts in more modes in terms of fermionic gates, *i.e.,* , the complexity between $|\mathcal{G}_B^N\rangle$ and $U_{n_1}(\alpha_1)\cdots U_{n_k}(\alpha_k)\,|\mathcal{G}_B^N\rangle$. Like for the single mode shift, the complexity would be independent of which bosonic ground state we are considering. Thus for simplicity as in the last section, one should focus on the case that $|\mathcal{G}_B^N\rangle$ is chosen to be the fermionic vacuum $|0\rangle$. The procedure is quite similar, first we have to obtain the transformation between the old and new basis in the following way,

$$\begin{aligned}\hat{c}_l &= U_{n_k}^\dagger(\alpha_k)U_{n_{k-1}}^\dagger(\alpha_{k-1})\cdots U_{n_1}^\dagger(\alpha_1)c_l U_{n_1}(\alpha_1)U_{n_2}(\alpha_2)\cdots U_{n_k}(\alpha_k)\\ &= \sum_{j,m,\ldots,i,q} R_{lj}^{(k)}(\alpha_k,n_k)R_{jm}^{(k-1)}(\alpha_{k-1},n_{k-1})\cdots R_{iq}^{(1)}(\alpha_1,n_1)c_q\end{aligned} \tag{5.60}$$

where

$$U_{n_k}^\dagger(\alpha_k)c_l U_{n_k}(\alpha_k) = \sum_j R_{lj}^{(k)}(\alpha_k,n_k)c_j, \tag{5.61}$$

and the entries of $R^{(k)}(\alpha_k,n_k)$ can be read out from (5.47) and (5.48). Since $U_{n_k}^\dagger(\alpha_k)$s are all commuting among themselves, $R^{(k)}(\alpha_k,n_k)$s forming a matrix representation are totally commuting as a result. In general, the arguments α_k are complex numbers $\alpha_k = |\alpha_k|e^{i\theta_k}$; one overall phase can be reabsorbed with a redefinition of c_j and $\tilde{c}_j$ as in (5.53). The numerical results we obtained for the two-mode shifts show that the complexity is in fact independent of both phases. We conjecture that this is true in general, although we cannot give a proof.

Result with $p = 1$ norm Applying the method in the last Section 5.3.2 for two-mode shifts $U_{n_1}(\alpha_1)$ and $U_{n_2}(\alpha_2)$, one could obtain the complexity $\mathcal{C}_{p=1}$ plotted as in Figure 5.4a where n_1 and n_2 are taken to be $n_1 = 10$ and $n_2 = 17$. From the plot, we can see that for the $|\alpha_2| = 0$

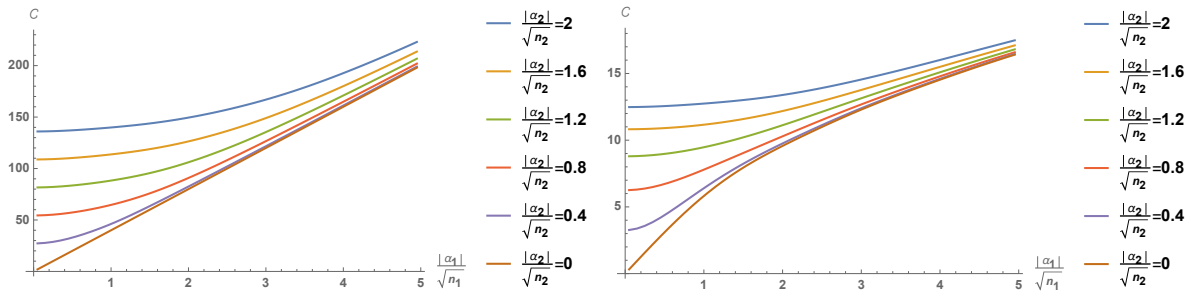

(a) Two-mode shifts, $\mathcal{C}_{p=1}$ **(b)** Two-mode shifts, $\mathcal{C}_{p=2}$

Figure 5.4: Complexity for two-mode shifts with $n_1 = 10, n_2 = 17$. The cutoff is chosen to be $N = 200$ for the two-mode shift covariance matrice, which is similar to one of the diagonal blocks in (5.55).

curve, the complexity is a linear function of $|\alpha_1|$ with a proportionality constant being $4\sqrt{n_1}$. While for the other $|\alpha_2| \neq 0$ curves, we see that as $|\alpha_1|$ becomes dominant they asymptotes to be

linear in $|\alpha_1|$ again with the same slope as for the curve $|\alpha_2| = 0$. Therefore, from the shape of the curves, we could deduce that the complexity for two-mode shift is

$$\mathcal{C}_{p=1}(|\mathcal{G}_B^N\rangle\,, U_{n_1}(\alpha_1)U_{n_2}(\alpha_2)\,|\mathcal{G}_B^N\rangle) = 4\sqrt{n_1|\alpha_1|^2 + n_2|\alpha_2|^2}, \tag{5.62}$$

which fits nicely with the results and reduces to (5.58) when $|\alpha_2| = 0$. It is reasonable to suppose that the result will generalize to multi-mode shifts as follows:

$$\mathcal{C}_{p=1}(|\mathcal{G}_B^N\rangle\,, U_{n_1}(\alpha_1)U_{n_2}(\alpha_2)\cdots U_{n_k}(\alpha_k)\,|\mathcal{G}_B^N\rangle) = 4\sqrt{\sum_{i=1}^{k} n_i|\alpha_i|^2}\,. \tag{5.63}$$

Result with $p = 2$ norm We plot the complexity $\mathcal{C}_{p=2}$ with the same setup in Figure 5.4b. As in Figure 5.4a, the complexity increases as either α_1 or α_2 increases, and all the curves converge to a certain curve as $\frac{|\alpha_1|}{\sqrt{n_1}}$ becomes much larger than $\frac{|\alpha_2|}{\sqrt{n_2}}$, which is expected since then the effect of the first shifting mode becomes dominant.

Finally, the upper bound for the complexity with *Schatten* $p = 2$ norm is given by

$$\mathcal{C}_{p=2}(|\mathcal{G}_B^N\rangle\,, U_{n_1}(\alpha_1)U_{n_2}(\alpha_2)\,|\mathcal{G}_B^N\rangle) \leq 4\sqrt{n_1|\alpha_1|^2 + n_2|\alpha_2|^2}\,, \tag{5.64}$$

and similarly for the general case.

5.4 A class of Fermionic and Bosonic Bi-Gaussian States

In the previous sections, we have shown that the bosonic coherent states of the type in (5.38) are fermionic gaussian states and we have also seen how to obtain the corresponding complexity by using Fubini-Study method and Nielsen method in terms of bosonic gates and fermionic gates respectively. However the bosonic coherent states are only a subset of all the fermionic gaussian state, whereas a state that is fermionic gaussian is not generically also bosonic gaussian.

In this section we show that there is a large class of states that are simultaneously bosonic and fermionic gaussian. This allows us to study the effect that different choices of gates have on the complexity of a given state, since in the fermionic description we allow gates that are fermion bilinears, whereas in the bosonic description we use gates that are bosonic bilinears. Notice that neither set of gates is a subset of the other, so we cannot establish a priori a bound between the two complexities.

5.4.1 A Bosonisation Identity

Starting with the fundamental bosonisation formula (5.13), it is possible to obtain the following relation [200]:

$$:i\psi^\dagger(x)\partial_x\psi(x):= \frac{2\pi^2}{L^2}(\hat{N} + \hat{N}^2) + \frac{\pi}{L}\partial_x\phi(x) + \frac{1}{2}:(\partial_x\phi(x))^2: + \frac{2\pi}{L}\hat{N}\partial_x\phi(x) + \frac{i}{2}\partial_x^2\phi(x)\,. \tag{5.65}$$

Taking the integral over space of this relation, we obtain on the two sides the fermionic and bosonic hamiltonian respectively, which is the basic property of the bosonisation formalism. Formula

(5.65) shows that the equality holds at the level of the hamiltonian density, up to total derivative terms which, crucially for our purposes, are linear in the boson field, hence fermion bilinears, if we work on a subspace of fixed particle number. For definiteness we can consider the case $\hat{N} = 0$, *i.e.*, , the module with fermion number zero. Therefore if we consider the inhomogeneous hamiltonian $H_f = \int dx f(x) :i\psi^\dagger(x)\partial_x\psi(x):$, dependent on an arbitrary function $f(x)$, the corresponding ground state will be fermionic gaussian, and also bosonic gaussian.

It is unlikely that further identities of this type exist, therefore we conjecture that the states obtained this way are the only ones that are gaussian in both descriptions. If we write down the same relation in Fourier components, taking

$$f(x) = \sum_k f_k e^{i\frac{2\pi k x}{L}} \tag{5.66}$$

and integrating each term of (5.65) multiplied by $f(x)$ over the whole space $[-L/2, L/2]$ gives

$$\int_{-L/2}^{L/2} \frac{dx}{2\pi} f(x)\partial_x\phi(x) = -i\sum_{n>0}\sqrt{n}(f_n b_n^\dagger - f_{-n}b_n), \tag{5.67}$$

$$\int_{-L/2}^{L/2} \frac{dx}{2\pi} f(x) :(\partial_x\phi(x))^2: = -\frac{2\pi}{L}\sum_{m,n>0}\sqrt{mn}(f_{m+n}b_m^\dagger b_n^\dagger + f_{-m-n}b_m b_n - 2f_{n-m}b_n^\dagger b_m), \tag{5.68}$$

$$\int_{-L/2}^{L/2} \frac{dx}{2\pi} f(x)(i\partial_x^2\phi(x)) = \frac{2\pi i}{L}\sum_{n>0} n^{3/2}(f_n b_n^\dagger + f_{-n}b_n), \tag{5.69}$$

$$\int_{-L/2}^{L/2} \frac{dx}{2\pi} f(x) :i\psi^\dagger(x)\partial_x\psi(x): = \frac{2\pi}{L}\sum_{l,k} k f_{l-k} :c_l^\dagger c_k: = \frac{2\pi}{L}\sum_{l,k} k :c_{k+l}^\dagger c_k: f_l, \tag{5.70}$$

putting all terms together we have the following relation

$$\begin{aligned}\sum_l l :c_l^\dagger c_l: f_0 + \sum_{n\neq 0,l}\left(l + \frac{n - 2\hat{N} - 1}{2}\right) c_{l+n}^\dagger c_l f_n \\ = \frac{1}{2}(\hat{N} + \hat{N}^2)f_0 - \frac{1}{2}\sum_{m,n>0}\sqrt{mn}(f_{m+n}b_m^\dagger b_n^\dagger + f_{-m-n}b_m b_n - 2f_{n-m}b_n^\dagger b_m)\,.\end{aligned} \tag{5.71}$$

Once again we see that identifying the coefficient of f_0, we obtain the usual identity for fermionic and bosonic Hamiltonians

$$\sum_k k :c_k^\dagger c_k: = \sum_{m>0} m b_m^\dagger b_m + \frac{1}{2}(\hat{N} + \hat{N}^2). \tag{5.72}$$

5.4.2 An Example with One Mode

We consider now one particular example of states in this family, corresponding to a function that has only Fourier modes $n = \pm 2$. The operator identity for f_2 which can be read from eq. (5.71) is

$$\sum_l \left(l + \frac{1 - 2\hat{N}}{2}\right) c_{l+2}^\dagger c_l = -\frac{1}{2}b_1^\dagger b_1^\dagger + \sum_{m>0}\sqrt{(m+2)m}\, b_{m+2}^\dagger b_m, \tag{5.73}$$

and for f_{-2} we have the hermitian conjugate of the above. The two identities will help build the following unitary operator $W_f(\beta) = W_b(\beta)$, given in terms of fermionic modes and bosonic

modes, respectively, as

$$W_f(\beta) = \exp\left(\sum_l \left(l + \frac{1-2\hat{N}}{2}\right)(\beta c_{l+2}^\dagger c_l - \beta^* c_l^\dagger c_{l+2})\right), \tag{5.74}$$

$$W_b(\beta) = \exp\left(-\frac{\beta}{2} b_1^\dagger b_1^\dagger + \frac{\beta^*}{2} b_1 b_1 + \sum_{m>0} \sqrt{m(m+2)}\,(\beta b_{m+2}^\dagger b_m - \beta^* b_m^\dagger b_{m+2})\right). \tag{5.75}$$

We will assume $\beta \in \mathbb{R}$ and focus on the sector $\hat{N} = 0$ in the following part with the reference state being the fermionic vacuum $|0\rangle$. The adjoint action of these operators on the modes cannot be obtained in an analytically closed form as in (5.47), (5.48). We must resort to a fully numerical computation. We put a cutoff on the number of modes, find the matrices representing $\frac{1}{\beta}\ln W_f$ and $\frac{1}{\beta}\ln W_b$, respectively R_f and R_b, and compute the exponential of those two matrices, which give the change of basis $\tilde{\xi}_i^f = (e^{\beta R_f})_{ij}\xi_j^f$ and $\tilde{\xi}_i^b = (e^{\beta R_b})_{ij}\xi_j^b$. The relative covariance matrix is then computed as in (2.58),(2.63), and the eigenvalues are found numerically. There is one case when we can find an exact result: the bosonic covariance Δ_b has the form $\Delta_b(\beta) = e^{\beta R_b} e^{\beta R_b^T}$, and

$$R_b = \begin{pmatrix} A_b & S_b \\ S_b & A_b \end{pmatrix} \sim \begin{pmatrix} A_b + S_b & 0 \\ 0 & A_b - S_b \end{pmatrix} \tag{5.76}$$

where A_b is antisymmetric and S_b is symmetric, which is consistent with the fact that $\Delta_b \in Sp(2N)$. Equation (5.76) means that $\ln \Delta_b$ can always be block diagonalized as

$$\ln \Delta_b(\beta) = \begin{pmatrix} \ln\left(e^{\beta(A_b+S_b)} e^{\beta(S_b-A_b)}\right) & 0 \\ 0 & \ln\left(e^{\beta(A_b-S_b)} e^{\beta(-A_b-S_b)}\right) \end{pmatrix}. \tag{5.77}$$

We notice that if one of the two blocks is positive definite, the other would be negative definite, due to the fact that the eigenvalues of Δ_b always come in pairs $e^{\pm r}$ (this is because Δ_b is symplectic and orthogonal). In this case one can show that the antisymmetric part does not contribute to the complexity; then it is easy to see that, setting $A_b = 0$ in (5.77), the complexity $\mathcal{C}_{p=1}$ can be computed exactly and is linear in the trace of the symmetric part S_b. However we do not have a criterion to determine when the blocks will be postive definite.

Result with $p = 1$ norm The results are shown in Figure 5.5. The behavior appears to be very different for bosons and fermions. The bosonic complexity (see Figure 5.5a) grows linearly without bound; this linear growth can be explained, as discussed above, by the positive-definiteness of the blocks of the covariance matrix. On comparison, the fermionic complexity is oscillating (see Figure 5.5b) in a way that suggests a quasi-periodic function. The maximum complexity of the first peak seems to grow linearly w.r.t. the logarithm of the cutoff $\ln(N)$ as in Figure 5.6a, this is consistent with the fact that the orthogonal group $SO(2N)$ becomes non-compact as $N \to \infty$. For bosons, on the other hand, this particular class of states has a complexity that is independent of the cutoff, even though the transformation at finite β mixes all the modes among themselves and not just a finite number of them.

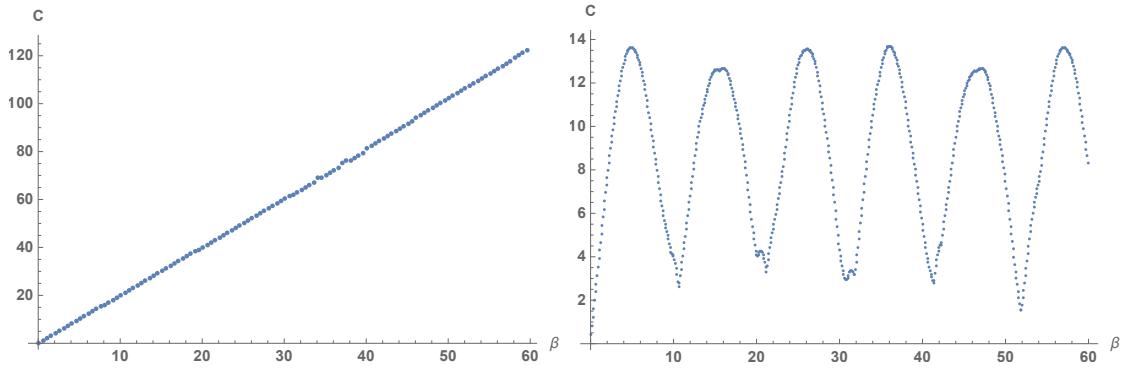

(a) Boson, $\mathcal{C}_{p=1}$, $N = 40$ **(b)** Fermion, $\mathcal{C}_{p=1}$, $N = 40$

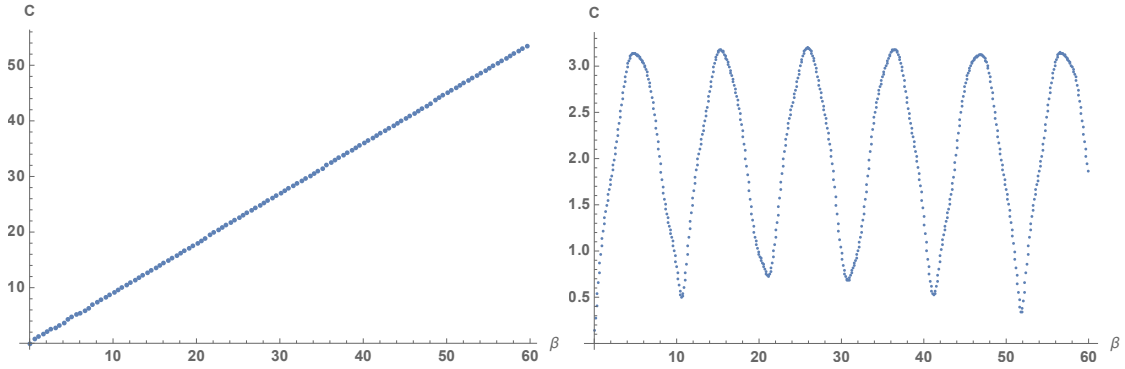

(c) Boson, $\mathcal{C}_{p=2}$, $N = 40$ **(d)** Fermion, $\mathcal{C}_{p=2}$, $N = 40$

Figure 5.5: The complexity for bosonic and fermionic gaussian states with $p = 1$ and $p = 2$ norms. (a) and (c) represent the bosonic case while (b) and (d) represent the fermionic case. The cutoff is chosen to be $N = 40$.

Result with $p = 2$ norm The complexities for gaussian states complexity with $p = 2$ norm are plotted in Figure 5.5c for the bosonic case and in Figure 5.5d for fermionic one. The trends appear to be similar as the $p = 1$ case, except that the values of the complexity are smaller.

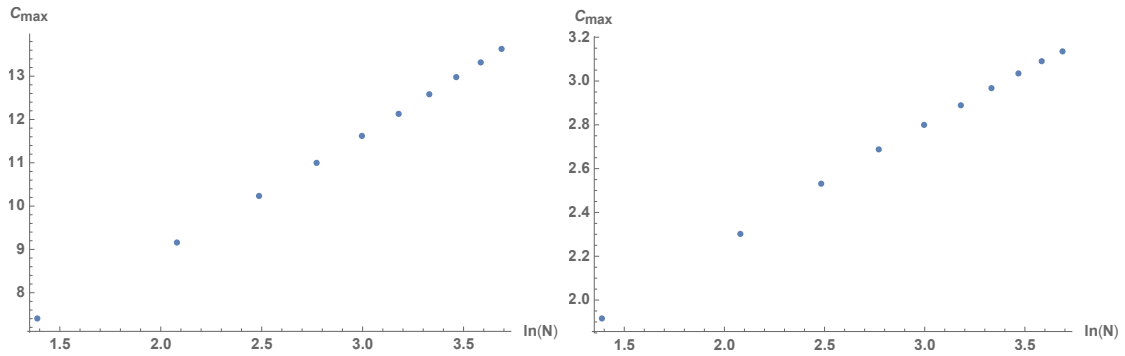

(a) $\mathcal{C}_{p=1}$ v.s. $\ln(N)$ **(b)** $\mathcal{C}_{p=2}$ v.s. $\ln(N)$

Figure 5.6: The maximum complexity for the fermionic case grows w.r.t. the logarithm of the cutoff, linearly for the $p = 1$ norm and quasi-linearly for the $p = 2$ norm.

5.4.3 An Example with Two Modes

We consider next a function $f(x)$ with two modes; the simplest case would be to use the operator identities for $f_{\pm 2}$ and $f_{\pm 3}$. In this case, the unitary operator for fermions

$$W_f(\beta,\gamma) = \exp\Bigg[\sum_l \left(l + \frac{1-2\hat{N}}{2}\right)\left(\beta c^\dagger_{l+2}c_l - \beta^* c^\dagger_l c_{l+2}\right) + \sum_l \left(l+1-\hat{N}\right)\left(\gamma c^\dagger_{l+3}c_l - \gamma^* c^\dagger_l c_{l+3}\right)\Bigg], \tag{5.78}$$

and for bosons

$$W_b(\beta,\gamma) = \exp\Bigg[-\frac{\beta}{2}b^\dagger_1 b^\dagger_1 + \frac{\beta^*}{2}b_1 b_1 + \sum_{m>0}\sqrt{m(m+2)}\left(\beta b^\dagger_{m+2}b_m - \beta^* b^\dagger_m b_{m+2}\right) - \sqrt{2}\gamma b^\dagger_1 b^\dagger_2 + \sqrt{2}\gamma^* b_1 b_2 + \sum_{m>0}\sqrt{m(m+3)}\left(\gamma b^\dagger_{m+3}b_m - \gamma^* b^\dagger_m b_{m+3}\right)\Bigg], \tag{5.79}$$

depend on two parameters, β and γ, coupling to the $n = 2$ and $n = 3$ mode respectively. For simplicity, we consider the case where β and γ are real and proportional to each other as $\gamma = m\beta$. In Figure 5.7, we plotted the complexity for both the bosonic state (Figure 5.7a and 5.7c) and the fermionic state (Figure 5.7b and 5.7d) as a function of β and for various values of m. We notice that in the bosonic case, the mixing of the modes does not have a dramatic effect (although the curves are no longer exactly linear), while for fermions the quasi-periodic behavior is destroyed. Again we observe that the qualitative features are the same using the $p = 1$ and the $p = 2$ norm.

5.5 Conclusion

In this chapter, we made a first step to consider the relations between fermionic and bosonic field theory complexity. We investigate such relations in the $2D$ free boson/free fermion model, where a highly nonlinear exact relation between the scalar field and the fermion field is present, encoded in eq. (5.13) that expresses the fermion field as the vertex operator of the scalar field. In this setup, the fermonic Fock space can be decomposed into modules according to their fermionic number (see eq. (5.18)), and each module can be identified with the bosonic Hilbert space. Moreover, the space of quadratic operators in one description is mapped to a space of non-quadratic ones in the other, and this allows us to study how the choice of the set of allowed gates influences the complexity of an operator.

In the current framework of calculable field theory complexity, not all the states can be treated on equal footing. We identified two classes of states that can be considered from both sides. The first type is bosonic-coherent and fermionic-gaussian, a direct consequence of eq. (5.12) where a single bosonic operator is a sum of bilinears of fermionic ones. We applied the *Fubini-Study* metric method on the bosonic side, with the analytical results given in (5.37) for a single mode shift and in (5.43) a generalization to multi-mode shift. The general multi-mode result shows that different modes are orthogonal in the FS metric which is a flat Euclidean metric. On the fermionic side, we applied instead the *Nielsen* method developed in [66], with numerical result

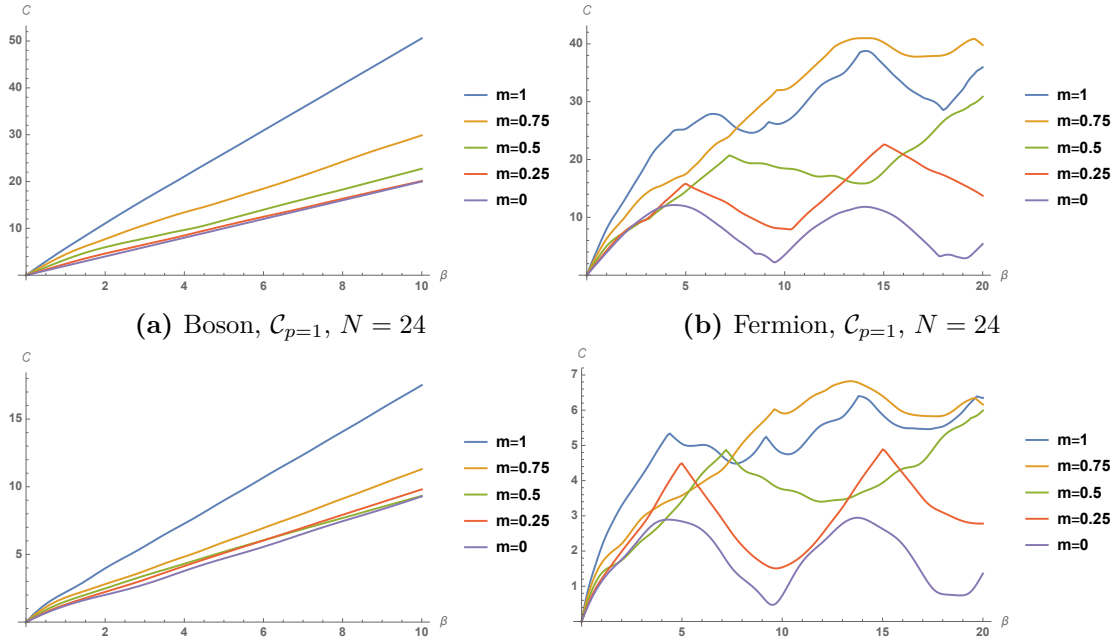

(a) Boson, $\mathcal{C}_{p=1}$, $N = 24$ **(b)** Fermion, $\mathcal{C}_{p=1}$, $N = 24$

(c) Boson, $\mathcal{C}_{p=2}$, $N = 24$ **(d)** Fermion, $\mathcal{C}_{p=2}$, $N = 24$

Figure 5.7: The complexity for bosonic and fermionic gaussian states with $p = 1$ and $p = 2$ norms. (a) and (c) represent the bosonic case while (b) and (d) represent the fermionic case. The cutoff is chosen to be $N = 24$ and the ratio varies from 0 to 1 with an interval of 0.25.

plotted in Figure 5.2, 5.4a for *Schatten* $p = 1$ norm, and Figure 5.3, 5.4b for $p = 2$ norm. Based on those numerics, an analytical result for multimode shift with $p = 1$ norm is obtained in eq. (5.63), which differ from the bosonic result (5.43) by an extra dependence on the mode number. This means that if we assign a mode-number dependent cost in the bosonic case, the two results would be equivalent up to a total factor. This result is a bit surprising, since it is for the $p = 2$ norm that we can interpret the complexity in terms of Riemannian geometry, so we should expect that the FS metric would compare more directly to that case. The $p = 1$ norm gives the space the structure of a *Finsler* manifold. It would be interesting to understand better the structure of this geometry; this could also shed some light on the relation between bosonic states and fermionic states holographically, since bosonic coherent states in the bulk constitute a sector of states that can be explcitly described both in the bulk and in the boundary (see the recent work [202]).

The second class of states is identified through the relation (5.65) which is a local (in space) relation between bosonic bilinears and fermionic ones, thus relating the gaussian states on both sides. These states can be understood as the ground states for an inhomogeneous Hamiltonian, obtained integrating (5.65) with an arbitrary function $f(x)$, that has the interpretation of a space-dependent Fermi velocity. We obtain a one-function family of bigaussian states, out of which we studied some of the simplest cases using *Nielsen* method. For the case of a function with the only Fourier component $f_{\pm 2} = \alpha$, the numerical results for bosons and fermions are plotted in Figure 5.5, which show qualitatively the same behavior using the $p = 1$ and $p = 2$ norm. The most notable features are: the bosonic complexity grows linearly with α, and is independent of the UV cutoff, while the fermionic complexity is roughly periodic in α, reaching peaks with value scaling

like $\ln N$ in the cutoff. This shows that the states are special in some sense, since a generic point in the group manifold $SO(2N)$ would be at a distance $\sim \sqrt{N}$ from the identity (at least in the $p = 2$ norm). We also considered the next simplest two-mode case, with components f_2 and f_3. The results, plotted in Figure 5.7, show that the effect of the mixing of the modes is small on the bosonic complexity, but more dramatic one on the fermionic one. It would be interesting to understand what is the behavior for a generic function f.

Incidentally, it would be also interesting to know whether these bi-Gaussian states have applictions in situations of physical interest (*e.g.*, in problems of electron transport in 1D [203]).

A natural extension of our work would be to consider the interacting model, namely the massless Thirring fermion model [204] that is dual to a free compact boson. In this case one can hope that the free theory on one side will give insight into the complexity of an interacting theory. The massive Thirring model is dual to a sin-Gordon model, it would be interesting to see if this case could be analyzed using integrability techniques.

Chapter 6

Berry Curvature as A Probe of Bulk Curvature

This Chapter is based on the work [21].

The rapid growth in the study of the interdisciplinary domain between the quantum information and the quantum gravity has initiated vast room in exploring the gauge-gravity dual in various manners. The fundamental spirit laid by Ryu and Takayanagi [11] is that the bulk spacetime is emerged from the quantum field theory living on the bounday. An intuition one can think of comes from the tensor network construction, where the bulk geometry is built via a coarse graining process from the boundary [152]. In a way, it tells us that the quantum information can indeed be encoded through some bulk geometric quantities, such as the bulk codimensional-two surface to encode the entanglement entropy of the subregion it anchors at, and the bulk codimensional-one volume to encode the quantum complexity of the boundary states as has been shown in Chapter 3. In this chapter, we are trying to argue that another quantity, which is so natural but yet not understood holographically, called the Riemann curvature, will be able to encode the Berry curvature of the boundary modular Hilbert spaces. This further strengthens the subregion duality in the entanglement wedge and offers a new probe of the duality.

6.1 Entanglement as a Connection

Subregion duality has taught us that the physics in a bulk entanglement wedge, i.e. its geometry, quantum state and dynamics of local quantum fields, can be recovered from the state ρ and operator algebra $\mathcal{A}(\mathcal{O})$ of its dual CFT subregion [85, 86, 205, 206]. The cornerstone of this important insight was the duality between the bulk modular flow and boundary modular flow induced by the modular Hamiltonians on both sides [82, 207, 208] within the code subspace [205]

$$H_{\text{mod}}^{\text{CFT}} = \frac{A}{4G_{\text{N}}} + H_{\text{mod}}^{\text{bulk}}\,, \tag{6.1}$$

with the modular Hamiltonians defined as the logarithm of the reduced density matrix of the subregion $H_{\text{mod}} = -\log\rho$ and A the area operator of the HRRT surface [11, 84] bounding the entanglement wedge.

In this chapter, we utilize relation (6.1) to make precise how boundary entanglement "builds"

the bulk spacetime [209, 210] by sewing together entanglement wedges to produce its global geometry. In ordinary differential geometry, spacetime is constructed by consistently gluing small patches of Minkowski space, which are the local tangent spaces of a base manifold. Central to this task is the *spacetime connection* that relates the Lorentz frames of nearby tangent spaces and endows spacetime with its curvature. Adopting this spirit, we explain how holographic spacetimes are assembled by the set of entanglement wedges by means of a geometric connection, which we propose is determined microscopically by the entanglement structure of the dual CFT state. The curvature of this entanglement connection reflects the bulk curvature in a way we make precise in Section 6.3.

Our central idea is to treat entanglement as a quantum notion of connection between subsystems [211]. All correlation functions within a CFT subregion A, endowed with the modular Hamiltonian H^A_{mod} are invariant under the unitary evolution generated by modular zero-modes Q^A_i commutes with the modular Hamiltonian

$$\left[Q^A_i, H_{\text{mod},A}\right] = 0\,, \tag{6.2}$$

where i marks a basis of the zero-mode subalgebra. For a physicist with access only to A, these symmetries of her local state translate to the freedoms of choosing her overall zero-mode frame. On the other hand, entanglement in the global CFT state renders the *relative zero-mode frame* of different modular Hamiltonians physical, establishing a map between the algebras localized in different subregions, as we explain in Section 6.2.1. Our proposal is to think of this zero mode ambiguity of subregions as a *gauge symmetry in the space of modular Hamiltonians*. The relative modular frame is then encoded in the connection between the relevant bundles —the modular Berry connection [212] which we define for arbitrary states in Section 6.2.2.

The bulk meaning of this zero-mode ambiguity of CFT subregions follows from relation (6.1). At leading order in G_{N}, bulk modular zero modes consist of large diffeomorphisms that do not vanish at the HRRT surface. These are the gravitational edge modes [213] or asymptotic symmetries [214, 215] of the extremal surface and, as we show in Section 6.3.1, they consist of internal diffeomorphisms and local boost transformations on the 2D plane normal to the HRRT surface. While the edge-mode frame for every given wedge can be chosen at will, the bulk spacetime allows us to compare frames of different wedges. When the extrinsic curvature of the HRRT surface is small compared to the Riemann curvature of the bulk spacetime, the bulk modular connection becomes the *relative embedding* of the local coordinate systems located around the surfaces, which is a central result in equations (6.44)−(6.46) of this chapter. The curvature of the modular Berry connection includes the bulk Riemann tensor as one of its components, as we demonstrate in detail in Section 6.3.2 and 6.3.3.

The gravitational connection of Section 6.3 and the CFT connection of Section 6.2 encode the relations of modular Hamiltonians on the two sides of AdS/CFT and are constructed by identical sets of rules. By virtue of (6.1) we, therefore, propose in Section 6.4 that the two different kinds of connections are related by the holographic duality. This provides a direct holographic link between the bulk curvature and the Berry curvature for the modular Hamiltonians of the CFT state. We conclude with a discussion of some conceptual and technical applications of the tools

developed in this work.

6.2 Modular Berry Connection

6.2.1 A toy example

The central idea underlying this work is that entanglement plays the role of a connection for subsystems of a quantum state [211]. In close analogy to the ordinary geometric connection of General Relativity which relates the Lorentz frames of nearby tangent spaces, the structure of entanglement defines the relation between the Hilbert space bases of different subsystems.

The simplest illustration of this idea involves a system of two qubits A and B in a maximally entangled state[1]:

$$|\psi\rangle_{AB} = \sum_{ij} W_{ij}|i\rangle_A|j\rangle_B. \tag{6.3}$$

The reduced density matrix of each qubit is maximally mixed. Both ρ_A and ρ_B are invariant under unitary transformations on the respective Hilbert space, which translates to a symmetry of expectation values for operators localized in A or B:

$$\begin{aligned}\langle\sigma^i_A\rangle &= \langle U^\dagger_A\sigma^i_A U_A\rangle,\\ \langle\sigma^i_B\rangle &= \langle U^\dagger_B\sigma^i_B U_B\rangle.\end{aligned} \tag{6.4}$$

Here $U_A, U_B \in SU(2)$ and $\sigma^i_{A,B}$ $(i = x, y, z)$ are the Pauli operators that generate the algebra of observables for the corresponding qubit. Each qubit is, therefore, endowed with a 'local' $SU(2)$ symmetry; in the absence of any external system of reference, the choice of the local unitary frame for A or B is simply a matter of convention.

Due to the entanglement of the two qubits in (6.3), however, expectation values of $\sigma^i_A\sigma^j_B$ are not invariant under independent unitary rotations U_A and U_B. This reflects the fact that the global state fixes the *relative* unitary frame of the subsystems. More precisely, $|\psi\rangle_{AB}$ defines an anti-linear map between the two Hilbert spaces[2]

$$|i\rangle_A \to |\tilde{i}\rangle_B = {}_A\langle i|\psi\rangle_{AB} = \sum_j W_{ij}|j\rangle_B\,, \tag{6.5}$$

that can also be expressed as an anti-linear map between the operators on the two Hilbert spaces

$$\begin{aligned}\sigma_A|i\rangle_A \to \tilde{\sigma}_B|\tilde{i}\rangle_B &= {}_A\langle i|\sigma^\dagger_A|\psi\rangle_{AB}\,, \quad \forall|i\rangle_A\\ \Rightarrow\quad \tilde{\sigma}_{B,ij} &= W_{ki}\,\sigma^*_{A,kl}\,W^{-1}_{jl}.\end{aligned} \tag{6.6}$$

The operators $\tilde{\sigma}_B$ are a simple example of the mirror operators of σ_A as discussed in [217], with $|\psi\rangle_{AB}$ a cyclic and separating vector for the algebra of operators acting on subsystem A.

It follows from definition (6.5) that the map between the two Hilbert spaces transforms under

[1] The maximal entanglement can be seen from tracing out the degrees of freedom for instance in B, then $\rho_A = \sum_{i,j,k,l} W_{ij}W^*_{lk}\delta_{jl}\,|i\rangle_A\,\langle k| = \sum_{ik}|i\rangle_A\,\langle k|$, where we have used that the W is unitary.

[2] Curious readers could refer to [216] for more details on how the anti-linear mapping works.

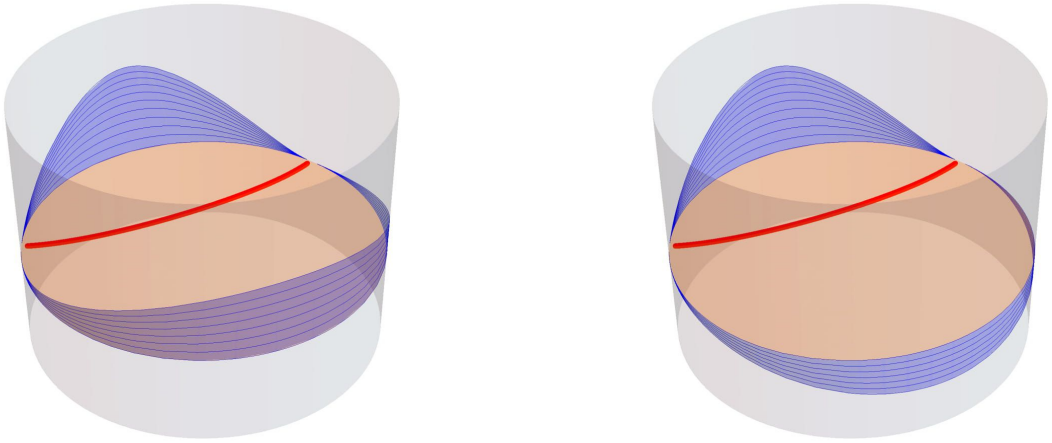

Figure 6.1: A holographic representation of eqs. (6.3)-(6.7): the global state W_{ij} of a bipartite holographic CFT is prepared by a tensor network that fills a spatial slice of the bulk spacetime (orange). The division of the CFT is illustrated with a red line that cuts through the bulk. The panels show two general examples of 'gauge transformations' of 'Wilson line' W. The focus of this chapter will be on those gauge transformations, which localize on HRRT surfaces.

the action of a local $SU(2)$ symmetry on each qubit as:

$$W_{ij} \to U^{\dagger}_{A,\,ik} W_{kl}\, U_{B,\,lj}. \tag{6.7}$$

By virtue of (6.5), (6.6) and (6.7), the matrix W_{ij} can be interpreted as an open Wilson line between the Hilbert spaces of the two qubits, with a form dictated by the pattern of entanglement. From a heuristic ER=EPR viewpoint, W_{ij} can be thought of as the gravitational Wilson line threading the quantum wormhole connecting the qubits [210].

Our main interest is in applying these observations to holographic duality; see Figure 6.1. If we divide a holographic CFT into two subregions A and B, a global pure state can likewise be represented as a matrix W_{ij} that is analogous to (6.3). We can think of this matrix as being prepared by a tensor network that fills a spatial slice of the bulk spacetime. Under changes of bases in A and in B, the matrix also transforms as in (6.7), i.e. as a Wilson line. What are the corresponding Wilson loops? Are they non-trivial and what feature of the bulk spacetime do they probe? We will answer these questions in the following part of this chapter. One highlight is that the holonomies of the entanglement connection probe the curvature of the dual spacetime. We interpret this as an indication that the pattern of entanglement of subsystems and the pattern of physical Wilson line dressing in gauge theories ought to be considered on equal footing.

The remainder of this section is devoted to formulating the quantum notion of connection when the subsystems of interest are subregions of a CFT, in arbitrary states. As in all geometric problems that involve a connection, the correct mathematical formalism here is that of fiber bundles. A reminder of the relevant concepts from differential geometry, as well as a description of the fiber bundle at hand, is given in Figure 6.2.

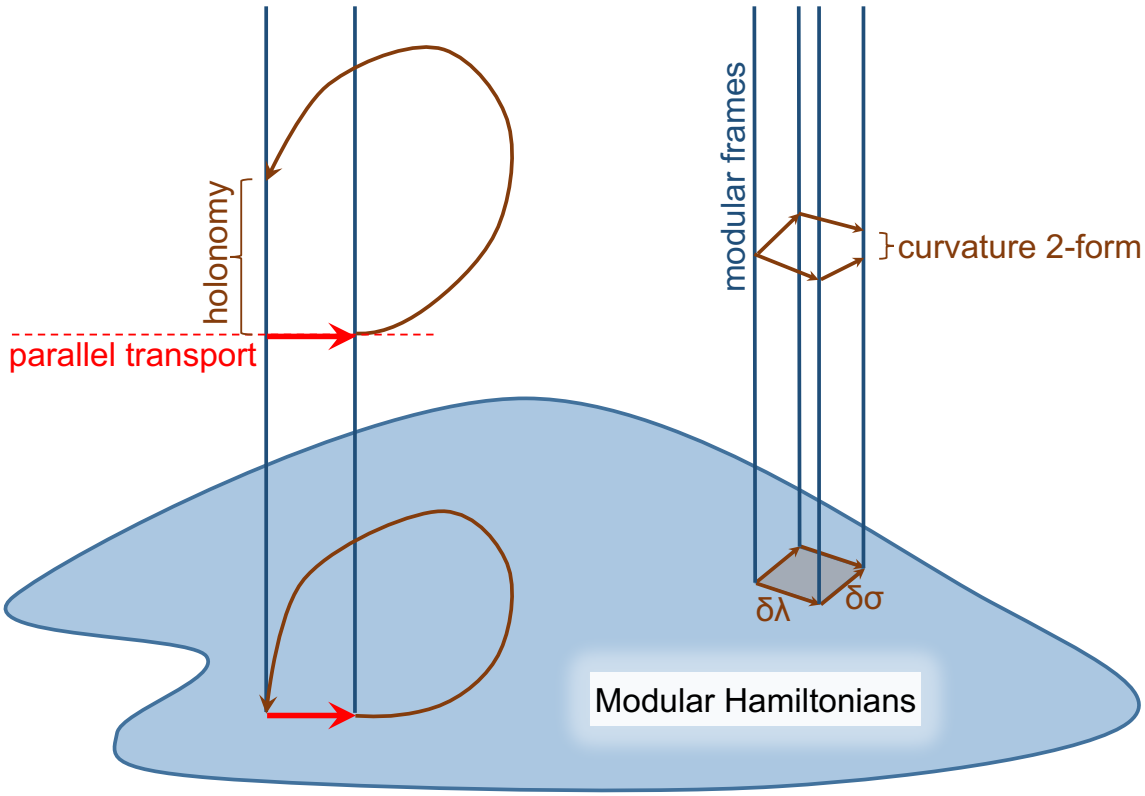

Figure 6.2: The fiber bundle structure of the modular connection. The base comprises different modular Hamiltonians and the fibers are modular zero mode frames.

6.2.2 Gauging the modular zero modes

Every subregion A of a CFT selects an algebra of operators $\mathcal{A}_A$ that is localized in it, and a modular Hamiltonian H_{mod} which encodes the reduced state in A via $H_{\text{mod}} = -\log \rho_A$. Strictly speaking, density matrices are not well-defined objects in quantum field theory and become meaningful only in the presence of a UV cutoff. In contrast, the sum of the modular Hamiltonians of $\mathcal{A}_A$ and its commutant $\mathcal{A}_{\bar{A}}$ is well-defined in the continuum and any rigorous construction should directly refer these two-sided operators.

We emphasize that our discussion is inherently two-sided. In order to postpone a few minor subtleties for conceptual clarity, however, we choose to phrase our initial presentation in terms of single-sided H_{mod}s and comment on its two-sided version in subsection 6.2.3.

Modular zero modes as local symmetries. Hermitian operators Q_i^A obeying

$$\left[Q_i^A, H_{\text{mod},A}\right] = 0\,, \tag{6.8}$$

are called *modular zero modes*. The unitary flow generated by Q_i defines an automorphism of $\mathcal{A}_A$ that is a *symmetry* of subregion A: The transformation

$$O \to U_Q^\dagger(s_i)\, O\, U_Q(s_i) \quad \forall\, O \in \mathcal{A}_A\,, \tag{6.9}$$

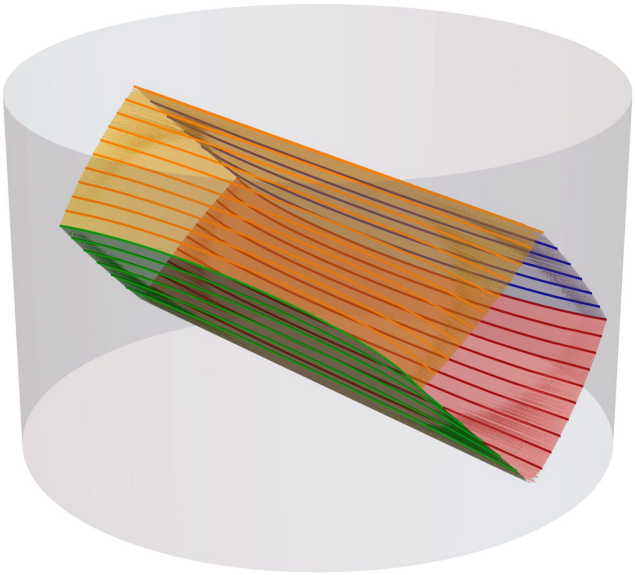

Figure 6.3: A closed trajectory in the space of CFT regions. To avoid clutter and to clarify the holographic application, here we display the family of corresponding RT surfaces in the bulk of AdS.

where $U_Q = e^{-i\sum_i Q_i s_i}$, maps the algebra into itself while preserving the expectation values of all of its elements in the given state. As a result, physical data localized in a subregion carry no information about its overall zero mode frame. This local ambiguity is, of course, irrelevant for all measurements or computations restricted to A. It is a gauge freedom, which spans the vertical (fiber) directions of our bundle.

A useful way of describing the zero-mode ambiguity is by switching to a 'Schrödinger picture.' The modular Hamiltonian is a Hermitian operator on the CFT Hilbert space, so it can be decomposed as

$$H_{\text{mod}} = U^\dagger \Delta U, \tag{6.10}$$

where a diagonal matrix Δ encodes the spectrum and a unitary U selects the basis of eigenvectors. Transformations generated by Q_i preserve the form of H_{mod} and, as a result, the basis U in (6.10) is only determined up to a gauge transformation consisting of right multiplication by U_Q:[3]

$$U \to U' = UU_Q. \tag{6.11}$$

Modular Berry connection as the relative zero-mode frame. Consider now a continuous family of connected CFT subregions parametrized by λ and their modular Hamiltonians $H_{\text{mod}}(\lambda)$. (See Figure 6.3.) The relations between these modular Hamiltonians can be conveniently expressed in terms of two families of operators: One describing the change of spectrum

[3] In other words, there is an equivalence class of CFT bases defined by $U \sim UU_Q$, in which H_{mod} has identical matrix elements.

and another the precession of the basis as we vary λ. In particular, using decomposition (6.10), the λ-derivative of $H_{\rm mod}(\lambda)$ is organized as

$$\dot{H}_{\rm mod} = [\dot{U}^\dagger U, H_{\rm mod}] + U^\dagger \dot{\Delta} U, \tag{6.12}$$

where $\dot{} \equiv \partial_\lambda$ and we have suppressed the λ-dependence of all operators for clarity. This shape-derivative derivative of $H_{\rm mod}$ may cause some discomfort to the careful reader, since the density matrices of different subregions formally live in different Hilbert spaces. For an infinitesimal transformation of the region's boundary, however, this computation is in fact under control, as was shown in [218]. The trick is to think of the shape deformation as sourcing a stress-tensor insertion at the subregion's boundary. The calculation requires a delicate treatment of the cutoff but it yields sensible results both in the CFT [218] and holographically [219]. In case this comment does not alleviate the reader's distress, we emphasize again that the discussion can be entirely expressed in terms of the full modular operators $H_{\rm mod}(\lambda) + H_{\rm mod}(\lambda^c)$, with λ^c the complement of region λ, which are well-defined operators on the full CFT Hilbert space, and refer them to subsection 6.2.3 for a detailed comment.

The second term on the right hand side of (6.12) encodes the change in the spectrum of $H_{\rm mod}$ and, since $[U^\dagger \dot{\Delta} U, H_{\rm mod}] = 0$, it belongs to the local algebra of modular zero modes. We can isolate this spectrum changing piece by introducing a projector P_0^λ onto the zero-mode sector of $H_{\rm mod}(\lambda)$. The latter can formally be constructed in terms of modular flow[4]

$$P_0^\lambda[V] \equiv \lim_{\Lambda\to\infty} \frac{1}{2\Lambda} \int_{-\Lambda}^{\Lambda} ds\; e^{iH_{\rm mod}(\lambda)s}\, V e^{-iH_{\rm mod}(\lambda)s}\,, \tag{6.13}$$

or in a Hilbert space representation simply as:

$$P_0^\lambda[V] \equiv \sum_{E,q_a,q_a'} |E,q_a\rangle\langle E,q_a|V|E,q_a'\rangle\langle E,q_a'|, \tag{6.14}$$

where $|E,q_a\rangle$ are simultaneous eigenstates of $H_{\rm mod}(\lambda)$ and a commuting set of zero modes Q_a, with eigenvalues E and q_a respectively. For systems with finite-dimensional Hilbert spaces, the zero-mode projector takes another useful form. Hermitian operators on a Hilbert space $\mathcal{H}$ with $\dim(\mathcal{H}) = D$ form a vector space and $\{\mathbb{I}, T_i\}$, where T_i the $SU(D)$ generators, form a complete basis which is orthonormal with respect to the Frobenius inner product $(T_i|T_j) = \frac{1}{D}\mathrm{Tr}\,[T_i T_j] = \delta_{ij}$. One can, therefore, find an orthonormal basis of modular zero modes $\{Q_i\}$, $[Q_i, H_{\rm mod}] = 0$ and $(Q_i|Q_j) = \delta_{ij}$ and define the projector:

$$P_0[V] = \sum_i (Q_i|V)Q_i = \sum_i \frac{1}{D}\mathrm{Tr}[Q_i V]Q_i. \tag{6.15}$$

An application of P_0^λ on both sides of eq. (6.12) then equates the spectrum changing operator

[4] This formula should be taken with a grain of salt since there can be Hermitian eigen-operators of the modular Hamiltonian $[H_{\rm mod}, V] = \kappa V$ which necessarily have imaginary eigenvalues, leading to exponential contributions to the integral (6.13).

to the zero mode component of $\dot{H}_{\text{mod}}$:

$$U^\dagger \dot{\Delta} U = P_0^\lambda[\dot{H}_{\text{mod}}(\lambda)]. \tag{6.16}$$

The operator $\dot{U}^\dagger(\lambda)U(\lambda)$ in (6.12), in turn, encodes the change of basis accompanying an infinitesimal shape variation of the region. Combining eq. (6.12) and (6.16) the relative basis operator is defined as the solution to equation:

$$\dot{H}_{\text{mod}} - P_0^\lambda[\dot{H}_{\text{mod}}] = [\dot{U}^\dagger U, H_{\text{mod}}(\lambda)]. \tag{6.17}$$

As is apparent, (6.17) fixes $\dot{U}^\dagger(\lambda)U(\lambda)$ only up to addition of zero modes. This ambiguous zero mode component is precisely the information we seek and it leads us to introduce the modular Berry connection:

Definition 1 *Consider the space of CFT subregions $\mathcal{K}$, parametrized by a set of coordinates λ^i.*[5] *The* ***modular Berry connection*** *is a 1-form in $\mathcal{K}$ that encodes the* ***relative zero mode frame*** *of infinitesimally separated modular Hamiltonians $H_{mod}(\lambda^i)$ and $H_{mod}(\lambda^i + \delta\lambda^i)$ and is given by:*

$$\Gamma(\lambda^i, \delta\lambda^i) = P_0^\lambda[\partial_{\lambda^i} U^\dagger U]\, \delta\lambda^i, \tag{6.18}$$

where P_0^λ is the projector onto the zero-mode sector of $H_{mod}(\lambda^i)$ given by (6.13) or (6.14). Under a λ-dependent gauge transformation (6.11), the connection (6.18) transforms as:

$$U(\lambda) \to U'(\lambda) = U(\lambda)U_Q(\lambda) \;\Rightarrow\; \Gamma \to \Gamma' = U_Q^\dagger\, \Gamma\, U_Q - U_Q^\dagger \partial_{\lambda^i} U_Q\, \delta\lambda^i\,. \tag{6.19}$$

For the readers who may find expression (6.18) for the Berry connection unfamiliar or confusing, in Appendix C.1 we include a short illustration of how (6.18) reduces to the standard Berry connection [220, 221] when applied to a family of pure states.

Modular parallel transport and holonomies. Granted a connection on a bundle, we can define a covariant derivative

$$D_\lambda^{(r)} = \partial_\lambda + \Gamma^{(r)}, \tag{6.20}$$

where $\Gamma^{(r)}$ is an appropriate representation of connection (6.18). This covariant derivative generates *parallel transport*. Any charged object, parallel transported along a closed loop $\mathcal{C}$, returns to its starting point transformed by the holonomy of $\mathcal{C}$.

Consider now a continuous 1-parameter family of modular Hamiltonians of a QFT state, $H_{\text{mod}}(\lambda)$, $\lambda \in [0, 1]$, which forms a closed loop $H_{\text{mod}}(0) = H_{\text{mod}}(1)$. The operator $U(\lambda)$ from eq. (6.10), which encodes the local choice of basis in every subregion, is charged under the zero modes with transformation rule (6.11). Therefore, we can compute the modular Berry holonomy of our closed loop by solving the transport problem for U.

Parallel transport of $U(\lambda_0)$ assigns a basis $\tilde{U}(\lambda)$ to the modular Hamiltonians $H_{\text{mod}}(\lambda)$ for all

[5] The index i here can be discrete or continuous. For subregions of quantum field theories in d spacetime dimensions, which is our main focus in this chapter, λ^i stands for the shape and location of the subregion's boundary.

$\lambda \in [0,1]$, with the initial conditon $\tilde{U}(\lambda_0) = U(\lambda_0)$. For an infinitesimal step $\delta\lambda$ away from λ_0, $\tilde{U}$ is equal to

$$\tilde{U}(\lambda_0 + \delta\lambda) \approx U(\lambda_0) + \delta\lambda\, D_\lambda U(\lambda_0) = U(\lambda_0 + \delta\lambda) + U(\lambda_0) P_0^{\lambda_0}[\dot{U}^\dagger U]\delta\lambda. \tag{6.21}$$

Multiplying both sides of (6.21) with $\tilde{U}^\dagger(\lambda_0)$ from the left, we observe that the operator $V_{\delta\lambda} = \tilde{U}^\dagger \frac{\delta}{\delta\lambda}\tilde{U}$ that generates the parallel transport of the basis obeys the conditions:

$$\begin{aligned} &\dot{H}_{\rm mod} - P_0^\lambda[\dot{H}_{\rm mod}] = [V_{\delta\lambda}(\lambda), H_{\rm mod}], \\ &P_0^\lambda[V_{\delta\lambda}(\lambda)] = 0. \end{aligned} \tag{6.22}$$

Equations (6.22) *define* the modular Berry transport. In section 6.2.4, we solve this transport problem in two tractable examples and compute the modular curvature.

What are the modular zero modes? An important comment is in order. In a typical CFT state, the only symmetries of the modular Hamiltonian of a subregion are generated by $H_{\rm mod}$ itself or the zero-modes of any globally conserved charges—or they are phase rotations of individual modular eigenstates. However, in anticipation of a connection to holography, it is important to recall that the equivalence of the bulk and boundary modular operators (6.1) proposed by JLMS [82] holds within a code subspace

$$P_{\rm code} H_{\rm mod} P_{\rm code} = \frac{A}{4G_N} + H_{\rm bulk}\,, \tag{6.23}$$

as articulated in the error correction framework of [205]. In connecting our CFT discussion to the bulk we are, therefore, not interested in exact zero-modes but only in approximate ones, constructed by the requirement that they commute with the code subspace projection of $H_{\rm mod}$

$$[Q_i, P_{\rm code} H_{\rm mod} P_{\rm code}] = 0. \tag{6.24}$$

We discuss the importance of this point in more detail in Section 6.4.

6.2.3 Comment on two-sided modular Hamiltonians

Having concluded the presentation of our CFT formalism in the language of subregion modular Hamiltonians, we wish to illustrate that the construction can be phrased directly in terms of the full modular Hamiltonians of CFT bipartitions, $H_{\rm full}(\lambda) \equiv H_{\rm mod}(\lambda) + H_{\rm mod}(\lambda^c)$, with λ^c the complement of region λ. This is important because it is $H_{\rm full}(\lambda)$, and not $H_{\rm mod}(\lambda)$, that generate a well-defined unitary flow in continuum quantum field theories.

First note that the zero-modes of the single-sided modular Hamiltonians (6.8) are obviously a subset of zero-modes of the full modular operator. However, $H_{\rm full}$ has a much larger set of zero-modes $\tilde{Q}_i$. These generate unitary transformations on the entire Hilbert space that do not necessarily factorize to products of unitary operators on the two complementary subregions. Intuitively, they are transformations that are allowed to change the density matrix ρ_λ but preserve $\rho_\lambda \otimes \rho_{\lambda^c}^{-1}$. The fiber bundle associated to the full modular Hamiltonians has, therefore, a much

larger gauge group than the one for the single-sided H_{mod}s.

Nevertheless, the modular Berry holonomies associated to a given global state $|\psi\rangle$ are identical for the two problems. The reason is that the Hilbert space vector $|\psi\rangle$ "spontaneously breaks" the symmetry group of $H_{\text{full}}(\lambda)$ to the subgroup that preserves the state:

$$U_{\tilde{Q}_i}|\psi\rangle = |\psi\rangle. \tag{6.25}$$

As a result, parallel transport will only generate holonomies valued in the much smaller subgroup of zero-modes (6.25) which is shared between the two-sided and single-sided modular operators. The vanishing of the Berry curvature components along the extra zero-mode directions of H_{full} implies that there is a globally consistent gauge in which the relevant projection of the connection vanishes everywhere and the computation reduces to the one presented in the previous section.

6.2.4 Modular Berry holonomy examples

CFT_2 Vacuum

We now put our definition (6.18) to work and explicitly compute the modular curvature in a tractable, illustrative example: the vacuum of a CFT_2 on a circle. This was computed previously in [212] by exploiting the geometry of the space of CFT intervals, or kinematic space [222, 223]. This subsection establishes the consistency of the general rules proposed here with the results of [212].

The (two-sided) vacuum modular Hamiltonian of an interval is an element of the conformal algebra. The global $SO(2,2)$ symmetry algebra of a CFT_2 decomposes to a pair of commuting $SO(2,1)$ subalgebras, which act on left-moving and right-moving null coordinates x^+ and x^-, respectively. The commutation relations are

$$[L_0, L_1] = -L_1\,, \qquad [L_0, L_{-1}] = L_{-1}\,, \qquad [L_1, L_{-1}] = 2L_0\,, \tag{6.26}$$

and similarly for $\bar{L}_i$.

The modular Hamiltonian of the interval with endpoints at $x_L^\mu = (a^+, a^-)$ and $x_R^\mu = (b^+, b^-)$ is the generator of the boost transformation that preserves x_L and x_R and has the form

$$H_{\text{mod}} = K_+ + K_-,$$

where K_+ and K_- are linear combinations of $L_{-1,0,1}$ and $\bar{L}_{-1,0,1}$. Their coefficients are functions of the endpoint coordinates of the interval; we derive them in Appendix C.2.

In order to compute modular Berry holonomies, we need to solve the parallel transport problem for the basis of the modular Hamiltonian. For example, given two nearby modular Hamiltonians $K_+(a^+, b^+)$ and $K_+(a^+ + da^+, b^+)$, we need to find an operator $V_{\delta a^+}$ that solves equations (6.22). Using the explicit form of the modular Hamiltonian (C.7) and the conformal algebra, we find that

$$\partial_{a^+} K_+ = \frac{1}{2\pi i}\,[\partial_{a^+} K_+,\, K_+]\,, \tag{6.27}$$

so in this case parallel transport is generated by $(1/2\pi i)\,\partial_{a^+} K_+$. More details of the calculation,

as well as parallel transport along more general trajectories in the space of CFT intervals, are given in Appendix C.2.

The modular Berry curvature can now be computed straightforwardly:

$$R[\delta a^+, \delta b^+] = -\frac{1}{2\pi i}\frac{K_+}{\sin^2\left(b^+ - a^+\right)/2},$$
$$R[\delta a^-, \delta b^-] = -\frac{1}{2\pi i}\frac{K_-}{\sin^2\left(b^- - a^-\right)/2}. \tag{6.28}$$

This exercise can also be applied to the computation of holonomies for modular Hamiltonians of ball-shaped regions in the vacuum of higher dimensional CFTs.

Null deformations and modular inclusions

The solution to the modular Berry transport becomes tractable in another interesting example: Families of modular Hamiltonians for subregions with null separated boundaries, in a CFT_d vacuum. The origin of the simplification in this case is not conformal symmetry but, more interestingly, an algebraic QFT theorem for *half-sided modular inclusions* [224].

Two operator subalgebras $\mathcal{A}_1$ and $\mathcal{A}_2 \subset \mathcal{A}_1$ are said to form a *modular inclusion* if modular evolution by $H_{\text{mod},1}$ maps $\mathcal{A}_2$ into itself for all *positive* modular times:

$$U^\dagger_{\text{mod},1}(s)\mathcal{A}_2 U_{\text{mod},1}(s) \subset \mathcal{A}_2, \quad \forall s > 0. \tag{6.29}$$

The half-sided modular inclusion theorem then states that the modular Hamiltonians of included algebras satisfy the commutator:

$$[H_2, H_1] = 2\pi i(H_2 - H_1). \tag{6.30}$$

In the CFT_d vacuum, when two subregions are related by an infinitesimal null deformation $x^\mu_{e.s.} \to x^\mu_{e.s.} + u^\mu(x_{e.s})$ their algebras are indeed included and (6.30) directly implies:

$$\left[\frac{\delta H_{\text{mod}}}{\delta u(x)}, H\right] = 2\pi i \frac{\delta H_{\text{mod}}}{\delta u(x)}. \tag{6.31}$$

The null functional derivative of the modular Hamiltonian $\frac{\delta H_{\text{mod}}}{\delta u(x)}$ is, therefore, an eigen-operator of H with non-zero eigenvalue $2\pi i$ that satisfies (6.22). The parallel transport operator for null deformations is then:

$$V_{\delta u} = \frac{1}{2\pi i}\frac{\delta H_{\text{mod}}}{\delta u(x)}. \tag{6.32}$$

6.3 Entanglement Wedge Connection

6.3.1 Modular zero modes in the bulk

The link between our CFT discussion and the bulk gravity theory is the JLMS relation [82, 207, 208]. The modular Hamiltonian of a boundary subregion is holographically mapped to

$$H_{\text{mod}} = \frac{A}{4G_N} + H^{\text{bulk}}_{\text{mod}} \tag{6.33}$$

where A is the HRRT surface area operator and $H^{\text{bulk}}_{\text{mod}}$ the modular Hamiltonian of the bulk QFT state in the associated entanglement wedge. This operator equivalence holds within the subspace of the CFT Hilbert space that corresponds to effective field theory excitations about a given spacetime background, called the code subspace [205].

An important consequence of (6.33) is that, for all holographic states of interest, H_{mod} admits a geometric description in a small neighborhood of the HRRT surface [206,225]. The area operator in Einstein gravity is identified with the Noether charge for diffeomorphisms ζ^M_{mod} that asymptote to a homogenous boost near the RT surface. Moreover, for finite energy bulk states, $H^{\text{bulk}}_{\text{mod}}$ reduces to its vacuum expression in the same neighborhood, implementing the above boost transformation on the matter fields. This renders the, generally non-local, H_{mod} a geometric boost generator at the edge of the entanglement wedge.

To make our discussion concrete, we partially fix the gauge to be orthonormal to the HRRT surface

$$\begin{aligned} g = &\Big(\eta_{\alpha\beta} + w_{\alpha\beta|\gamma}(y)\, x^\gamma + \mathcal{O}(x^2)\Big) dx^\alpha \otimes dx^\beta + \Big(2\sigma_{i\alpha|\beta}(y)\, x^\beta + \mathcal{O}(x^2)\Big) dx^\alpha \otimes dy^i + \\ &+ \Big(\gamma_{ij}(y) + K_{ij|\alpha}(y)\, x^\alpha + \mathcal{O}(x^2)\Big) dy^i \otimes dy^j \,, \end{aligned} \tag{6.34}$$

where y^i, $i = 2, \ldots, d$ is some choice of coordinates along the minimal surface directions and x^α, $\alpha = 0, 1$ parametrize distances along two orthogonal transverse directions, with the extremal surface at $x^\alpha = 0$. The boost generated by the CFT modular Hamiltonian in the gauge (6.34) reads:

$$\begin{aligned} \zeta^\alpha_{\text{mod}} &\overset{x^\alpha \sim 0}{\to} 2\pi \epsilon^{\alpha\beta} x_\beta, \\ \zeta^i_{\text{mod}} &\overset{x^\alpha \sim 0}{\to} 0. \end{aligned} \tag{6.35}$$

This approximation for the modular flow is valid within a neighborhood with size set by the normal extrinsic curvature of the HRRT surface $x^+ K_{ij|+}$, $x^- K_{ij|-} \ll 1$ where $x^\pm$ normal light-like coordinates [206]. Beyond this regime, modular flow gets modified by generically non-local contributions. Our entire discussion in this section assumes the validity of approximation (6.35). We will discuss how the corrections restrict the regime of validity of our results in Section 6.3.3.

Bulk modular zero modes. As is the case for the modular Hamiltonian itself, the zero modes will generally be non-local operators in the bulk wedge, defined by $\left[Q_i, H^{\text{bulk}}_{\text{mod}}\right] = 0$. Near the extremal surface, however, due to the geometric action of H_{mod} a class of zero modes will reduce

to generators of spacetime transformations:

$$Q = \zeta^M(y^i)\partial_M + \mathcal{O}(x^+ K_{ij|+},\, x^- K_{ij|-}). \tag{6.36}$$

These need to preserve the location and area of the HRRT surface and commute with the modular boost (6.35), which translates to the condition

$$[\zeta, \zeta_{\rm mod}]^M = \zeta^N \partial_N \zeta^M_{\rm mod} - \zeta^N_{\rm mod} \partial_N \zeta^M = 0, \tag{6.37}$$

where the indice $M = 0, 1, \ldots, d$ covers both the transverse directions and tangential directions to the RT surface. Moreover, we demand that the diffeomorphisms generated by (6.36) are non-trivial. In a spacetime with no boundary, all spacetime transformations have vanishing generators, as a result of the constraint equations of gravity. When boundaries exist, however, diffeomorphisms that act non-trivially on them are endowed with non-vanishing Noether charges.

An entanglement wedge has two boundaries: The standard asymptotic boundary used to define CFT correlators and the boundary selected by the HRRT surface. Large diffeomorphisms that do not vanish asymptotically give rise to the boundary conformal group and they are not relevant for us here. On the other hand, diffeomorphisms that act non-trivially on the HRRT surface have Noether charge[6] [227]

$$Q_\zeta = -\frac{1}{4\pi G_N} \int_{RT} d^2x \sqrt{\gamma}\, \epsilon^{\alpha\beta} \nabla_\alpha \zeta_\beta \,, \tag{6.38}$$

and constitute bulk zero-modes when $Q_\zeta \neq 0$ and (6.37) is satisfied. The modular boost is, of course, one of them, with a Noether charge equal to the area of the extremal surface in Planck units.

The symmetry group selected by the above requirements consists of diffeomorphisms along the minimal surface directions and location-dependent boosts in its normal plane. In gauge (6.34) the zero-modes read

$$\begin{aligned} \zeta^\alpha &\overset{x^\alpha \sim 0}{\longrightarrow} \omega(y)\, \epsilon^{\alpha\beta} x_\beta, \\ \zeta^i &\overset{x^\alpha \sim 0}{\longrightarrow} \zeta^i_0(y) + 0 \cdot x \end{aligned} \tag{6.39}$$

where in the second line we chose to explicitly emphasize the vanishing transverse derivative of the $i-$th component, $\partial_\alpha \zeta^i\big|_{x^\alpha = 0} = 0$, as demanded by (6.37). It follows that the class of zero modes $\zeta^i \partial_i$ map the HRRT surface to itself while preserving its normal frame, a fact that will play a crucial role in section 6.3.2.

Transformations (6.39) are the gravitational edge modes discussed in [213] and the analogue of the horizon symmetries of [215] where our RT surface replaces their black hole horizon. As in our CFT discussion, the vector fields (6.39) generate symmetries of the physics near $x^\alpha = 0$ in a given wedge and will be treated as local gauge transformations on the space of entanglement wedges. We should note that, in general, there exist other zero-modes as well, e.g. edge-modes of bulk

[6] A more clear and thorough analysis on the conserved currents and Noether charges using the Wald-Iyer formalism could be found in [226].

gauge fields, that generate extra components of the modular Berry connection. The gravitational edge-modes discussed here, however, are universally present in holographic theories and for this reason we choose to focus our discussion on them.

6.3.2 Relative edge-mode frame as a connection

Consider now two entanglement wedges, λ and $\lambda + \delta\lambda$, whose HRRT surfaces are infinitesimally separated from each other. Each wedge is equipped with a vector field $\zeta^M_{\text{mod}}(x;\lambda)$ generating the corresponding modular flow near its HRRT surface. Moreover, each wedge comes with its own arbitrary choice of zero-mode frame, which given (6.39) is simply an internal coordinate system on the extremal surface and a hyperbolic angle coordinate on its transverse 2D plane. Figure 6.4 below zooms in on a small fragment of four extremal surfaces and displays their zero-mode frames.

The key idea now is that the geometry of the global spacetime enables us to compare the two zero mode frames. What makes this possible is the existence of diffeomorphisms $x^M \to x^M + \xi^M(x)$, which map one extremal surface to the other, allowing us to relate the coordinate systems in their neighborhoods. Bulk diffeomorphisms, therefore, play the role of the relative basis operator $\dot{U}^\dagger U$ (6.17) in our CFT discussion.

Mapping the modular boost generators. It is instructive to proceed in parallel with our CFT construction of Section 6.2.2. The λ-variation of the modular Hamiltonian in the bulk becomes the difference of the vector fields $\zeta^M_{\text{mod}}(x;\lambda)$ and $\zeta^M_{\text{mod}}(x;\lambda+\delta\lambda)$. As in CFT, this can generally be organized into two contributions as follows

$$\delta_\lambda \zeta^M_{\text{mod}}(x;\lambda) = [\xi(x;\lambda,\delta\lambda), \zeta_{\text{mod}}(x;\lambda)]^M + P_0^\lambda[\delta_\lambda \zeta^M_{\text{mod}}(x;\lambda)]\,, \tag{6.40}$$

where $\delta_\lambda\zeta^M_{\text{mod}}$ is the difference between the two modular generators and P_0 is the bulk projector onto zero modes discussed in more detail below (see eq. (6.46)). The vector field $\xi(x;\lambda,\delta\lambda)$ is a diffeomorphism rotating the basis of the modular Hamiltonian, which in the geometric regime is simply the local coordinate system. On the other hand, the zero-mode projection describes the change in the spectrum. Condition (6.40) is the direct bulk analogue of CFT equation (6.17).

Equation (6.40) determines the diffeomorphism ξ up to additive contributions by zero-mode transformations (6.39). A formal but explicit solution to the general problem can be obtained as follows. First, we introduce the transverse location $\delta x^\alpha = \delta x^\alpha(y^i;\lambda,\delta\lambda)$ of the HRRT surface $\lambda+\delta\lambda$ relative to λ. Crucially, δx^α is determined simply by the deformation $\delta x^\mu_{\partial B}$ of the boundary subregion the surface is anchored at. This follows from equation

$$\delta_{\delta x} K_\alpha = -\eta_{\alpha\beta}\gamma^{ij}\nabla_i\nabla_j\delta x^\beta + \gamma^{ij}R_{i(\alpha\beta)j}\delta x^\beta - K_{\alpha;ij}K_\beta{}^{ij}\delta x^\beta = 0\,, \tag{6.41}$$

where $K_{\alpha;ij} = \mathcal{L}_\alpha g_{ij}$ is the normal extrinsic curvature and $K_\alpha = \gamma^{ij}K_{\alpha;ij}$, which ensures the new surface at δx^α is also extremal, as discussed in detail in [219]. Eq. (6.41) fixes the form of δx^α in terms of its boundary condition $\delta x^\mu_{\partial B}$.

Second, we recall that the vector field ζ_{mod} generates boosts on the normal 2-D plane of the HRRT surface. $\zeta_{\text{mod}}(\lambda+\delta\lambda)$ therefore needs to also have the form (6.35) in normal coordinates about $\lambda+\delta\lambda$. To express this requirement, we introduce a pair of normal vectors on the new

surface $n_\alpha{}^M(y;\lambda+\delta\lambda) = \delta^M_\alpha + \delta n_\alpha{}^M(y) + \mathcal{O}(\delta n^2)$, where $\alpha = 0, 1$ with $n_\alpha \cdot n_\beta = \eta_{\alpha\beta}$.[7] Imposing both conditions on $\xi(x;\lambda,\delta\lambda)$ then leads to the following solution of eq. (6.40):

$$\begin{aligned}\xi^M(x^M;\lambda,\delta\lambda) = &-\delta^M_\alpha\,\delta x^\alpha - \left(\delta n_\alpha{}^M + \Gamma^M_{\alpha\beta}\,\delta x^\beta\right) x^\alpha \\ &+ \omega(y)\delta^M_\alpha\,\epsilon^\alpha{}_\beta x^\beta + \delta^M_i\,\zeta^i_0(y),\end{aligned} \tag{6.42}$$

where Γ^M_{NK} are the Christoffel symbols in gauge (6.34). A detailed derivation of $\xi(x;\lambda,\delta\lambda)$ is given given in Appendix C.3. The expression for the diffeomorphism ξ in an arbitrary gauge can, of course, be obtained simply by a change of coordinates in (6.42).

The quantities $\omega(y)$ and $\zeta^i_0(y)$ are arbitrary functions of the minimal surface coordinates representing the edge-mode ambiguity in ξ^M. The arbitrariness in $\omega(y)$ is precisely our freedom in selecting a pair of orthonormal vectors $n_\alpha{}^M$ among the family of Lorentz equivalent pairs, as can be seen by the transformation of $\delta n_a{}^M$ under a local Lorentz boost on the surface's transverse plane

$$\delta n_\beta{}^\alpha \to \delta n_\beta{}^\alpha + \omega(y)\epsilon_\beta{}^\alpha. \tag{6.43}$$

The zero-mode ω can, therefore, be absorbed into the redefinition of $\delta n_\alpha{}^M$. The undetermined function $\zeta^i_0(y)$, in turn, expresses our freedom to pick the coordinate system on the surface $\lambda+\delta\lambda$ at will.

Bulk modular connection. The ambiguous edge-mode part in the solution of (6.40) encodes the *relative zero-mode frame* of the two entanglement wedges. In order to define the bulk modular connection we, therefore, need to perform a zero-mode projection of the diffeomorphism ξ^M, mapping between the two coordinate systems at λ and $\lambda+\delta\lambda$. In covariant form, the zero-mode component of the vector field ξ that *defines* modular connection in the bulk reads[8]

$$\Gamma(\lambda,\delta\lambda) = \Omega[\xi]\mathcal{L}_\Omega + Z^i[\xi]\mathcal{L}_{Z^i} \tag{6.44}$$

where $\mathcal{L}_\Omega$ and $\mathcal{L}_{Z^i}$ are the Lie derivatives generating the corresponding asymptotic symmetries of the HRRT surface (6.39), and

$$\begin{aligned}\Omega[\xi(\lambda,\delta\lambda)] &= \frac{1}{2}\epsilon^{\alpha\beta} n_\alpha{}^M\,\partial_M\left(n_{\beta N}\xi^N\right)|_{RT} \\ &= \frac{1}{2}\epsilon^{\alpha\beta}\left(n_{\alpha M}\,\Delta_{\delta\lambda} n_\beta{}^M + n_{\alpha M}\,\Gamma^M_{\gamma K}\delta x^\gamma\, n_\beta{}^K\right), \end{aligned} \tag{6.45}$$

$$Z^i[\xi(\lambda,\delta\lambda)] = -t^i_N \xi^N|_{RT}\,. \tag{6.46}$$

Here $n_\alpha{}^M(\lambda)$ $(\alpha = 0, 1)$ are two unit normal vectors on the extremal surface λ with $n_\alpha \cdot n_\beta = \eta_{\alpha\beta}$ and t^{iN} $(i = 2, \ldots, d)$ are the corresponding tangents. We also introduced $\Delta_{\delta\lambda}$ for the 'internal'

[7] There is of course no unique choice. There is a continuous family of normal vectors related by local Lorentz transformations, which will be important later on.

[8] It is straightforward to confirm that the definition of the zero-mode projector $P[\xi] = -\Omega[\xi]\epsilon^\alpha{}_\beta x^\beta\partial_\alpha - Z^i[\xi]\partial_i$ satisfies $P \circ P = P$, is itself a zero-mode and it annihilates the vector Lie bracket $[\xi, \zeta_{\text{mod}}]$, as any consistent projector should.

covariant derivative associated to the $d-2$-dimensional diffeomorphism subgroup

$$\Delta_{\delta\lambda} = \delta\lambda \frac{\partial}{\partial\lambda} + Z^i[\xi]\mathcal{L}_{Z^i}. \tag{6.47}$$

It is very important here that the zero-mode $\mathcal{L}_{Z^i}$ preserves the normal frame, as explained around eq. (6.39), and, therefore, provides a canonical map between normal vectors at different locations on the same HRRT surface, allowing the construction of the internal covariant derivative (6.47).

Expression (6.45) for the boost component of $\Gamma(\lambda, \delta\lambda)$ is, by definition, the spin connection for the normal frame of the HRRT surface. The role of the covariant derivative $\Delta_{\delta\lambda}$ is to *align the internal coordinates* of the nearby minimal surfaces before comparing the normal frames at the 'same location'. Thus, the curvature of our modular Berry connection computes the bulk Riemann curvature *when* the approximation (6.35) of the modular flow is justified. We explain this proviso in more detail in the next subsection.

6.3.3 Bulk modular curvature and parallel transport

Equipped with connection (6.44), the bulk modular curvature follows from the standard definition. It reads:

$$\begin{aligned} R_{\delta\lambda_1\delta\lambda_2} &= \delta_{\delta\lambda_1}\Gamma(\delta\lambda_2) - \delta_{\delta\lambda_2}\Gamma(\delta\lambda_1) + [\Gamma(\delta\lambda_1), \Gamma(\delta\lambda_2)] \\ &= \Big(\Delta_{\delta\lambda_1}\Omega(\delta\lambda_2) - \Delta_{\delta\lambda_2}\Omega(\delta\lambda_1)\Big)\mathcal{L}_\Omega \\ &+ \Big(\Delta_{\delta\lambda_1}Z^i(\delta\lambda_2) - \Delta_{\delta\lambda_2}Z^i(\delta\lambda_1)\Big)\mathcal{L}_{Z^i}\,, \end{aligned} \tag{6.48}$$

where $\Delta_{\delta\lambda}$ is given by expression (6.47). We illustrate the modular curvature in Figure 6.4.

The curvature (6.48) can be decomposed into two contributions: the curvature of the non-abelian group of surface diffeomorphisms

$$R^{(Z)}_{\delta\lambda_1\delta\lambda_2} = \Delta_{\delta\lambda_1}Z^i(\delta\lambda_2) - \Delta_{\delta\lambda_2}Z^i(\delta\lambda_1) \tag{6.49}$$

and the curvature of the abelian subgroup of local transverse boosts generated by $\mathcal{L}_\Omega$:

$$R^{(\Omega)}_{\delta\lambda_1\delta\lambda_2} = \Delta_{\delta\lambda_1}\Omega(\delta\lambda_2) - \Delta_{\delta\lambda_2}\Omega(\delta\lambda_1). \tag{6.50}$$

The appearance of the internal covariant derivative $\Delta_{\delta\lambda}$ in (6.50) is required by covariance because the orthogonal boosts are non-trivially fibered over the surface diffeomorphisms.

Relation to the bulk curvature. Expression (6.45) for the modular Berry connection is the spin connection for the normal frame of the extremal surfaces. This immediately implies that the $\mathcal{L}_\Omega$ component of the curvature (6.50) directly probes the bulk Riemann curvature.

At this point it is important, however, to recall that in approximation (6.35) of the modular flow as a boost generator we neglected terms of order $\mathcal{O}(x^+K_{ij|+},\, x^-K_{ij|-})$ where $K_{ij|\alpha}$ is the normal extrinsic curvature of the HRRT surface. These, generally non-local, contributions to the bulk modular Hamiltonian can generate corrections of order $\mathcal{O}(K_{ij|\alpha}\delta x^\alpha)$ to (6.45), which affect its curvature at orders $\mathcal{O}(K^2, \partial K)$. Since the modular curvature computed by naïvely employing

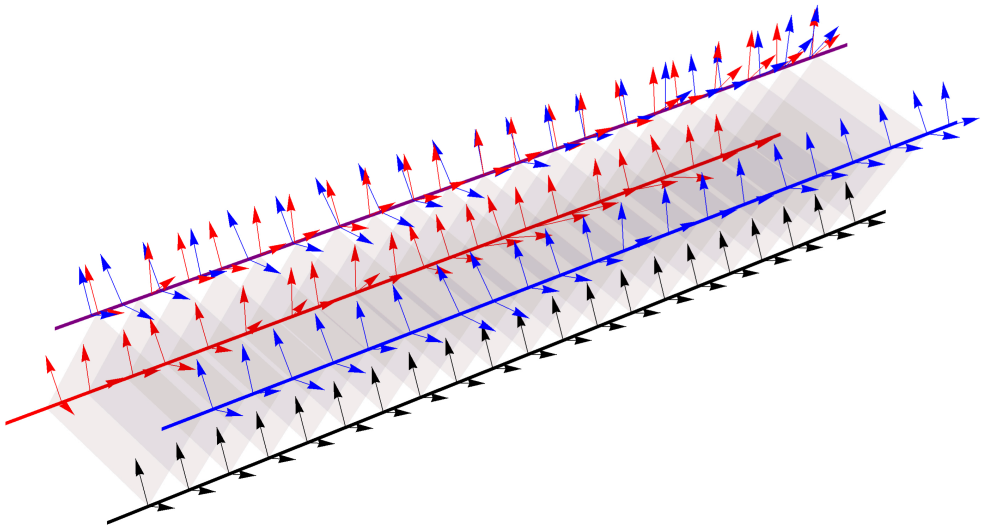

Figure 6.4: Modular Berry curvature in the bulk. The modular zero mode frames are marked with pairs of arrows that stand for the normal vectors $n_\alpha^M(\lambda, y)$ (which transform under orthogonal boosts); the distances between neighboring pairs reflect the extremal surface diffeomorphism frame. We parallel transport a zero mode frame from the bottom surface to the top surface along two different paths (red and blue); the mismatch between the resulting frames is the modular curvature. The mismatch between the locations of the red and blue arrows on the top is the surface diffeomorphism component of the curvature (6.49) while the mismatch between their directions is the boost component of the curvature (6.50).

approximation (6.35) at every step is the bulk Riemann curvature, our computation of (6.42) is under control only when there is a hierarchy between the bulk Riemann curvature and the normal extrinsic curvature of the HRRT surface

$$R \gg K^2, \partial K. \tag{6.51}$$

The curvature of the geometric connection (6.45, 6.46) is an approximation to the modular Berry connection at leading order in a $K^2/R, \partial K/R$ expansion.

Condition (6.51) can be intuitively understood as follows: The geometric approximation to the bulk modular flow confines us within a distance of order $\mathcal{O}(1/K)$ from the extremal surface. If this distance is also small compared to the Riemann curvature, spacetime looks effectively flat, and the boost of the normal frame resulting from parallel transporting the surface is comparable to the corrections neglected in the approximation (6.35). The modular Berry curvature, therefore, reliably measures the bulk curvature in the neighborhood of an RT surface when the surfaces considered obey (6.51).

Modular parallel transport. Assuming (6.51), we can illustrate the modular parallel transport geometrically. Consider a family of minimal surfaces $\gamma(\lambda)$ with $\lambda \in [0, 1]$ that form a closed loop $\gamma(0) = \gamma(1)$. In a neighborhood of every minimal surface $\gamma(\lambda)$ we can define a coordinate system $x_\lambda^M = (x_\lambda^\alpha, y_\lambda^i)$, where x_λ^α $(\alpha = 0, 1)$ measures distances from $\gamma(\lambda)$ along two orthogonal directions. These are simply local choices for the edge-mode frames of the corresponding entan-

glement wedges. As we explained in the previous section, these different localized coordinate patches are related to each other by the diffeomorphisms (6.42):

$$x^M_{\lambda+\delta\lambda} = x^M_\lambda + \xi^M(x;\lambda,d\lambda). \tag{6.52}$$

The 'gluing' diffeomorphism ξ is of course subject to the zero mode ambiguity, which is the focus of this chapter.

Given the connection (6.44), we can define a covariant derivative

$$\nabla_\lambda = \frac{\delta}{\delta\lambda} + \Gamma(\lambda,\delta\lambda) \tag{6.53}$$

which generates the parallel transport. Applied to the coordinate frames x^M_λ, parallel transport assigns a canonical frame $\tilde{x}^M_\lambda$ to every surface $\gamma(\lambda)$, given an initial condition $\tilde{x}^M_{\lambda_0} = x^M_{\lambda_0}$. For an infinitesimal step $\delta\lambda$, the parallel transported frame becomes:

$$\begin{aligned}\tilde{x}^M_{\lambda+\delta\lambda} &= \tilde{x}^M_\lambda + \delta\lambda\,\nabla_\lambda \tilde{x}^M_\lambda \\ &= x^M_{\lambda+\delta\lambda} + \Big(\Omega(\lambda,\delta\lambda)\epsilon^{\alpha\beta}\tilde{x}_{\lambda\beta}\frac{\partial}{\partial\tilde{x}^\alpha_\lambda} + Z^i(\lambda,\delta\lambda)\frac{\partial}{\partial\tilde{y}^i_\lambda}\Big)\tilde{x}^M_\lambda \\ &= \tilde{x}^M_\lambda + \xi^M(\tilde{x};\lambda,\delta\lambda) + \left(\frac{1}{2}\epsilon^\gamma{}_\delta\partial_\gamma\xi^\delta\right)|_{\tilde{x}^\alpha=0}\delta^M_\alpha\epsilon^{\alpha\beta}\tilde{x}_{\lambda\beta} - \delta^M_i\xi^i|_{\tilde{x}^\alpha=0}\end{aligned} \tag{6.54}$$

In the second step we used the explicit form of the zero-mode generators in the local orthonormal gauge (6.39) and in the third step we used the formulas (6.45, 6.46) for the components of the connection Ω, Z^i. An application of the projector (6.46) to (6.54) reveals that the diffeomorphism $\tilde{\xi}^M(\lambda,\delta\lambda)$ generating parallel transport of the edge-mode frame

$$\tilde{x}^M_{\lambda+\delta\lambda} = \tilde{x}^M_\lambda + \tilde{\xi}^M(\tilde{x};\lambda,\delta\lambda) \tag{6.55}$$

indeed has vanishing zero mode components.

The modular parallel transport in the bulk can be summarized as a geometric flow, which at every step:

1. maps between the two modular boost generators (up to zero modes),
2. is always orthogonal to the extremal surface,
3. preserves the hyperbolic angles between adjacent points on the normal 2-D plane.

We can covariantly express these conditions as follows:

$$\delta_\lambda\zeta^M_{\rm mod}(x;\lambda) - P^\lambda_0[\delta_\lambda\zeta^M_{\rm mod}(x;\lambda)] = \Big[\tilde{\xi}(x;\lambda,\delta\lambda),\zeta_{\rm mod}(x;\lambda)\Big]^M, \tag{6.56}$$

$$\frac{1}{2}\epsilon^{\alpha\beta}n_\alpha\cdot\partial\left(n_\beta\cdot\tilde{\xi}\right)|_{RT} = 0, \tag{6.57}$$

$$t^i\cdot\tilde{\xi}\Big|_{RT} = 0 \tag{6.58}$$

which are direct bulk analogues of the CFT conditions (6.22).

Following these rules we can transport the surface around a closed loop in the space of extremal surfaces, returning to its original location in the end. A comparison of the original and transported

coordinate frames in its vicinity will reveal a location-dependent boost transformation on its normal plane and a diffeomorphism of the internal coordinates. This is the bulk modular Berry holonomy. We saw an example of it in Figure 6.4, which shows the computation of the modular curvature—that is, the holonomy of an infinitesimal loop. But the picture is the same for larger loops, for example the loop shown in Figure 6.3.

6.3.4 Example: Pure AdS_3

This subsection mirrors the discussion of the boundary modular Berry connection in the vacuum of a two-dimensional CFT. In Appendix C.2 we identify the operator that generates modular parallel transport from boundary interval λ to interval $\lambda + \delta\lambda$. In doing so, we only exploit the global conformal algebra $SO(2,1) \times SO(2,1)$.

But this $SO(2,1) \times SO(2,1)$ is also the algebra of the Killing vector fields of AdS_3. In particular, equations (C.11-C.12), (C.15) and (C.16) hold for the corresponding Killing vector fields. As a consequence, the Killing vector field that represents (C.15) is a solution of equation (6.40). We also know it has no zero mode component to be projected out

$$P_0^{\lambda}[\delta_\lambda \zeta^M_{\text{mod}}(x;\lambda)] = 0 \tag{6.59}$$

because—as was the case for operator $V_{\delta\lambda}$ in the boundary discussion—it too lives in eigenspaces of the adjoint action of ζ_{mod} that are orthogonal to the 0-eigenspace. In summary, the Killing vector field that corresponds to $V_{\delta\lambda}$ generates the bulk modular parallel transport in pure AdS_3.

To understand bulk modular parallel transport geometrically, consider an initial HRRT surface that is a diagonal of a static slice of AdS_3:

$$\lambda = (a^+, b^+, a^-, b^-) \equiv (\theta_L + t_L, \theta_R + t_R, \theta_L - t_L, \theta_R - t_R) = (-\pi/2, \pi/2, -\pi/2, \pi/2)\,. \tag{6.60}$$

The analysis for other initial geodesics is identical up to an overall AdS_3 isometry. The task is to interpret

$$\text{equation (C.15)} = \frac{1}{2\pi i}\left(-\partial_{a^+}K_+ + \partial_{b^+}K_+ + \partial_{a^-}K_- - \partial_{b^-}K_-\right),$$

the $SO(2,1) \times SO(2,1)$ algebra element that generates modular parallel transport, as an AdS_3 Killing vector field. In the representation (C.6), the action of (C.15) on the boundary is:

$$\frac{1}{2}\frac{da^+}{d\lambda}\Big(\sin x^+ + 1\Big)\partial_+ - \frac{1}{2}\frac{db^+}{d\lambda}\Big(\sin x^+ - 1\Big)\partial_+ + \frac{1}{2}\frac{da^-}{d\lambda}(\sin x^- + 1)\partial_- - \frac{1}{2}\frac{db^-}{d\lambda}(\sin x^- - 1)\partial_- \tag{6.61}$$

Going to θ and t-coordinates on the boundary, this becomes:

$$\begin{aligned}
&\frac{1}{2}\left(-\frac{d(b^+ - a^+)}{d\lambda}\sin(\theta + t) - \frac{d(b^- - a^-)}{d\lambda}\sin(\theta - t) + \frac{d(a^+ + b^+ + a^- + b^-)}{d\lambda}\right)\partial_\theta \\
&+ \frac{1}{2}\left(-\frac{d(b^+ - a^+)}{d\lambda}\sin(\theta + t) + \frac{d(b^- - a^-)}{d\lambda}\sin(\theta - t) + \frac{d(a^+ + b^+ - a^- - b^-)}{d\lambda}\right)\partial_t
\end{aligned} \tag{6.62}$$

Let us survey what this solution means in the bulk of AdS_3.

One option is to move from λ to:

$$\lambda + \delta\lambda = (-\pi/2 + d\lambda, \pi/2 + d\lambda, -\pi/2 + d\lambda, \pi/2 + d\lambda) \tag{6.63}$$

In this case, parallel transport is carried out by this global conformal symmetry:

$$V_{\delta\lambda} = 2\partial_\theta \,. \tag{6.64}$$

It is easy to see that the corresponding symmetry of AdS_3 is a global rotation about its center, which maps the geodesic λ to $\lambda + \delta\lambda$. Mapping the special interval (6.60) to a general initial λ, we recognize the following rule of parallel transport:

Case 1: If two geodesics live on a common $\mathbb{H}_2$ subspace of pure AdS_3 and intersect, bulk modular parallel transport is a rigid rotation about their intersection point which preserves their common $\mathbb{H}_2$. This rule for bulk modular parallel transport, dubbed 'rotation without slipping,' was first explained in [212].

Another case is to move from λ to:

$$\lambda + \delta\lambda = (-\pi/2 + d\lambda, \pi/2 + d\lambda, -\pi/2 - d\lambda, \pi/2 - d\lambda) \,. \tag{6.65}$$

In this case, parallel transport is carried out by this global conformal symmetry:

$$V_{\delta\lambda} = 2\partial_t \,. \tag{6.66}$$

This is a rigid time translation in AdS_3. Once again, mapping the special interval (6.60) to a general initial λ, we recognize the following rule of parallel transport:

Case 2: If two geodesics λ and $\lambda + \delta\lambda$ live on a common AdS_2 subspace of pure AdS_3 and do not intersect, bulk modular parallel transport is a global time translation that preserves their common AdS_2. This time translation also preserves that timelike geodesic in AdS, which connects the points of closest approach between λ and $\lambda + \delta\lambda$.

There are two other basic cases, which depend on the relative signs of $da^+/d\lambda$, $db^+/d\lambda$, $da^-/d\lambda$ and $db^-/d\lambda$. Altogether, these four basic cases span the four dimensions of kinematic space [212, 222]. The most general case is of course a linear combination of the four. Its detailed geometric meaning will be discussed in [228].

Along any trajectory in the space of geodesics, parallel transport is generated by an AdS_3 isometry, which at each step maps geodesic λ to geodesic $\lambda + \delta\lambda$. When we close a loop, we generate a finite AdS_3 isometry that maps the initial geodesic back to itself. Such isometries are spanned by the orthogonal boost and rigid translation along the said geodesic. Of course, we have reached the same conclusion in eqs. (6.28): in the language of Sec. 6.2.4, the orthogonal boost is generated by $K_+ + K_-$ and the longitudinal translation by $K_+ - K_-$.

6.4 The Proposal and Implications

In this chapter, we proposed a link between the curvature of spacetime and the relations between modular Hamiltonians of the dual CFT state. Our key observation on the boundary is that the set of subregion modular Hamiltonians is endowed with a *gauge symmetry*, consisting of rotating the basis of each H_{mod} by a zero-mode transformation. The relative zero-mode frame is then promoted to a gauge connection with a non-vanishing curvature. This is a notion of curvature, which—as first recognized in [211]—is directly associated to the entanglement pattern of the state. It can be studied by applying the ideas of Berry, Wilczek and Zee [220, 221] to the set of modular Hamiltonians.

Modular Berry holonomies as an entanglement measure The characterization of multi-partite entanglement is a famously unsolved problem. Unlike two-partite entanglement, which is entirely characterized by the spectrum of the modular Hamiltonians, it is not known what quantities are sufficient to classify different forms of multi-partite entanglement.[9] Modular Berry holonomies are a promising quantity in this regard. One way in which one might probe multi-system entanglement is to group the systems into two sets and study how the resulting bipartite entanglement varies as the grouping evolves. This is a description of the modular Berry-Wilson loop. Because the focus of this chapter is on holographic applications of the modular Berry connection, we leave an exploration of its uses for classifying entanglement to the future.

Modular Berry holonomies in holography In the bulk, modular flow admits a simple geometric description sufficiently close to the corresponding HRRT surface. This allowed us to translate the CFT rules of modular parallel transport to entanglement wedges and derive a bulk avatar of the modular Berry connection. Our main result is that for HRRT surfaces that satisfy condition (6.51) the modular Berry connection reduces to a geometric connection encoding the spin connection for the normal surface frame and the relative embedding of the internal coordinates. Its curvature is, therefore, a holographic probe of the bulk Riemann curvature. A somewhat different CFT Berry connection recently appeared in the discussion of holographic complexity [123, 232], while the algebra of modular Hamiltonians was used for bulk reconstruction in [225, 233]. Our feeling is that there is an overarching framework connecting these results to the ideas we presented here.

Error correction and bulk locality. Our proposed holographic relation between modular Berry curvature and bulk spacetime curvature hinges on the validity of the JLMS relation (6.1). The latter is the only bridge between our CFT and bulk discussions. The error correction framework for the AdS/CFT dictionary [205] clarified that the equivalence of bulk and boundary modular Hamiltonians (6.1) holds within the code subspace, namely the subspace of the CFT Hilbert space describing bulk low energy excitations about a specific background. It is therefore implicit in our construction that in the holographic context the H_{mod} appearing in equations (6.8) and (6.17) is actually the restriction of the exact CFT modular Hamiltonian to the code subspace $H_{\text{mod}} = P_{\text{code}} H^{\text{exact}}_{\text{mod}} P_{\text{code}}$.

[9] Although there exist classification schemes that are customized to specific systems like qubits [229–231].

The code subspace projection is more than just a technicality; it is directly responsible for endowing the boundary modular Hamiltonian with the right zero-mode algebra. In a typical CFT state, the symmetries of the modular Hamiltonian are either generated by H_{mod} itself and the conserved global charges of the CFT, if any, or they are simple phase rotations of individual modular eigenstates. On the other hand, the existence of a *local, semiclassical* bulk requires a set of zero-modes that generate the asymptotic symmetry group of the HRRT surface (6.39). The essential task of the projector P_{code} is to introduce the correct group of approximate zero-modes. In the absence of any currently known, bulk-independent way for identifying the appropriate code subspaces in the boundary theory, the modular zero-mode algebra and the corresponding modular Berry holonomies can serve as a useful guiding principle.

On the role of soft modes. There is an aspect of our story that played a supporting role in our main presentation but we believe deserves more attention. This is the new, to our knowledge, use of gravitational edge modes of subregions to probe the curvature of their embedding spacetime. Edge modes have been subject to a lot of recent studies due to their relation to soft theorems and the memory effect [214], the construction of the physical phase space of subsystems in gauge theories [213, 227, 234, 235], the definition of entanglement entropy [236, 237], and, more speculatively, to the black hole information problem [215, 238]. In our work, the relative edge mode frame of infinitesimally separated regions acquired a new physical interpretation as a gravitational connection with curvature that depends on the background spacetime.

One moral of our treatment is that soft modes are unphysical, gauge degrees of freedom from the perspective of a given subregion but their holonomies contain physical geometric information. This informs the recent discussion regarding the physical significance of soft modes [227, 239, 240]. It will be illuminating to formulate our ideas more rigorously in the canonical formalism along the lines of [213], where we believe they may offer a useful framework for describing surface translations. It is also worthwhile to apply them in backgrounds that are not asymptotically AdS.

We also learned that we can 'implant' soft hair on the boundary of a subregion by transporting it around a closed loop. It is interesting to compare the latter with the more operational way of exciting soft modes by sending shockwaves that cross the boundary of the subregion [214]. Intuitively, the shockwaves of [214] can be thought of as the 'experimental' protocol for shifting the location of the horizon—an idealized version of which is the transport problem we have formulated. To construct a closed loop of surfaces we could apply two shockwaves along different directions, in two different orderings. The edge-mode holonomy in this setup measures the soft graviton component of the commutator of the two shockwaves. It would be interesting to understand this heuristic picture in detail. The appearance of shockwave commutators also suggests an intriguing possible relation to the physics of chaos [14, 241].[10]

Bulk gauge field holonomies. An interesting playground for our ideas is the case of holographic CFTs with global symmetries. The conserved charges give rise to a new set of modular zero-modes, which are holographically mapped to the edge modes of the dual bulk gauge field.

[10] We thank Beni Yoshida for this comment.

The relevant component of the modular Berry curvature should then be reflected in the local field strength of the gauge field along an HRRT surface. This setup is, in a sense, simpler than the gravitational case we discussed in this work and could allow for more computations. For example, it would be an interesting exercise to repeat the computations we did for pure AdS_3 with a bulk gauge field turned on.

Gravitation and gauge field dynamics? A particularly exciting question we leave for future study is whether our proposed perspective on the bulk gravitational and gauge connections can shed light on the emergence of their dynamics [242]. An excitation of the CFT state gets imprinted on the modular Hamiltonians in its future causal cone and thus affects the modular Berry connection. As a result, the latter is ultimately promoted to a dynamical object. Whether the laws governing this evolution take a useful form, however, remains to be seen. It is worth noting that an appealing feature of our approach is that it treats all gauge fields, including gravity, on equal footing. All bulk holonomies have the same microscopic origin in the CFT: the entanglement pattern of the state as encoded in the relative bases of modular Hamiltonians. A dynamical law of the sort we speculate here would constitute a unified holographic description of gravitational and gauge interactions.

Chapter 7

Conclusions

Throughout the whole thesis, we have been fascinated by and have made efforts to understand how quantities in quantum information theory can be encoded geometrically in the semi-classical gravity theory. It is along the line towards a better understanding of the quantum gravity, which have attracted theorists for the past sixty years.

Based on this spirit, we started with a quantity that is proposed to depict the scrambling behavior inside the black hole, called quantum complexity, which is essentially a difficulty measure from one state to another in the modern quantum circuit language. Our aim is to understand the universality of the two bulk proposals, *i.e.,* "Complexity=Volume" (CV) and "Complexity=Action" (CA), by using a rather simple thin brane model in AdS_3, *albeit* without a black hole in the spacetime. The two proposals have been tested in many gravitational systems which show agreement with each other at least in terms of the divergence structure. However, our analysis tend to discriminate the two in this simple setup, in the sense that the CV result has a tension dependent logarithmic divergence while this behavior is not present in CA result. This is the first case to show such an evident contrast between the two conjectures, leading us to think what the universality really means in terms of complexity, since in comparison with the entanglement entropy where the logarithmic divergence preserves the universal information, the same consideration might not hold in understanding holographic complexity. Nevertheless, this should still be an open question and should be more clear as we get a kind of holographic measure of circuit complexity, which will be among the future research programs of the author.

In the QFT consideration of the circuit complexity, which should be regarded as the boundary exploration in the AdS/CFT context, we would like to understand explicitly how the gate choices can influence the circuit complexity. With resort to free bosonized model in two dimension, we realized that changing the gate set, from bosonic type to ferminonic one, is NOT guaranteed to change the result completely. As we have shown, in the "bosonic coherent-fermionic Gaussian" case, the two result are comparable with an inhomogeneous choice of the penalty factor for the fermionic gates, while in the bi-Gaussian case, the two gate choices respond dramatically different as we augment the UV cutoff and can not be tuned to eliminate the discrepancy by playing with the penalty factor. In the latter case, the necessity for reconsidering the universal information shows up again, as only the fermionic result shows a numerical *log*(cutoff) dependence. This means that by a proper selection of the allowable gates to form a set, it could possibly lead to

some more preferred result, *albeit* not yet in a systematic manner. This manipulation might look too subjective, however, it renders a way to consider the holographic measure of circuit complexity, which might favor a certain set of gates, the holographic gate set. This is merely a speculation at the moment, which might give rise to some interesting work in the future.

As an episode, we re-looked at the thin brane model in details, with the hope to understand better how the universal information of the two-point functions for stress tensor in dCFT_2 can be stored in the canonical holographic manner. In the literature, it has been shown that only one new parameter other than the central charges arises for those two-point functions, which determines the energy transport coefficients across the interface. Instead of the commonly acknowledged duality which states that the partner for the brane tension is the boundary entropy in the dCFT, our analysis points out that the brane tension actually encodes the transport property of the dCFT in terms of the transmission or reflection coefficients. Our statement looks more reasonable as the topological interface corresponds to zero brane tension but can have arbitrary boundary entropy. An interesting direction for further application of our result is to relate to the "island" proposal in evaporating black holes, which is worthy of investigation.

In the last part, we would like to understand if there could some other bulk geometric quantities that can encode certain information on the boundary, which is other than quantities defined in hypersurfaces or actions in a certain region. Our study shows that there is in fact a pair that can be dual to each other which has not yet received enough attention, it is the bulk Riemann curvature and the Berry curvature in the space of modular Hamiltonians. We have been able to establish the duality in a general asymptotic AdS background, and have tested the conjecture in a simple example of $\text{AdS}_3/\text{CFT}_2$ which shows a nice agreement due to the simplicity of this system and the nice symmetry decomposition $SO(2,2) = SL(2,\mathbb{R}) \times SL(2,\mathbb{R})$. This study in principle opens up a new direction along the entanglement wedge reconstruction, and it would be interesting to investigate if the technique used here would help define a complexity measure since the Berry connection is an affine connection between different states.

The studies in the thesis have initiated some interesting directions in the understanding of how certain quantum information is encoded in a geometric manner in gravity, as mentioned above. Hopefully, those considerations will be further investigates and lead to some contributions to the community towards a better understanding of quantum gravity and quantum information.

Appendix A

Several Derivations for the Defect Toy Model

A.1 Derivation of the Light Cone using Global Coordinates

In this appendix we derive the light cone surface of subsection 3.1.3 using the (ϕ, θ) coordinate system. Since the form of the null surface is identical in conformally equivalent spacetimes, we will study null geodesics in the metric

$$ds^2 = -dt^2 + d\phi^2 + \sin^2\phi \; d\theta^2 \tag{A.1}$$

which is a conformal rescaling of the metric (3.8). The geodesic equations read,[1]

$$\ddot{t} = 0, \qquad \ddot{\phi} = \frac{1}{2}\sin(2\phi)\,\dot{\theta}^2, \qquad \ddot{\theta} = -2\cot\phi\,\dot{\theta}\,\dot{\phi}\,, \tag{A.2}$$

where the derivatives are taken with respect to some parameter σ along the null geodesics and the requirement that the geodesics are null reads

$$-1 + \dot{\phi}^2 + \sin^2\phi\,\dot{\theta}^2 = 0. \tag{A.3}$$

The first equation in (A.2) is consistent with having the geodesics parameterized by t, namely $\sigma = t$. Integrating the last equation in (A.2) yields

$$\dot{\theta} = \frac{a}{\sin^2\phi}, \tag{A.4}$$

where a is an integration constant. Next, we substitute the result from eq. (A.4) into the null constraint (A.3) which yields

$$\dot{\phi} = \pm\sqrt{1 - \frac{a^2}{\sin^2\phi}}. \tag{A.5}$$

Solutions to eqs. (A.4)-(A.5) automatically satisfy the second equation in (A.2). Before we proceed in finding the explicit solution for the null geodesics, let us pause and briefly comment on the

[1] Of course, since we are working with the equations of motion of the squared line element, under the conformal rescaling the parametrization of the null geodesics could change.

properties of eqs. (A.4)-(A.5). If we start from the boundary and look at inwards and future oriented null rays we will choose the minus branch of eq. (A.5) since ϕ is decreasing as we move into the bulk. The constant of integration a determines the angular orientation (θ) of the null geodesic as it falls into the bulk according to eq. (A.4). For instance for $a = 0$ we will have a geodesic which follows a line of constant θ and this is the geodesic which determines the boundary of the WDW patch in vacuum AdS_3 without the defect. For other values of a there is a particular value of the radial coordinate $\phi = \sin^{-1}|a|$ for which $\dot{\phi} = 0$ and the geodesic turns back toward the boundary. Let us focus on the upper half of the WDW patch and study future oriented geodesics starting from the boundary. Integrating the minus branch of the differential equation (A.5) we obtain the solution

$$t = c_2 - \cos^{-1}\left(\frac{\cos\phi}{\sqrt{1-a^2}}\right) \qquad \text{where} \qquad \sin^{-1}|a| \leq \phi \leq \pi/2. \tag{A.6}$$

The initial condition $\phi(t = 0) = \pi/2$ fixes $c_2 = \pi/2$. Finally we can solve the equation for $\dot{\theta}$, which gives

$$\theta = c_3 + \tan^{-1}(a \tan t) \qquad \text{where} \qquad 0 \leq t \leq \pi/2, \tag{A.7}$$

and the initial condition $\theta(t = 0) = 0$ for the null rays originating from $(t, \phi, \theta) = (0, \pi/2, 0)$ fixes $c_3 = 0$.[2]

We also present in the following an equation which describes the shape of the lightcone constructed from these null rays. We will focus on the part of the surface for negative angles $\theta < 0$ which fixes the new component of the boundary of the WDW patch in the defect region, see figure 3.3. First, from eq. (A.6) with $c_2 = \pi/2$ we extract a

$$a = -\sqrt{1 - \frac{\cos^2\phi}{\sin^2 t}} \qquad \text{for} \qquad \theta < 0. \tag{A.8}$$

Substituting this value into eq. (A.7) together with $c_3 = 0$ for the null lightcone originating from the boundary at $\theta = 0$ we obtain

$$\tan\theta + \sqrt{\tan^2 t - \frac{\cos^2\phi}{\cos^2 t}} = 0 \qquad \text{or} \qquad \cos\theta = \frac{\cos t}{\sin\phi}\,. \tag{A.9}$$

One can also relate this analysis to the (y, r) coordinate one by verifying that lines of constant a (or t) correspond to a constant value of the coordinate y (or r) respectively, see eq. (3.9). More explicitly we have

$$a = \tanh y, \qquad \tanh r = \cos t. \tag{A.10}$$

A cross section of the light cone surface for different values of t is depicted by the green slices in figure 3.4 where we have used the following coordinates for the plot

$$x = \frac{\phi}{\pi/2}\cos\theta, \qquad y = \frac{\phi}{\pi/2}\sin\theta. \tag{A.11}$$

[2] For the null rays originating from $\theta(t = 0) = \pi$ we have $c_3 = \pi$ but since the picture is symmetric we will focus on the null rays originating from $\theta(t = 0) = 0$.

A.2 Contributions to the Subregion CA Outside the Defect Region

In this appendix we evaluate the contributions to the subregion CA proposal outside the defect region for a subregion which is symmetric around the defect. This also gives the result for the subregion complexity from the CA proposal in empty AdS_3 in global coordinates for a subregion of the same size. The projections of the various regions used in this calculation onto the $t = 0$ time slice are illustrated in figure 3.11. In what follows we will work in the (t, ϕ, θ) coordinates of eq. (3.8). The relevant conversions can be found in eqs. (3.5), (3.7) and (3.9).

Preliminaries It will be useful to have expressions for the various surfaces in the relevant coordinates; these are: the boundary of the WDW patch (S_3 in figure 3.11)

$$\phi = \pi/2 - t, \tag{A.12}$$

the boundary of the entanglement wedge, see eq. (A.9) ($S_6 \cup S_7$ in figure 3.11)

$$\sin\phi\cos\theta = \cos(\theta_R - t), \tag{A.13}$$

the cutoff surface ($S_1 \cup S_5$ in figure 3.11)

$$\phi = \frac{\pi}{2} - \hat{\delta}, \tag{A.14}$$

the joint at the intersection of the WDW patch and the entanglement wedge (J_4 in figure 3.11)

$$\cos\theta = \frac{\sin(\theta_R + \phi)}{\sin\phi} \qquad \text{and} \qquad t = \pi/2 - \phi = \tan^{-1}\left(\frac{\cos\theta - \cos\theta_R}{\sin\theta_R}\right), \tag{A.15}$$

the point at the intersection of the joint J_4 and the $\theta = 0$ surface

$$\phi = \frac{\pi}{2} - \frac{\theta_R}{2}, \qquad t = \frac{\theta_R}{2} \qquad \text{and} \qquad \theta = 0, \tag{A.16}$$

while the point at the intersection of the joint J_4 and the cutoff surface is given by

$$t = \hat{\delta}, \qquad \phi = \pi/2 - \hat{\delta} \qquad \text{and} \qquad \theta = \cos^{-1}\left(\frac{\cos(\theta_R - \hat{\delta})}{\cos\hat{\delta}}\right) = \theta_R - \hat{\delta} + \mathcal{O}(\hat{\delta}^2). \tag{A.17}$$

The RT surface J_7 is given by

$$t = 0 \qquad \text{and} \qquad \sin\phi\cos\theta = \cos\theta_R, \tag{A.18}$$

the point at the intersection of the RT surface and the surface $\theta = 0$

$$\phi = \frac{\pi}{2} - \theta_R, \qquad t = 0 \qquad \text{and} \qquad \theta = 0, \tag{A.19}$$

the joint J_1 where the cutoff surface intersects the entanglement wedge

$$\phi = \frac{\pi}{2} - \hat{\delta}, \qquad \cos\theta = \frac{\cos(\theta_R - t)}{\cos\hat{\delta}}, \tag{A.20}$$

and finally, the point at the intersection of the RT surface and the cutoff

$$\theta = \cos^{-1}\left(\frac{\cos\theta_R}{\cos\hat{\delta}}\right) = \theta_R + \mathcal{O}(\hat{\delta}^2) \quad \text{and} \quad t = 0. \tag{A.21}$$

It will also be useful to have the surface data for the entanglement wedge in terms of the (t, ϕ, θ) coordinates. The null boundary of the entanglement wedge is given in eq. (A.13) and can be parameterized similarly to eqs. (A.6)-(A.7) with the substitution $t \to \theta_R - t$ in the relevant places

$$x^\mu = (t, \phi, \theta) = \left(t, \cos^{-1}\left(\sqrt{1-a^2}\sin(\theta_R - t)\right), \tan^{-1}\left(a\tan(\theta_R - t)\right)\right), \tag{A.22}$$

where a is constant along a given null geodesic parameterized by t. The surface information in this coordinate system with the parametrization $\lambda = t/\mathcal{N}_{\text{EW}}$ is

$$\begin{aligned} k^\mu_{\text{EW}} &= \mathcal{N}_{\text{EW}}\left(1, \frac{\sqrt{1-a^2}}{\sqrt{1+a^2\tan^2(\theta_R - t)}}, -\frac{a\sec^2(\theta_R - t)}{1+a^2\tan^2(\theta_R - t)}\right), \\ \kappa_{\text{EW}} &= 2\mathcal{N}_{\text{EW}}\cot(\theta_R - t), \qquad \gamma^{\text{EW}}_{aa} = \frac{L^2}{(1-a^2)^2}. \end{aligned} \tag{A.23}$$

We may also determine the values of a and t at the point where the entanglement wedge intersects RT surface and the cutoff surface

$$t = 0, \qquad \text{and} \qquad a_{\max} = \sqrt{1 - \frac{\sin^2\hat{\delta}}{\sin^2\theta_R}} = 1 - \frac{\hat{\delta}^2}{2\sin^2\theta_R} + \mathcal{O}(\hat{\delta}^4) \tag{A.24}$$

as well as the point where it intersects the cutoff surface and the WDW patch

$$t = 0, \qquad \text{and} \qquad a_{\min} = \sqrt{1 - \frac{\sin^2\hat{\delta}}{\sin^2(\theta_R - \hat{\delta})}} = 1 - \frac{\hat{\delta}^2}{2\sin^2\theta_R} - \frac{\cot\theta_R}{\sin^2\theta_R}\hat{\delta}^3 + \mathcal{O}(\hat{\delta}^4). \tag{A.25}$$

Below, we will only be able to extract the divergent pieces of the subregion CA proposal outside the defect region analytically and will leave some of the finite pieces as implicit integral expressions.

Bulk Contributions The bulk contribution B_2 under the WDW patch reads

$$\begin{aligned} B_2 &= -\frac{L}{4\pi G_{\text{N}}}\int_{\frac{\pi}{2}-\frac{\theta_R}{2}}^{\frac{\pi}{2}-\hat{\delta}} d\phi\,\frac{\sin\phi}{\cos^3\phi}\int_0^{\cos^{-1}\left(\frac{\sin(\theta_R+\phi)}{\sin\phi}\right)} d\theta\int_0^{\frac{\pi}{2}-\phi} dt \\ &= -\frac{L}{4\pi G_{\text{N}}}\left(\frac{\theta_R}{\hat{\delta}} + \ln\hat{\delta}\right) + \text{finite}. \end{aligned} \tag{A.26}$$

Next, we evaluate the bulk contribution of the region under the entanglement wedge. We subdivide it into two parts, B_4 and B_5, as indicated in figure 3.11, along a line of constant $\phi = \frac{\pi}{2} - \frac{\theta_R}{2}$. The part B_4 is finite and reads

$$B_4 = -\frac{L}{4\pi G_{\rm N}} \int_{\frac{\pi}{2}-\theta_R}^{\frac{\pi}{2}-\frac{\theta_R}{2}} d\phi \, \frac{\sin\phi}{\cos^3\phi} \int_0^{\cos^{-1}\left(\frac{\cos\theta_R}{\sin\phi}\right)} d\theta \int_0^{\theta_R - \cos^{-1}(\cos\theta\sin\phi)} dt = \text{finite}. \tag{A.27}$$

The part B_5 extends all the way to the cutoff and reads

$$\begin{aligned} B_5 =& -\frac{L}{4\pi G_{\rm N}} \int_{\frac{\pi}{2}-\frac{\theta_R}{2}}^{\frac{\pi}{2}-\hat{\delta}} d\phi \, \frac{\sin\phi}{\cos^3\phi} \int_{\cos^{-1}\left(\frac{\sin(\theta_R+\phi)}{\sin\phi}\right)}^{\cos^{-1}\left(\frac{\cos\theta_R}{\sin\phi}\right)} d\theta \int_0^{\theta_R - \cos^{-1}(\cos\theta\sin\phi)} dt \\ =& \frac{L}{8\pi G_{\rm N}} \ln\hat{\delta} + \text{finite}. \end{aligned} \tag{A.28}$$

Therefore, the total bulk contribution reads

$$I_{\rm bulk,out} = -\frac{L}{\pi G_{\rm N}} \left(\frac{\theta_R}{\hat{\delta}} + \frac{1}{2}\ln\hat{\delta} \right) + \text{finite}, \tag{A.29}$$

where we have included a factor of four to account for the two sides of the defect as well as the contributions above and below the $t = 0$ time slice.

Surface Contributions We proceed by evaluating the various surface contributions. We start with the cutoff surface. In the region under the WDW patch (S_1), this is a simple modification of our previous calculation in eq. (3.31). All we have to do is modify the limits of integration as follows

$$S_1 = \frac{L}{8\pi G_{\rm N}} \int_0^{\hat{\delta}} dt \int_0^{\theta_R - \hat{\delta} + \mathcal{O}(\hat{\delta}^2)} d\theta \, \frac{\cos\hat{\delta}}{\sin^2\hat{\delta}} \left(\cos\hat{\delta} + \frac{1}{\cos\hat{\delta}} \right) = \frac{L\,\theta_R}{4\pi G_{\rm N}\hat{\delta}} + \text{finite}. \tag{A.30}$$

The part of the cutoff surface under the entanglement wedge is similarly given by

$$S_5 = \frac{L}{8\pi G_{\rm N}} \int_{\theta_R - \hat{\delta} + \mathcal{O}(\hat{\delta}^2)}^{\theta_R + \mathcal{O}(\hat{\delta}^2)} d\theta \int_0^{\theta_R - \theta + \mathcal{O}(\hat{\delta}^2)} dt \, \frac{\cos\hat{\delta}}{\sin^2\hat{\delta}} \left(\cos\hat{\delta} + \frac{1}{\cos\hat{\delta}} \right) = \text{finite}. \tag{A.31}$$

Next, we evaluate the contributions of the various null surfaces. We start with the null boundary of the WDW patch which requires a simple modification to the integration limits in eq. (3.35)

$$\begin{aligned} S_3 =& \frac{L}{8\pi G_{\rm N}} \int_0^{\theta_R - \hat{\delta} + \mathcal{O}(\hat{\delta}^2)} d\theta \int_{\hat{\delta}}^{\tan^{-1}\left(\frac{\cos\theta - \cos\theta_R}{\sin\theta_R}\right)} \left(\frac{\ln\left(\frac{2\ell_{ct}\mathcal{N}_3}{\sin(2t)}\right) + 2\cos^2 t}{\sin^2 t} \right) dt \\ =& \frac{L}{8\pi G_{\rm N}} \left(\frac{\theta_R}{\hat{\delta}} \left[\ln\left(\frac{\ell_{ct}\mathcal{N}_3}{\hat{\delta}}\right) + 1 \right] + \ln\hat{\delta}\,[2 + \ln(\ell_{ct}\mathcal{N}_3)] - \frac{1}{2}\ln^2\hat{\delta} \right) + \text{finite}. \end{aligned} \tag{A.32}$$

For the null boundary of the entanglement wedge, we will divide the integration region along a line of constant $a = a_{\rm min}$, see eq. (A.25), as indicated in figure 3.11. This yields

$$S_6 = -\frac{L\mathcal{N}_{\rm EW}}{4\pi G_{\rm N}} \int_{a_{\rm min}}^{a_{\rm max}} da \int_0^{\theta_R - \sin^{-1}\left(\frac{\sin\hat{\delta}}{\sqrt{1-a^2}}\right)} \frac{\cot(\theta_R - t)}{(1-a^2)} dt = \mathcal{O}(\hat{\delta}^2), \tag{A.33}$$

and

$$S_7 = -\frac{L\mathcal{N}_{\rm EW}}{4\pi G_{\rm N}}\int_0^{a_{\min}} da \int_0^{t_{\max}} \frac{\cot(\theta_R - t)}{(1-a^2)} dt = \text{finite}, \tag{A.34}$$

where $t_{\max}$ solves the equation

$$\sin t_{\max} = \sqrt{1-a^2}\sin(\theta_R - t_{\max}). \tag{A.35}$$

Joint contributions The joint at the intersection between the WDW patch and the cylindrical cutoff surface is similar to the expression (3.36) and reads

$$J_3 = -\frac{L}{8\pi G_{\rm N}}\int_0^{\theta_R - \hat{\delta} + \mathcal{O}(\hat{\delta}^2)} \cot\hat{\delta}\ln\left(\frac{\mathcal{N}_3 L}{\sin\hat{\delta}}\right) d\theta = -\frac{L}{8\pi G_{\rm N}}\left(\frac{\theta_R}{\hat{\delta}} - 1\right)\ln\left(\frac{\mathcal{N}_3 L}{\hat{\delta}}\right). \tag{A.36}$$

For the joint at the intersection of the entanglement wedge and the cutoff surface we obtain

$$\begin{aligned} J_1 &= -\frac{1}{8\pi G_{\rm N}}\int \sqrt{\gamma^{\rm EW}}\ln|k^\mu_{\rm EW} s^{(1)}_\mu| da \\ &= -\frac{L}{8\pi G_{\rm N}}\int_{a_{\min}}^{a_{\max}} \frac{1}{1-a^2}\ln\left(\frac{2LN_{\rm EW}\sqrt{\cos^2\hat{\delta} - a^2}}{\sin(2\hat{\delta})}\right) da = \mathcal{O}(\hat{\delta}), \end{aligned} \tag{A.37}$$

where we used eqs. (3.29) and (A.23) for the relevant normal vectors. Next, we evaluate the joint at the intersection of the entanglement wedge and the WDW patch. We use the normal vectors in eq. (A.23) and (3.33) and substitute the value of t at the joint using eq. (A.35)

$$\begin{aligned} J_4 &= \frac{L}{8\pi G_{\rm N}}\int_0^{a_{\min}} \frac{1}{1-a^2}\left(\ln\frac{L^2\mathcal{N}_3\mathcal{N}_{\rm EW}\csc^2\theta_R}{2(1-a^2)} + \ln\frac{(2-a^2+2\sqrt{1-a^2}\cos\theta_R)^2}{1+\sqrt{1-a^2}\cos\theta_R}\right) da \\ &= \frac{L}{8\pi G_{\rm N}}\left(\ln^2\hat{\delta} - \ln\hat{\delta}\ln\left(\frac{L^2\mathcal{N}_3\mathcal{N}_{\rm EW}}{2}\right)\right) + \text{finite}. \end{aligned} \tag{A.38}$$

Finally, the joint between the past and future boundaries of the entanglement wedge reads

$$\begin{aligned} J_7 &= -\frac{L}{8\pi G_{\rm N}}\int_0^{a_{\max}} \frac{da}{1-a^2}\ln\left(\frac{L^2\mathcal{N}^2_{\rm EW}\csc^2\theta_R}{1-a^2}\right) \\ &= -\frac{L}{8\pi G_{\rm N}}\left(\ln^2\hat{\delta} - \ln\hat{\delta}\ln\left(L^2\mathcal{N}^2_{\rm EW}\right)\right) + \text{finite}. \end{aligned} \tag{A.39}$$

Adding together the various joint and surface contributions yields

$$I_{\rm sj,out} = \frac{L}{2\pi G_{\rm N}}\left(\frac{\theta_R}{\hat{\delta}}\left[\ln\left(\frac{\ell_{ct}}{L}\right) + 3\right] + \ln\hat{\delta}\left[1 + \ln\left(\frac{2\ell_{ct}}{L}\right)\right]\right) + \text{finite}, \tag{A.40}$$

and of course we see that the various constant related to the choice of parametrization canceled out.

Total divergence Combining eqs. (A.29) and (A.40), we obtain the total divergence for the vacuum AdS_3 portion of the CA proposal for an entangling region which is symmetric around

the defect

$$\mathcal{C}^{\text{vac}}_{A,\text{sub}} = \frac{1}{\pi}\left(I_{\text{sj,out}} + I_{\text{bulk,out}}\right) = \frac{L}{2\pi^2 G_{\text{N}}}\left(\frac{\theta_R}{\hat{\delta}}\left[\ln\left(\frac{\ell_{ct}}{L}\right)+1\right] + \ln\hat{\delta}\,\ln\left(\frac{2\ell_{ct}}{L}\right)\right) + \text{finite}. \tag{A.41}$$

This concludes the derivation of eq. (3.90).

A.3 Subregion CV in the Poincaré patch

In the global coordinates, we are constrained to consider the case where the two patches glued together share the same cosmological constant. However, if we consider the Poincaré patch, we can glue together two AdS_3 patches with different AdS radii along the location of the defect. The backreacted metric reads [130, 155, 170]

$$ds^2 = \frac{L^2}{z'^2}(-dt^2+dz'^2+dx'^2)\,\Theta(z'+x'\tan\beta) + \frac{R^2}{z^2}(-dt^2+dz^2+dx^2)\,\Theta(z-x\tan\alpha), \tag{A.42}$$

where $\Theta(z)$ is the Heaviside theta function and the two patches have different AdS radii R and L. The matching condition is given by

$$\frac{R}{\sin\alpha} = \frac{L}{\sin\beta} = -\frac{\cot\alpha+\cot\beta}{8\pi G_{\text{N}}\lambda}, \tag{A.43}$$

where $\lambda > 0$ is the tension of the brane, see eq. (3.1). Stability of the gravitational solution requires that $\pi \geq \alpha, \beta \geq \pi/2$, see [155]. In the case with no defect ($\lambda = 0$) the matching condition (A.43) implies that the two AdS radii are equal $L = R$ and that $\alpha = \beta = \pi/2$. However note that in general $L = R$ does not imply that there is no defect. We will think of the two patches as being drawn alongside each other, see figure A.1. In this case the two coordinates systems (t, x, z), and (t, x', z') are related through a rotation in the $x - z$ plane as follows

$$\begin{pmatrix} z' \\ x' \end{pmatrix} = \begin{pmatrix} -\cos(\alpha+\beta) & \sin(\alpha+\beta) \\ -\sin(\alpha+\beta) & -\cos(\alpha+\beta) \end{pmatrix}\begin{pmatrix} z \\ x \end{pmatrix}. \tag{A.44}$$

Figure A.1 illustrates a constant time slice of our setup. The regions $\mathcal{D}_L$ and $\mathcal{D}_R$ are extensions of the AdS space due to the existence of the defect. We will consider the subregion complexity for a subregion which is anchored at the boundary at $x = a$ (right) and $x' = -b$ (left). Without loss of generality, we will everywhere assume that $a > b > 0$.

It is natural to continue to choose the cutoff in the regions $\mathcal{C}_L$ and $\mathcal{C}_R$, to match the usual Fefferman-Graham expansion, with $z' = \delta$ and $z = \delta$, respectively. In the defect region we suggest to extend the cutoff surface smoothly using a circular arc, similarly to what was done in subsection 3.1.2.[3] Focusing on the defect extensions $\mathcal{D}_R$ and $\mathcal{D}_L$, it will be useful to define a

[3] One could in principle consider choosing two different cutoffs for the FG expansions on each side of the defect, connected by an interpolating curve in the defect region. For example one such choice was presented in [130] where the author considers cutoffs of constant z everywhere (including the defect region). The relation between the two cutoffs is determined by holding the scale factor of the metric fixed. The resulting cutoff is continuous but not smooth across the interface. In our case, these choices would not influence the logarithmic (defect-dependent) contribution to the complexity which is expected to be universal, see section 3.5.

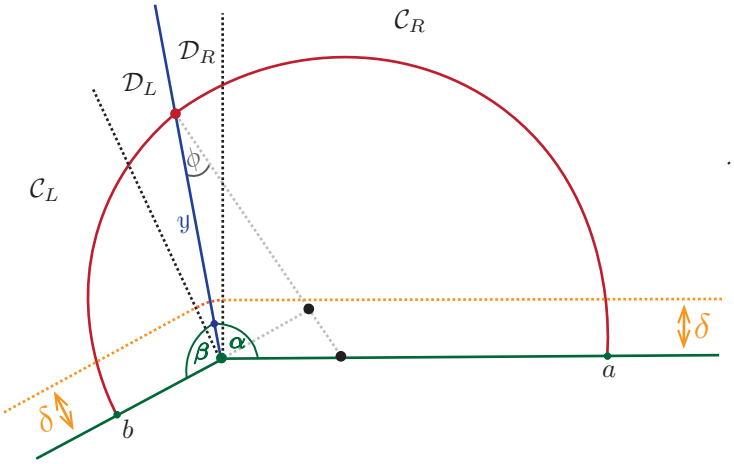

Figure A.1: Constant time slice of the two AdS_3 patches, glued together along the straight blue line representing the defect. α (right) and β (left) are the opening angles of the patches on each side of the defect. The defect extends the space and its contribution is encoded in the regions $\mathcal{D}_L, \mathcal{D}_R$, while $\mathcal{C}_L, \mathcal{C}_R$ are the parts of the AdS_3 spaces outside the defect extension. The cutoff is represented by a dotted orange curve and is extended as a circular arc in the region of the defect. The red curve represents the RT surface corresponding to the region anchored at the AdS boundary at points a and b. It consists of two circular arcs of different radii which are connected smoothly at the location of the defect. The centers of the relevant nested circles are depicted as black dots.

radial coordinates in the $x - z$ plane as

$$x = \rho \cos\theta, \qquad z = \rho \sin\theta. \tag{A.45}$$

In terms of these coordinates the metric reads

$$ds^2 = \frac{R^2}{\rho^2 \sin^2\theta}\left(-dt^2 + d\rho^2 + \rho^2 d\theta^2\right), \tag{A.46}$$

and the cutoff extension is given by

$$\rho = \delta. \tag{A.47}$$

The RT surfaces on each side of the defect are parts of circular arcs in the $x - z$ coordinates which are perpendicular to the boundary. They can be described by the following equations

$$(x - O_A)^2 + z^2 = R_A^2, \qquad (x' - O_B)^2 + z'^2 = R_B^2, \tag{A.48}$$

where O_A and O_B indicate the positions of the centers of the circular arcs and R_A and R_B indicate their Radii in the right/left patches respectively. The matching condition across the defect indicates that the circles are tangent at the location of the defect (see, e.g., [155]). One is then led to the conclusion that the two centers as well as the location where the arcs intersect the defect lie along a single line. We define the angle between this line and the defect as ϕ, see figure A.1.

The geometry is completely fixed by the angles α and β as well as the sizes of the relevant

boundary regions a (right) and b (left), see figure A.1. The angle ϕ is given by the solution to the equation

$$\frac{a}{b} = \left(\frac{\tan\frac{\alpha}{2}\tan\frac{\phi}{2}+1}{\tan\frac{\alpha}{2}\tan\frac{\phi}{2}-1}\right)\left(\frac{\tan\frac{\beta}{2}\tan\frac{\phi}{2}+1}{\tan\frac{\beta}{2}\tan\frac{\phi}{2}-1}\right) \tag{A.49}$$

which satisfies $\sin\alpha > \sin\phi$ and $\sin\beta > \sin\phi$, or explicitly

$$\tan\frac{\phi}{2} = \frac{(a+b)\sin\frac{\alpha+\beta}{2} - \sqrt{(a+b)^2\sin^2\left(\frac{\alpha-\beta}{2}\right)+4ab\sin\alpha\sin\beta}}{2(a-b)\sin\frac{\alpha}{2}\sin\frac{\beta}{2}}. \tag{A.50}$$

The various "lengths"[4] indicated in figure A.1 are given by

$$\begin{aligned} R_A &= a\frac{\sin\alpha}{\sin\alpha+\sin\phi}, & R_B &= b\frac{\sin\beta}{\sin\beta-\sin\phi}, \\ O_A &= a\frac{\sin\phi}{\sin\alpha+\sin\phi}, & O_B &= b\frac{\sin\phi}{\sin\beta-\sin\phi}, \end{aligned} \tag{A.51}$$

and the "length" along the defect up to the meeting point is given by

$$y = a\,\frac{\sin(\alpha+\phi)}{\sin\alpha+\sin\phi} = b\,\frac{\sin(\beta-\phi)}{\sin\beta-\sin\phi}, \tag{A.52}$$

or explicitly

$$y = \frac{(a-b)\sin\left(\frac{\beta-\alpha}{2}\right)+\sqrt{(a+b)^2\sin^2\left(\frac{\beta-\alpha}{2}\right)+4ab\sin\alpha\sin\beta}}{2\sin\left(\frac{\alpha+\beta}{2}\right)}, \tag{A.53}$$

cf. eq. (B.3) of [155].

We will focus on the subregion complexity, since the boundary is infinite and hence the complexity of the full space is (IR) divergent. We have divided the integration region into four regions – $\mathcal{C}_R$ and $\mathcal{C}_L$ outside the defect region and $\mathcal{D}_R$ and $\mathcal{D}_L$ inside the defect region. The various volumes read

$$\begin{aligned} \mathcal{C}_R &= R^2\int_\delta^{\sqrt{R_A^2-O_A^2}}\frac{dz}{z^2}\int_0^{O_A+\sqrt{R_A^2-z^2}}dx + R^2\int_{\sqrt{R_A^2-O_A^2}}^{R_A}\frac{dz}{z^2}\int_{O_A-\sqrt{R_A^2-z^2}}^{O_A+\sqrt{R_A^2-z^2}}dx \\ &= R^2\left(\frac{a}{\delta}-\frac{\pi}{2}-\sin^{-1}\left(\frac{\sin\phi}{\sin\beta}\right)\right), \end{aligned} \tag{A.54}$$

and

$$\mathcal{C}_L = L^2\int_\delta^{\sqrt{R_B^2-O_B^2}}\frac{dz'}{z'^2}\int_{O_B-\sqrt{R_B^2-z'^2}}^{0}dx' = L^2\left(\frac{b}{\delta}-\frac{\pi}{2}+\sin^{-1}\left(\frac{\sin\phi}{\sin\beta}\right)\right), \tag{A.55}$$

[4] Here we indicate the length without the overall conformal factor namely, $\sqrt{x^2+z^2}$ or $\sqrt{x'^2+z'^2}$.

outside the defect region and

$$\mathcal{D}_R = R^2 \int_{\pi/2}^{\alpha} \frac{d\theta}{\sin^2\theta} \int_{\delta}^{O_A \cos\theta + \sqrt{R_A^2 - O_A^2 \sin^2\theta}} \frac{d\rho}{\rho} = R^2 \left(\cot\alpha \ln\left(\frac{\delta}{y}\right) - \phi + \sin^{-1}\left(\frac{\sin\phi}{\sin\alpha}\right)\right), \tag{A.56}$$

and

$$\mathcal{D}_L = L^2 \int_{\pi-\beta}^{\pi/2} \frac{d\theta}{\sin^2\theta} \int_{\delta}^{O_B \cos\theta + \sqrt{R_B^2 - O_B^2 \sin^2\theta}} \frac{d\rho}{\rho} = L^2 \left(\cot\beta \ln\left(\frac{\delta}{y}\right) + \phi - \sin^{-1}\left(\frac{\sin\phi}{\sin\beta}\right)\right), \tag{A.57}$$

inside the defect region. Of course we notice that the left and right patch results are related by the exchange $\phi \to -\phi$, $\alpha \to \beta$, $a \to b$ and $R \to L$.

Summing all the contributions together, multiplying by the relevant factors of proportionality $1/(G_{\text{N}}R)$ and $1/(G_{\text{N}}L)$ for the right and left patches respectively, see eq. (2.45), and expressing the result in terms of the central charges, $c_R \equiv \frac{3R}{2G_{\text{N}}}$ and $c_L \equiv \frac{3L}{2G_{\text{N}}}$, yields

$$\begin{aligned} \mathcal{C}_V^{\text{poincare}} = {} & \frac{2(c_R\, a + c_L\, b)}{3\delta} + \frac{2}{3}\left(c_R \cot\alpha + c_L \cot\beta\right) \ln\left(\frac{\delta}{y}\right) \\ & - \frac{2c_R}{3}\left(\frac{\pi}{2} + \phi\right) - \frac{2c_L}{3}\left(\frac{\pi}{2} - \phi\right). \end{aligned} \tag{A.58}$$

where ϕ is defined in eq. (A.50), y is defined in eq. (A.53) and α and β are determined from the matching conditions (A.43) in terms of the two cosmological constants and the data of the defect.

Finally, let us study the limit of equal cosmological constant which yields $\alpha = \beta$, $c_R = c_L \equiv c_T$ and as a consequence $y = \sqrt{ab}$. This yields the following complexity

$$\mathcal{C}_V^{\text{poincare}} = \frac{2c_T}{3}\left(\frac{a+b}{\delta} - 2\sinh y^* \ln\left(\frac{\delta}{\sqrt{ab}}\right) - \pi\right) \tag{A.59}$$

where we have used eq. (A.43) and eq. (3.3) to relate $\cot\alpha = -\sinh y^*$. This can be seen as the large boundary size $a, b \ll L_{\mathcal{B}}$ limit of the global coordinate result of eq. (3.69) where we have used $\theta_R = a/L_{\mathcal{B}}$ and $\theta_L = -b/L_{\mathcal{B}}$ in order to perform the expansion in eqs. (3.70) and (3.69).

A similar analysis to the one we have performed in subsection 3.3.2 for the subregion CA conjecture can be performed here as well. We leave this extension for future work.

Appendix B

Orthogonality of the rotational matrix $M(n)$ for $\alpha \in \mathbb{R}$

The orthogonality is independent of the bosonic mode n, for simplicity, in this section we will take $n = 1$, thus neglect the explicit dependence of n for the matrices. Since A and B are both symmetric, which means

$$MM^T = \begin{pmatrix} A^2 + B^2 & BA - AB \\ AB - BA & A^2 + B^2 \end{pmatrix}. \tag{B.1}$$

To prove the orthogonality of M is to show that $(A^2 + B^2)_{ik} = \delta_{ik}$ and $(AB - BA)_{ik} = 0$, this will be given explicitly in the following part.

B.1 $(A^2 + B^2)_{ik} = \delta_{ik}$

To start with, k is required to be $k = i + 2m (m \in \mathbb{Z})$ since it is easy to see that if k and i differ by an odd number the corresponding entry would give zero. The diagonal entries correspond to the case $m = 0$, which are given as

$$\begin{aligned} (A^2 + B^2)_{ii} &= \sum_r A_{i(i+2r)} A_{(i+2r)i} + B_{i(i+2r+1)} B_{(i+2r+1)i} \\ &= \sum_r J^2_{|2r|} + \sum_r J^2_{|2r+1|} \\ &= J_0^2 + 2\sum_{r=1} J_r^2 = 1 \end{aligned} \tag{B.2}$$

which is known as Neumann's theorem of Bessel functions. Without loss of generality, we will assume that $m > 0$ in the following case for the off-diagonal entries. The calculation shows

$$\begin{aligned}(A^2+B^2)_{ik} &= \sum_{r>m}(-1)^m J_{2r}J_{2(r-m)} + \sum_{r\geq m}(-1)^m J_{(2r+1)}J_{2(r-m)+1} \\ &+ \sum_{0\leq r\leq m}(-1)^m J_{2r}J_{2(m-r)} + \sum_{0\leq r<m}(-1)^{m+1}J_{2r+1}J_{-1-2(r-m)} \\ &+ \sum_{r<0}(-1)^m(J_{-2r}J_{2(m-r)} + J_{-2r-1}J_{-1-2(r-m)}) \\ &= (-1)^m\sum_{r\geq 1}J_rJ_{2m+r} + (-1)^m\sum_{r=0}^{2m}(-1)^r J_rJ_{2m-r} + (-1)^m\sum_{r\geq 1}J_rJ_{2m+r} \\ &= (-1)^m\left(\sum_{r=0}^{2m}(-1)^r J_rJ_{2m-r} + 2\sum_{r\geq 1}J_rJ_{2m+r}\right) = 0 \end{aligned} \tag{B.3}$$

where in the second step we used the property of Bessel function $J_{-l} = (-1)^l J_l$ and the last step is another theorem of Neumann. Therefore, we have proved that

$$A^2 + B^2 = \mathbb{1} \tag{B.4}$$

is an identity matrix.

B.2 $(AB - BA)_{ik} = 0$

In this case, the non-zero entries would require $k = 2m + 1 (m \in \mathbb{Z})$. The calculation follows,

$$\begin{aligned}(AB)_{i(i+2m+1)} &= \sum_r A_{i(2r+i)}B_{(2r+i)(i+2m+1)} \\ &= \sum_r (-1)^r i^{|(2(m-r)+1|-1}J_{2|r|}J_{|2(m-r)+1|}\end{aligned} \tag{B.5}$$

and

$$\begin{aligned}(BA)_{i(i+2m+1)} &= \sum_r B_{i(2r+1+i)}A_{(2r+i)(i+2m+1)} \\ &= \sum_r (-1)^{m-r} i^{|2r+1|-1}J_{2|m-r|}J_{|2r+1|} \\ &= \sum_r (-1)^r i^{|(2(m-r)+1|-1}J_{2|r|}J_{|2(m-r)+1|}\end{aligned} \tag{B.6}$$

therefore,

$$(AB - BA)_{ik} = 0. \tag{B.7}$$

Combining (B.4) and (B.7), one shows that M is an orthogonal matrix as expected.

Appendix C

Modular Berry Connection

C.1 Berry connection

Consider a family of normalized pure states $\rho(\lambda) = |\psi(\lambda)\rangle\langle\psi(\lambda)|$. Each state is invariant under the transformation $U(\lambda) = \exp\Big(i\theta(\lambda)|\psi(\lambda)\rangle\langle\psi(\lambda)|\Big)$, which simply rotates the vector $|\psi(\lambda)\rangle$ by a phase $\theta(\lambda)$. The operators $U(\lambda)$ are therefore the modular zero modes in this simple example.

The variation of the state under an infinitesimal change of λ is

$$\partial_\lambda \rho = (\partial_\lambda|\psi\rangle)\,\langle\psi| + |\psi\rangle\,(\partial_\lambda\langle\psi|) = [V, \rho]\,, \tag{C.1}$$

where we defined the anti-Hermitian operator

$$V = (\partial_\lambda|\psi\rangle)\,\langle\psi| - |\psi\rangle\,(\partial_\lambda\langle\psi|)\ . \tag{C.2}$$

This is clearly not unique since any addition of zero-modes to V respects equation (C.1). This reflects our freedom to independently rotate the phases of $|\psi(\lambda)\rangle$ and $|\psi(\lambda+\delta\lambda)\rangle$.

According to (6.18), the modular Berry connection is the projection of $V(\lambda)$ onto the zero modes of $\rho(\lambda)$ which, using the projector (6.14), reads:

$$\Gamma = P_0^\lambda[V(\lambda)] = \Big(\langle\psi|\partial_\lambda\psi\rangle - \langle\partial_\lambda\psi|\psi\rangle\Big)|\psi\rangle\langle\psi|\,. \tag{C.3}$$

This is the familiar Berry connection [220, 221].

C.2 Modular connection for CFT vacuum

The two-sided modular Hamiltonian for an interval in the CFT vacuum can be written in terms of the conformal generators as $H_{\text{mod}} = K_+ + K_-$, with:

$$K_+ = s_1 L_1 + s_0 L_0 + s_{-1} L_{-1}\,, \tag{C.4}$$

$$K_- = t_1 \bar{L}_1 + t_0 \bar{L}_0 + t_{-1} \bar{L}_{-1}. \tag{C.5}$$

The coefficients s_i, t_i are determined, up to an overall multiplicative constant, by the requirement that the generators K_+ and K_- preserve the left-moving and right-moving null coordinates of

the interval endpoints (a^+, b^+) and (a^-, b^-), respectively. Working in the representation

$$L_{-1} = ie^{-ix^+}\partial_+ \qquad \text{and} \qquad L_0 = i\partial_+ \qquad \text{and} \qquad L_1 = ie^{ix^+}\partial_+, \tag{C.6}$$

with an identical action of the $\bar{L}_i$s on the x^- null coordinate, we find:

$$\begin{aligned} s_1 &= \tfrac{2\pi\cot(b^+-a^+)/2}{e^{ia^+}+e^{ib^+}}, & t_1 &= -\tfrac{2\pi\cot(b^--a^-)/2}{e^{ia^-}+e^{ib^-}}, \\ s_0 &= -2\pi\cot(b^+-a^+)/2, & t_0 &= 2\pi\cot(b^--a^-)/2, \\ s_{-1} &= \tfrac{2\pi\cot(b^+-a^+)/2}{e^{-ia^+}+e^{-ib^+}}, & t_{-1} &= -\tfrac{2\pi\cot(b^--a^-)/2}{e^{-ia^-}+e^{-ib^-}}. \end{aligned} \tag{C.7}$$

We found the overall magnitude of H_{mod} by demanding that $\exp(-H_{\text{mod}}/2)$—a finite $SO(2,1) \times SO(2,1)$ transformation—map an interval to its complement.

The generator of modular parallel transport is defined by the conditions:

$$\partial_{a^+} K_+ = [V_{\delta a^+}, K_+]\,, \tag{C.8}$$

$$P_0[V_{\delta a^+}] = 0\,. \tag{C.9}$$

In the vacuum of a two-dimensional CFT, any single-interval modular Hamiltonian can be mapped to any other using conformal transformations. This is the reason for the absence of the spectrum changing operator appearing on the left hand side of the general equation (6.22). The same fact guarantees that $V_{\delta a^+}$ is an element of the conformal algebra, so it is a linear combination of the generators (C.6).

To find $V_{\delta a^+}$ explicitly, it is convenient to decompose the conformal algebra into eigenoperators of the adjoint action of the modular Hamiltonian:

$$[K_+, E_\kappa] = \kappa E_\kappa\,. \tag{C.10}$$

The three solutions of equation (C.10) are:

$$[K_+, K_+] = 0\,,$$

$$[K_+, \partial_{a^+} K_+] = -2\pi i\, \partial_{a^+} K_+\,, \tag{C.11}$$

$$[K_+, \partial_{b^+} K_+] = +2\pi i\, \partial_{b^+} K_+\,. \tag{C.12}$$

This immediately implies eq. (6.27), i.e.:

$$V_{\delta a^+} = \frac{1}{2\pi i}\, \partial_{a^+} K_+\,. \tag{C.13}$$

Eq. (C.9) is automatically satisfied because $\partial_{a^+} K_+$ and K_+ live in orthogonal eigenspaces of the eigenvalue equation (C.10).

It is easy to consider a more general direction in kinematic space (space of CFT intervals.) Say we go from $H_{\text{mod}}(\lambda)$ (here $\lambda = (a^+, b^+, a^-, b^-)$) to $\lambda + \delta\lambda$. The change in the modular Hamiltonian is:

$$\partial_\lambda H_{\text{mod}} \equiv (\partial a^+/\partial\lambda)\, \partial_{a^+} K_+ + (\partial b^+/\partial\lambda)\, \partial_{b^+} K_+ + (\partial a^-/\partial\lambda)\, \partial_{a^-} K_- + (\partial b^-/\partial\lambda)\, \partial_{b^-} K_-\,. \tag{C.14}$$

The operator

$$V_{\delta\lambda} = \frac{1}{2\pi i}\left(\frac{\partial a^+}{\partial\lambda}\partial_{a^+}K_+ - \frac{\partial b^+}{\partial\lambda}\partial_{b^+}K_+ - \frac{\partial a^-}{\partial\lambda}\partial_{a^-}K_- + \frac{\partial b^-}{\partial\lambda}\partial_{b^-}K_-\right) \tag{C.15}$$

solves

$$[V_{\delta\lambda}, H_{\text{mod}}] = \partial_\lambda H_{\text{mod}}. \tag{C.16}$$

It also satisfies (C.9) because it lives outside the zero-eigenspace of $[H_{\text{mod}}, E_\kappa] = \kappa E_\kappa$, the latter being generated by K_+ and K_-. Therefore, (C.15) is the generator of modular parallel transport.

C.3 Solution to the equation governing $H^{\text{bulk}}_{\text{mod}}$

In this part, we consider the solution to eq. (6.40). Consider an entanglement wedge λ and a coordinate system $x^M = (x^\alpha, y^i)$ in the neighborhood of its RT surface. x^α denotes distances along two directions orthogonal to the RT surface and y^i is a choice of internal surface coordinates.

Since we are ultimately interested in comparing the frames of two nearby extremal surfaces, the form of the metric in the vicinity of the RT surface is important. It is convenient to introduce normal geodesic coordinates $\sigma^M = (\sigma^a(x), y^i)$, where $\sigma^a(x)\eta_{ab}\sigma^b(x)$ measures the geodesic distance of a nearby point x from the minimal surface and $\frac{\sigma^a}{\sigma}$ is the unit tangent vector to the same geodesic at its starting point on the surface. In an expansion around the surface, this coordinate system is:

$$x^M(\sigma^\alpha, y^i) = \sigma^M - \frac{1}{2}\Gamma^M_{\alpha\beta}(y)\sigma^\alpha\sigma^\beta + \mathcal{O}(\sigma^3)\,. \tag{C.17}$$

The advantage of the σ-coordinates is that they set the components $\Gamma^M_{\alpha\beta}$ of the Christofel connection to zero, so they constitute the analog of the local inertial frame for a surface.

For as long as we focus on a small neighborhood of the RT surface ($\sigma^+K_{ij|+}$, $\sigma^-K_{ij|-} \ll 1$) the action of the modular Hamiltonian is expected to be local and, therefore, it can be described by a vector field $\zeta^M_{(\lambda)}(\sigma)$ generating a geometric flow. About the surface, the modular flow generator has the form

$$\begin{aligned}\zeta^a_{(\lambda)} &= 2\pi\epsilon^a{}_b\sigma^b\,,\\ \zeta^i_{(\lambda)} &= 0\,.\end{aligned} \tag{C.18}$$

The λ-derivative of the modular boost. Consider now a nearby entanglement wedge $\lambda+\delta\lambda$ whose RT surface is separated from that of λ by $\delta\sigma^\alpha(y_i)$ in the orthogonal directions. Its modular boost generator $\tilde{\zeta}^M_{(\lambda+\delta\lambda)}$ will have the same form (C.18) in the normal frame of the new wedge. Let $n_a{}^M(\tilde{y};\lambda+\delta\lambda)$ $(a=0,1)$ be two orthonormal vectors at every point $\tilde{y}^i$ on the HRRT surface of $\lambda+\delta\lambda$ and denote by s^a distances along $n_a{}^M$. Then the map $(\sigma^a(s^a,\tilde{y}^i), y^i(s^a,\tilde{y}^i))$, at first non-trivial order in the separation of the two surfaces, is:

$$\begin{aligned}\sigma^a &= \delta\sigma^a(\tilde{y}) + s^a + \delta n_b{}^a s^b + \mathcal{O}(s^2, \delta\sigma^2, \delta n^2)\,,\\ y^i &= \tilde{y}^i + \delta n_b{}^i s^b + \mathcal{O}(s^2, \delta\sigma^2, \delta n^2)\,.\end{aligned} \tag{C.19}$$

Here $\delta n_a{}^M \equiv n_a{}^M(\lambda+\delta\lambda) - n_a{}^M(\lambda)$ and we have used the fact that, in the orthonormal gauge we are using, the normal vectors on the λ surface are $n_a{}^M(\lambda) = \delta_a^M$.

It is important to note that the choice of normal coordinates s^a is not unique, since any local Lorentz boost on the orthogonal plane

$$\delta n_b{}^a \to \delta n_b{}^a + \omega(\tilde{y})\epsilon_b{}^a \tag{C.20}$$

will yield an equally acceptable pair of normal directions. There is, therefore, an ambiguity in the map between the normal frames of two nearby minimal surfaces. This ambiguity will be important in what follows.

Since the vector field $\tilde{\zeta}^M_{(\lambda+\delta\lambda)}$ has the form (C.18) in the s^a-coordinates, we can use transformation (C.19) to map it back to the σ-coordinates and compute the difference of the two modular boost generators:

$$\begin{aligned}\delta_\lambda \zeta^M = &-\delta_a^M \epsilon^a{}_b \delta\sigma^b - \delta_a^M \epsilon^a{}_b \delta n_c{}^b \sigma^c + \delta n_a{}^M \epsilon^a{}_b \sigma^b \\ &+ \mathcal{O}(s^2, \delta\sigma^2, \delta n^2)\,.\end{aligned} \tag{C.21}$$

Zero-mode component of (C.21). The next step is to compute the zero mode component of $\delta_\lambda\zeta^M$ and subtract it to obtain an equation for the Lie bracket of ξ with ζ_λ. Applying the projector (6.46) to the right hand side of (C.21), we find:

$$\Omega\left(\delta_\lambda\zeta\right) = -\frac{1}{2}\epsilon^{ab}\partial_a\left(\eta_{bc}\delta_\lambda\zeta^c\right)\Big|_{\sigma^a=0} = 0\,, \tag{C.22}$$

$$Z^i\left(\delta_\lambda\zeta\right) = \delta_\lambda\zeta^i\Big|_{\sigma^a=0} = 0\,. \tag{C.23}$$

Equation (C.21) contains no zero mode components, so no extra subtraction is necessary.

The bulk modular connection. By plugging the result (C.21) into equation (6.40) we obtain an equation for the diffeomorphism ξ that can be straightforwardly solved to get

$$\xi^M = -\delta_a^M\,\delta\sigma^a - \delta n_a{}^M\,\sigma^a\,. \tag{C.24}$$

The solution (C.24) is not unique, because the vector Lie bracket $[\xi,\zeta]$ has a kernel. The family of solutions to (6.40) are related to (C.24) (and each other) by:

$$\xi^M \to \xi^M + \omega(\tilde{y}^i)\delta_a^M\,\epsilon^a{}_b\,\sigma^b + \delta_i^M\,\zeta_0^i(\tilde{y}_i)\,. \tag{C.25}$$

As discussed in the main text, this is simply an addition of modular zero modes. The first term, corresponding to a spatially varying boost along the orthogonal RT surface directions, can be absorbed in the ambiguity (C.20) in the local choice of normal vectors on the RT surface of $\lambda+\delta\lambda$. The second term, in turn, allows the internal coordinate systems on λ and $\lambda+\delta\lambda$ to be related by an infinitesimal element of the $(d-2)$-dimensional surface diffeomorphim subgroup.

It instructive to transform the result (C.24) back to the general normal gauge x^M using (C.17).

Some direct computation yields the following general solution (up to zero modes):

$$\xi^M = -\delta^M_a \, \delta\sigma^a - \left(\delta n_a{}^M + \Gamma^M_{ab} \, \delta\sigma^b \right) \, x^a \, . \tag{C.26}$$

Bibliography

[1] A. Einstein and M. Großman, *Entwurf einer verallgemeinerten Relativitätstheorie und einer Theorie der Gravitation*, *Monatshefte für Mathematik und Physik* **26** (1915) A38–A38.

[2] C. Misner, K. Thorne and J. Wheeler, *Gravitation*. W. H. Freeman and company, 1973.

[3] A. Einstein, *Über einen die erzeugung und verwandlung des lichtes betreffenden heuristischen gesichtspunkt*, *Annalen der Physik* **322** (1905) 132–148.

[4] N. Bohr, *I. On the constitution of atoms and molecules*, *The London, Edinburgh, and Dublin Philosophical Magazine and Journal of Science* **26** (1913) 1–25.

[5] J. M. Maldacena, *The Large N limit of superconformal field theories and supergravity*, *Int. J. Theor. Phys.* **38** (1999) 1113–1133, [hep-th/9711200].

[6] C. B. Thorn, *Reformulating string theory with the 1/N expansion*, in *The First International A.D. Sakharov Conference on Physics*, pp. 0447–454, 5, 1991. hep-th/9405069.

[7] G. 't Hooft, *Dimensional reduction in quantum gravity*, *Conf. Proc. C* **930308** (1993) 284–296, [gr-qc/9310026].

[8] L. Susskind, *The World as a hologram*, *J. Math. Phys.* **36** (1995) 6377–6396, [hep-th/9409089].

[9] G. Policastro, D. T. Son and A. O. Starinets, *The Shear viscosity of strongly coupled N=4 supersymmetric Yang-Mills plasma*, *Phys. Rev. Lett.* **87** (2001) 081601, [hep-th/0104066].

[10] E. V. Shuryak, *What RHIC experiments and theory tell us about properties of quark-gluon plasma?*, *Nucl. Phys. A* **750** (2005) 64–83, [hep-ph/0405066].

[11] S. Ryu and T. Takayanagi, *Holographic derivation of entanglement entropy from AdS/CFT*, *Phys. Rev. Lett.* **96** (2006) 181602, [hep-th/0603001].

[12] T. Hirata and T. Takayanagi, *AdS/CFT and strong subadditivity of entanglement entropy*, *JHEP* **02** (2007) 042, [hep-th/0608213].

[13] M. Headrick and T. Takayanagi, *A Holographic proof of the strong subadditivity of entanglement entropy*, *Phys. Rev. D* **76** (2007) 106013, [0704.3719].

[14] S. H. Shenker and D. Stanford, *Black holes and the butterfly effect*, *JHEP* **03** (2014) 067, [1306.0622].

[15] X. Dong, *The Gravity Dual of Renyi Entropy*, *Nature Commun.* **7** (2016) 12472, [1601.06788].

[16] D. Stanford and L. Susskind, *Complexity and Shock Wave Geometries*, *Phys. Rev.* **D90** (2014) 126007, [1406.2678].

[17] A. R. Brown, D. A. Roberts, L. Susskind, B. Swingle and Y. Zhao, *Holographic Complexity Equals Bulk Action?*, *Phys. Rev. Lett.* **116** (2016) 191301, [1509.07876].

[18] S. Chapman, D. Ge and G. Policastro, *Holographic Complexity for Defects Distinguishes Action from Volume*, *JHEP* **05** (2019) 049, [1811.12549].

[19] C. Bachas, S. Chapman, D. Ge and G. Policastro, *Energy Reflection and Transmission at 2D Holographic Interfaces*, 2006.11333.

[20] D. Ge and G. Policastro, *Circuit Complexity and 2D Bosonisation*, *JHEP* **10** (2019) 276, [1904.03003].

[21] B. Czech, J. De Boer, D. Ge and L. Lamprou, *A modular sewing kit for entanglement wedges*, *JHEP* **11** (2019) 094, [1903.04493].

[22] E. Witten, *Anti-de Sitter space and holography*, *Adv. Theor. Math. Phys.* **2** (1998) 253–291, [hep-th/9802150].

[23] S. Gubser, I. R. Klebanov and A. M. Polyakov, *Gauge theory correlators from noncritical string theory*, *Phys. Lett. B* **428** (1998) 105–114, [hep-th/9802109].

[24] J. Polchinski, *Introduction to Gauge/Gravity Duality*, in *Theoretical Advanced Study Institute in Elementary Particle Physics: String theory and its Applications: From meV to the Planck Scale*, pp. 3–46, 10, 2010. 1010.6134. DOI.

[25] O. Aharony, S. S. Gubser, J. M. Maldacena, H. Ooguri and Y. Oz, *Large N field theories, string theory and gravity*, *Phys. Rept.* **323** (2000) 183–386, [hep-th/9905111].

[26] K. Skenderis, *Lecture notes on holographic renormalization*, *Class. Quant. Grav.* **19** (2002) 5849–5876, [hep-th/0209067].

[27] M. Parikh and P. Samantray, *Rindler-AdS/CFT*, *JHEP* **10** (2018) 129, [1211.7370].

[28] D. Kabat, G. Lifschytz, S. Roy and D. Sarkar, *Holographic representation of bulk fields with spin in AdS/CFT*, *Phys. Rev. D* **86** (2012) 026004, [1204.0126].

[29] I. R. Klebanov and E. Witten, *AdS / CFT correspondence and symmetry breaking*, *Nucl. Phys. B* **556** (1999) 89–114, [hep-th/9905104].

[30] D. Z. Freedman, S. D. Mathur, A. Matusis and L. Rastelli, *Correlation functions in the CFT(d) / AdS(d+1) correspondence*, *Nucl. Phys. B* **546** (1999) 96–118, [hep-th/9804058].

[31] P. Di Francesco, P. Mathieu and D. Senechal, *Conformal Field Theory*. Graduate Texts in Contemporary Physics. Springer-Verlag, New York, 1997, 10.1007/978-1-4612-2256-9.

[32] J. Brown and M. Henneaux, *Central Charges in the Canonical Realization of Asymptotic Symmetries: An Example from Three-Dimensional Gravity*, *Commun. Math. Phys.* **104** (1986) 207–226.

[33] H. Saida and J. Soda, *Statistical entropy of BTZ black hole in higher curvature gravity*, *Phys. Lett. B* **471** (2000) 358–366, [gr-qc/9909061].

[34] P. Kraus and F. Larsen, *Microscopic black hole entropy in theories with higher derivatives*, *JHEP* **09** (2005) 034, [hep-th/0506176].

[35] J. R. David, G. Mandal and S. R. Wadia, *Microscopic formulation of black holes in string theory*, *Phys. Rept.* **369** (2002) 549–686, [hep-th/0203048].

[36] P. Kraus, *Lectures on black holes and the AdS(3) / CFT(2) correspondence*, *Lect. Notes Phys.* **755** (2008) 193–247, [hep-th/0609074].

[37] D. Tong, *The holographic dual of* $AdS_3 \times S^3 \times S^3 \times S^1$, *JHEP* **04** (2014) 193, [1402.5135].

[38] L. Eberhardt, M. R. Gaberdiel and W. Li, *A holographic dual for string theory on* $AdS_3 \times S^3 \times S^3 \times S^1$, *JHEP* **08** (2017) 111, [1707.02705].

[39] S. Deser and A. Schwimmer, *Geometric classification of conformal anomalies in arbitrary dimensions*, *Phys. Lett. B* **309** (1993) 279–284, [hep-th/9302047].

[40] S. N. Solodukhin, *Boundary terms of conformal anomaly*, *Phys. Lett. B* **752** (2016) 131–134, [1510.04566].

[41] D. Fursaev, *Conformal anomalies of CFT's with boundaries*, *JHEP* **12** (2015) 112, [1510.01427].

[42] M. Henningson and K. Skenderis, *The Holographic Weyl anomaly*, *JHEP* **07** (1998) 023, [hep-th/9806087].

[43] G. M. Shore, *The c and a-theorems and the Local Renormalisation Group*. SpringerBriefs in Physics. Springer, Cham, 2017, 10.1007/978-3-319-54000-9.

[44] M. Duff, *Observations on Conformal Anomalies*, *Nucl. Phys. B* **125** (1977) 334–348.

[45] Z. Komargodski and A. Schwimmer, *On Renormalization Group Flows in Four Dimensions*, *JHEP* **12** (2011) 099, [1107.3987].

[46] A. Zamolodchikov, *Irreversibility of the Flux of the Renormalization Group in a 2D Field Theory*, *JETP Lett.* **43** (1986) 730–732.

[47] S. de Haro, S. N. Solodukhin and K. Skenderis, *Holographic reconstruction of space-time and renormalization in the AdS / CFT correspondence*, *Commun. Math. Phys.* **217** (2001) 595–622, [hep-th/0002230].

[48] K. Skenderis and S. N. Solodukhin, *Quantum effective action from the AdS / CFT correspondence*, *Phys. Lett. B* **472** (2000) 316–322, [hep-th/9910023].

[49] C. Bachas, S. Chapman, D. Ge and G. Policastro, *in preparation*.

[50] T. Quella, I. Runkel and G. M. Watts, *Reflection and transmission for conformal defects*, *JHEP* **04** (2007) 095, [hep-th/0611296].

[51] M. Meineri, J. Penedones and A. Rousset, *Colliders and conformal interfaces*, *JHEP* **02** (2020) 138, [1904.10974].

[52] C. Bachas, J. de Boer, R. Dijkgraaf and H. Ooguri, *Permeable conformal walls and holography*, *JHEP* **06** (2002) 027, [hep-th/0111210].

[53] M. Mintchev, E. Ragoucy and P. Sorba, *Reflection transmission algebras*, *J. Phys. A* **36** (2003) 10407, [hep-th/0303187].

[54] P. Hayden and J. Preskill, *Black holes as mirrors: Quantum information in random subsystems*, *JHEP* **09** (2007) 120, [0708.4025].

[55] T. Hartman and J. Maldacena, *Time Evolution of Entanglement Entropy from Black Hole Interiors*, *JHEP* **05** (2013) 014, [1303.1080].

[56] J. M. Maldacena, *Eternal black holes in anti-de Sitter*, *JHEP* **04** (2003) 021, [hep-th/0106112].

[57] A. R. Brown, D. A. Roberts, L. Susskind, B. Swingle and Y. Zhao, *Complexity, action, and black holes*, *Phys. Rev.* **D93** (2016) 086006, [1512.04993].

[58] G. W. Gibbons and S. W. Hawking, *Action Integrals and Partition Functions in Quantum Gravity*, *Phys. Rev.* **D15** (1977) 2752–2756.

[59] J. W. York, Jr., *Role of conformal three geometry in the dynamics of gravitation*, *Phys. Rev. Lett.* **28** (1972) 1082–1085.

[60] K. Parattu, S. Chakraborty, B. R. Majhi and T. Padmanabhan, *A Boundary Term for the Gravitational Action with Null Boundaries*, *Gen. Rel. Grav.* **48** (2016) 94, [1501.01053].

[61] G. Hayward, *Gravitational action for spacetimes with nonsmooth boundaries*, *Phys. Rev. D* **47** (Apr, 1993) 3275–3280.

[62] D. Brill and G. Hayward, *Is the gravitational action additive?*, *Phys. Rev.* **D50** (1994) 4914–4919, [gr-qc/9403018].

[63] L. Lehner, R. C. Myers, E. Poisson and R. D. Sorkin, *Gravitational action with null boundaries*, *Phys. Rev.* **D94** (2016) 084046, [1609.00207].

[64] D. Carmi, R. C. Myers and P. Rath, *Comments on Holographic Complexity*, *JHEP* **03** (2017) 118, [1612.00433].

[65] R. Jefferson and R. C. Myers, *Circuit complexity in quantum field theory*, *JHEP* **10** (2017) 107, [1707.08570].

[66] L. Hackl and R. C. Myers, *Circuit complexity for free fermions*, *JHEP* **07** (2018) 139, [1803.10638].

[67] S. Chapman, M. P. Heller, H. Marrochio and F. Pastawski, *Toward a Definition of Complexity for Quantum Field Theory States*, *Phys. Rev. Lett.* **120** (2018) 121602, [1707.08582].

[68] P. Caputa, N. Kundu, M. Miyaji, T. Takayanagi and K. Watanabe, *Liouville action as path-integral complexity: From continuous tensor networks to AdS/CFT*, *JHEP* **11** (2017) 097, [1706.07056].

[69] A. Bhattacharyya, P. Caputa, S. R. Das, N. Kundu, M. Miyaji and T. Takayanagi, *Path-Integral complexity for perturbed CFTs*, *JHEP* **07** (2018) 086, [1804.01999].

[70] R.-Q. Yang, Y.-S. An, C. Niu, C.-Y. Zhang and K.-Y. Kim, *Principles and symmetries of complexity in quantum field theory*, *Eur. Phys. J.* **C79** (2019) 109, [1803.01797].

[71] R.-Q. Yang, Y.-S. An, C. Niu, C.-Y. Zhang and K.-Y. Kim, *More on complexity of operators in quantum field theory*, *JHEP* **03** (2019) 161, [1809.06678].

[72] A. Bhattacharyya, A. Shekar and A. Sinha, *Circuit complexity in interacting QFTs and RG flows*, *JHEP* **10** (2018) 140, [1808.03105].

[73] R. Khan, C. Krishnan and S. Sharma, *Circuit Complexity in Fermionic Field Theory*, *Phys. Rev.* **D98** (2018) 126001, [1801.07620].

[74] F. M. Paula, T. R. de Oliveira and M. S. Sarandy, *Geometric quantum discord through the schatten 1-norm*, *Phys. Rev. A* **87** (Jun, 2013) 064101.

[75] S. Chapman, J. Eisert, L. Hackl, M. P. Heller, R. Jefferson, H. Marrochio et al., *Complexity and entanglement for thermofield double states*, *SciPost Phys.* **6** (2019) 034, [1810.05151].

[76] M. Rangamani and T. Takayanagi, *Holographic Entanglement Entropy*, vol. 931. Springer, 2017, 10.1007/978-3-319-52573-0.

[77] R. Haag, *Local Quantum Physics: Fields, Particles, Algebras*. Theoretical and Mathematical Physics. Springer Berlin Heidelberg, 1996.

[78] J. Bisognano and E. Wichmann, *On the Duality Condition for a Hermitian Scalar Field*, *J. Math. Phys.* **16** (1975) 985–1007.

[79] H. Casini, M. Huerta and R. C. Myers, *Towards a derivation of holographic entanglement entropy*, *JHEP* **05** (2011) 036, [1102.0440].

[80] W. G. Unruh, *Notes on black-hole evaporation*, *Phys. Rev. D* **14** (Aug, 1976) 870–892.

[81] R. E. Peierls, *The commutation laws of relativistic field theory*, *Proceedings of the Royal Society of London. Series A, Mathematical and Physical Sciences* **214** (1952) 143–157.

[82] D. L. Jafferis, A. Lewkowycz, J. Maldacena and S. J. Suh, *Relative entropy equals bulk relative entropy*, *JHEP* **06** (2016) 004, [1512.06431].

[83] M. Ohya and D. Petz, *Quantum entropy and its use*. Texts and monographs in physics. Springer-Verlag, 1993.

[84] V. E. Hubeny, M. Rangamani and T. Takayanagi, *A Covariant holographic entanglement entropy proposal*, *JHEP* **07** (2007) 062, [0705.0016].

[85] X. Dong, D. Harlow and A. C. Wall, *Reconstruction of Bulk Operators within the Entanglement Wedge in Gauge-Gravity Duality*, *Phys. Rev. Lett.* **117** (2016) 021601, [1601.05416].

[86] A. Almheiri, X. Dong and D. Harlow, *Bulk Locality and Quantum Error Correction in AdS/CFT*, *JHEP* **04** (2015) 163, [1411.7041].

[87] D. Harlow, *TASI Lectures on the Emergence of Bulk Physics in AdS/CFT*, *PoS* **TASI2017** (2018) 002, [1802.01040].

[88] A. Reynolds and S. F. Ross, *Divergences in Holographic Complexity*, *Class. Quant. Grav.* **34** (2017) 105004, [1612.05439].

[89] L. Susskind, *Computational Complexity and Black Hole Horizons; Addendum to Computational Complexity and Black Hole Horizons*, *Fortsch. Phys.* **64** (2016) 24–43, Addendum: 44–48, [arXiv:1402.5674,1403.5695].

[90] D. Carmi, S. Chapman, H. Marrochio, R. C. Myers and S. Sugishita, *On the Time Dependence of Holographic Complexity*, *JHEP* **11** (2017) 188, [1709.10184].

[91] S. Chapman, H. Marrochio and R. C. Myers, *Holographic complexity in Vaidya spacetimes. Part I*, *JHEP* **06** (2018) 046, [1804.07410].

[92] S. Chapman, H. Marrochio and R. C. Myers, *Holographic complexity in Vaidya spacetimes. Part II*, *JHEP* **06** (2018) 114, [1805.07262].

[93] Y. Zhao, *Complexity and Boost Symmetry*, *Phys. Rev.* **D98** (2018) 086011, [1702.03957].

[94] A. R. Brown, H. Gharibyan, H. W. Lin, L. Susskind, L. Thorlacius and Y. Zhao, *Complexity of Jackiw-Teitelboim gravity*, *Phys. Rev.* **D99** (2019) 046016, [1810.08741].

[95] K. Goto, H. Marrochio, R. C. Myers, L. Queimada and B. Yoshida, *Holographic Complexity Equals Which Action?*, *JHEP* **02** (2019) 160, [1901.00014].

[96] A. Akhavan, M. Alishahiha, A. Naseh and H. Zolfi, *Complexity and Behind the Horizon Cut Off*, *JHEP* **12** (2018) 090, [1810.12015].

[97] M. Alishahiha, K. Babaei Velni and M. R. Tanhayi, *Complexity and Near Extremal Charged Black Branes*, 1901.00689.

[98] M. Alishahiha, A. Faraji Astaneh, M. R. Mohammadi Mozaffar and A. Mollabashi, *Complexity Growth with Lifshitz Scaling and Hyperscaling Violation*, *JHEP* **07** (2018) 042, [1802.06740].

[99] B. Swingle and Y. Wang, *Holographic complexity of Einstein-Maxwell-Dilaton gravity*, *JHEP* **09** (2018) 106, [1712.09826].

[100] N. Andrei et al., *Boundary and Defect CFT: Open Problems and Applications*, 2018. 1810.05697.

[101] O. Aharony, O. DeWolfe, D. Z. Freedman and A. Karch, *Defect conformal field theory and locally localized gravity*, *JHEP* **07** (2003) 030, [hep-th/0303249].

[102] T. Azeyanagi, A. Karch, T. Takayanagi and E. G. Thompson, *Holographic calculation of boundary entropy*, *JHEP* **03** (2008) 054, [0712.1850].

[103] Y. Sato and K. Watanabe, *Does Boundary Distinguish Complexities?*, *JHEP* **11** (2019) 132, [1908.11094].

[104] P. Braccia, A. L. Cotrone and E. Tonni, *Complexity in the presence of a boundary*, *JHEP* **02** (2020) 051, [1910.03489].

[105] I. Affleck and A. W. Ludwig, *Universal noninteger 'ground state degeneracy' in critical quantum systems*, *Phys. Rev. Lett.* **67** (1991) 161–164.

[106] M. Flory, *A complexity/fidelity susceptibility g-theorem for $AdS_3/BCFT_2$*, *JHEP* **06** (2017) 131, [1702.06386].

[107] J. de Boer, E. Llabrés, J. F. Pedraza and D. Vegh, *Chaotic strings in AdS/CFT*, *Phys. Rev. Lett.* **120** (2018) 201604, [1709.01052].

[108] S. Ryu and T. Takayanagi, *Aspects of Holographic Entanglement Entropy*, *JHEP* **08** (2006) 045, [hep-th/0605073].

[109] B. Czech, J. L. Karczmarek, F. Nogueira and M. Van Raamsdonk, *The Gravity Dual of a Density Matrix*, *Class. Quant. Grav.* **29** (2012) 155009, [1204.1330].

[110] M. Headrick, V. E. Hubeny, A. Lawrence and M. Rangamani, *Causality & holographic entanglement entropy*, *JHEP* **12** (2014) 162, [1408.6300].

[111] M. Alishahiha, *Holographic Complexity*, *Phys. Rev.* **D92** (2015) 126009, [1509.06614].

[112] R.-Q. Yang, *Complexity for quantum field theory states and applications to thermofield double states*, *Phys. Rev. D* **97** (2018) 066004, [1709.00921].

[113] R.-Q. Yang, C. Niu, C.-Y. Zhang and K.-Y. Kim, *Comparison of holographic and field theoretic complexities for time dependent thermofield double states*, *JHEP* **02** (2018) 082, [1710.00600].

[114] K. Hashimoto, N. Iizuka and S. Sugishita, *Time evolution of complexity in Abelian gauge theories*, *Phys. Rev. D* **96** (2017) 126001, [1707.03840].

[115] A. P. Reynolds and S. F. Ross, *Complexity of the AdS soliton*, *Class. Quant. Grav.* **35** (2018) 095006, [1712.03732].

[116] D. W. F. Alves and G. Camilo, *Evolution of complexity following a quantum quench in free field theory*, *JHEP* **06** (2018) 029, [1804.00107].

[117] H. A. Camargo, P. Caputa, D. Das, M. P. Heller and R. Jefferson, *Complexity as a novel probe of quantum quenches: universal scalings and purifications*, *Phys. Rev. Lett.* **122** (2019) 081601, [1807.07075].

[118] P. Caputa, N. Kundu, M. Miyaji, T. Takayanagi and K. Watanabe, *Anti-de Sitter space from optimization of path integrals in conformal field theories*, *Phys. Rev. Lett.* **119** (2017) 071602, [1703.00456].

[119] P. Caputa and J. M. Magan, *Quantum Computation as Gravity*, *Phys. Rev. Lett.* **122** (2019) 231302, [1807.04422].

[120] J. M. Magán, *Black holes, complexity and quantum chaos*, *JHEP* **09** (2018) 043, [1805.05839].

[121] T. Takayanagi, *Holographic Spacetimes as Quantum Circuits of Path-Integrations*, *JHEP* **12** (2018) 048, [1808.09072].

[122] T. Ali, A. Bhattacharyya, S. Shajidul Haque, E. H. Kim and N. Moynihan, *Time Evolution of Complexity: A Critique of Three Methods*, *JHEP* **04** (2019) 087, [1810.02734].

[123] A. Belin, A. Lewkowycz and G. Sárosi, *Complexity and the bulk volume, a new York time story*, *JHEP* **03** (2019) 044, [1811.03097].

[124] C. A. Agón, M. Headrick and B. Swingle, *Subsystem Complexity and Holography*, *JHEP* **02** (2019) 145, [1804.01561].

[125] C. G. Callan, I. R. Klebanov, A. W. W. Ludwig and J. M. Maldacena, *Exact solution of a boundary conformal field theory*, *Nucl. Phys.* **B422** (1994) 417–448, [hep-th/9402113].

[126] S. Chapman, H. Marrochio and R. C. Myers, *Complexity of Formation in Holography*, *JHEP* **01** (2017) 062, [1610.08063].

[127] I. Papadimitriou and K. Skenderis, *Correlation functions in holographic RG flows*, *JHEP* **10** (2004) 075, [hep-th/0407071].

[128] M. Gutperle and A. Trivella, *Note on entanglement entropy and regularization in holographic interface theories*, *Phys. Rev. D* **95** (2017) 066009, [1611.07595].

[129] T. Faulkner, M. Guica, T. Hartman, R. C. Myers and M. Van Raamsdonk, *Gravitation from Entanglement in Holographic CFTs*, *JHEP* **03** (2014) 051, [1312.7856].

[130] C. Bachas, *Asymptotic symmetries of AdS_2 branes*, in *Proceedings, Meeting on Strings and Gravity : Tying the Forces Together : 5th Francqui Colloquium: Brussels, Belgium, October, 19-21, 2001*, pp. 9–17, 2003. hep-th/0205115.

[131] W. Israel, *Singular hypersurfaces and thin shells in general relativity*, *Nuovo Cim.* **B44S10** (1966) 1.

[132] R. Abt, J. Erdmenger, H. Hinrichsen, C. M. Melby-Thompson, R. Meyer, C. Northe et al., *Topological Complexity in AdS_3/CFT_2*, *Fortsch. Phys.* **66** (2018) 1800034, [1710.01327].

[133] P. Calabrese and J. L. Cardy, *Entanglement entropy and quantum field theory*, *J. Stat. Mech.* **0406** (2004) P06002, [hep-th/0405152].

[134] M. Guo, J. Hernandez, R. C. Myers and S.-M. Ruan, *Circuit Complexity for Coherent States*, *JHEP* **10** (2018) 011, [1807.07677].

[135] J. L. Cardy, *Boundary Conditions, Fusion Rules and the Verlinde Formula*, *Nucl. Phys.* **B324** (1989) 581–596.

[136] K. Sakai and Y. Satoh, *Entanglement through conformal interfaces*, *JHEP* **12** (2008) 001, [0809.4548].

[137] M. Gutperle and J. D. Miller, *Entanglement entropy at CFT junctions*, *Phys. Rev.* **D95** (2017) 106008, [1701.08856].

[138] P. Bueno and R. C. Myers, *Universal entanglement for higher dimensional cones*, *JHEP* **12** (2015) 168, [1508.00587].

[139] C. P. Herzog and K.-W. Huang, *Boundary Conformal Field Theory and a Boundary Central Charge*, *JHEP* **10** (2017) 189, [1707.06224].

[140] J. Polchinski and L. Thorlacius, *Free fermion representation of a boundary conformal field theory*, *Phys. Rev.* **D50** (1994) R622–R626, [hep-th/9404008].

[141] T. Takayanagi, *Holographic Dual of BCFT*, *Phys. Rev. Lett.* **107** (2011) 101602, [1105.5165].

[142] M. Fujita, T. Takayanagi and E. Tonni, *Aspects of AdS/BCFT*, *JHEP* **11** (2011) 043, [1108.5152].

[143] D. Bak, M. Gutperle and S. Hirano, *A Dilatonic deformation of AdS(5) and its field theory dual*, *JHEP* **05** (2003) 072, [hep-th/0304129].

[144] A. B. Clark, D. Z. Freedman, A. Karch and M. Schnabl, *Dual of the Janus solution: An interface conformal field theory*, *Phys. Rev.* **D71** (2005) 066003, [hep-th/0407073].

[145] A. Karch and L. Randall, *Locally localized gravity*, *JHEP* **05** (2001) 008, [hep-th/0011156].

[146] O. DeWolfe, D. Z. Freedman and H. Ooguri, *Holography and defect conformal field theories*, *Phys. Rev. D* **66** (2002) 025009, [hep-th/0111135].

[147] K. Jensen and A. O'Bannon, *Holography, Entanglement Entropy, and Conformal Field Theories with Boundaries or Defects*, *Phys. Rev. D* **88** (2013) 106006, [1309.4523].

[148] H.-C. Chang and A. Karch, *Entanglement Entropy for Probe Branes*, *JHEP* **01** (2014) 180, [1307.5325].

[149] C. Bachas and M. Petropoulos, *Anti-de Sitter D-branes*, *JHEP* **02** (2001) 025, [hep-th/0012234].

[150] D. Bak, M. Gutperle and S. Hirano, *Three dimensional Janus and time-dependent black holes*, *JHEP* **02** (2007) 068, [hep-th/0701108].

[151] G. Evenbly and G. Vidal, *Quantum Criticality with the Multi-scale Entanglement Renormalization Ansatz*, *ArXiv e-prints* (Sept., 2011) , [1109.5334].

[152] B. Swingle, *Entanglement Renormalization and Holography*, *Phys. Rev.* **D86** (2012) 065007, [0905.1317].

[153] G. Vidal, *Entanglement Renormalization*, *Phys. Rev. Lett.* **99** (2007) 220405, [cond-mat/0512165].

[154] G. Vidal, *Class of Quantum Many-Body States That Can Be Efficiently Simulated*, *Phys. Rev. Lett.* **101** (2008) 110501.

[155] B. Czech, P. H. Nguyen and S. Swaminathan, *A defect in holographic interpretations of tensor networks*, *JHEP* **03** (2017) 090, [1612.05698].

[156] E. Wong and I. Affleck, *Tunneling in quantum wires: A Boundary conformal field theory approach*, *Nucl. Phys. B* **417** (1994) 403–438, [cond-mat/9311040].

[157] M. Oshikawa and I. Affleck, *Boundary conformal field theory approach to the critical two-dimensional Ising model with a defect line*, *Nucl. Phys. B* **495** (1997) 533–582, [cond-mat/9612187].

[158] A. Karch and L. Randall, *Open and closed string interpretation of SUSY CFT's on branes with boundaries*, *JHEP* **06** (2001) 063, [hep-th/0105132].

[159] M. Porrati, *Mass and gauge invariance 4. Holography for the Karch-Randall model*, *Phys. Rev. D* **65** (2002) 044015, [hep-th/0109017].

[160] T. Kimura and M. Murata, *Transport Process in Multi-Junctions of Quantum Systems*, *JHEP* **07** (2015) 072, [1505.05275].

[161] M. Billó, V. Gonçalves, E. Lauria and M. Meineri, *Defects in conformal field theory*, *JHEP* **04** (2016) 091, [1601.02883].

[162] S. R. Coleman and F. De Luccia, *Gravitational Effects on and of Vacuum Decay*, *Phys. Rev. D* **21** (1980) 3305.

[163] M. Cvetic, S. Griffies and S.-J. Rey, *Static domain walls in N=1 supergravity*, *Nucl. Phys. B* **381** (1992) 301–328, [hep-th/9201007].

[164] T. Hartman, S. Kundu and A. Tajdini, *Averaged Null Energy Condition from Causality*, *JHEP* **07** (2017) 066, [1610.05308].

[165] J. Fuchs, M. R. Gaberdiel, I. Runkel and C. Schweigert, *Topological defects for the free boson CFT*, *J. Phys. A* **40** (2007) 11403, [0705.3129].

[166] C. Bachas and I. Brunner, *Fusion of conformal interfaces*, *JHEP* **02** (2008) 085, [0712.0076].

[167] J. R. Fliss, X. Wen, O. Parrikar, C.-T. Hsieh, B. Han, T. L. Hughes et al., *Interface contributions to topological entanglement in abelian chern-simons theory*, *Journal of High Energy Physics* **2017** (Sep, 2017) .

[168] M. Gutperle and J. D. Miller, *Topological interfaces in chern-simons theory and the ads3/cft2 correspondence*, *Physical Review D* **99** (Jan, 2019) .

[169] M. Chiodaroli, M. Gutperle and L.-Y. Hung, *Boundary entropy of supersymmetric Janus solutions*, *JHEP* **09** (2010) 082, [1005.4433].

[170] J. Erdmenger, M. Flory and M.-N. Newrzella, *Bending branes for DCFT in two dimensions*, *JHEP* **01** (2015) 058, [1410.7811].

[171] M. Gutperle and J. D. Miller, *Entanglement entropy at holographic interfaces*, *Phys. Rev. D* **93** (2016) 026006, [1511.08955].

[172] M. Banados, *Three-dimensional quantum geometry and black holes*, *AIP Conf. Proc.* **484** (1999) 147–169, [hep-th/9901148].

[173] V. Balasubramanian, P. Kraus and A. E. Lawrence, *Bulk versus boundary dynamics in anti-de Sitter space-time*, *Phys. Rev.* **D59** (1999) 046003, [hep-th/9805171].

[174] M. Rooman and P. Spindel, *Uniqueness of the asymptotic AdS(3) geometry*, *Class. Quant. Grav.* **18** (2001) 2117–2124, [gr-qc/0011005].

[175] K. Krasnov, *On holomorphic factorization in asymptotically AdS 3-D gravity*, *Class. Quant. Grav.* **20** (2003) 4015–4042, [hep-th/0109198].

[176] D. T. Son and A. O. Starinets, *Minkowski space correlators in AdS / CFT correspondence: Recipe and applications*, *JHEP* **09** (2002) 042, [hep-th/0205051].

[177] C. Herzog and D. Son, *Schwinger-Keldysh propagators from AdS/CFT correspondence*, *JHEP* **03** (2003) 046, [hep-th/0212072].

[178] K. Skenderis and B. C. van Rees, *Real-time gauge/gravity duality: Prescription, Renormalization and Examples*, *JHEP* **05** (2009) 085, [0812.2909].

[179] B. Carter, *Essentials of classical brane dynamics*, *Int. J. Theor. Phys.* **40** (2001) 2099–2130, [gr-qc/0012036].

[180] E. D'Hoker, J. Estes and M. Gutperle, *Exact half-BPS Type IIB interface solutions. I. Local solution and supersymmetric Janus*, *JHEP* **06** (2007) 021, [0705.0022].

[181] E. D'Hoker, J. Estes and M. Gutperle, *Exact half-BPS Type IIB interface solutions. II. Flux solutions and multi-Janus*, *JHEP* **06** (2007) 022, [0705.0024].

[182] C. Bachas and I. Lavdas, *Massive Anti-de Sitter Gravity from String Theory*, *JHEP* **11** (2018) 003, [1807.00591].

[183] G. Penington, *Entanglement Wedge Reconstruction and the Information Paradox*, 1905.08255.

[184] A. Almheiri, N. Engelhardt, D. Marolf and H. Maxfield, *The entropy of bulk quantum fields and the entanglement wedge of an evaporating black hole*, *JHEP* **12** (2019) 063, [1905.08762].

[185] A. Almheiri, R. Mahajan, J. Maldacena and Y. Zhao, *The Page curve of Hawking radiation from semiclassical geometry*, *JHEP* **03** (2020) 149, [1908.10996].

[186] H. Z. Chen, Z. Fisher, J. Hernandez, R. C. Myers and S.-M. Ruan, *Information Flow in Black Hole Evaporation*, *JHEP* **03** (2020) 152, [1911.03402].

[187] M. Rozali, J. Sully, M. Van Raamsdonk, C. Waddell and D. Wakeham, *Information radiation in BCFT models of black holes*, *JHEP* **05** (2020) 004, [1910.12836].

[188] H. Geng and A. Karch, *Massive Islands*, 2006.02438.

[189] H. Z. Chen, R. C. Myers, D. Neuenfeld, I. A. Reyes and J. Sandor, *Quantum Extremal Islands Made Easy, Part I: Entanglement on the Brane*, 2006.04851.

[190] L. Susskind and Y. Zhao, *Switchbacks and the Bridge to Nowhere*, 1408.2823.

[191] L. Susskind, *Entanglement is not enough*, *Fortsch. Phys.* **64** (2016) 49–71, [1411.0690].

[192] L. Susskind, *Three Lectures on Complexity and Black Holes*, 2018. 1810.11563.

[193] C. Holzhey, F. Larsen and F. Wilczek, *Geometric and renormalized entropy in conformal field theory*, *Nucl. Phys.* **B424** (1994) 443–467, [hep-th/9403108].

[194] M. R. Dowling and M. A. Nielsen, *The geometry of quantum computation*, *arXiv e-prints* (Dec, 2006) quant–ph/0701004, [quant-ph/0701004].

[195] D. A. Roberts and B. Yoshida, *Chaos and complexity by design*, *JHEP* **04** (2017) 121, [1610.04903].

[196] T. Ali, A. Bhattacharyya, S. Shajidul Haque, E. H. Kim and N. Moynihan, *Post-Quench Evolution of Distance and Uncertainty in a Topological System: Complexity, Entanglement and Revivals*, 1811.05985.

[197] J. Watrous, *Quantum Computational Complexity*, 0804.3401.

[198] R. Cleve, *An introduction to quantum complexity theory*, quant-ph/9906111.

[199] J. Cotler, M. R. Mohammadi Mozaffar, A. Mollabashi and A. Naseh, *Renormalization Group Circuits for Weakly Interacting Continuum Field Theories*, 1806.02831.

[200] J. von Delft and H. Schoeller, *Bosonization for beginners - refermionization for experts*, *Annalen der Physik* **510** (Nov., 1998) 225–305, [cond-mat/9805275].

[201] I. Bengtsson and K. Zyczkowski, *Geometry of Quantum States: An Introduction to Quantum Entanglement*. Cambridge University Press, New York, NY, USA, 2006.

[202] A. Bernamonti, F. Galli, J. Hernandez, R. C. Myers, S.-M. Ruan and J. Simón, *First Law of Holographic Complexity*, *Phys. Rev. Lett.* **123** (2019) 081601, [1903.04511].

[203] T. Giamarchi, *Quantum Physics in One Dimension*. Oxford University Press, Oxford, UK, 2003.

[204] A. O. Gogolin, A. A. Nersesian and A. M. Tsvelik, *Bosonization and strongly correlated systems*. 2004.

[205] D. Harlow, *The Ryu–Takayanagi Formula from Quantum Error Correction*, *Commun. Math. Phys.* **354** (2017) 865–912, [1607.03901].

[206] T. Faulkner and A. Lewkowycz, *Bulk locality from modular flow*, *JHEP* **07** (2017) 151, [1704.05464].

[207] T. Faulkner, A. Lewkowycz and J. Maldacena, *Quantum corrections to holographic entanglement entropy*, *JHEP* **11** (2013) 074, [1307.2892].

[208] D. L. Jafferis and S. J. Suh, *The Gravity Duals of Modular Hamiltonians*, *JHEP* **09** (2016) 068, [1412.8465].

[209] M. Van Raamsdonk, *Building up spacetime with quantum entanglement*, *Gen. Rel. Grav.* **42** (2010) 2323–2329, [1005.3035].

[210] J. Maldacena and L. Susskind, *Cool horizons for entangled black holes*, *Fortsch. Phys.* **61** (2013) 781–811, [1306.0533].

[211] B. Czech, L. Lamprou and L. Susskind, *Entanglement Holonomies*, 1807.04276.

[212] B. Czech, L. Lamprou, S. Mccandlish and J. Sully, *Modular Berry Connection for Entangled Subregions in AdS/CFT*, *Phys. Rev. Lett.* **120** (2018) 091601, [1712.07123].

[213] W. Donnelly and L. Freidel, *Local subsystems in gauge theory and gravity*, *JHEP* **09** (2016) 102, [1601.04744].

[214] A. Strominger, *Lectures on the Infrared Structure of Gravity and Gauge Theory*, 1703.05448.

[215] S. W. Hawking, M. J. Perry and A. Strominger, *Superrotation Charge and Supertranslation Hair on Black Holes*, *JHEP* **05** (2017) 161, [1611.09175].

[216] J. Mielczarek and T. Trześniewski, *Gauge fields and quantum entanglement*, 1911.10208.

[217] K. Papadodimas and S. Raju, *State-Dependent Bulk-Boundary Maps and Black Hole Complementarity*, *Phys. Rev.* **D89** (2014) 086010, [1310.6335].

[218] T. Faulkner, R. G. Leigh, O. Parrikar and H. Wang, *Modular Hamiltonians for Deformed Half-Spaces and the Averaged Null Energy Condition*, *JHEP* **09** (2016) 038, [1605.08072].

[219] A. Lewkowycz and O. Parrikar, *The holographic shape of entanglement and Einstein's equations*, *JHEP* **05** (2018) 147, [1802.10103].

[220] M. V. Berry, *Quantal phase factors accompanying adiabatic changes*, *Proc. R. Soc. Lond. A* **392** (March, 1984) 45–57.

[221] F. Wilczek and A. Zee, *Appearance of gauge structure in simple dynamical systems*, *Phys. Rev. Lett.* **52** (Jun, 1984) 2111–2114.

[222] B. Czech, L. Lamprou, S. McCandlish, B. Mosk and J. Sully, *A Stereoscopic Look into the Bulk*, *JHEP* **07** (2016) 129, [1604.03110].

[223] J. de Boer, F. M. Haehl, M. P. Heller and R. C. Myers, *Entanglement, holography and causal diamonds*, *JHEP* **08** (2016) 162, [1606.03307].

[224] H. Casini, E. Teste and G. Torroba, *Modular Hamiltonians on the null plane and the Markov property of the vacuum state*, *J. Phys.* **A50** (2017) 364001, [1703.10656].

[225] T. Faulkner, M. Li and H. Wang, *A modular toolkit for bulk reconstruction*, *JHEP* **04** (2019) 119, [1806.10560].

[226] D. Harlow and J.-Q. Wu, *Covariant phase space with boundaries*, 1906.08616.

[227] J. Camps, *Superselection Sectors of Gravitational Subregions*, *JHEP* **01** (2019) 182, [1810.01802].

[228] B. Czech, Y. D. Olivas and Z.-z. Wang, *Holographic integral geometry with time dependence*, 1905.07413.

[229] V. Coffman, J. Kundu and W. K. Wootters, *Distributed entanglement*, *Phys. Rev.* **A61** (2000) 052306, [quant-ph/9907047].

[230] F. Verstraete, J. Dehaene, B. De Moor and H. Verschelde, *Four qubits can be entangled in nine different ways*, *Physical Review A* **65** (Apr, 2002) .

[231] W. Dur, G. Vidal and J. I. Cirac, *Three qubits can be entangled in two inequivalent ways*, *Phys. Rev.* **A62** (2000) 062314, [quant-ph/0005115].

[232] A. Belin, A. Lewkowycz and G. Sárosi, *The boundary dual of the bulk symplectic form*, *Phys. Lett.* **B789** (2019) 71–75, [1806.10144].

[233] D. Kabat and G. Lifschytz, *Emergence of spacetime from the algebra of total modular Hamiltonians*, *JHEP* **05** (2019) 017, [1812.02915].

[234] X. Dong, D. Harlow and D. Marolf, *Flat entanglement spectra in fixed-area states of quantum gravity*, *JHEP* **10** (2019) 240, [1811.05382].

[235] J. Kirklin, *Unambiguous Phase Spaces for Subregions*, *JHEP* **03** (2019) 116, [1901.09857].

[236] W. Donnelly, *Entanglement entropy and nonabelian gauge symmetry*, *Class. Quant. Grav.* **31** (2014) 214003, [1406.7304].

[237] W. Donnelly and A. C. Wall, *Entanglement entropy of electromagnetic edge modes*, *Phys. Rev. Lett.* **114** (2015) 111603, [1412.1895].

[238] S. Haco, S. W. Hawking, M. J. Perry and A. Strominger, *Black Hole Entropy and Soft Hair*, *JHEP* **12** (2018) 098, [1810.01847].

[239] R. Bousso and M. Porrati, *Soft Hair as a Soft Wig*, *Class. Quant. Grav.* **34** (2017) 204001, [1706.00436].

[240] R. Bousso and M. Porrati, *Observable Supertranslations*, *Phys. Rev.* **D96** (2017) 086016, [1706.09280].

[241] J. Maldacena, S. H. Shenker and D. Stanford, *A bound on chaos*, *JHEP* **08** (2016) 106, [1503.01409].

[242] D. Harlow, *Wormholes, Emergent Gauge Fields, and the Weak Gravity Conjecture*, *JHEP* **01** (2016) 122, [1510.07911].

RÉSUMÉ

La dualité holographique donne un moyen d'encoder certaines informations quantiques dans une théorie gravitationnelle semi-classique. Dans cette thèse, nous commençons par une étude de la complexité quantique, en considérant l'universalité de deux conjectures holographiques, "Complexité = Volume" (CV) et "Complexité = Action" (CA), en termes d'un modèle avec une brane mince dans AdS_3. Notre résultat montre que la structure de divergences pour les deux cas n'est pas identique car le CV a une divergence logarithmique supplémentaire dépendante de la tension de la brane. Bien que des considérations préliminaires sur la complexité en théorie des champs favorisent le CA, la question de l'universalité reste ouverte. Ensuite, nous passons à une étude sur la dépendance de la complexité d'un circuit quantique du choix des portes. Un calcul explicite dans le modèle de fermions bosonisées en deux dimensions montre que l'influence du choix de l'ensemble de portes est différente pour différents sous-ensembles d'états considérés: elle est non significative pour les états "cohérente bosonique-Gaussien fermionique", bien que radicalement différent dans les états bi-Gaussien. Puis, nous reconsidérons le modèle à brane mince de manière holographique canonique, constatant que la tension de la brane est liée aux coefficients de transport d'énergie définis dans le dCFT ainsi qu'à l'entropie de bord sur l'interface, ce qui était connu dans la littérature. Dans la dernière partie, nous proposons une nouvelle quantité géométrique dans le bulk, duelle à la courbure de Berry dans l'espace des Hamiltoniens modulaires de bord, qui est la courbure de Riemann au voisinage de la surface de Hubeny-Rangamani-Takayanagi. Une vérification de cette conjecture a été faite en AdS_3 pur qui montre un bon accord en raison de la simplicité et des symétries du système.

MOTS CLÉS

Théorie des Cordes, Dualité Holographique, Gravité Quantique, et Information Quantique.

ABSTRACT

The holographic duality renders a way to encode certain quantum information in a semi-classical gravity theory. In this thesis, we start with the quantum complexity, considering the universality of its two holographic conjectures, "Complexity=Volume" (CV) and "Complexity=Action" (CA), in terms of the thin brane model in AdS_3. Our result shows that the divergence structures for the two are not identical as CV has an extra brane tension dependent logarithmic divergence. Though preliminary considerations on the field theory side of complexity favor CA, the universality question is still kept open. Next we move to a study on the gate dependence of circuit complexity by explicit calculation in the two-dimensional bosonized model where we show that the influence of the gate set choice is different for different subsets of states under consideration, not significant for "bosonic coherent-fermionic Gaussian" case, while dramatically different in the bi-Gaussian case. Then, we reconsider the thin-brane model in the canonical holographic manner, finding that the brane tension is related to the energy transport coefficients defined in the dCFT, in addition to the relation to the boundary entropy of the interface which has been commonly advertised in the literature. In the last part, we propose a new bulk geometric quantity dual to the Berry curvature in the space of boundary modular Hamiltonians, which is the Riemann curvature in the vicinity of the Hubeny-Rangamani-Takayanagi surface. A sanity test has been done in pure AdS_3 which shows a nice agreement due to the simplicity and nice symmetries of this system.

KEYWORDS

String Theory, Holographic Duality, Quantum Gravity, and Quantum Information.